

## Chapter 6

# Optimum Waveform Estimation

### 6.1 Introduction

In Chapters 2, 3, and 4 we discussed deterministic design techniques and developed the basic ideas of beam patterns, array gain, sidelobe control, and null placement. In Chapter 5 we developed statistical representations of space-time random processes.

In Chapters 6–10, we utilize the statistical representation of the signal and noise processes to design array processors that are optimum in a statistical sense. The first step is to define the objectives of the array processor. We consider the following objectives in the remainder of the text:

- (i) The first objective of interest is to **estimate the waveform** of a plane-wave signal impinging on the array in the presence of noise and interfering signals. More generally, we want to estimate the waveform of  $D$  plane-wave signals impinging on the array in a similar environment. This problem is sometimes called the “signal copy” problem in the literature. This objective will lead us to beamformers that are optimum in a statistical sense. They are the statistical analog to the deterministic beamformers in Chapters 2–4. In Chapter 6, we assume that the appropriate statistics are known. In Chapter 7, we assume that the necessary statistics must be measured from the data and are led to adaptive beamformers.
- (ii) The second objective of interest is to **detect** the presence or absence of a signal that impinges on the array as a plane-wave or a spatially spread

signal. More generally, we want to detect which signal belonging to a finite alphabet is present.

This problem is the spatial generalization of the optimum detection problem that we studied in Parts 1 and 3 of DEMT ([VT68], [VT01a]). We study this objective in Chapter 10. In most cases, the spatial aspects of the problem lead to the same beamformers as in Chapters 6 and 7.

- (iii) The third objective of interest is to **estimate the direction of arrival** of  $D$  plane waves that are impinging on the array in the presence of interference and noise. In most cases of interest, the spatial spectral matrix  $\mathbf{S}_x$  and the noise level  $\sigma_w^2$  are unknown. Thus, we formulate the problem as a more general **parameter estimation problem**, in which there are  $D$  desired parameters plus a set of unwanted (or nuisance) parameters.

This problem is the spatial generalization of the parameter estimation problem that we studied in Parts 1 and 3 of DEMT ([VT68] and [VT01a]). We study this problem in Chapters 8 and 9.

There is a problem contained in this third objective that deserves special mention. This is the case in which the array manifold vector is either unknown or is perturbed from its nominal position. In some application our focus is on the signal DOAs and we treat array parameters as nuisance parameters. In another application, the value of the array parameters is also important. This latter case is known as the **array calibration** problem. We treat it briefly in Chapter 9, but do not discuss it in detail.

All of the problems within this objective are characterized by a **finite** parameter set. We want to estimate some (or all) of the parameters in this set.

- (iv) The fourth objective of interest is to **estimate the spatial spectrum** of the space-time process that is impinging on the array. If we model the space-time field parametrically as in Section 5.6, then the basic ideas (but not the details) carry over from the parameter estimation problem. However, in many applications, a parametric model is not appropriate and we utilize non-parametric spatial spectrum estimation. We do not cover non-parametric estimation in the text. In Chapter 9, we cite several references on spectrum estimation.

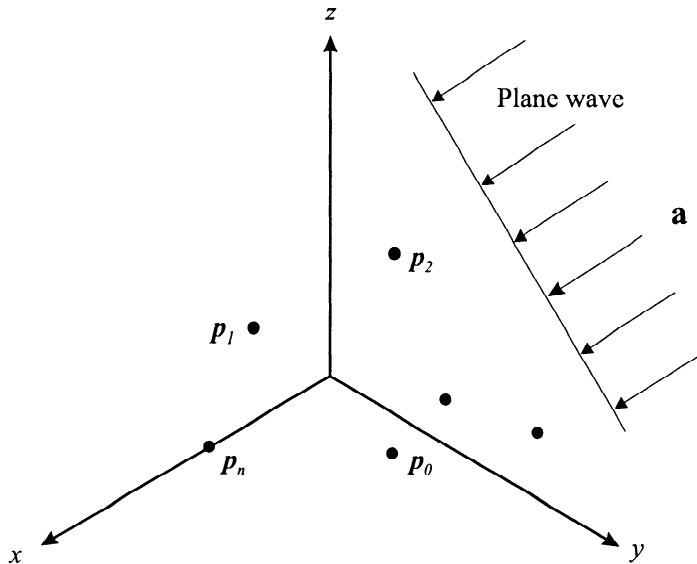


Figure 6.1 Sensor array with single plane-wave signal.

In the course of the remainder of the text we amplify on these objectives and suggest excursions. It is important to always keep the desired objective in mind when evaluating the array processor, because a particular processor may appear under several different objectives and its performance will be evaluated according to different criteria.

For example, in Section 6.2.1, we develop a beamformer referred to as the minimum variance distortionless response (MVDR) or Capon beamformer. It also appears in the parameter estimation context in Chapter 9 and would appear in the non-parametric spatial spectrum estimation problem if we developed it. We must evaluate its performance in the context of the specific objective.

The basic models that we utilize in this chapter are shown in Figures 6.1 through 6.5. The array consists of \$N\$ sensors located in a 3-D space. Normally we assume isotropic sensors, but we show how to modify the results to take element patterns into account. In Figure 6.1, we show a single plane-wave signal propagating along \$\mathbf{a}\_s\$. The temporal characteristics of the signal of interest include known signals, signals with random parameters, random processes, and unknown nonrandom signals. This includes a large number of communications, radar, sonar, and seismic problems. In Figure 6.2(a), we show multiple plane-wave signals propagating along \$\mathbf{a}\_i; i = 1, \dots, L\_s\$.

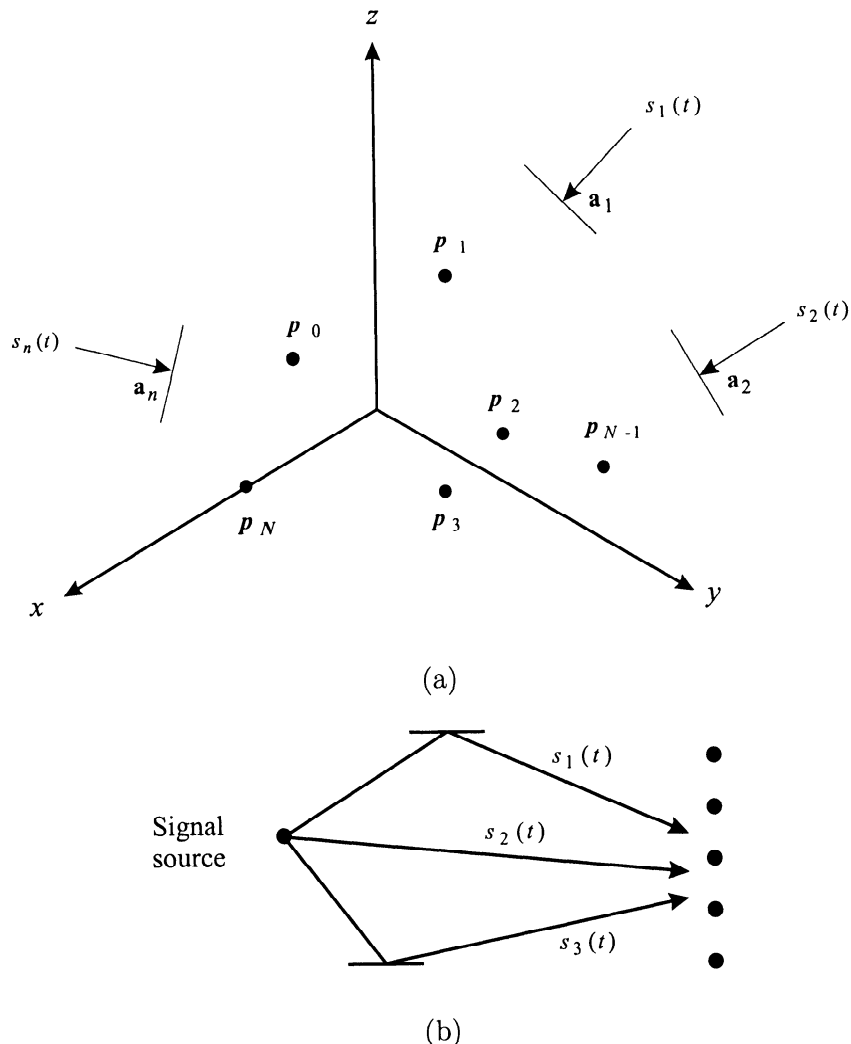


Figure 6.2 (a) Multiple plane-wave signals; (b) multipath environment.

The model arises in the multipath environments of communications, radar, sonar, and seismic environments, as shown in Figure 6.2(b). The temporal characteristics of the signals can vary as in the single-signal case. The third signal case of interest is shown in Figure 6.3(a). Here the signal source has a continuous distribution in frequency-wavenumber space. This model can arise in communications systems (e.g., the tropospheric scatter model shown in Figure 6.3(b)) or sonar systems (Figure 6.3(c)) as well as other areas. For spatially spread signals, the temporal characteristics are modeled as a random processes.

Various noise models are used with these signal models. Our model always assumes that there is a non-zero sensor noise that is uncorrelated from sensor to sensor. A typical discrete interference model is shown in Figure 6.4. Here the external interference consists of a set of plane-wave signals. In the radar and communications area, this is a realistic model for jammers. In the sonar case, it can represent discrete noise sources such as propellers. These noises can be either continuous-wave (CW) signals, modulated signals, narrowband random processes, or wideband random processes. A typical continuous noise field is shown in Figure 6.5. These fields occur frequently in the sonar and radar area.

In all of our work in this chapter we assume that the statistical characteristics of the signal and noise fields are known. We also assume the array characteristics (e.g., location, element patterns) are known. We look at the effect of imprecise or erroneous knowledge of these characteristics, but defer the study of unknown environments to a later chapter. In addition, we focus our attention on the case where the signal and noise processes are stationary and the observation interval is long.

In Section 6.2, we begin our discussion by modeling the signal as an unknown nonrandom signal propagating along some known direction and develop the concept of an optimum distortionless filter that guarantees that any signal propagating along the specified direction will pass through the filter undistorted and the output noise power is minimized. If the noise is a sample function from a Gaussian random process then the output of the optimum distortionless filter is the maximum likelihood estimate of the signal. We refer to this filter as the minimum variance distortionless response (MVDR) filter.

We then consider the case in which the signal is a sample function from a random process and design the optimum linear processor to generate the minimum mean-square error (MMSE) estimate of the signal. The result is the vector version of the Wiener filter that we studied in Chapter 6 of DEMT I [VT68], [VT01a]. We demonstrate that the optimum processor consists of

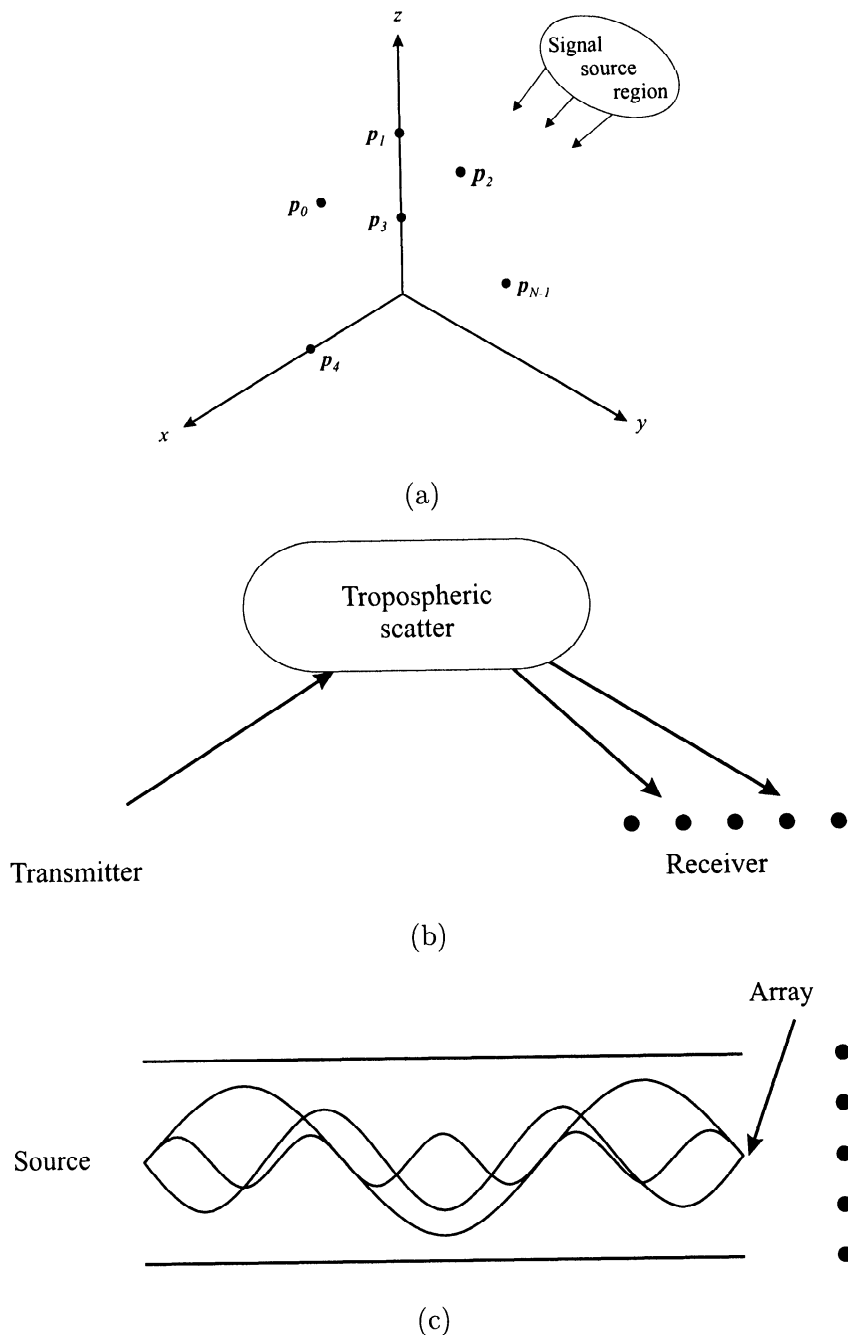


Figure 6.3 (a) Spatially spread signals; (b) troposphere; (c) sonar.

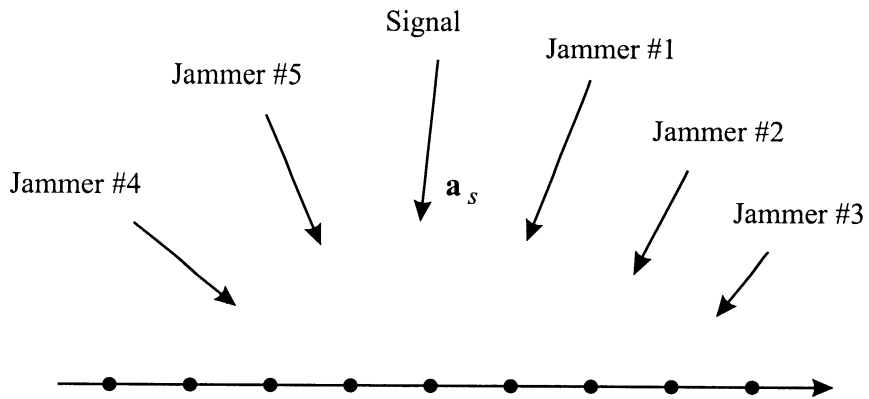


Figure 6.4 Discrete interference model.

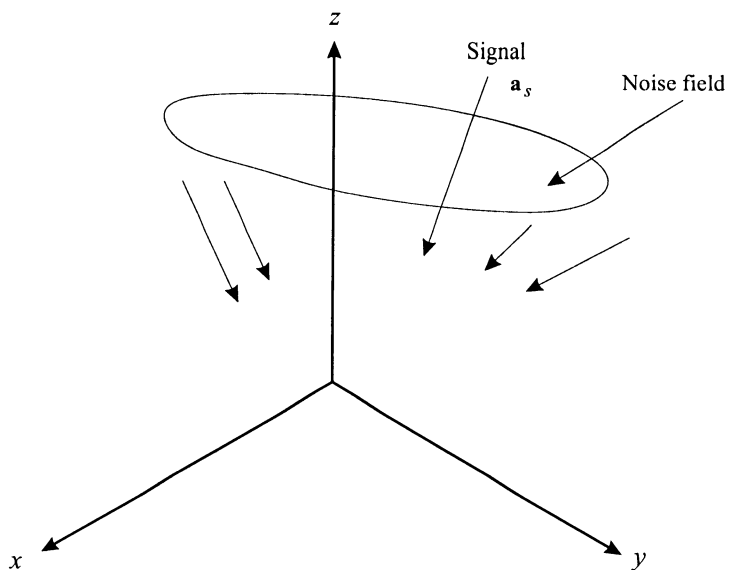


Figure 6.5 Continuous noise field.

an optimum beamformer followed by an optimum scalar filter. We then show that if the signal and noise processes are Gaussian, the optimum linear processor is generating the conditional mean (thus, no nonlinear processor could do better).

We show that if the signal is a single plane wave, then the optimum matrix processor (i.e., the optimum beamformer) is the same for either signal model.

We then examine two other beamformers. The first maximizes the output *SNR*. For a single plane-wave signal, this criterion leads to the same optimum beamformer as the MMSE beamformer. Thus for single plane-wave signals we have a criterion-invariant receiver. The second beamformer assumes that we know (or can measure)  $\mathbf{S}_x(\omega)$  but do not know the spectral matrix of the noise component ( $\mathbf{S}_n(\omega)$ ). We choose a steering direction and find the optimum distortionless filter for that direction. We refer to this as the minimum power distortionless response (MPDR) filter. If the steering direction corresponds to the actual signal direction, then the MPDR beamformer reduces to the MVDR beamformer. Later we examine the effects of a mismatch.

All of the results in Section 6.2 apply to arbitrary noise fields. In Section 6.3, we examine the case in which the interference consists of a set of discrete plane waves and find explicit solutions for the optimum beamformers and their performance. We introduce the idea of an eigenbeam receiver as a realization of the optimum processor.

In Section 6.4, we study spatially spread interference. We use the physical noise models from Section 5.3 and the ARMA models from Section 5.6 to model the interference and study the performance of the MVDR and MPDR beamformers with this type of interference.

In Section 6.5, we extend the results to the case in which there are multiple desired plane-wave signals. The results are a logical extension of single plane-wave signals. However, the resulting beamformer has some interesting properties.

A major problem in applying optimum beamformers in operational systems is the potential sensitivity to mismatches between the actual environment and the model used to derive the optimum beamformer.

In Section 6.6, we analyze how the performance of the MVDR beamformer is affected by various types of mismatch. Typical mismatches include DOA mismatch, sensor gain and phase perturbations, and sensor position perturbations. The MVDR beamformer degrades gracefully. However, we find that the performance of the MPDR beamformer degrades rapidly under mismatch. We introduce a technique called diagonal loading to improve

robustness.

In Section 6.7, we incorporate additional linear constraints in order to further improve the robustness of the beamformer. We derive the linear constrained minimum variance (LCMV) and the linear constrained minimum power (LCMP) beamformer. We find that, with the addition of diagonal loading, these beamformers are reasonably robust. We also introduce a generalized sidelobe canceller realization of the beamformer.

In Section 5.5, we showed how the use of an orthogonal expansion in terms of eigenvalues and eigenvectors enabled us to represent the set of plane-wave signals and interference in a subspace. In Section 6.8, we develop beamformers that perform an eigendecomposition of  $\mathbf{S}_x$ . A subset of the eigenvalues and eigenvectors is used to construct the beamformer. Two types of eigenvector beamformers, eigenspace beamformers and dominant-mode rejection beamformers, are developed and analyzed. In the known spectrum case, they have the potential to provide improved performance in the presence of mismatch. In Chapter 7, we see that, in the real-world case, where we have to estimate  $\mathbf{S}_x$  or an equivalent statistic, they offer additional advantages.

In Section 6.9, we consider the case in which we first form a reduced-dimension beamspace by processing the data with a small set of non-adaptive beams that span the sector of interest. We then process the beam outputs using an adaptive processor. We find that there are a number of advantages to this technique.

In Section 6.10, we consider the use of quadratic constraints to improve beamformer robustness. We introduced it in Section 6.6 to motivate diagonal loading. We revisit it to more fully exploit its potentials and to set the stage for variable diagonal loading in Chapter 7.

In Section 6.11, we develop an algorithm to minimize the squared error between a desired beam pattern and the actual beam pattern over a region of  $w\text{-k}$  space. We minimize the output power subject to a constraint on the squared error. This approach leads to a beamformer that is referred to as a soft-constraint beamformer. It is a generalization of diagonal loading that is useful in some applications.

In Section 6.12, we consider the case in which the desired signal and the interference are coherent ( $|\rho| = 1$ ) or correlated ( $|\rho| \neq 0$ ). We find that, as  $|\rho|$  approaches one, there is significant performance degradation because the desired signal is cancelled. We introduce a technique called spatial smoothing to obtain beamformers that will operate in a coherent environment.

In Section 6.13, we consider broadband beamformers. The frequency-

domain implementation is a straightforward extension of our narrowband results because of our use of the frequency-domain snapshot model. The time-domain implementation requires an extension of the narrowband time-domain model in Section 5.2.

In Section 6.14, we summarize our results and discuss some of the issues that remain to be explored.

The structure of Chapter 6 is shown in Table 6.1. Most of the material in the first part of this chapter appeared in “Chapter II-5: Multi-dimensional and Multi-variable Processes” [VT69], which was part of the course notes for my course in Advanced Topics in Detection and Estimation Theory taught at M.I.T. in the Spring term of 1969. Although these notes were unpublished, they had a significant underground distribution. Some of the material had been published earlier in [VT66b] and [VT66a] with the grandiose title, “A Unified Theory for Optimum Array Processing.” Other references include [VT64], [VT65], and [VT68]. The material was intended to be the last chapter in DEMT III [VT71] and [VT01b], but was omitted because of space limitations. Some of it appeared subsequently in [Bag76]. Other early work in the area covered by this chapter includes Bryn [Bry62], Middleton and Groginsky [MG64], Schweppe [Sch68], Gaardner [Gaa66] [Gaa67], Burg [Bur64], Pritchard [Pri63], [Pri51], Vanderkulk [Van63], Childers and Reed [CR65], Becker and Cron [BC65], Faran and Hills [FH53], Kelly [Kel65], Price [Pri53], [Pri54], [Pri56], Wolf [Wol59], Capon et al. [CGK67], Edelbute et al. [EFK67], Mermoz [Mer64] and Middleton [Mid60]. The material starting in Section 6.6 is new and is based on a large number of journal articles, conference papers, and books that have appeared in this area over the last 30 years.

It is worthwhile re-emphasizing that throughout this chapter we assume that the signal and the interference statistics are known. In Chapter 7, we develop adaptive beamformers that estimate the appropriate statistics from the incoming data. We would expect that these adaptive beamformers will converge to one of the beamformers in this chapter if the processes are stationary and the observation time approaches infinity. Thus, we might consider the beamformers in this chapter to be the “steady-state” version of the corresponding adaptive beamformer.

Even if a particular beamformer developed in this chapter has good performance, it does not guarantee that its adaptive version will have good performance (or be computationally feasible). However, if the beamformer’s performance assuming known statistics is poor, then it is unlikely that the adaptive version will be useful.

Table 6.1 Structure of Chapter 6.

Optimum Beamformers	6.2 Single PW Signal MVDR, MPDR MMSE	6.5 Multiple PW Signals MVDR, MPDR MMSE	
Interference Models	6.3 Discrete SPW, MPW Sensitivity Eigenbeams	6.4 Spatially Spread Acoustic noise models ARMA models	
Model Mismatch	6.6 Mismatch Steering vector Array perturbations Noise models		
Constraints	6.7 Linear Constraints Directional Derivative Eigenvector Quiescent pattern	6.10 Quadratic Constraints Fixed diagonal loading Variable DL	6.11 Soft Constraints Generalized diagonal loading
Reduced Dimension	6.8 Eigenspace Principal components Cross spectral	6.9 Beamspace BS-MPDR BS-LCMP	
Coherent Signals	6.12 Coherent Signals Signal nulling FB averaging Spatial smoothing		
Broadband Beamformers	6.13 Broadband Frequency domain Time domain		

Therefore, the purpose of this chapter is to develop a collection of beamformers that have good properties in a known statistics environment. These beamformers serve as candidates for adaptive implementations.

It is important to understand the notation we use in the chapter. We use the frequency-domain snapshot model developed in Section 5.2.1. We assume that the approximations developed in that section are valid. Therefore, the input to the array processor is a sequence of statistically independent circular complex Gaussian random vectors,  $\mathbf{X}_{\Delta T}(\omega_m, k)$ ,  $m = -(M-1)/2 \leq m \leq (M-1)/2$ ,  $k = 1, \dots, K$ . Sections 6.2–6.12 consider narrowband beamformers. Because  $\mathbf{X}_{\Delta T}(\omega_{m_1}, k)$  and  $\mathbf{X}_{\Delta T}(\omega_{m_2}, k)$  are statistically independent, the narrowband beamformers for each frequency bin are uncoupled. Therefore, it is convenient to suppress the  $m$  subscript of  $\omega$ . The discussion assumes that the spatial spectral matrix is known and is the same for each snapshot. Therefore it is convenient to suppress the  $k$ -dependence. Chapter 7 focusses on the behavior as a function of  $k$ . The approximations in Section 5.2.1 replace the mean and covariance of  $\mathbf{X}_{\Delta T}(\omega_m, k)$  with  $\mathbf{m}_x(\omega_m, k)$  and  $\mathbf{S}_x(\omega_m)$ , respectively. Therefore it is convenient to suppress the  $\Delta T$  subscript. Thus, to keep the notation as simple as possible,  $\mathbf{X}(\omega)$  will be used in Sections 6.2–6.12 to represent  $\mathbf{X}_{\Delta T}(\omega_m, k)$ .

In many cases, the  $\omega$ -dependence will also be suppressed and  $\mathbf{X}$  will be used. Occasionally, one or more of the subscripts or indices will be used to make a specific point.

It is also useful to note that, since Sections 6.2–6.12 deal with narrowband beamformers, the entire development could have been done in the time domain. For the same spatial characteristics of the signals and noise, the resulting weight vectors in the beamformers are identical.

## 6.2 Optimum Beamformers

In this section, we derive optimum beamformers for plane-wave signals being received in the presence of a noise field and analyze their performance. We consider four models. The objective of the optimum beamformer is to estimate the signal waveform.

In Section 6.2.1, we assume that the noise is a sample function of a random process with known second-order statistics, but the signal is an unknown nonrandom plane-wave signal arriving from a known direction. We derive the optimum linear array processor to provide the minimum variance unbiased estimate of the signal waveform. We show that this criterion is the same as requiring the array processor to be a distortionless filter (i.e.,

any waveform coming from the specified signal direction will pass through the filter undistorted) and find the distortionless filter that minimizes the output variance. Finally, we show that if the noise process is Gaussian, then the output of the optimum distortionless filter is the maximum likelihood estimate of the signal waveform.

In Section 6.2.2, we assume that the signals and noises are sample functions of stationary random processes and that their second-order statistics are known. Initially, we consider a single plane-wave signal arriving at the array from a known direction. We derive the optimum linear array processor to estimate the signal waveform using a MMSE criterion. Finally, we observe that if the signal and noise processes are Gaussian, then the optimum linear array processor is optimum over the class of all processors.

In Section 6.2.3, we utilize the signal and noise model of Section 6.2.2. However, now we assume that the criterion is maximum output *SNR*. We show that the optimum processor consists of the same matrix operation as in the second model followed by a different scalar filter.

In Section 6.2.4, we consider a fourth model. This model is closely related to the first model. In this model we select a steering direction that we believe the signal is arriving from. However, the actual signal may be arriving from a different direction. In addition, we assume that we know (or can measure) the statistics of the total received waveform  $\mathbf{x}(t)$ , but do not know the statistics of the signal and noise components. We derive the distortionless filter for the specified steering direction that minimizes the mean square output power. We refer to the processor derived using this model as the minimum power distortionless response (MPDR) beamformer. When the signal direction and the steering direction coincide, the MPDR beamformer reduces to the MVDR beamformer. In other cases, there may be a significant difference in performance.

In Section 6.2.6, we extend the results to multiple plane-wave signals.

### 6.2.1 Minimum Variance Distortionless Response (MVDR) Beamformers

In this section, we consider the first model that was described at the beginning of the section. This is the case in which the signal is nonrandom but unknown. In the initial discussion, we consider the case of single plane-wave signal.

The frequency-domain snapshot consists of signal plus noise,

$$\mathbf{X}(\omega) = \mathbf{X}_s(\omega) + \mathbf{N}(\omega). \quad (6.1)$$

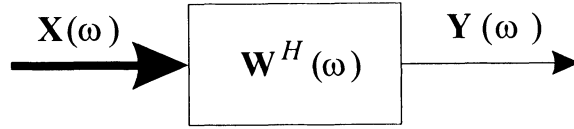


Figure 6.6 Matrix processor.

The signal vector can be written as

$$\mathbf{X}_s(\omega) = F(\omega)\mathbf{v}(\omega : \mathbf{k}_s), \quad (6.2)$$

where  $F(\omega)$  is the frequency-domain snapshot of the source signal and  $\mathbf{v}(\omega : \mathbf{k}_s)$  is the array manifold vector for a plane wave with wavenumber  $\mathbf{k}_s$ . The noise snapshot,  $\mathbf{N}(\omega)$  is a zero-mean random vector with spectral matrix,

$$\mathbf{S}_n(\omega) = \mathbf{S}_c(\omega) + \sigma_w^2 \mathbf{I}. \quad (6.3)$$

Later we will add the assumption that  $\mathbf{N}(\omega)$  is a zero-mean circular complex Gaussian random vector.

### 6.2.1.1 Minimum variance distortionless response (MVDR) beamformer

We process  $\mathbf{X}(\omega)$  with a matrix operation  $\mathbf{W}^H(\omega)$  as shown in Figure 6.6. The dimension of  $\mathbf{W}^H(\omega)$  is  $1 \times N$ .

The first criterion of interest is called the distortionless criterion. It is required that, in the absence of noise,

$$Y(\omega) = F(\omega), \quad (6.4)$$

for any  $F(\omega)$ . Under this constraint, we wish to minimize the variance of  $Y(\omega)$  in the presence of noise. Thus, we write

$$Y(\omega) = F(\omega) + Y_n(\omega), \quad (6.5)$$

and minimize  $E [|Y_n(\omega)|^2]$ .

The constraint of no distortion implies

$$\mathbf{W}^H(\omega)\mathbf{v}(\omega : \mathbf{k}_s) = 1. \quad (6.6)$$

The mean square of the output noise is,

$$E [|Y_n|^2] = \mathbf{W}^H(\omega)\mathbf{S}_n(\omega)\mathbf{W}(\omega). \quad (6.7)$$

We want to minimize  $E[|Y_n|^2]$  subject to the constraint in (6.6).<sup>1</sup>

Before doing this, we state a second criterion that leads to the same minimization problem.

This second criterion is called the minimum variance unbiased estimate criterion.<sup>2</sup> Here we require that  $Y(\omega)$  be the minimum variance unbiased estimate of  $F(\omega)$ . This implies

$$E[Y(\omega)] = F(\omega). \quad (6.8)$$

Thus, using (6.5) in (6.8),

$$\begin{aligned} E[Y(\omega)] &= E[F(\omega)] + E[N(\omega)] \\ &= E[F(\omega)], \end{aligned} \quad (6.9)$$

for any  $F(\omega)$ . This equality implies

$$\mathbf{W}^H(\omega)\mathbf{v}(\omega : \mathbf{k}_s) = 1, \quad (6.10)$$

which is identical to the constraint in (6.6).

Thus we have the same minimization problem as before. We now solve this problem by imposing the constraint in (6.6) by using a Lagrange multiplier. The function that we minimize is

$$\begin{aligned} F &\triangleq \mathbf{W}^H(\omega)\mathbf{S}_{\mathbf{n}}(\omega)\mathbf{W}(\omega) + \lambda(\omega) \left[ \mathbf{W}^H(\omega)\mathbf{v}(\omega : \mathbf{k}_s) - 1 \right] \\ &\quad + \lambda^*(\omega) \left[ \mathbf{v}^H(\omega : \mathbf{k}_s)\mathbf{W}(\omega) - 1 \right]. \end{aligned} \quad (6.11)$$

Taking the complex gradient with respect to  $\mathbf{W}^H(\omega)$  and solving gives

$$\mathbf{W}_o^H(\omega) = -\lambda(\omega)\mathbf{v}^H(\omega : \mathbf{k}_s)\mathbf{S}_{\mathbf{n}}^{-1}(\omega). \quad (6.12)$$

To evaluate  $\lambda(\omega)$ , we use the constraint in (6.6), which gives

$$\lambda(\omega) = - \left[ \mathbf{v}^H(\omega : \mathbf{k}_s)\mathbf{S}_{\mathbf{n}}^{-1}(\omega)\mathbf{v}(\omega : \mathbf{k}_s) \right]^{-1}. \quad (6.13)$$

Thus,

$\mathbf{W}_o^H(\omega) = \Lambda(\omega : \mathbf{k}_s)\mathbf{v}^H(\omega : \mathbf{k}_s)\mathbf{S}_{\mathbf{n}}^{-1}(\omega),$

(6.14)

---

<sup>1</sup>The idea of combining multiple inputs in a statistically optimum manner under the constraint of no signal distortion is due to Darlington [Dar58]. An interesting discussion of the method is contained in Brown and Nilsson's text [BN62].

<sup>2</sup>This criterion was first considered for this application by Levin [Lev64].

where

$$\Lambda(\omega : \mathbf{k}_s) \triangleq \left[ \mathbf{v}^H(\omega : \mathbf{k}_s) \mathbf{S}_{\mathbf{n}}^{-1}(\omega) \mathbf{v}(\omega : \mathbf{k}_s) \right]^{-1}. \quad (6.15)$$

The matrix processor in (6.14) and (6.15) is referred to as the MVDR beamformer and was first derived by Capon [Cap69]. It is sometimes referred to as the Capon beamformer.

For notational simplicity, it is convenient to suppress  $\omega$  and  $\mathbf{k}_s$  in these formulas.

$$\mathbf{v}_s \triangleq \mathbf{v}(\omega_c : \mathbf{k}_s), \quad (6.16)$$

$$\mathbf{S}_{\mathbf{n}}(\omega) \triangleq \mathbf{S}_{\mathbf{n}}, \quad (6.17)$$

$$\Lambda_s \triangleq \mathbf{v}^H \mathbf{S}_{\mathbf{n}}^{-1} \mathbf{v}. \quad (6.18)$$

Then,

$$\mathbf{w}_o^H = \Lambda_s \mathbf{v}^H \mathbf{S}_{\mathbf{n}}^{-1} \quad (6.19)$$

or

$$\mathbf{w}_{mvdr}^H = \Lambda_s \mathbf{v}^H \mathbf{S}_{\mathbf{n}}^{-1}, \quad (6.20)$$

where the subscript emphasizes the optimization criterion.

### 6.2.1.2 Maximum likelihood estimators

We consider the same model as in Section 6.2.1.1 except the assumption that  $\mathbf{N}(\omega)$  is a circular complex Gaussian random vector is added. The likelihood function at  $\omega_m$  is

$$l_R(\omega_m) = \left[ \mathbf{X}^H(\omega_m) - F^*(\omega_m) \mathbf{v}^H(\omega_m) \right] \mathbf{S}_{\mathbf{n}}^{-1}(\omega_m) \left[ \mathbf{X}(\omega_m) - F(\omega_m) \mathbf{v}(\omega_m) \right], \quad (6.21)$$

where constant multipliers and additive terms that do not depend on  $F(\omega_m)$  have been dropped.

Taking the complex gradient with respect to  $F^*(\omega_m)$ , setting the result equal to zero and solving the resulting equation gives

$$\hat{\mathbf{F}}(\omega_m)|_{ml} = \frac{\mathbf{v}^H(\omega_m) \mathbf{S}_{\mathbf{n}}^{-1}(\omega_m) \mathbf{X}(\omega_m)}{\mathbf{v}^H(\omega_m) \mathbf{S}_{\mathbf{n}}^{-1}(\omega_m) \mathbf{v}^H(\omega_m)}. \quad (6.22)$$

The estimate in (6.22) is identical to the output of the MVDR processor in (6.14) with  $\omega = \omega_m$ .

The reason for introducing  $\omega_m$  in (6.21) is that, in order to find the ML estimate of  $f(t)$ , the joint ML estimate of  $F(\omega_m)$ ,  $m = -(M-1)/2 \leq m \leq$

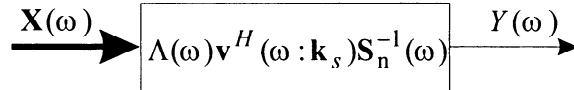


Figure 6.7 Minimum variance distortionless response (MVDR) processor.

$(M - 1)/2$  is required. Then  $f(t)|_{ml}$  is reconstructed using (5.36). However, because the frequency-domain snapshots for  $\omega_{m_1} \neq \omega_{m_2}$  are statistically independent, the joint likelihood function is a sum of the likelihood functions in (6.21) over  $m$ . The resulting  $F(\omega_m)|_{ml}$  are independent.

The output of the optimum distortionless (or MVDR) matrix is the ML estimate of  $F(\omega_m)$  and can be used to generate  $f(t)|_{ml}$ .<sup>3</sup> The important point is that the ML derivation did not assume a linear operation (matrix multiplication) on  $\mathbf{X}(\omega_m)$ . As in the scalar case, the Gaussian model leads to a linear processor.

This ML result has occasionally caused confusion in the literature. The MVDR filter provides the ML estimate of the signal  $f(t)$  when the signal wavenumber (direction of arrival) is known and  $\mathbf{S}_n(\omega)$  is known. In Chapters 8 and 9, we will estimate the DOA of the signal. In most cases, the MVDR filter scanned in wavenumber space does not provide the ML estimate of the signal's DOA.

### 6.2.1.3 Array gain

We denote the matrix filter in Figure 6.7 by  $\mathbf{W}_o^H(\omega)$  where subscript “ $o$ ” denotes optimum:

$$\mathbf{W}_{mvdr}^H \triangleq \mathbf{W}_o^H(\omega) = \Lambda(\omega)\mathbf{v}^H(\omega : \mathbf{k}_s)\mathbf{S}_n^{-1}(\omega). \quad (6.23)$$

The array gain at a particular frequency  $\omega$  is given by the ratio of the signal spectrum to the noise spectrum at the output of the distortionless filter compared to the ratio at the input. The spectrum of the noise component of  $Y(\omega)$  is

$$\begin{aligned} S_{y_n}(\omega) &= \mathbf{W}_o^H(\omega)\mathbf{S}_n(\omega)\mathbf{W}_o(\omega) \\ &= \mathbf{v}^H(\omega)\mathbf{S}_n^{-1}(\omega)\mathbf{S}_n(\omega)\mathbf{S}_n^{-1}(\omega)\mathbf{v}(\omega) \cdot \Lambda^2(\omega) \\ &= \Lambda(\omega). \end{aligned} \quad (6.24)$$

Since the  $\mathbf{W}_o^H(\omega)$  is distortionless,

$$S_{y_s}(\omega) = S_f(\omega). \quad (6.25)$$

---

<sup>3</sup>This result was first obtained by Kelly and Levin [KL64].

If we assume that the noise spectrum at each sensor is the same, then the input  $SNR$  at each sensor is  $\frac{S_f(\omega)}{S_n(\omega)}$ . Therefore,

$$\begin{aligned} A_o(\omega : \mathbf{k}_s) &= \frac{S_f(\omega)}{\Lambda(\omega)} / \frac{S_f(\omega)}{S_n(\omega)} = \frac{S_n(\omega)}{\Lambda(\omega)} \\ &= S_n(\omega) \mathbf{v}^H(\omega : \mathbf{k}_s) \mathbf{S}_n^{-1}(\omega) \mathbf{v}(\omega : \mathbf{k}_s). \end{aligned} \quad (6.26)$$

We define a normalized spectral matrix  $\rho_n(\omega)$  by the relation,

$$\mathbf{S}_n(\omega) = S_n(\omega) \rho_n(\omega). \quad (6.27)$$

Then,

$$A_o(\omega : \mathbf{k}_s) = \mathbf{v}^H(\omega : \mathbf{k}_s) \rho_n^{-1}(\omega) \mathbf{v}(\omega : \mathbf{k}_s). \quad (6.28)$$

Suppressing  $\omega$  and  $\mathbf{k}_s$ , (6.28) can be written as

$$A_o = \mathbf{v}_s^H \rho_n^{-1} \mathbf{v}_s. \quad (6.29)$$

Recall from Chapter 2 that the conventional delay-and-sum beamformer is

$$\mathbf{W}_c^H(\omega) = \frac{1}{N} \mathbf{v}^H(\omega : \mathbf{k}_s). \quad (6.30)$$

The output noise is

$$S_{y_{nc}}(\omega) = \frac{1}{N^2} \mathbf{v}^H(\omega : \mathbf{k}_s) \mathbf{S}_n(\omega) \mathbf{v}(\omega : \mathbf{k}_s), \quad (6.31)$$

and the resulting array gain is

$$A_c(\omega : \mathbf{k}_s) = \frac{N^2}{\mathbf{v}^H(\omega : \mathbf{k}_s) \rho_n(\omega) \mathbf{v}(\omega : \mathbf{k}_s)}, \quad (6.32)$$

or, suppressing  $\omega$  and  $\mathbf{k}_s$ ,

$$A_c = \frac{N^2}{\mathbf{v}_s^H \rho_n \mathbf{v}_s}. \quad (6.33)$$

Whenever the  $\rho(\omega)$  matrix is diagonal, (i.e., the noises at the different sensors are uncorrelated) the conventional and optimum receivers are identical and the two array gains are identical:

$$A_o(\omega : \mathbf{k}_s) = A_c(\omega : \mathbf{k}_s) = N. \quad (6.34)$$

In other cases,

$$A_o(\omega : \mathbf{k}_s) \geq A_c(\omega : \mathbf{k}_s). \quad (6.35)$$

### 6.2.2 Minimum Mean-Square Error (MMSE) Estimators

In this section, we find the optimum linear matrix processor whose output is the MMSE estimate of a desired signal snapshot  $D(\omega)$ .

#### 6.2.2.1 Single plane-wave signal

We first consider the problem of a single plane-wave signal in noise. Thus,

$$\mathbf{X}(\omega) = F(\omega)\mathbf{v}(\omega : \mathbf{k}_s) + \mathbf{N}(\omega), \quad (6.36)$$

where the source signal snapshot,  $F(\omega)$ , is a scalar zero-mean random variable with variance  $S_f(\omega)$ . The signal and noise snapshots are uncorrelated. We assume that  $\mathbf{N}(\omega)$  contains a spatial white noise component so that

$$\mathbf{S}_n(\omega) = \mathbf{S}_c(\omega) + \sigma_w^2 \mathbf{I}. \quad (6.37)$$

The spectral matrix of  $\mathbf{X}(\omega)$  is

$$\mathbf{S}_x(\omega) = S_f(\omega)\mathbf{v}(\omega : \mathbf{k}_s)\mathbf{v}^H(\omega : \mathbf{k}_s) + \mathbf{S}_n(\omega). \quad (6.38)$$

For convenience we have assumed the noise snapshot has the same statistics at each sensor. The case of unequal values follows directly.

The desired snapshot  $D(\omega)$  is equal to the source snapshot,  $F(\omega)$ . The matrix processor is an  $N \times 1$  matrix denoted by  $\mathbf{H}(\omega)$  whose output is  $\hat{D}(\omega)$ . The mean-square error is

$$\begin{aligned} \xi &= E \left\{ |D(\omega) - \mathbf{H}(\omega)\mathbf{X}(\omega)|^2 \right\} \\ &= E \left\{ (D(\omega) - \mathbf{H}(\omega)\mathbf{X}(\omega)) (D^*(\omega) - \mathbf{X}^H(\omega)\mathbf{H}^H(\omega)) \right\}. \end{aligned} \quad (6.39)$$

Taking the complex gradient with respect to  $\mathbf{H}^H(\omega)$  and setting the result equal to zero gives,

$$E [D(\omega)\mathbf{X}^H(\omega)] - \mathbf{H}(\omega)E [\mathbf{X}(\omega)\mathbf{X}^H(\omega)] = \mathbf{0}, \quad (6.40)$$

or

$$\mathbf{S}_{d\mathbf{x}^H}(\omega) = \mathbf{H}_o(\omega)\mathbf{S}_x(\omega). \quad (6.41)$$

Thus,

$\mathbf{H}_o(\omega) = \mathbf{S}_{d\mathbf{x}^H}(\omega)\mathbf{S}_x^{-1}(\omega).$

(6.42)

From (6.36) and the uncorrelated signal and noise assumption we obtain

$$S_{d\mathbf{x}^H}(\omega) = S_f(\omega)\mathbf{v}^H(\omega : \mathbf{k}_s). \quad (6.43)$$

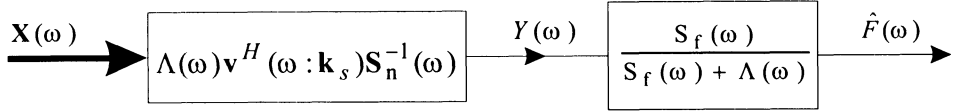


Figure 6.8 MMSE processor.

Then,

$$\mathbf{H}_o(\omega) = S_f(\omega)\mathbf{v}^H(\omega : \mathbf{k}_s)\mathbf{S}_{\mathbf{x}}^{-1}(\omega). \quad (6.44)$$

Inverting (6.38) using the matrix inversion formula, we obtain

$$\mathbf{S}_{\mathbf{x}}^{-1}(\omega) = \mathbf{S}_{\mathbf{n}}^{-1} - \mathbf{S}_{\mathbf{n}}^{-1}S_f\mathbf{v}(1 + \mathbf{v}^H\mathbf{S}_{\mathbf{n}}^{-1}S_f\mathbf{v})^{-1}\mathbf{v}^H\mathbf{S}_{\mathbf{n}}^{-1}, \quad (6.45)$$

where we have suppressed the  $\omega$  and  $\mathbf{k}_s$  arguments on the right side of the equation. Defining

$$\Lambda^{-1}(\omega) = \mathbf{v}^H(\omega : \mathbf{k}_s)\mathbf{S}_{\mathbf{n}}^{-1}(\omega)\mathbf{v}(\omega : \mathbf{k}_s), \quad (6.46)$$

and substituting (6.45) into (6.44), we obtain,

$$\mathbf{H}_o(\omega) = \frac{S_f(\omega)}{S_f(\omega) + \Lambda(\omega)} \cdot \Lambda(\omega)\mathbf{v}^H(\omega : \mathbf{k}_s)\mathbf{S}_{\mathbf{n}}^{-1}(\omega). \quad (6.47)$$

The MMSE processor is shown in Figure 6.8. We see that it consists of the optimum distortionless matrix followed by a scalar multiplier.

Substituting (6.47) into (6.39) gives the optimum mean-square error:

$$\xi_o(\omega) = \frac{S_f(\omega)\Lambda(\omega)}{S_f(\omega) + \Lambda(\omega)}, \quad (6.48)$$

which can also be written as

$$\xi_o(\omega) = \frac{S_f(\omega) \begin{bmatrix} S_n(\omega) \\ A_o(\omega) \end{bmatrix}}{S_f(\omega) + \begin{bmatrix} S_n(\omega) \\ A_o(\omega) \end{bmatrix}}. \quad (6.49)$$

The effect of the array is completely characterized by the optimum array gain  $A_o(\omega : \mathbf{k}_s)$ .

We look at optimum array gains for various signal and noise environments in Sections 6.3–6.5.

### 6.2.2.2 Conditional mean estimators

In the previous sections, we have assumed that the second-order statistics of the signal and noise processes are known and then found the optimum linear MMSE matrix processor. From our results with scalar waveforms in DEMT I ([VT68], [VT01a], e.g., pp. 476–479) we would expect that if we assume that the signal and noise processes are vector Gaussian random processes, then the optimum processor will be a linear processor. The proof of this conjecture follows in a straightforward manner.

The frequency-domain snapshot is

$$\mathbf{X}(\omega_m) = F(\omega_m)\mathbf{v}(\omega_m) + \mathbf{N}(\omega_m). \quad (6.50)$$

The MMSE estimation is the mean of the *a posteriori* probability density of  $F(\omega_m)$ , given  $\mathbf{X}(\omega_m)$ . This mean is referred to as the conditional mean.

The probability density of  $\mathbf{X}(\omega_m)$ , given  $F(\omega_m)$ , is

$$\begin{aligned} p_{\mathbf{X}(\omega_m)|F(\omega_m)}(\cdot) &= c_1 \exp \left\{ - \left[ \mathbf{X}^H(\omega_m) - F^*(\omega_m)\mathbf{v}^H(\omega_m) \right] \right. \\ &\quad \left. \mathbf{S}_n^{-1}(\omega_m) [\mathbf{X}(\omega_m) - F(\omega_m)\mathbf{v}(\omega_m)] \right\}. \end{aligned} \quad (6.51)$$

The probability density of  $F(\omega_m)$  is

$$p_{F(\omega_m)}(\cdot) = c_2 \exp \left\{ -F^*(\omega_m)S_f^{-1}(\omega_m)F(\omega_m) \right\}. \quad (6.52)$$

Using Bayes rule, the *a posteriori* density at  $\omega_m$  is,

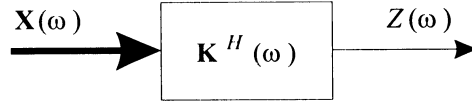
$$\begin{aligned} p_{F(\omega_m)|\mathbf{X}(\omega_m)}(\cdot) &= c_3 \exp \left[ -F^*(\omega_m)S_f^{-1}(\omega_m)F(\omega_m) \right] \\ &\cdot \exp \left[ \mathbf{X}^H(\omega_m)\mathbf{S}_n^{-1}(\omega_m)\mathbf{X}(\omega_m) - F^*(\omega_m)\mathbf{v}^H(\omega_m)\mathbf{S}_n^{-1}(\omega_m)\mathbf{X}(\omega_m) \right. \\ &\quad \left. - \mathbf{X}^H(\omega_m)\mathbf{S}_n^{-1}(\omega_m)F(\omega_m)\mathbf{v}(\omega_m) + F^*(\omega_m)\mathbf{v}^H(\omega_m)\mathbf{S}_n^{-1}(\omega_m) \right. \\ &\quad \left. \mathbf{v}(\omega_m)F(\omega_m) \right]. \end{aligned} \quad (6.53)$$

Defining

$$H_S^{-1}(\omega_m) = \frac{1}{\Lambda(\omega_m)} + \frac{1}{S_f(\omega_m)}, \quad (6.54)$$

where  $\Lambda(\omega_m)$  was defined in (6.15), (6.53) can be written as

$$\begin{aligned} p_{F(\omega_m)|\mathbf{X}(\omega_m)}(\cdot) &= c_4 \exp \left\{ \left[ F^*(\omega_m) - \mathbf{X}^H(\omega_m)\mathbf{S}_n^{-1}(\omega_m)\mathbf{v}(\omega_m)H_S^*(\omega_m) \right] \right. \\ &\quad \left. H_S^{-1}(\omega_m) \left[ F(\omega_m) - H_S(\omega_m)\mathbf{v}^H(\omega_m)\mathbf{S}_n^{-1}(\omega_m) \right. \right. \\ &\quad \left. \left. \mathbf{X}(\omega_m) \right] \right\}. \end{aligned} \quad (6.55)$$

Figure 6.9 Maximum *SNR* processor.

Thus, the conditional mean is,

$$\begin{aligned} \hat{F}(\omega_m) &= H_S(\omega_m)\mathbf{v}^H(\omega_m)\mathbf{S}_n^{-1}(\omega_m)\mathbf{X}(\omega_m) \\ &= \frac{S_f(\omega_m)}{S_f(\omega_m) + \Lambda(\omega_m)} \cdot \Lambda(\omega_m)\mathbf{v}^H(\omega_m)\mathbf{S}_n^{-1}(\omega_m)\mathbf{X}(\omega_m), \end{aligned} \quad (6.56)$$

which corresponds to the operation in (6.47) with  $\omega = \omega_m$ . The resulting mean-square error at  $\omega_m$  is

$$\xi(\omega_m) = H_S(\omega_m) = \frac{S_f(\omega_m)\Lambda(\omega_m)}{S_f(\omega_m) + \Lambda(\omega_m)}. \quad (6.57)$$

Therefore, whenever the Gaussian model is utilized, the optimum MMSE processor will be the linear processor derived in Section 6.2.1.1.

### 6.2.3 Maximum Signal-to-Noise Ratio (**SNR**)

In the two preceding sections we found the optimum receiver for different criteria. For the single plane-wave signal case, both criteria and signal models led to the same matrix operation. The effect of the array was contained in the array gain. A logical question is, “if we maximized the array gain, would the optimum receiver be different?” It is straightforward to demonstrate that the resulting matrix processor is identical to the processor in the previous sections. Note that, since the input *SNR* is fixed, maximizing the output *SNR* maximizes the array gain.

The system of interest is shown in Figure 6.9. The *SNR* at frequency  $\omega$  is,

$$\frac{S}{N} \triangleq \frac{\mathbf{K}^H(\omega)\mathbf{S}_{x_s}(\omega)\mathbf{K}(\omega)}{\mathbf{K}^H(\omega)\mathbf{S}_n(\omega)\mathbf{K}(\omega)}, \quad (6.58)$$

which is a ratio of two quadratic forms.

For notational ease and in anticipation of the final answer, we define<sup>4</sup>

$$\beta \triangleq S/N. \quad (6.59)$$

---

<sup>4</sup>This derivation is due to N. Owsley (private communication).

Taking the complex gradient of (6.58) with respect to  $\mathbf{K}^H$  and setting the result to zero gives

$$\frac{\mathbf{S}_{\mathbf{x}_s} \mathbf{K} (\mathbf{K}^H \mathbf{S}_{\mathbf{n}} \mathbf{K}) - \mathbf{S}_{\mathbf{n}} \mathbf{K} (\mathbf{K}^H \mathbf{S}_{\mathbf{x}_s} \mathbf{K})}{(\mathbf{K}^H \mathbf{S}_{\mathbf{n}} \mathbf{K})^2} = \mathbf{0}, \quad (6.60)$$

where we have suppressed the  $\omega$  dependence. This implies

$$\beta \mathbf{S}_{\mathbf{n}} \mathbf{K} = \mathbf{S}_{\mathbf{x}_s} \mathbf{K}, \quad (6.61)$$

or

$$\beta \mathbf{K} = [\mathbf{S}_{\mathbf{n}}^{-1} \mathbf{S}_{\mathbf{x}_s}] \mathbf{K}. \quad (6.62)$$

This result is familiar as the eigenvalue problem. Setting  $\mathbf{K}$  equal to any eigenvector of  $[\mathbf{S}_{\mathbf{n}}^{-1} \mathbf{S}_{\mathbf{x}_s}]$  will satisfy (6.62). However, we want to maximize  $\beta = S/N$ , so we choose the eigenvector corresponding to the largest eigenvalue. This result is valid for an arbitrary spectral matrix  $\mathbf{S}_{\mathbf{x}_s}(\omega)$ .

For the special case of a plane-wave signal,

$$\mathbf{S}_{\mathbf{x}_s}(\omega) = S_f(\omega) \mathbf{v}(\omega : \mathbf{k}_s) \mathbf{v}^H(\omega : \mathbf{k}_s). \quad (6.63)$$

Substituting (6.63) into (6.62) gives

$$\beta \mathbf{K} = \mathbf{S}_{\mathbf{n}}^{-1} S_f \mathbf{v} \mathbf{v}^H \mathbf{K}, \quad (6.64)$$

where the  $\omega$  dependence is suppressed. The solution to (6.64) is

$$\mathbf{K} = \mathbf{S}_{\mathbf{n}}^{-1} \mathbf{v}, \quad (6.65)$$

and

$$\beta = \left( \frac{S}{N} \right) = S_f(\mathbf{v}^H \mathbf{S}_{\mathbf{n}}^{-1} \mathbf{v}). \quad (6.66)$$

The matrix operation for maximizing the *SNR* is identical to the MVDR beamformer and the MMSE beamformer. (The constant  $\Lambda(\omega : \mathbf{k}_s)$  in (6.24) does not appear but can be included.) For homogeneous noise, (6.66) can be written as

$$\begin{aligned} \frac{S}{N} &= \frac{S_f(\omega)}{S_n(\omega)} \mathbf{v}^H(\omega : \mathbf{k}_s) \boldsymbol{\rho}^{-1}(\omega) \mathbf{v}(\omega : \mathbf{k}_s) \\ &= \frac{S_f(\omega)}{S_n(\omega)} A_o(\omega : \mathbf{k}_s). \end{aligned} \quad (6.67)$$

We see that, for a wide class of criteria, the optimum processor is an MVDR beamformer followed by a scalar filter that depends on the criterion. In [VT66a], we termed this a “criterion-invariant receiver.” The important implication is that the MVDR beamformer creates a signal subspace (in this case, 1-D) where all subsequent processing takes place.

### 6.2.4 Minimum Power Distortionless Response (MPDR) Beamformers

The final beamformer that we develop is referred to as the minimum power distortionless response (MPDR) beamformer. It is closely related to the MVDR beamformer of Section 6.2.1.

The model has two new features. The first is that we will match the distortionless filter  $\mathbf{w}^H$  to a plane wave arriving from the direction  $\mathbf{a}_m$ . Defining

$$\mathbf{v}_m \triangleq \mathbf{v}(\omega : \mathbf{a}_m), \quad (6.68)$$

we require

$$\mathbf{w}^H \mathbf{v}_m = \mathbf{W}^H(\omega) \mathbf{v}(\omega : \mathbf{a}_m) = 1. \quad (6.69)$$

We refer to  $\mathbf{v}_m$  as the **steering vector**. Ideally, we would like the steering vector to correspond exactly to the signal vector,

$$\mathbf{v}_m = \mathbf{v}_s, \quad (6.70)$$

but in many cases this may not be true.

The second feature of the model is that we assume that  $\mathbf{S}_x(\omega)$ , the spectral matrix of the entire input, is available to design the beamformer. By contrast, our previous models assumed that  $\mathbf{S}_n(\omega)$  and  $\mathbf{v}(\omega : \mathbf{k}_s)$  were available (the MMSE model also assumed knowledge of  $\mathbf{S}_f(\omega)$ ). We want to minimize the total output power subject to the constraint in (6.69). The derivation is identical to that in (6.11)–(6.14). The result is

$$\boxed{\mathbf{w}_{mpdr}^H = \frac{\mathbf{v}_m^H \mathbf{S}_x^{-1}}{\mathbf{v}_m^H \mathbf{S}_x^{-1} \mathbf{v}_m}.} \quad (6.71)$$

In the majority of the literature, this beamformer is also referred to as an MVDR beamformer. We use a different name to emphasize that we are using  $\mathbf{S}_x^{-1}$  instead of  $\mathbf{S}_n^{-1}$ .

It is straightforward to verify that, if  $\mathbf{v}_m = \mathbf{v}_s$ , then

$$\mathbf{w}_{mpdr}^H = \mathbf{w}_{mvdr}^H \quad (6.72)$$

(see Problem 6.2.2).

When  $\mathbf{v}_s \neq \mathbf{v}_m$ , the beamformers are different. In this chapter,  $\mathbf{S}_x$  is assumed to be known. However, in actual applications,  $\mathbf{S}_x$  is estimated. The estimate  $\hat{\mathbf{S}}_x$  will be constructed with the actual  $\mathbf{v}_s$ , not the model  $\mathbf{v}_m$ . This is the source of the problem with mismatched signals. In Sections 6.6 and 6.7 we will study the effects of steering vector mismatch on the performance

of MVDR and MPDR beamformers. This steering vector mismatch can be caused by signal direction mismatch, array perturbations, or frequency mismatch. We will find that the presence of the signal in  $\mathbf{S}_x(\omega)$  can cause significant degradation in the receiver performance when  $\mathbf{v}_s \neq \mathbf{v}_m$ . We will devote a significant amount of effort to the design of beamformers that are robust to mismatch. The array gain for the MPDR beamformer is

$$A_{mpdr} = \frac{|\mathbf{v}_m^H \mathbf{S}_x^{-1} \mathbf{v}_s|^2}{\mathbf{v}_m^H \mathbf{S}_x^{-1} \boldsymbol{\rho}_n \mathbf{S}_x^{-1} \mathbf{v}_m}. \quad (6.73)$$

### 6.2.5 Summary

In this section, we have considered a single plane-wave signal in the presence of interference and noise. We have shown that, for several important criteria, the optimum beamformer is the MVDR (or Capon) beamformer specified by (6.14) and (6.15). When  $\omega$  and  $\mathbf{k}_s$  are suppressed, it can be written as

$$\mathbf{w}_{mvdr}^H = \frac{\mathbf{v}_s^H \mathbf{S}_n^{-1}}{\mathbf{v}_s^H \mathbf{S}_n^{-1} \mathbf{v}_s}. \quad (6.74)$$

This beamformer is widely used in applications where it is possible to measure or estimate  $\mathbf{S}_n(w)$ .

In applications where the signal is always present we use the MPDR beamformer specified by (6.71).

In Section 6.3, we examine the performance of the MVDR and MPDR beamformers for discrete interference. In Section 6.4, we examine their performance for spatially spread interference.

## 6.3 Discrete Interference

In this section, we consider an important special case in which the noise consists of a set of  $D$  interfering plane-wave signals plus uncorrelated noise. We assume that  $D + 1$  is less than  $N$ , the number of array elements.

The key result is that in this model the optimum beamformer generates  $D + 1$  sufficient statistics and then combines them. Thus the problem is reduced to a  $(D + 1)$ -dimensional “signal-plus-interference” subspace rather than the original  $N$ -dimensional element space. This leads to significant simplification in the processor.

In Section 6.3.1, we consider a single interfering signal to illustrate the basic ideas. In Section 6.3.2, we consider  $D$  interfering signals and develop a “directional interference beamformer.” In Section 6.3.3, we summarize our results.

### 6.3.1 Single Plane-wave Interfering Signal

In this case, we consider a single plane-wave desired signal with array manifold  $\mathbf{v}(\omega : \mathbf{k}_s)$  and a noise process consisting of a single plane-wave interfering signal with array manifold  $\mathbf{v}(\omega : \mathbf{k}_1)$  plus a white noise component at each sensor with spectral height  $\sigma_w^2$ . We will find the optimum distortionless filter, the array gain of the optimum and conventional beamformer, and the beam pattern of the optimum beamformer. The single plane-wave interferer case illustrates many results that can be generalized to multiple interfering signals.

For a single directional noise,

$$\mathbf{S}_n(\omega) = \sigma_w^2 \mathbf{I} + M_1(\omega) \mathbf{v}(\omega : \mathbf{k}_1) \mathbf{v}^H(\omega : \mathbf{k}_1), \quad (6.75)$$

where  $M_1(\omega)$  is the spectrum of the interfering signal. Suppressing  $\omega$  and  $\mathbf{k}$ , (6.75) becomes

$$\mathbf{S}_n = \sigma_w^2 \mathbf{I} + M_1 \mathbf{v}_1 \mathbf{v}_1^H. \quad (6.76)$$

Using the matrix inversion lemma,

$$\mathbf{S}_n^{-1} = \frac{1}{\sigma_w^2} \left[ \mathbf{I} - \frac{M_1}{\sigma_w^2 + NM_1} \mathbf{v}_1 \mathbf{v}_1^H \right]. \quad (6.77)$$

The noise spectrum at each sensor is

$$S_n = (\sigma_w^2 + M_1). \quad (6.78)$$

Using (6.77) in (6.23) gives

$$\mathbf{w}_{mvdr}^H = \mathbf{w}_o^H = \frac{\Lambda}{\sigma_w^2} \mathbf{v}_s^H \left[ \mathbf{I} - \frac{M_1}{\sigma_w^2 + NM_1} \mathbf{v}_1 \mathbf{v}_1^H \right]. \quad (6.79)$$

Now define

$$\rho_{s1} \triangleq \frac{\mathbf{v}_s^H \mathbf{v}_1}{N}, \quad (6.80)$$

which is the **spatial correlation coefficient** between the desired signal and the interference. Note that

$$\rho_{s1} = B_c(\mathbf{k}_1 : \mathbf{k}_s), \quad (6.81)$$

is the conventional beam pattern aimed as  $\mathbf{k}_s$  (the signal wavenumber) and evaluated at  $\mathbf{k}_1$  (the interferer wavenumber).

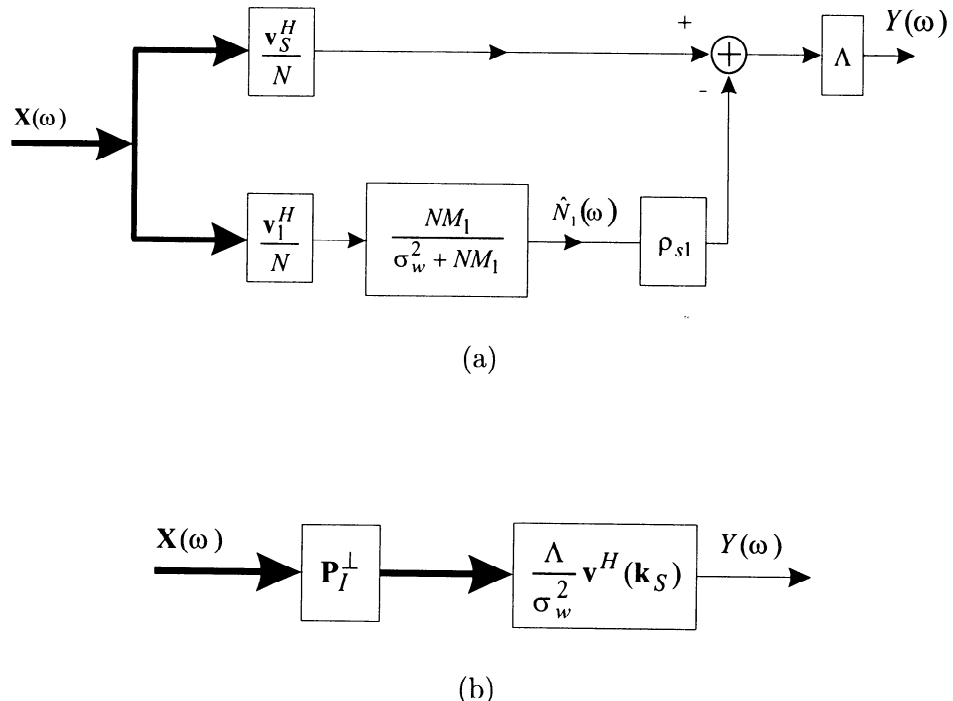


Figure 6.10 Optimum MVDR processor: single plane-wave interferer; (a) general case; (b) high *INR*.

Then (6.79) reduces to

$$\mathbf{w}_o^H = \frac{\Lambda N}{\sigma_w^2} \left[ \frac{\mathbf{v}_s^H}{N} - \rho_{s1} \frac{NM_1}{\sigma_w^2 + NM_1} \cdot \frac{\mathbf{v}_1^H}{N} \right]. \quad (6.82)$$

The normalizing coefficient  $\Lambda$  is given by

$$\begin{aligned} \Lambda &= \left\{ \frac{1}{\sigma_w^2} \mathbf{v}_s^H \left[ \mathbf{I} - \frac{M_1}{\sigma_w^2 + NM_1} \mathbf{v}_1 \mathbf{v}_1^H \right] \mathbf{v}_s \right\}^{-1} \\ &= \left\{ \frac{1}{\sigma_w^2} N \left[ 1 - \frac{NM_1}{\sigma_w^2 + NM_1} |\rho_{s1}|^2 \right] \right\}^{-1}. \end{aligned} \quad (6.83)$$

The resulting beamformer is shown in Figure 6.10(a). We see that the beamformer is generating two “spatial” sufficient statistics, one corresponding to the desired signal and one to the interfering signal, and then combining them optimally. Note that each of the spatial processors is precisely a conventional beamformer pointed at the signal and interferer, respectively.

The bottom path has a logical interpretation. It is easy to verify that  $\hat{n}_1(t)$  is the minimum mean-square estimate of  $n(t)$  (use (6.47) with  $M_1 = S_f$  and  $\mathbf{S}_n = \sigma_w^2 \mathbf{I}$ ) in the absence of the desired signal. We then subtract a fraction of the estimate corresponding to the spatial correlation of the two signals.

We observe that, if  $NM_1 \gg \sigma_w^2$ , then (6.79) can be written as

$$\begin{aligned}\mathbf{w}_o^H &= \frac{\Lambda}{\sigma_w^2} \mathbf{v}_s^H \left[ \mathbf{I} - \mathbf{v}_1 \left[ \mathbf{v}_1^H \mathbf{v}_1 \right]^{-1} \mathbf{v}_1^H \right] \\ &= \frac{\Lambda}{\sigma_w^2} \mathbf{v}_s^H \mathbf{P}_I^\perp,\end{aligned}\quad (6.84)$$

where  $\mathbf{P}_I^\perp$  is the projection matrix onto the subspace orthogonal to the interference. The resulting processor is shown in Figure 6.10(b). The beamformer is placing a perfect null on the interfering signal.

The optimum array gain is obtained by substituting (6.78) and (6.83) into (6.26) to obtain

$$A_o = N \left( 1 + \frac{M_1}{\sigma_w^2} \right) \left( 1 - \frac{NM_1}{\sigma_w^2 + NM_1} |\rho_{s1}|^2 \right), \quad (6.85)$$

$$A_o = N(1 + \sigma_I^2) \left[ \frac{1 + N\sigma_I^2[1 - |\rho_{s1}|^2]}{1 + N\sigma_I^2} \right], \quad (6.86)$$

where

$$\sigma_I^2 \triangleq \frac{M_1}{\sigma_w^2} \triangleq INR. \quad (6.87)$$

Notice that optimum array gain depends on both  $\sigma_I^2$ , which is an interference-to-white noise ratio (*INR*), and  $\rho_{s1}$ , which is the spatial correlation between the signal and the interference.

The limiting cases of (6.85) are of interest. For large  $N\sigma_I^2$ ,

$$A_o(\omega : \mathbf{k}_s) \simeq N(1 + \sigma_I^2)[1 - |\rho_{s1}|^2], \quad (6.88)$$

so, for large *INRs*, the array gain can be quite large if  $|\rho_{s1}| \neq 1$ .

For  $|\rho_{s1}| = 1$ , (i.e., collinear signal and interference),

$$A_o(\omega : \mathbf{k}_s) = N \frac{1 + \sigma_I^2}{1 + N\sigma_I^2}, \quad (6.89)$$

which approaches 1 for large  $\sigma_I^2$ .

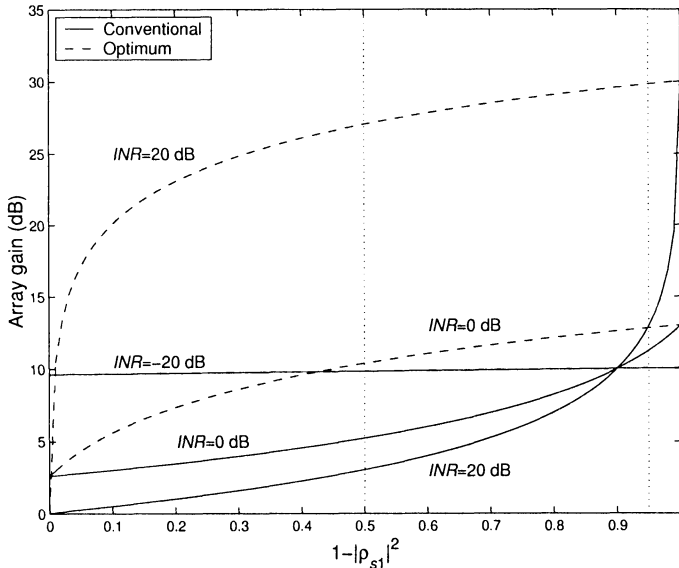


Figure 6.11 Array gain versus  $(1 - |\rho_{s1}|^2)$ : 10-element array: (a)  $INR = 0$  dB; (b)  $INR = 10$  dB; (c)  $INR = 20$  dB.

The conventional array gain is obtained by substituting (6.76) into (6.32) to obtain

$$A_c(\omega : \mathbf{k}_s) = \frac{N(1 + \sigma_I^2)}{1 + \sigma_I^2 N |\rho_{s1}|^2}. \quad (6.90)$$

The optimum and conventional array gains are plotted in Figure 6.11 for  $N = 10$ . Note that the array geometry is embedded in  $\rho_{s1}$  through the conventional beam pattern (6.81) so that these results apply to an arbitrary array. We have also shown the HPBW line at  $|\rho_{s1}|^2 = 0.5$ . For  $|\rho_{s1}|^2$  to the left of this line, the interferer is inside the HPBW region of the main lobe. When we examine beam patterns in the examples, we find that this may cause pattern problems.

For large  $N$ , and

$$N\sigma_I^2 [1 - |\rho_{s1}|^2] \gg 1, \quad (6.91)$$

(6.86) becomes

$$A_o \cong N(1 + \sigma_I^2)(1 - |\rho_{s1}|^2). \quad (6.92)$$

Therefore, it is convenient to plot  $A_o/N$  as shown in Figure 6.12.

The beam pattern for the optimum array can be obtained by substituting

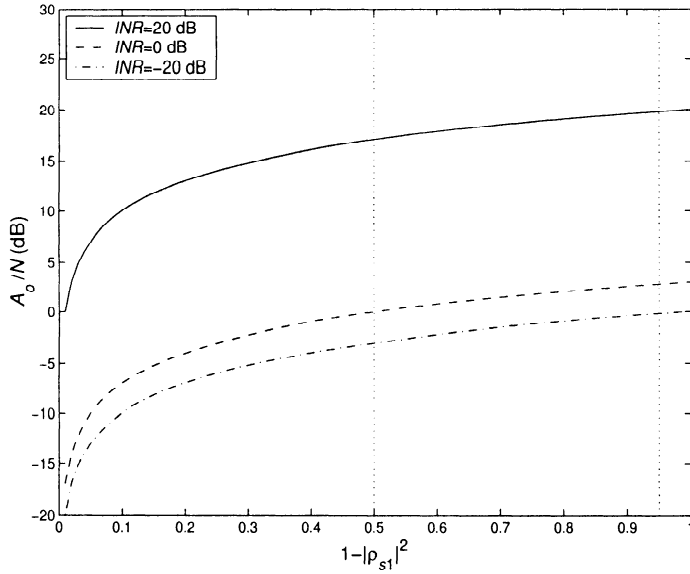


Figure 6.12 Normalized optimum array gain versus  $(1 - |\rho_{s1}|^2)$ .

(6.82) into (2.51). The result is

$$B_o(\omega : \mathbf{k}_s) = \frac{\Lambda N}{\sigma_w^2} \left[ \rho_{sa} - \frac{N\sigma_I^2 \rho_{s1}}{1 + N\sigma_I^2} \rho_{1a} \right], \quad (6.93)$$

where  $\Lambda$  is the normalizing function in (6.83) and we have suppressed the  $\omega$  dependence on the right side of (6.93). We observe that

$$\begin{aligned} \rho_{sa} &= \frac{1}{N} \mathbf{v}^H(\omega : \mathbf{k}_s) \mathbf{v}(\omega : \mathbf{k}) \\ &= B_c(\mathbf{k} : \mathbf{k}_s), \end{aligned} \quad (6.94)$$

which is just the conventional beam pattern for a delay-and-sum array beamformer pointed at  $\mathbf{k}_s$ , and that

$$\rho_{1a} = \frac{1}{N} \mathbf{v}^H(\omega : \mathbf{k}_1) \mathbf{v}(\omega : \mathbf{k}) = B_c(\mathbf{k} : \mathbf{k}_1) \quad (6.95)$$

is just the conventional beam pattern for a delay-and-sum array beamformer pointed at  $\mathbf{k}_1$ .

Thus, we can interpret the optimum array pattern as the conventional beam pattern pointed at the signal minus a constant times the conventional

beam pattern pointed at the interferer

$$B_o(\omega, \mathbf{k} : \mathbf{k}_s) = \frac{\Lambda(\omega) \cdot N}{\sigma_w^2} \cdot \left[ B_c(\omega, \mathbf{k} : \mathbf{k}_s) - \frac{N\sigma_I^2}{1 + N\sigma_I^2} \cdot B_c(\mathbf{k}_1 : \mathbf{k}_s) B_c(\mathbf{k} : \mathbf{k}_1) \right]. \quad (6.96)$$

Note that this result follows directly from Figure 6.10.

The value of the multiplying constant depends on two factors. The first is the value at  $\mathbf{k}_1$  of the conventional beam pattern aimed at  $\mathbf{k}_s$ . If the interferer happened to be at a perfect null in the conventional pattern, there would be no effect and therefore no reason to subtract it. If the interferer is at a sidelobe of the conventional pattern, we would need to subtract a proportional amount. The second term depends on the value of  $N\sigma_I^2$ . As  $N\sigma_I^2 \rightarrow \infty$ , this term approaches one.

The combined effect of the two terms is to create a partial null in the beam pattern at  $\mathbf{k}_1$ . The value of the beam pattern at  $\mathbf{k}_1$  is

$$B_o(\mathbf{k}_1 : \mathbf{k}_s) = \frac{\Lambda(\omega)}{\sigma_w^2} \cdot N B_c(\mathbf{k}_1 : \mathbf{k}_s) \left( \frac{1}{1 + N\sigma_I^2} \right), \quad (6.97)$$

as  $N\sigma_I^2$  goes to infinity the optimum array pattern has a perfect null at the direction of the interferer. For finite *INR*, it creates a partial null (or notch) whose depth is adjusted to minimize the output variance.

All of the discussion up to this point applies to an arbitrary array. We now specialize the results to a linear uniformly spaced array.

Consider the standard 10-element linear array along the  $z$ -axis. From (2.92), the conventional beam pattern for an array pointed at broadside ( $u_s = 0$ ) is

$$B_c(u) = \frac{1}{N} \frac{\sin\left(\frac{N\pi u}{2}\right)}{\sin\left(\frac{\pi u}{2}\right)}, \quad (6.98)$$

where  $u = \cos \theta$ .

It is useful to divide  $u$ -space into three regions in order to analyze the MVDR processor:

$$\text{SIDELOBE REGION: } 0.2 \leq |u| \leq 1.0,$$

$$\text{OUTER MAIN LOBE: } 0.045 \leq |u| < 0.2,$$

$$\text{HPBW REGION: } 0 < |u| < 0.045.$$

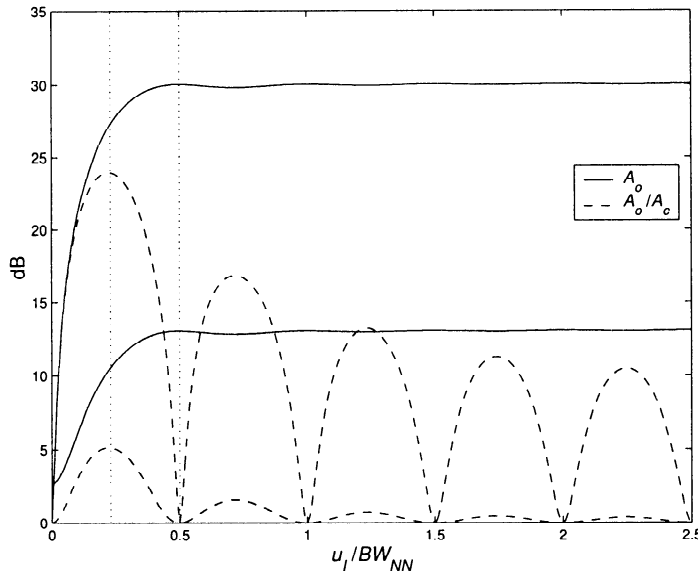


Figure 6.13  $A_o$  and  $A_o/A_c$  versus  $u_I/BW_{NN}$ ;  $INR = 0$  dB and 20 dB.

We assume the interferer arrives from  $u_I$ . In Figure 6.13, we plot  $A_o$  as a function of  $u_I/BW_{NN}$ . We also plot  $A_o/A_c$  as a function of  $u_I$  and observe that its maximum is at the HPBW point. We see that as soon as the interferer is outside the main lobe ( $u_I > 0.5BW_{NN}$ ) the optimum array gain is  $(N \cdot INR)$  dB. The conventional array gain has the same behavior as the beam pattern in  $u$ -space.

In Figure 6.14(a) and 6.14(b), we show the optimum beam pattern for two values of  $u_I$  in the sidelobe region for an  $INR (\sigma_I^2)$  of 10 dB. In Figure 6.14(c) and (d), we show the optimum beam pattern for the same values of  $u_I$  in the sidelobe region for an  $INR (\sigma_I^2)$  of 20 dB. We see that the beam pattern is essentially the same as a conventional beam pattern except for the region near the null.

In Figure 6.15, we repeat Figure 6.14 for two values of  $u_I$  in the outer main-lobe region;  $u_I = 0.18$  and  $u_I = 0.09$ . For  $u_I = 0.18$ , the behavior is similar to the sidelobe region except for the growth of the sidelobe nearest to the null. However, at  $u_I = 0.09$ , two effects are apparent: (1) the main lobe has shifted to the left (away from the null) and its height is larger than unity; (2) the height of the right sidelobe is about -3 dB.

In Figure 6.16, we consider two values of  $u_I$  in the HPBW region;  $u_I = 0.0433$  and  $u_I = 0.02$ . We only show the beam pattern inside the  $BW_{NN}$ .

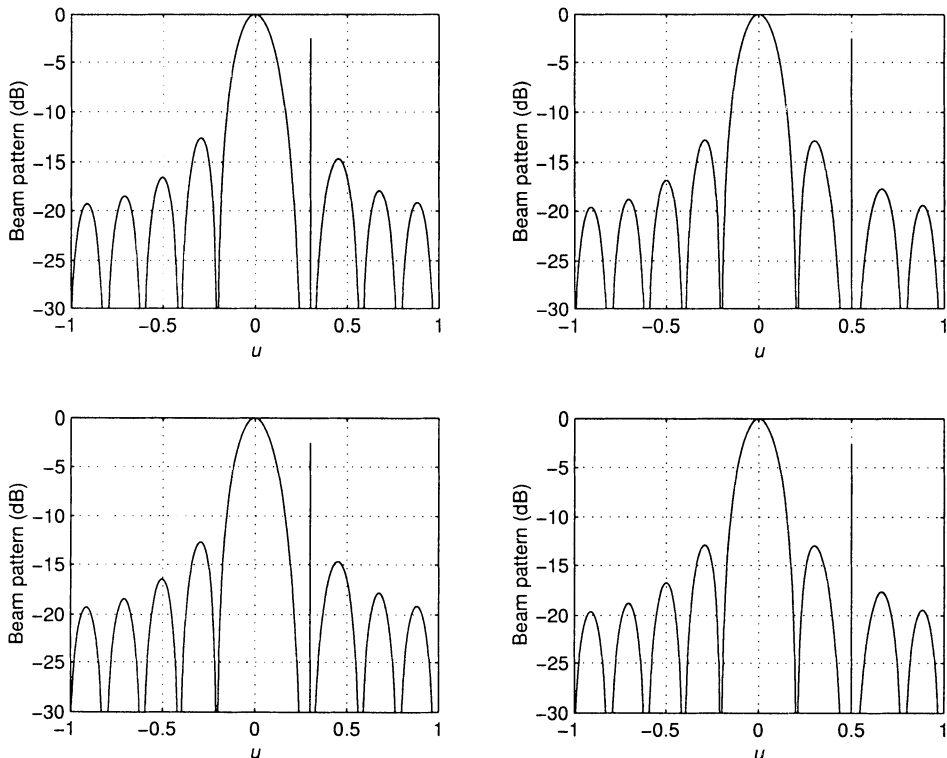


Figure 6.14 Optimum beam pattern for sidelobe interference: (a)  $\sigma_I^2 = 10$  dB,  $u_I = 0.30$ ; (b)  $\sigma_I^2 = 10$  dB,  $u_I = 0.50$ ; (c)  $\sigma_I^2 = 20$  dB,  $u_I = 0.30$ ; (d)  $\sigma_I^2 = 20$  dB,  $u_I = 0.50$ .

We see that the main lobe has split into two “sidelobes” whose heights are significantly larger (about 5 dB at the HPBW point) than the gain in the signal direction.

Thus, as the interferer moves inside the main lobe the peak of the optimum pattern is no longer pointed at the target and the “off-target” gain is significantly larger than the “on-target” gain, which is constrained to be one.

Due to the slope of the beam pattern at the MRA (in this case, when  $u_s = 0$ ), we would anticipate that the beamformer will be sensitive to signal DOA mismatch. In Section 6.6.2, we analyze DOA mismatch. We assume the signal actually arrives from  $u_a$  and derive an expression for the normalized array gain  $A_{mvdr}(\mathbf{v}_a : \mathbf{v}_m)/A_o(\mathbf{v}_m)$ . The result for the scenario in Figure 6.16 is shown in Figure 6.32. We see that the array gain is very sensitive to

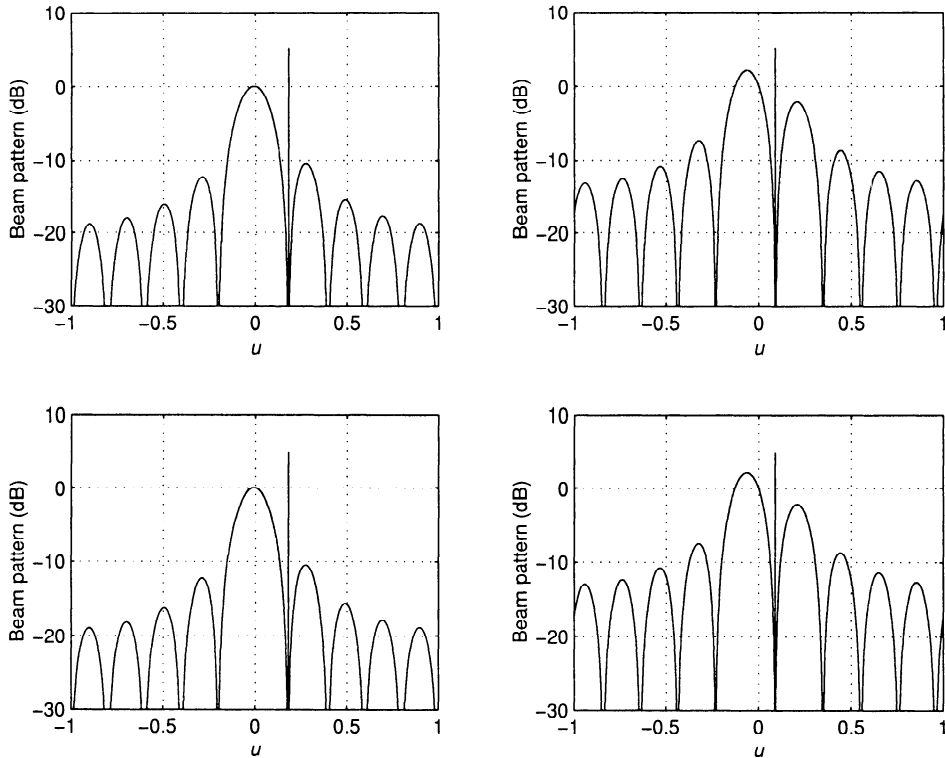


Figure 6.15 Optimum beam pattern for outer main-lobe interference: (a)  $\sigma_I^2 = 10 \text{ dB}$ ,  $u_I = 0.18$ ; (b)  $\sigma_I^2 = 10 \text{ dB}$ ,  $u_I = 0.09$ ; (c)  $\sigma_I^2 = 20 \text{ dB}$ ,  $u_I = 0.18$ ; (d)  $\sigma_I^2 = 20 \text{ dB}$ ,  $u_I = 0.09$ .

mismatch. In some applications, the variation may be acceptable. However, in most cases, we will want to impose additional constraints in order to maintain reasonably constant performance in the presence of small DOA mismatch.

If the mismatch between the model and actual environment is due to array perturbations, then the sensitivity functions that we encountered in Chapter 2 (2.209) is an appropriate measure.

The sensitivity function is the inverse of the white noise gain,

$$T(\psi_s) = A_w^{-1}(\psi_s) = \left| \mathbf{w}_{do}^H(\psi_s) \right|^2. \quad (6.99)$$

For the single interferer case, the sensitivity function is obtained by substi-

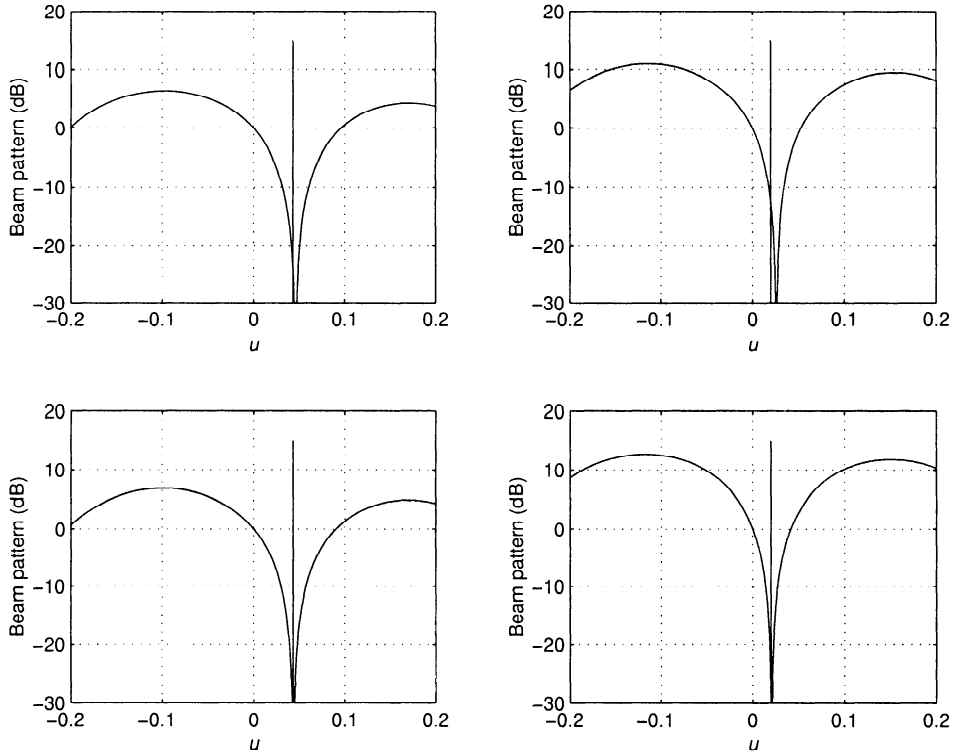


Figure 6.16 Optimum beam pattern for interference inside HPBW: (a)  $\sigma_I^2 = 10 \text{ dB}$ ,  $u_I = 0.0433$ ; (b)  $\sigma_I^2 = 10 \text{ dB}$ ,  $u_I = 0.02$ ; (c)  $\sigma_I^2 = 20 \text{ dB}$ ,  $u_I = 0.0433$ ; (d)  $\sigma_I^2 = 20 \text{ dB}$ ,  $u_I = 0.02$ .

tuting (6.82) and (6.83) into (6.99) to give

$$T = \frac{1}{N} \frac{1 + 2N\sigma_I^2\alpha^2 + N^2\sigma_I^4\alpha^2}{(1 + N\sigma_I^2\alpha^2)^2}, \quad (6.100)$$

where

$$\alpha^2 = 1 - |\rho_{s1}|^2. \quad (6.101)$$

The sensitivity function is plotted versus  $\alpha^2$  in Figure 6.17(a). This plot is valid for an arbitrary array. In Figure 6.17(b), we plot  $T$  versus  $u_I/BW_{NN}$  for a standard linear array.

To compare  $A_o$  and  $A_c$  is interesting, but not particularly relevant, as we argued in Chapter 3 that we would seldom use uniform weighting. A more realistic comparison is to compare  $A_o$  to some of the patterns we designed in Chapter 3 (or Chapter 4 for planar arrays).

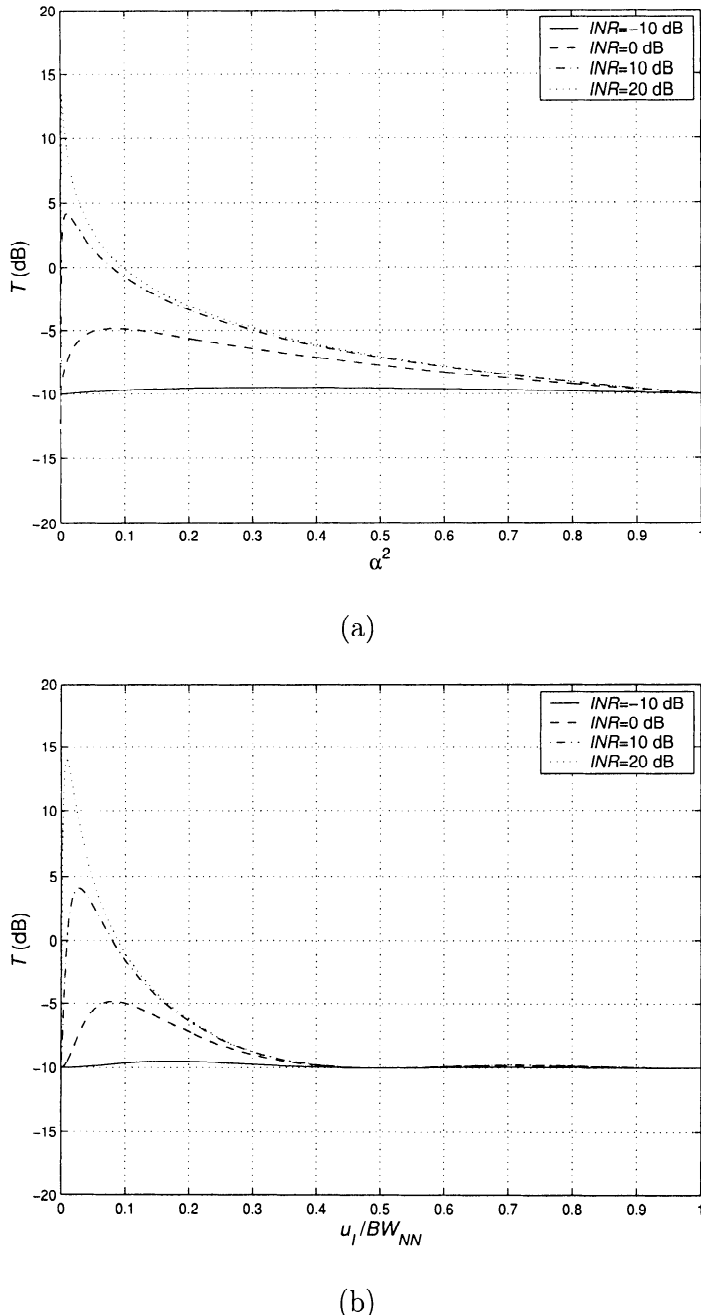


Figure 6.17 Sensitivity function,  $T(\alpha)$ : (a)  $T(\alpha)$  versus  $\alpha$  for arbitrary array; (b)  $T(\alpha)$  versus  $u_I/BW_{NN}$  for standard linear array.

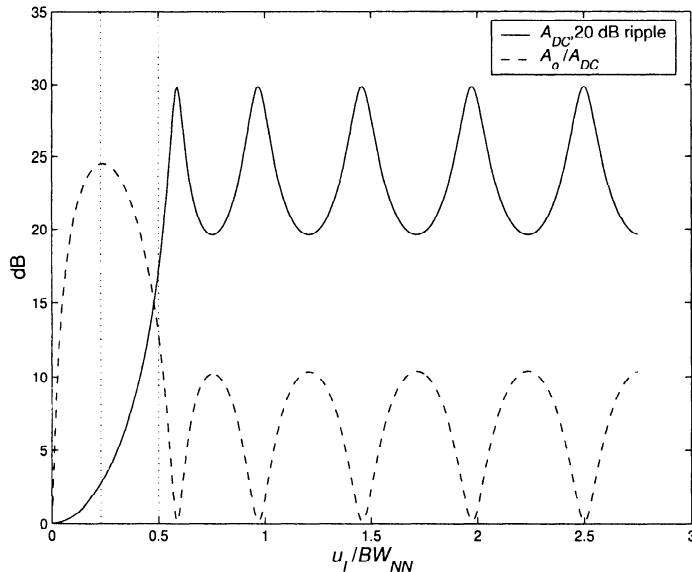


Figure 6.18 Array gain:  $A_{DC}$  and  $A_o/A_{DC}$  versus  $u_I/BW_{NN}$ ;  $INR = 20$  dB.

The array gain against white noise was computed for the weightings in Chapter 3 (recall that the white noise array gain  $A_w$  and directivity  $D$  are identical for a standard linear array). The array gain against directional noise (in the absence of white noise) is just the magnitude of the beam pattern squared. When the  $INR$  is near unity, we must calculate the array gain. However, for large  $INR$  we can use the value of the beam pattern squared.

In Figure 6.18, we plot the array gains and array gain ratios for the Dolph-Chebychev weighting. The result is what we would expect. Outside the main-lobe region, the array gain is just the beam pattern squared. Thus, for an  $INR$  of 20 dB, the performance may be acceptable. However, as the  $INR$  increases, the optimum array gain continues to improve ( $A_o \simeq N \cdot INR$ ) while the deterministic array gains remain the same.

We can summarize the main results as:

- (i) In the sidelobe region, the MVDR beamformer offers significant performance improvement for larger  $INR$  and gives an acceptable beam pattern.
- (ii) In the outer sidelobe region, the beam pattern of the MVDR beamformer starts to degenerate.

- (iii) In the HPBW region, the MVDR beamformer generates a solution that distorts the main lobe and is sensitive to model mismatch. One of the major issues that we discuss in later sections of this chapter is techniques to provide “main-lobe protection” when a strong interferer arrives in the HPBW region.

It is important to note that our comments about the MVDR beamformer are in the context of the objective of the beamformer. We are steering the beam in a specific direction  $u_m$ . Our objective is to reproduce a signal coming from that direction as accurately as possible. If the signal is a digital signal, we want to detect the bits with a minimum probability of error. We do not want the performance to degrade significantly for signal directions close to  $u_m$ . The allowable variation in  $u_a$  will depend on how wide an area in  $u$ -space is covered by a given steering direction.

In Chapters 8 and 9, we study DOA estimation. In this problem, and the spatial spectral estimation problem, we want the array processor to be very sensitive to the direction of arrival of the signal. We discuss the performance of the MVDR beamformer in that context in Section 9.2.

### 6.3.2 Multiple Plane-wave Interferers

In this section, we generalize the single interferer results from Section 6.3.1 to the case of  $D$  plane-wave interferers.

The realization of interest is shown in Figure 6.19. There are  $D$  paths, which are normalized steering and sum devices corresponding to the  $D$  interfering noises. Notice that they are not orthogonal. The other path is a normalized steer-and-sum device corresponding to the desired signal. The transform of the interfering noise can be written as

$$\mathbf{N}_c(\omega) = \sum_{i=1}^D N_i(\omega) \mathbf{v}(\omega : \mathbf{k}_i) \quad (6.102)$$

and

$$\mathbf{S}_{\mathbf{n}_c}(\omega) = \sum_{i=1}^D \sum_{j=1}^D S_{n_i n_j}(\omega) \mathbf{v}(\omega : \mathbf{k}_i) \mathbf{v}^H(\omega : \mathbf{k}_j). \quad (6.103)$$

We define an  $N \times D$  dimensional matrix,

$$\mathbf{V}_I = \left[ \begin{array}{c|c|c|c} \mathbf{v}(\mathbf{k}_1) & \mathbf{v}(\mathbf{k}_2) & \cdots & \mathbf{v}(\mathbf{k}_D) \end{array} \right], \quad (6.104)$$

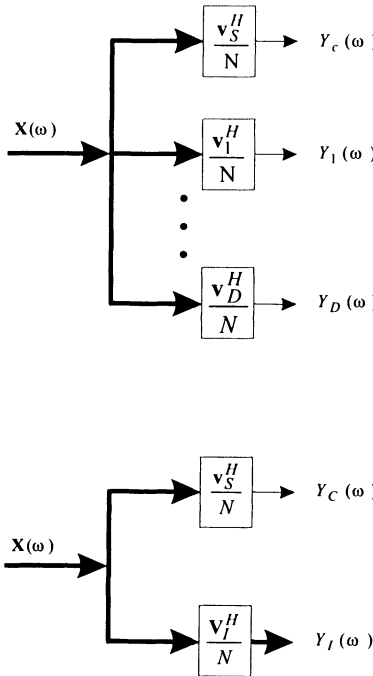


Figure 6.19 Directional noise receiver.

which represents the composite array manifold, and

$$\mathbf{S}_I = \begin{bmatrix} S_{11}(\omega) & S_{21}(\omega) & \cdots \\ S_{12}(\omega) & S_{22}(\omega) & \cdots \\ \vdots & \vdots & S_{DD}(\omega) \end{bmatrix}, \quad (6.105)$$

is the interference spectral matrix. We assume that the signal and interference are statistically independent.

Suppressing the  $\omega$  and  $\mathbf{k}_i$  dependence, the total interference plus white noise spectral matrix is

$$\mathbf{S}_n = \sigma_w^2 \mathbf{I} + \mathbf{V}_I \mathbf{S}_I \mathbf{V}_I^H. \quad (6.106)$$

Using the matrix inversion lemma

$$\mathbf{S}_n^{-1} = \frac{1}{\sigma_w^2} \mathbf{I} - \frac{1}{\sigma_w^2} \mathbf{V}_I (\mathbf{I} + \mathbf{S}_I \mathbf{V}_I^H \cdot \frac{1}{\sigma_w^2} \mathbf{V}_I)^{-1} \mathbf{S}_I \mathbf{V}_I^H \cdot \frac{1}{\sigma_w^2}. \quad (6.107)$$

Then, (6.107) can be written as

$$\mathbf{S}_n^{-1} = \frac{1}{\sigma_w^2} \left[ \mathbf{I} - \mathbf{V}_I \left( \mathbf{I} + \frac{\mathbf{S}_I}{\sigma_w^2} \mathbf{V}_I^H \mathbf{V}_I \right)^{-1} \frac{\mathbf{S}_I}{\sigma_w^2} \mathbf{V}_I^H \right]. \quad (6.108)$$

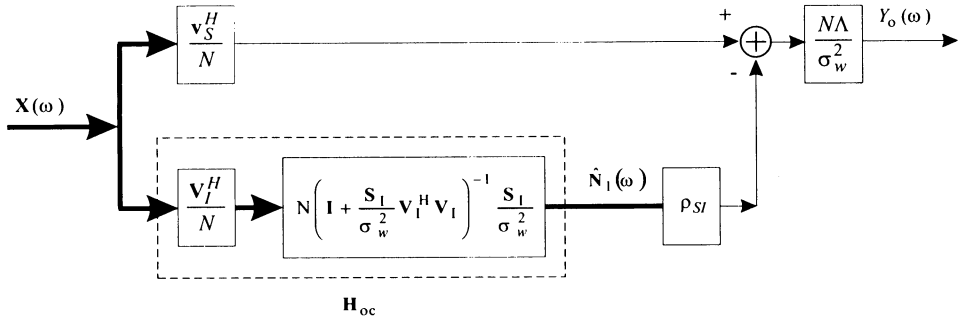


Figure 6.20 Optimal directional noise receiver.

From (6.23), the MVDR beamformer is

$$\begin{aligned}\mathbf{w}_o^H &= \Lambda \mathbf{v}_s^H \mathbf{S}_{\mathbf{n}}^{-1} \\ &= \frac{N\Lambda}{\sigma_w^2} \left[ \frac{\mathbf{v}_s^H}{N} - \boldsymbol{\rho}_{sI} \mathbf{H}_{oc} \right],\end{aligned}\quad (6.109)$$

where

$$\mathbf{H}_{oc} \triangleq \left[ \mathbf{I} + \frac{\mathbf{S}_I}{\sigma_w^2} \mathbf{V}_I^H \mathbf{V}_I \right]^{-1} \frac{\mathbf{S}_I}{\sigma_w^2} \mathbf{V}_I^H,\quad (6.110)$$

is a  $D \times N$  matrix. We shall see that  $\mathbf{H}_{oc}$  is the matrix filter whose output is the minimum mean-square error estimate of  $\mathbf{n}_I(t)$  in the absence of the desired signal.

The matrix  $\boldsymbol{\rho}_{sI}$  is the  $1 \times D$  spatial correlation matrix,

$$\boldsymbol{\rho}_{sI} \triangleq \frac{\mathbf{v}_s^H \mathbf{V}_I}{N}.\quad (6.111)$$

The resulting receiver is shown in Figure 6.20. Thus, the optimum receiver is estimating the directional noise vectors and then subtracting the component of the estimate that is correlated with the desired signal. The  $i$ th component of the spatial correlation matrix is

$$[\boldsymbol{\rho}_{sI}]_i = \frac{\mathbf{v}_s^H \mathbf{v}_i}{N} = B_c(\mathbf{k}_i : \mathbf{k}_s).\quad (6.112)$$

Similarly the  $ij$ th element of  $\mathbf{V}_I^H \mathbf{V}_I$  can be expressed as a conventional beam pattern

$$[\mathbf{V}_I^H \mathbf{V}_I]_{ij} = \mathbf{v}_i^H \mathbf{v}_j = NB_c(\mathbf{k}_j : \mathbf{k}_i).\quad (6.113)$$

Thus, all of the spatial relationships can be expressed in terms of conventional beam patterns.

The final term to be defined in (6.109) is  $\Lambda$ . Substituting (6.108) in (6.15), we obtain

$$\Lambda = \left\{ \frac{N}{\sigma_w^2} \left\{ 1 - \rho_{sI} \left[ \mathbf{I} + \frac{\mathbf{S}_I}{\sigma_w^2} \mathbf{V}_I^H \mathbf{V}_I \right]^{-1} \frac{\mathbf{S}_I}{\sigma_w^2} \cdot N \cdot \rho_{sI}^H \right\} \right\}^{-1}. \quad (6.114)$$

The first performance measure of interest is the array gain. The noise spectrum at a single sensor is

$$S_n = \mathbf{1}^T \mathbf{S}_I \mathbf{1} + \sigma_w^2. \quad (6.115)$$

Using (6.108) and (6.115) in (6.28) gives

$$A_o = N \left( 1 + \frac{\mathbf{1}^T \mathbf{S}_I \mathbf{1}}{\sigma_w^2} \right) (1 - N\alpha), \quad (6.116)$$

where

$$\alpha = \rho_{sI} \left[ \mathbf{I} + \frac{\mathbf{S}_I}{\sigma_w^2} \mathbf{V}_I^H \mathbf{V}_I \right]^{-1} \frac{\mathbf{S}_I}{\sigma_w^2} \rho_{sI}^H. \quad (6.117)$$

The  $\alpha$  can also be written as

$$\begin{aligned} \alpha &= \text{tr} \left[ \rho_{sI} \left[ \mathbf{I} + \frac{\mathbf{S}_I}{\sigma_w^2} \mathbf{V}_I^H \mathbf{V}_I \right]^{-1} \frac{\mathbf{S}_I}{\sigma_w^2} \rho_{sI}^H \right] \\ &= \text{tr} \left[ \rho_{sI}^H \rho_{sI} \left[ \mathbf{I} + \frac{\mathbf{S}_I}{\sigma_w^2} \mathbf{V}_I^H \mathbf{V}_I \right]^{-1} \frac{\mathbf{S}_I}{\sigma_w^2} \right]. \end{aligned} \quad (6.118)$$

The second measure of interest is the optimal beam pattern

$$B_o(\mathbf{k} : \mathbf{k}_s) = \frac{N\Lambda}{\sigma_w^2} \left[ \frac{\mathbf{v}_s^H}{N} - \rho_{sI} \left[ \mathbf{I} + \frac{\mathbf{S}_I}{\sigma_w^2} \mathbf{V}_I^H \mathbf{V}_I \right]^{-1} \frac{\mathbf{S}_I}{\sigma_w^2} \mathbf{V}_I^H \right] \mathbf{v}(\mathbf{k}). \quad (6.119)$$

Note that

$$\frac{\mathbf{V}_I^H \mathbf{v}_k}{N} = \begin{bmatrix} B_c(\mathbf{k} : \mathbf{k}_1) \\ B_c(\mathbf{k} : \mathbf{k}_2) \\ \vdots \\ B_c(\mathbf{k} : \mathbf{k}_D) \end{bmatrix} \triangleq \mathbf{B}_c(\mathbf{k} : \mathbf{k}_I) \quad (6.120)$$

is a  $D \times 1$  matrix of conventional beam patterns. This is what we would expect from the receiver configuration in Figure 6.20. Then (6.146) can be written as

$$B_o(\mathbf{k} : \mathbf{k}_s) = \frac{N\Lambda}{\sigma_w^2} \left[ B_c(\mathbf{k} : \mathbf{k}_s) - N \rho_{sI} \left[ \mathbf{I} + \frac{\mathbf{S}_I}{\sigma_w^2} \mathbf{V}_I^H \mathbf{V}_I \right]^{-1} \frac{\mathbf{S}_I}{\sigma_w^2} \mathbf{B}(\mathbf{k} : \mathbf{k}_I) \right]. \quad (6.121)$$

Thus, the optimal beam pattern is the weighted sum of  $D + 1$  conventional beam patterns corresponding to the desired and interfering signals.

If the interfering signals are uncorrelated, we can write

$$\frac{\mathbf{S}_I}{\sigma_w^2} \triangleq \begin{bmatrix} \sigma_1^2 & 0 & & \\ & \sigma_2^2 & & \\ & 0 & \ddots & \\ & & & \sigma_D^2 \end{bmatrix} \triangleq \boldsymbol{\sigma}_I^2. \quad (6.122)$$

Then, (6.109) can be written as

$$\boxed{\mathbf{w}_o^H = \frac{\Lambda \mathbf{v}_s^H}{\sigma_w^2} \left[ \mathbf{I} - \mathbf{V}_I \left[ [\boldsymbol{\sigma}_I^2]^{-1} + \mathbf{V}_I^H \mathbf{V}_I \right]^{-1} \mathbf{V}_I^H \right].} \quad (6.123)$$

For large  $\boldsymbol{\sigma}_I^2$ , this reduces to

$$\boxed{\mathbf{w}_o^H = \frac{\Lambda \mathbf{v}_s^H}{\sigma_w^2} \left[ \mathbf{I} - \mathbf{V}_I \left[ \mathbf{V}_I^H \mathbf{V}_I \right]^{-1} \mathbf{V}_I^H \right],} \quad (6.124)$$

which can be written as

$$\mathbf{w}_o^H = \frac{\Lambda}{\sigma_w^2} \mathbf{v}_s^H \mathbf{P}_I^\perp, \quad (6.125)$$

where  $\mathbf{P}_I$  is the projection matrix onto the interference subspace and  $\mathbf{P}_I^\perp$  is the projection onto a subspace orthogonal to the interference subspace. Thus, we are putting a null on each of the interfering signals.

The single plane-wave case illustrated many of the properties of the multiple plane-wave interference case. In the sidelobe region with multiple separated interferers, the effects are similar to the single interferer case.

We consider two examples to illustrate some interesting behavior.

### Example 6.3.1

Consider a standard 10-element linear array. The desired signal is at  $\psi = 0$ . There are two uncorrelated interfering signals located symmetrically about  $\psi = 0$ . In Figure 6.21, we show the optimum beam pattern for  $\sigma_I^2 = 20$  dB. We see that in the sidelobe region the optimum pattern has a deep notch at the locations of the interferers and the other lobes are well behaved. As the interferers move inside the main lobe, the optimum pattern has two large symmetric sidelobes plus three other sidelobes that are larger than the main lobe.

In Figure 6.22, we show the array gain as a function of  $u/BW_{NN}$  for various values of  $\sigma_I^2$  (for  $N \geq 10$ ).

### Example 6.3.2

Consider a standard linear array with 21 elements. (This is the same array as in Example 3.7.2.) We assume there are three interferers at  $u_1 = 0.21$ ,  $u_2 = 0.22$ , and  $u_3 = 0.23$ .

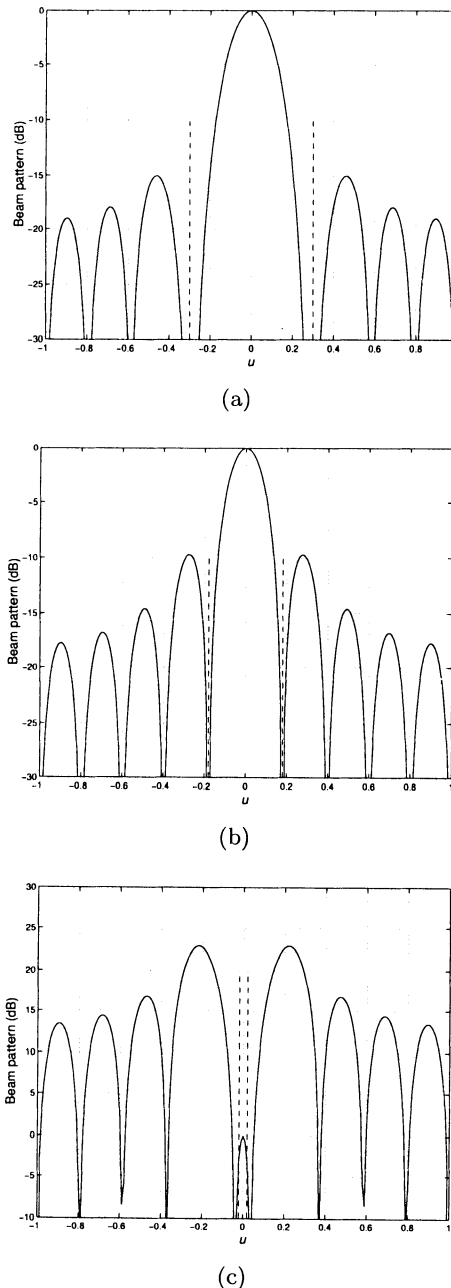


Figure 6.21 MVDR beam pattern: symmetric interference:  $INR = 20$  c  
 (a) sidelobe region,  $u = 0.3$ ; (b) outer main-lobe region,  $u = 0.18$ ; (c) HPB region,  $u = 0.02$ .

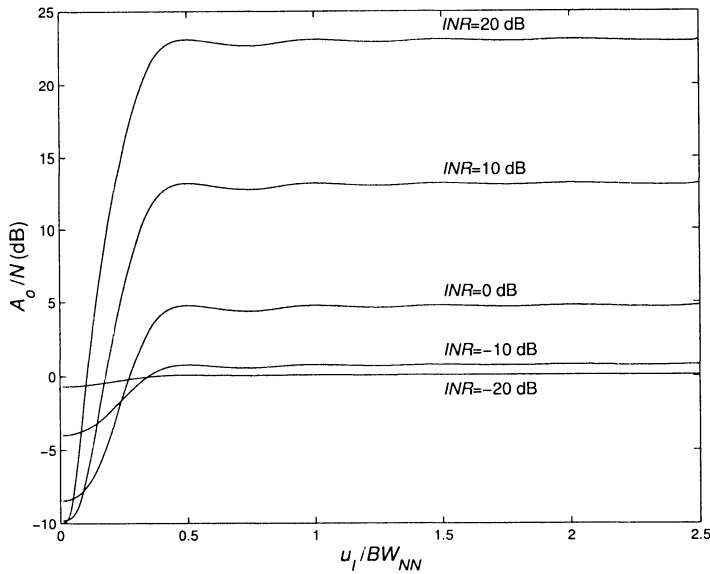


Figure 6.22 Array gain/ $N$  versus  $u_i/BW_{NN}$ .

The resulting beam pattern is shown in Figure 6.23 for several values of  $INR$ . The corresponding array gains are indicated.

We see that for  $\sigma_I^2 = 20$  dB; the pattern is still different from the result in Example 3.7.2 (Figure 3.40). (The MVDR preserves the main lobe and the first sidelobe.) This is because the MVDR beamformer does not need to create three nulls.

### 6.3.3 Summary: Discrete Interference

For discrete interference, the optimum receiver forms a signal plus interference subspace and then performs optimal processing in that subspace. We could have derived the optimum processor by arguing that the signal plus interference subspace forms a sufficient statistic for the optimization problem.

If the  $INR$  is modest, then the optimum processor forms notches (partial nulls) in the direction of the interfering signals. As the  $INR$  increases, these notches approach perfect nulls.

If the interferers are outside the main lobe, then the beam pattern of the optimum processor is well-behaved and we can obtain a significant improvement in array gain. If the interferers are inside the main lobe, the optimal solution creates large spurious lobes away from the desired MRA. We will look at several alternative approaches later, but will find that main-lobe

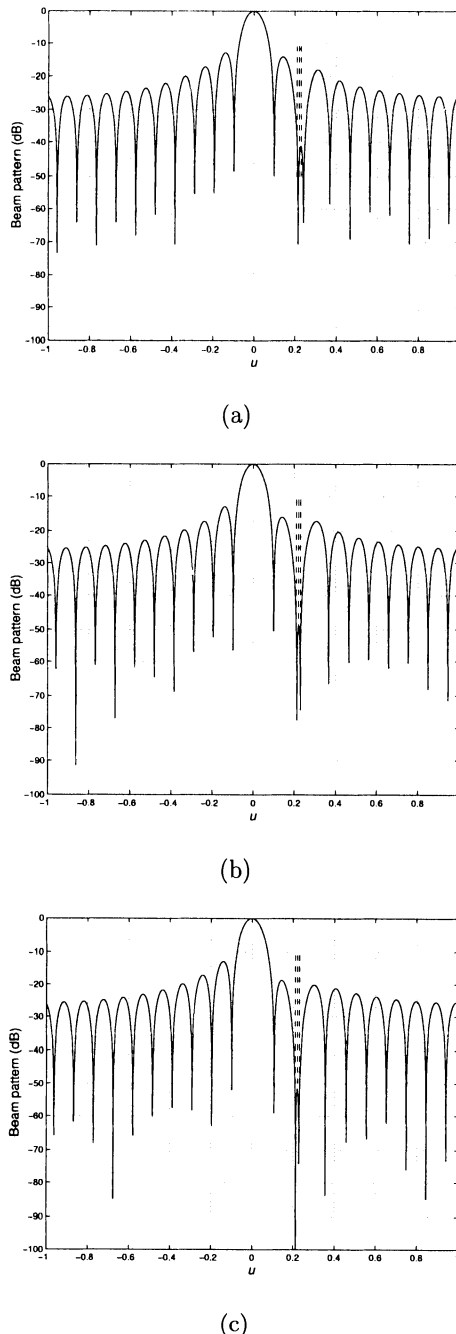


Figure 6.23 Beam pattern for three interferers:  $N=21$ ,  $u_s=0$ ,  $u_I=0.21, 0.22, 0.23$ ; (a)  $\sigma_I^2 = 0$  dB; (b)  $\sigma_I^2 = 10$  dB; (c)  $\sigma_I^2 = 20$  dB.

interference is a difficult problem.

## 6.4 Spatially Spread Interference

In this section, we consider the performance of the MVDR beamformer in the presence of spatially spread interference plus white noise. In Section 6.4.1, we consider the physical noise models that were developed in Section 5.3.3. In Section 6.4.2, we consider the ARMA models that were developed in Section 5.6.

### 6.4.1 Physical Noise Models

In Section 5.3.3 and the associated problems (e.g., Problems 5.3.1–5.3.3), we developed several noise models that corresponded to noise fields encountered in acoustic environments.

We consider two examples to illustrate the performance of an optimum processor in that environment.

#### Example 6.4.1

Consider a standard 10-element linear array oriented in the vertical direction (along the  $z$ -axis). The frequency-domain snapshots are

$$\mathbf{X}(\omega) = \mathbf{v}(\psi_T)F(\omega) + \mathbf{N}_c(\omega) + \mathbf{W}(\omega). \quad (6.126)$$

The noise contains a white component with spectral matrix  $\sigma_w^2 \mathbf{I}$  and a high-surface noise component whose spatial spectral matrix is

$$\mathbf{S}_{\mathbf{n}_c}(\omega) = \mathbf{S}_o(\omega) \left\{ \text{sinc}(k_o \Delta \mathbf{p}) + j\alpha \frac{1}{k_o \Delta \mathbf{p}} [\text{sinc}(k_o \Delta \mathbf{p}) - \cos(k_o \Delta \mathbf{p})] \cos \theta_p \right\}, \quad (6.127)$$

and  $\alpha = 1$  (see Problem 5.3.1). The surface noise and the white noise are uncorrelated. The optimum array gain is obtained by:

- (i) Evaluating  $S_o(\omega : \theta, \phi)$  at the sensor locations to obtain the spectral matrix  $\mathbf{S}_{\mathbf{n}_c}(\omega)$ .
- (ii) Find  $\mathbf{S}_n^{-1}(\omega) = [\mathbf{S}_{\mathbf{n}_c}(\omega) + \sigma_w^2 \mathbf{I}]^{-1}$  numerically.
- (iii) Substituting into (6.28) to find  $A_o$ .
- (iv) Substituting into (6.32) gives  $A_c$  for comparison.

In Figure 6.24 we show the results as a function of  $\theta_s$  for several values of  $\mathbf{S}_o(\omega)/\sigma_w^2$ .

#### Example 6.4.2 [Bag76]

We consider the same model as in Example 6.4.1 except  $\mathbf{S}_{\mathbf{n}_c}(\omega)$  corresponds to a high-layer noise environment. The spatial spectral matrix is

$$\begin{aligned} \mathbf{S}_{\mathbf{n}_c}(\omega) = & S_o(\omega) \left\{ \text{sinc}(k_o \Delta \mathbf{p}) + \alpha \left[ \left( \frac{3}{(k_o \Delta \mathbf{p})^2} - 1 \right) \text{sinc}(k_o \Delta \mathbf{p}) \right. \right. \\ & \left. \left. - \frac{3 \cos(k_o \Delta \mathbf{p})}{(k_o \Delta \mathbf{p})^2} \right] \left[ \frac{3 \cos(2\theta_p) + 1}{4} \right] \right\}, \end{aligned} \quad (6.128)$$

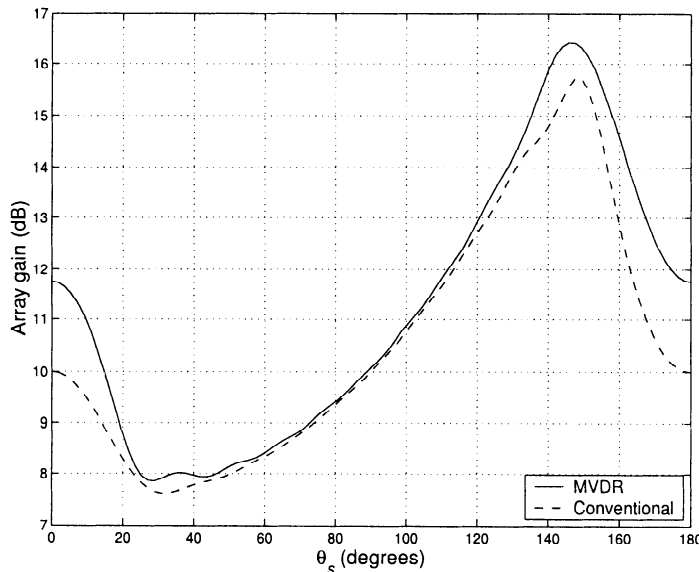


Figure 6.24 MVDR beamformer: array gain versus  $\theta_s$  for various  $\mathbf{S}_n(\omega_c)/\sigma_w^2$  levels; high surface noise.

with  $\alpha = 1$  (see Problem 5.3.2). We repeat the steps in Example 6.4.1 to obtain the optimum array gain and the conventional array gain. We show the results in Figure 6.25 as a function of  $\theta_s$  for several values of  $S_o(\omega)/\sigma_w^2$ .

### 6.4.2 ARMA Models

In this case, we assume that the spatially spread noise process can be modeled as an autoregressive process of order  $p$  where  $N$ , the number of sensor elements in the standard linear array, satisfies

$$N \geq 2p + 1. \quad (6.129)$$

In order to implement the optimum beamformer we need to evaluate  $\mathbf{S}_n^{-1}$ , where  $n(k)$  is an AR( $p$ ) process (see (5.308) and Figure 5.22). We first consider the case in which the sensor noise is negligible. Subsequently we consider the case of small sensor noise and then the general case.

A formula for  $\mathbf{S}_n^{-1}$  in terms of the AR parameters was given in (5.338). We give two examples.

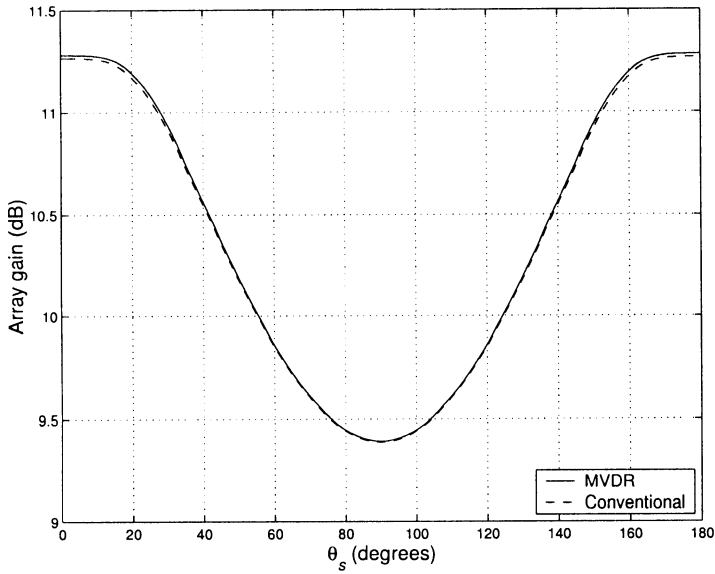


Figure 6.25 MVDR beamformer: array gain versus  $\theta_s$  for various  $\mathbf{S}_n(\omega_c)/\sigma_w^2$  levels; high layer noise.

For a complex AR(1) process,

$$\mathbf{S}_n^{-1} = \frac{1}{\sigma_u^2} \begin{bmatrix} 1 & a^*[1] & 0 & 0 & \cdots & 0 \\ a[1] & 1 + |a[1]|^2 & a^*[1] & 0 & \cdots & 0 \\ 0 & a[1] & 1 + |a[1]|^2 & a^*[1] & \cdots & 0 \\ \vdots & \vdots & \ddots & \ddots & \ddots & \vdots \\ 0 & 0 & \cdots & a[1] & 1 + |a[1]|^2 & a^*[1] \\ 0 & 0 & \cdots & 0 & a[1] & 1 \end{bmatrix}. \quad (6.130)$$

We observe that  $\mathbf{S}_n^{-1}$  is a Hermitian, persymmetric matrix, but it is not Toeplitz. We also observe that we can partition  $\mathbf{S}_n^{-1}$  as

$$\mathbf{S}_n^{-1} = \left[ \begin{array}{c|c} \mathbf{a}^* & \mathbf{0} \\ \hline \mathbf{B} & \\ \hline \mathbf{0} & \mathbf{J} \mathbf{a} \end{array} \right], \quad (6.131)$$

and the middle  $(N - 2) \times N$  matrix  $\mathbf{B}$  is a right circulant matrix as well as a banded Toeplitz matrix.

For a complex AR(2) process, we have,

$$\mathbf{S}_n^{-1} = \frac{1}{\sigma_u^2} \begin{bmatrix} 1 & a^*[1] & a^*[2] \\ a[1] & 1 + |a[1]|^2 & a^*[1] + a[1]a^*[2] \\ a[2] & a[1] + a^*[1]a[2] & 1 + |a[1]|^2 + |a[2]|^2 \\ \vdots & \ddots & \ddots \\ 0 & \cdots & a[1] + a^*[1]a[2] \\ 0 & \cdots & a[2] \\ 0 & \cdots & 0 \\ & & 0 & \cdots & 0 \\ & & a^*[2] & \cdots & 0 \\ & & a^*[1] + a[1]a^*[2] & \cdots & 0 \\ & & \ddots & \ddots & \vdots \\ & & 1 + |a[1]|^2 + |a[2]|^2 & a^*[1] + a[1]a^*[2] & a^*[2] \\ & & a[1] + a^*[1]a[2] & 1 + |a[1]|^2 & a^*[1] \\ & & a[2] & a[1] & 1 \end{bmatrix}. \quad (6.132)$$

For the AR( $p$ ), (5.338) can be written as

$$\left[ \mathbf{S}_n^{-1} \right]_{ij} = \frac{1}{\sigma^2} \sum_{k=1}^N (a[i-k]a^*[j-k] - a^*[N-i+k]a[N-j+k]) \quad i = 1, 2, \dots, N; j = 1, 2, \dots, N, \quad (6.133)$$

where  $a[k] = 0$  for  $k < 0$  and  $k > p$ .

We consider a simple example to illustrate the result.

#### Example 6.4.3

Consider an  $N$ -element standard linear array with  $\mathbf{n}(k)$  consisting of a complex AR(1) process and assume there is no observation noise. We assume  $N$  is odd.

Then, the MVDR filter is

$$\mathbf{w}_o^H = \Lambda \mathbf{v}^H(\psi_s) \mathbf{S}_n^{-1}, \quad (6.134)$$

and the optimum array gain is

$$A_o = [E [|n_i(k)|^2]] \Lambda^{-1} = \frac{\sigma_u^2}{(1 - |a[1]|^2)} \Lambda^{-1}, \quad (6.135)$$

where

$$\Lambda = [\mathbf{v}^H(\psi_s) \mathbf{S}_n^{-1} \mathbf{v}(\psi_s)]^{-1}. \quad (6.136)$$

The elements of the MVDR filter (omitting the  $\Lambda$  term temporarily) are obtained by using (6.130) in (6.14)

$$w'_{o1} = e^{j \frac{N-1}{2} \psi_s} [1 - |a_1| e^{-j(\psi_s - \psi_n)}], \quad (6.137)$$

$$\begin{aligned} w'_{on} &= e^{j[\frac{N-2}{2} - (n-1)]\psi_s} [-|a_1| e^{j(\psi_s - \psi_n)} + (1 + |a_1|^2) - |a_1| e^{-j(\psi_s - \psi_n)}] \\ &= e^{j[\frac{N-2}{2} - (n-1)]\psi_s} [(1 + |a_1|^2) - 2|a_1| \cos(\psi_s - \psi_n)] \\ n &= 2, 3, \dots, N-1, \end{aligned} \quad (6.138)$$

$$w'_{oN} = e^{-j\frac{N-1}{2}\psi_s} [1 - |a_1|e^{j(\psi_s - \psi_n)}] = w'^*_o, \quad (6.139)$$

where the prime denotes the absence of  $\Lambda$ .

The beam pattern for a standard 11-element linear array is shown in Figure 6.26. We see that as the peak of  $a_1$  moves inside the main lobe, the MVDR beamformer narrows the main lobe, causing a significant increase in the sidelobes.

To find the array gain, we substitute (6.130) into (6.28) and obtain

$$\begin{aligned} A_o &= \frac{1}{1 - |a_1|^2} [N - 2(N-1)|a_1|\cos(\psi_s - \psi_n) + (N-2)|a_1|^2] \\ &= \frac{1}{1 - |a_1|^2} [N(1 - |a_1|^2) - 2(N-1)|a_1|(|a_1| - \cos(\psi_s - \psi_n))] \\ &= N \left\{ 1 + \frac{2(N-1)}{N} \frac{|a_1|}{1 - |a_1|^2} (|a_1| - \cos(\psi_s - \psi_n)) \right\}. \end{aligned} \quad (6.140)$$

The array gain is plotted versus  $\Delta u/BW_{NN} = (u_s - u_n)/BW_{NN}$  in Figure 6.27 for several values of  $|a_1|$ .

As  $|a_1|$  approaches unity, the required *INR* for the no white noise assumption to be valid becomes higher. In these cases, the array gain is calculated numerically.

In Figure 6.28, the array gain is plotted versus  $\Delta u/BW_{NN}$  for various values of  $|a_1|$  and  $\sigma_x^2/\sigma_w^2$ . We also show the result for a single plane wave from Figure 6.13. We see that, as  $|a_1|$  increases, the array gain approaches the single plane-wave result. For small  $|a_1|$ , the interference is spread over more of  $u$ -space and the optimum beamformer is less effective. In the limit, as  $|a_1|$  goes to zero, the AR process is identical to white noise and  $A_o = 10.41$  dB.

## 6.5 Multiple Plane-wave Signals

In this section, we consider the case in which there are multiple desired plane-wave signals. In Section 6.5.1, we consider MVDR beamformers. In Section 6.5.2, we consider MMSE beamformers.

### 6.5.1 MVDR Beamformer

In this section, we find the optimum distortionless matrix processor for  $D$  plane-wave signals. Using the frequency-domain snapshot model,

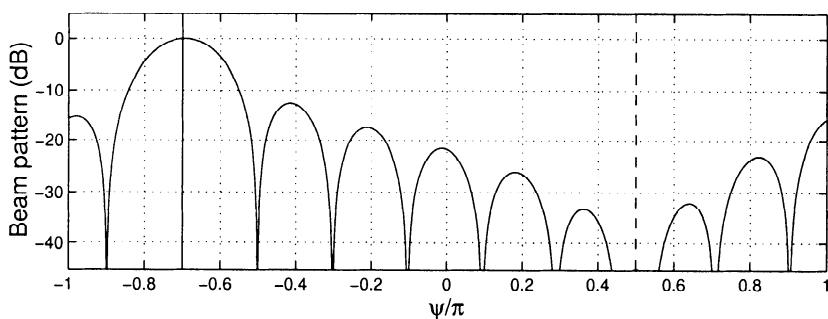
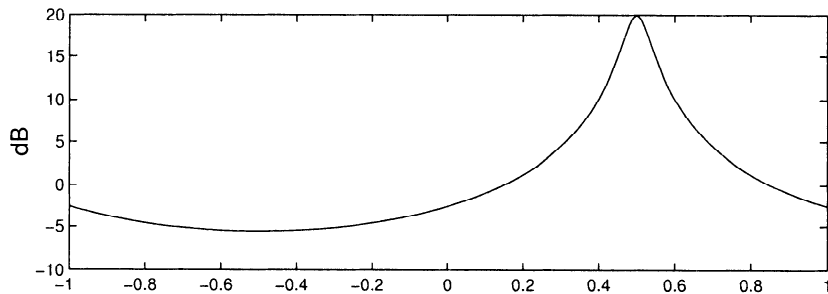
$$\mathbf{X}(\omega) = \mathbf{V}_s \mathbf{F}(\omega) + \mathbf{N}(\omega), \quad (6.141)$$

where  $\mathbf{V}_s$  is an  $N \times D$  array manifold matrix,

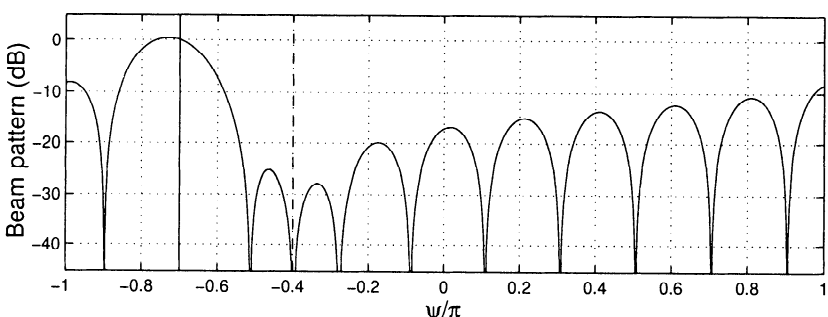
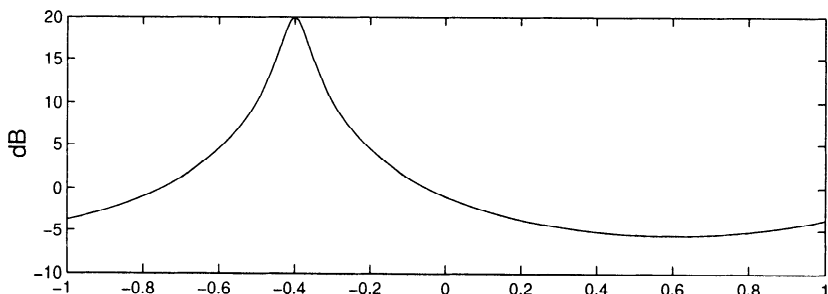
$$\mathbf{V}_s = \left[ \mathbf{v}(\omega : \mathbf{k}_1) \mid \mathbf{v}(\omega : \mathbf{k}_2) \mid \cdots \mid \mathbf{v}(\omega : \mathbf{k}_D) \right], \quad (6.142)$$

and

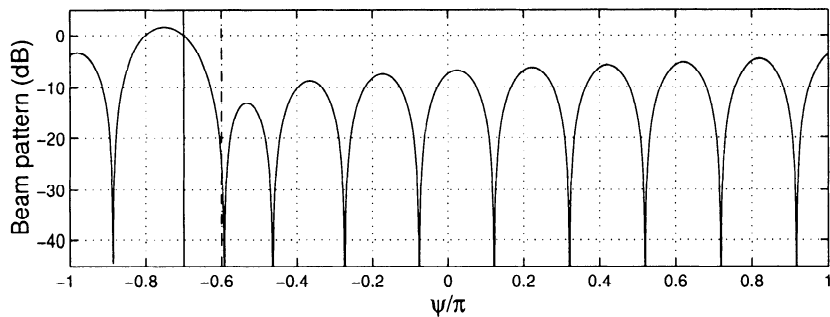
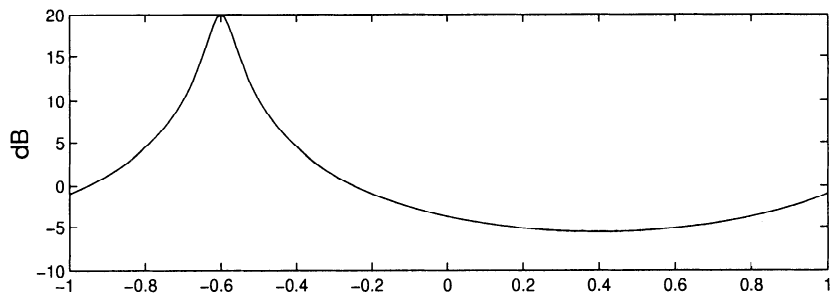
$$\mathbf{F}(\omega) = \begin{bmatrix} F_1(\omega) \\ F_2(\omega) \\ \vdots \\ F_D(\omega) \end{bmatrix} \quad (6.143)$$



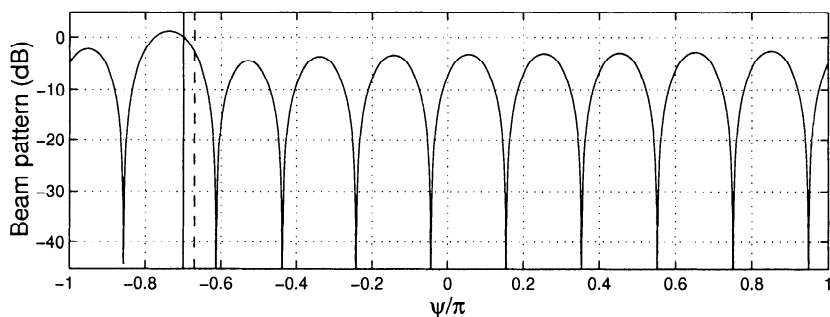
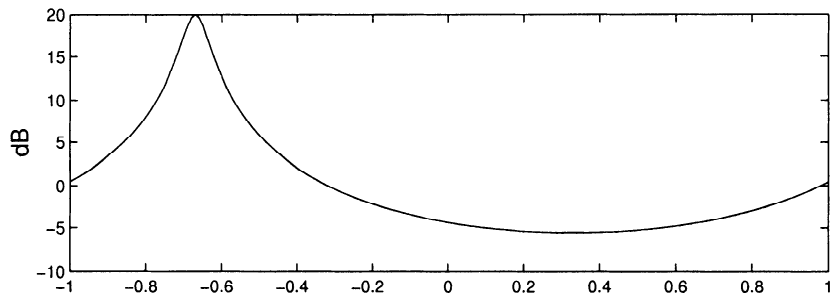
(a)



(b)



(c)



(d)

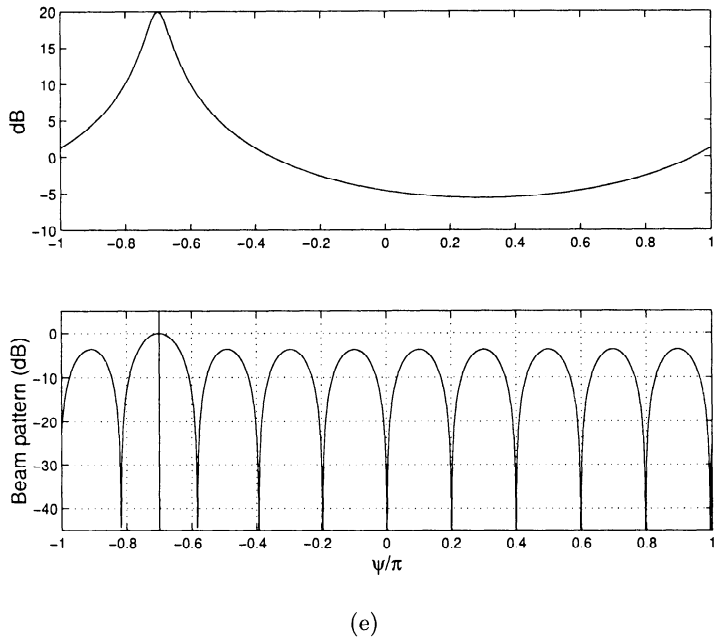


Figure 6.26 Optimum beam pattern: complex AR(1) interference in the absence of white noise:  $|a_1| = 0.9$ ; (a)  $\phi = 0.5\pi$ ; (b)  $\phi = -0.4\pi$ ; (c)  $\phi = -0.6\pi$ ; (d)  $\phi = -0.67\pi$ ; (e)  $\phi = -0.70\pi$ ; no additive white noise.

is the Fourier transform of an unknown nonrandom signal vector. The processor,  $\mathbf{W}^H(\omega)$ , is a  $D \times N$  distortionless matrix processor:

$$\mathbf{W}^H(\omega) = \begin{bmatrix} \mathbf{W}_1^H(\omega) \\ \mathbf{W}_2^H(\omega) \\ \vdots \\ \mathbf{W}_D^H(\omega) \end{bmatrix}. \quad (6.144)$$

Suppressing the  $\omega$  dependence, the distortionless criterion implies,

$$\begin{aligned} \mathbf{w}_1^H \mathbf{V} \mathbf{F} &= F_1, \\ \mathbf{w}_2^H \mathbf{V} \mathbf{F} &= F_2, \\ &\vdots \\ \mathbf{w}_D^H \mathbf{V} \mathbf{F} &= F_D. \end{aligned} \quad (6.145)$$

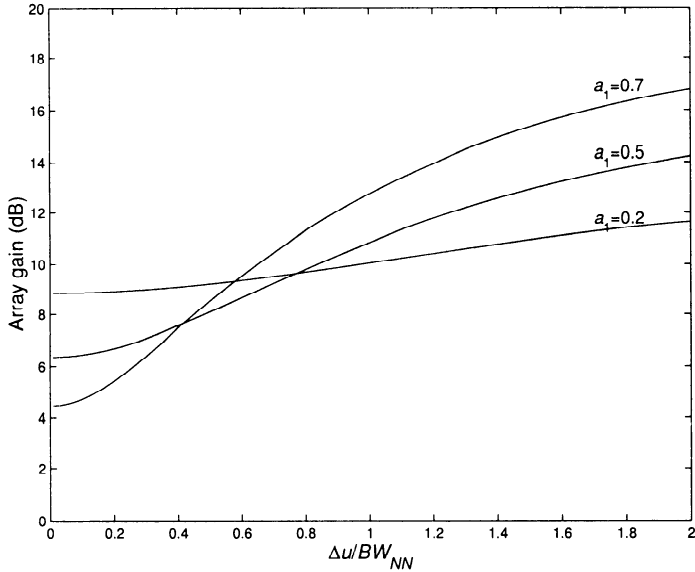


Figure 6.27 Array gain: complex AR(1) interference;  $A_o$  versus  $\Delta u/BW_{NN}$ ;  $|a_1| = 0.2, 0.5$  and  $0.7$ .

Because (6.145) must be satisfied for arbitrary  $\mathbf{F}$ , it places  $D$  constraints on each  $\mathbf{w}_i$ . For  $\mathbf{w}_1$ ,

$$\begin{aligned} \mathbf{w}_1^H \mathbf{v}_1 F_1 &= F_1, \\ \mathbf{w}_1^H \mathbf{v}_2 F_2 &= 0, \\ &\vdots \\ \mathbf{w}_1^H \mathbf{v}_D F_D &= 0. \end{aligned} \quad (6.146)$$

These constraints imply,

$$\begin{aligned} \mathbf{w}_1^H \mathbf{v}_1 &= 1, \\ \mathbf{w}_1^H \mathbf{v}_2 &= 0, \\ &\vdots \\ \mathbf{w}_1^H \mathbf{v}_D &= 0. \end{aligned} \quad (6.147)$$

or, for the  $i$ th beamformer,

$$\mathbf{w}_i^H \mathbf{v}_j = \delta_{ij} \quad i, j = 1, \dots, D. \quad (6.148)$$

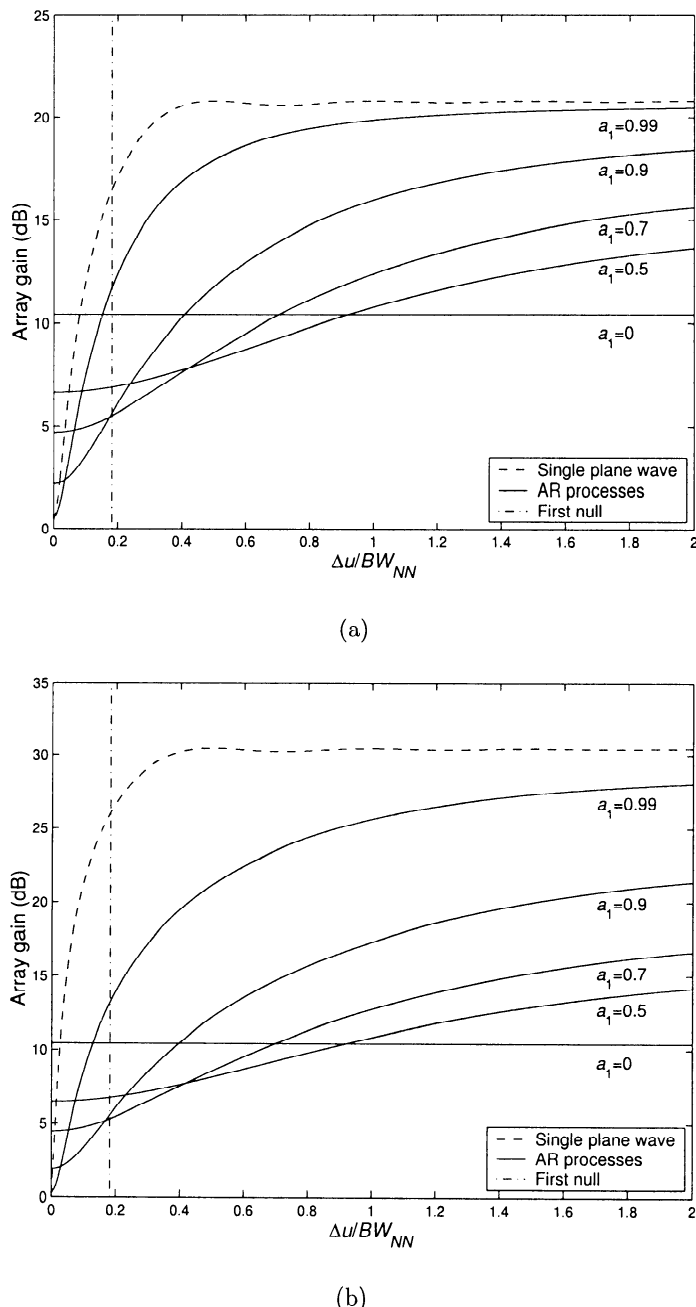


Figure 6.28 Array gain: complex AR(1) interference;  $A_o$  versus  $\Delta u/BW_{NN}$ ;  $|a_1| = 0.5, 0.7, 0.9$  and  $0.99$ ; (a)  $\sigma_x^2/\sigma_w^2 = 10$  dB; (b)  $\sigma_x^2/\sigma_w^2 = 20$  dB.

Therefore, the  $i$ th beamformer is distortionless with respect to the  $i$ th signal and puts a perfect null of the other  $D - 1$  signals. The output noise of the  $i$ th beamformer is

$$\sigma_{ni}^2 = \mathbf{w}_i^H \mathbf{S}_n \mathbf{w}_i. \quad (6.149)$$

We minimize  $\sigma_{ni}^2$  subject to the  $D$  constraints on  $\mathbf{w}_i$ . We define

$$G_i = \mathbf{w}_i^H \mathbf{S}_n \mathbf{w}_i + \sum_{j=1}^D \lambda_{ij}^* \left( \mathbf{w}_i^H \mathbf{v}_i - \delta_{ij} \right) + \sum_{j=1}^D \lambda_{ij} \left( \mathbf{v}_i^H \mathbf{w}_i - \delta_{ij} \right), \\ i = 1, \dots, D. \quad (6.150)$$

Minimizing gives

$$\mathbf{w}_i^H \mathbf{S}_n + \lambda_{ij} \mathbf{v}_j^H = 0, \quad i, j = 1, \dots, D, \quad (6.151)$$

or

$$\mathbf{w}_i^H = -\lambda_{ij} \mathbf{v}_j^H \mathbf{S}_n^{-1}, \quad i, j = 1, \dots, D. \quad (6.152)$$

Substituting (6.152) into (6.148) gives

$$-\lambda_{ii} \mathbf{v}_i^H \mathbf{S}_n^{-1} \mathbf{v}_i = 1, \quad i = 1, \dots, D. \quad (6.153)$$

$$-\lambda_{ij} \mathbf{v}_i^H \mathbf{S}_n^{-1} \mathbf{v}_j = 0, \quad i, j = 1, \dots, D, \quad (6.154)$$

or

$$-\lambda_{ij} \mathbf{v}_i^H \mathbf{S}_n^{-1} \mathbf{v}_j = \delta_{ij}, \quad i, j = 1, \dots, D. \quad (6.155)$$

We define a  $D \times D$  matrix  $\Lambda$  whose  $ij$ th element is  $\lambda_{ij}$ . Then (6.155) can be written in matrix notation as

$$-\Lambda[\mathbf{V}^H \mathbf{S}_n^{-1} \mathbf{V}] = \mathbf{I}, \quad (6.156)$$

or

$$\Lambda = -[\mathbf{V}^H \mathbf{S}_n^{-1} \mathbf{V}]^{-1}. \quad (6.157)$$

Then, the optimum distortionless beamformer can be written as

$$\boxed{\mathbf{W}_{do}^H = [\mathbf{V}^H \mathbf{S}_n^{-1} \mathbf{V}]^{-1} \mathbf{V}^H \mathbf{S}_n^{-1}.} \quad (6.158)$$

The output of  $\mathbf{W}_{do}^H$  is the  $D \times 1$  vector,

$$\hat{\mathbf{F}}_o = [\mathbf{V}^H \mathbf{S}_n^{-1} \mathbf{V}]^{-1} \mathbf{V}^H \mathbf{S}_n^{-1} \mathbf{X}, \quad (6.159)$$

which is also the minimum variance unbiased estimate of  $\mathbf{F}$ .

It is also straightforward to show that

$$\hat{\mathbf{F}}_{ml} = \hat{\mathbf{F}}_o, \quad (6.160)$$

if the Gaussian assumption is added.

For the special case of white homogeneous noise,

$$\mathbf{S}_n = \sigma_w^2 \mathbf{I}, \quad (6.161)$$

the optimum processor is

$$\boxed{\mathbf{W}_{do}^H = [\mathbf{V}^H \mathbf{V}]^{-1} \mathbf{V}^H}. \quad (6.162)$$

Thus,

$$\hat{\mathbf{F}}_o = [\mathbf{V}^H \mathbf{V}]^{-1} \mathbf{V}^H \mathbf{X}. \quad (6.163)$$

This result in (6.163) was first pointed out by Schweppe [Sch68]. As he did not include the derivation in the paper, it has been rediscovered in several subsequent papers.

It is useful to rewrite the result in (6.148) in a different manner. Consider the first signal and partition  $\mathbf{V}$  as,

$$\mathbf{V} = [\mathbf{v}_1 | \mathbf{V}_I]. \quad (6.164)$$

Then

$$\mathbf{V}^H \mathbf{V} = \left[ \begin{array}{c|c} \mathbf{v}_1^H \mathbf{v}_1 & \mathbf{v}_1^H \mathbf{V}_I \\ \hline \mathbf{V}_I^H \mathbf{v}_1 & \mathbf{V}_I^H \mathbf{V}_I \end{array} \right]. \quad (6.165)$$

Using (6.165) in (6.163) gives

$$\hat{F}_{ml1} = c \mathbf{v}_1^H \left\{ \mathbf{I} - \mathbf{V}_I (\mathbf{V}_I^H \mathbf{V}_I)^{-1} \mathbf{V}_I^H \right\} \mathbf{X}, \quad (6.166)$$

where  $c$  is the normalizing constant,

$$c = \left\{ \mathbf{v}_1^H [\mathbf{I} - \mathbf{V}_I (\mathbf{V}_I^H \mathbf{V}_I)^{-1} \mathbf{V}_I^H] \mathbf{v}_1 \right\}^{-1}. \quad (6.167)$$

The matrix in the brace is just a projection matrix onto the subspace defined by the columns of  $\mathbf{V}_I$  (the interference subspace):

$$\mathbf{P}_I \triangleq \mathbf{V}_I (\mathbf{V}_I^H \mathbf{V}_I)^{-1} \mathbf{V}_I^H. \quad (6.168)$$

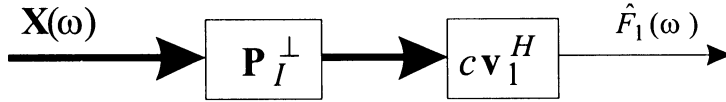


Figure 6.29 Optimum beamformer: multiple plane waves.

The complement of the projection matrix is

$$\mathbf{P}_I^\perp = \mathbf{I} - \mathbf{P}_I. \quad (6.169)$$

Then we can write

$$\hat{F}_{ml1} = c \mathbf{v}_1^H \mathbf{P}_I^\perp \mathbf{X}. \quad (6.170)$$

The representation in (6.169) and (6.170) emphasizes that when we want to simultaneously find the ML estimate of  $D$  plane-wave signal waveforms or construct a  $D \times N$  MVDR processor, the optimum receiver treats the  $i$ th signal ( $i = 1, 2, \dots, D$ ) as the desired signal and the other  $(D - 1)$  signals as interferers and puts “perfect” nulls on them. Note that this result only corresponds to (6.124) in the limiting case of large  $\sigma_f^2$ . The optimum beamformer is shown in Figure 6.29.

### 6.5.2 MMSE Processors

In this case the signal component of the received waveform consists of  $D$  plane-wave signals arriving from different directions. The source signals are sample functions from stationary zero-mean random processes that are uncorrelated with the noise field but may be correlated with each other. We define the **source signal snapshot vector** as a  $D \times 1$  complex vector,

$$\mathbf{F}(\omega) = \begin{bmatrix} F_1(\omega) \\ F_2(\omega) \\ \vdots \\ F_D(\omega) \end{bmatrix}. \quad (6.171)$$

The source spectral matrix is  $\mathbf{S}_f$  and is assumed to be of rank  $D$ . The array manifold matrix,  $\mathbf{V}_s$ , is an  $N \times D$  matrix,

$$\mathbf{V}_s = \left[ \mathbf{v}(\omega : \mathbf{k}_1) \mid \mathbf{v}(\omega : \mathbf{k}_2) \mid \cdots \mid \mathbf{v}(\omega : \mathbf{k}_D) \right], \quad (6.172)$$

where we have suppressed the  $\omega$  dependence on the left side of (6.172). The spectral matrix of the input is

$$\mathbf{S}_x = \mathbf{V}_s \mathbf{S}_f \mathbf{V}_s^H + \mathbf{S}_n. \quad (6.173)$$

We want to find the MMSE estimate of the  $D$  source signals. Thus, the desired signal snapshot vector  $\mathbf{D}(\omega)$  is a  $D \times 1$  vector,

$$\mathbf{D}(\omega) = \mathbf{F}(\omega), \quad (6.174)$$

and  $\mathbf{H}_o$  will be a  $D \times N$  matrix processor whose output is the desired estimate  $\hat{\mathbf{D}}(\omega)$ . The mean square error is defined as

$$\xi = E \left\{ \| \mathbf{D}(\omega) - \hat{\mathbf{D}}(\omega) \|^2 \right\}. \quad (6.175)$$

Proceeding as in the single plane-wave case, we obtain

$$\mathbf{H}_o = \mathbf{S}_{d\mathbf{x}^H} \mathbf{S}_{\mathbf{x}}^{-1}, \quad (6.176)$$

where

$$\mathbf{S}_{d\mathbf{x}^H} = \mathbf{S}_f \mathbf{V}_s^H. \quad (6.177)$$

Taking the inverse of  $\mathbf{S}_{\mathbf{x}}(\omega)$  gives

$$\mathbf{S}_{\mathbf{x}}^{-1} = \mathbf{S}_n^{-1} \left[ \mathbf{I} - \mathbf{V}_s (\mathbf{I} + \mathbf{S}_f \mathbf{V}_s^H \mathbf{S}_n^{-1} \mathbf{V}_s)^{-1} \mathbf{S}_f \mathbf{V}_s^H \mathbf{S}_n^{-1} \right], \quad (6.178)$$

where the  $\omega$  and  $\mathbf{k}_i (i = 1, \dots, D)$  dependence are suppressed. Then using (6.177) and (6.178) in (6.176), we have

$$\begin{aligned} \mathbf{H}_o &= \mathbf{S}_f \mathbf{V}^H \mathbf{S}_n^{-1} \left[ \mathbf{I} - \mathbf{V} (\mathbf{I} + \mathbf{S}_f \mathbf{V}^H \mathbf{S}_n^{-1} \mathbf{V})^{-1} \mathbf{S}_f \mathbf{V}^H \mathbf{S}_n^{-1} \right] \\ &= \mathbf{S}_f \mathbf{V}^H \mathbf{S}_n^{-1} - \mathbf{S}_f \mathbf{V}^H \mathbf{S}_n^{-1} \mathbf{V} (\mathbf{I} + \mathbf{S}_f \mathbf{V}^H \mathbf{S}_n^{-1} \mathbf{V})^{-1} \times \\ &\quad \mathbf{S}_f \mathbf{V}^H \mathbf{S}_n^{-1}. \end{aligned} \quad (6.179)$$

This can be put in more convenient form by rewriting the first term. Then

$$\begin{aligned} \mathbf{H}_o &= \left\{ (\mathbf{I} + \mathbf{S}_f \mathbf{V}^H \mathbf{S}_n^{-1} \mathbf{V}) (\mathbf{I} + \mathbf{S}_f \mathbf{V}^H \mathbf{S}_n^{-1} \mathbf{V})^{-1} \mathbf{S}_f \mathbf{V}^H \mathbf{S}_n^{-1} \right. \\ &\quad \left. - \mathbf{S}_f \mathbf{V}^H \mathbf{S}_n^{-1} \mathbf{V} (\mathbf{I} + \mathbf{S}_f \mathbf{V}^H \mathbf{S}_n^{-1} \mathbf{V})^{-1} \mathbf{S}_f \mathbf{V}^H \mathbf{S}_n^{-1} \right\}, \end{aligned} \quad (6.180)$$

which reduces to,

$$\boxed{\mathbf{H}_o = (\mathbf{I} + \mathbf{S}_f \mathbf{V}^H \mathbf{S}_n^{-1} \mathbf{V})^{-1} \mathbf{S}_f \mathbf{V}^H \mathbf{S}_n^{-1}.} \quad (6.181)$$

This result is the multiple plane-wave generalization of (6.47). The optimum processor is shown in Figure 6.30. Note that the first matrix operation

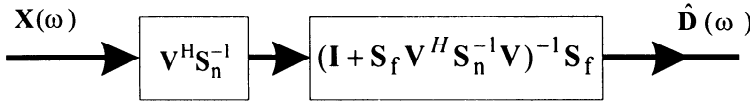


Figure 6.30 MMSE processor, multiple plane-wave signals.

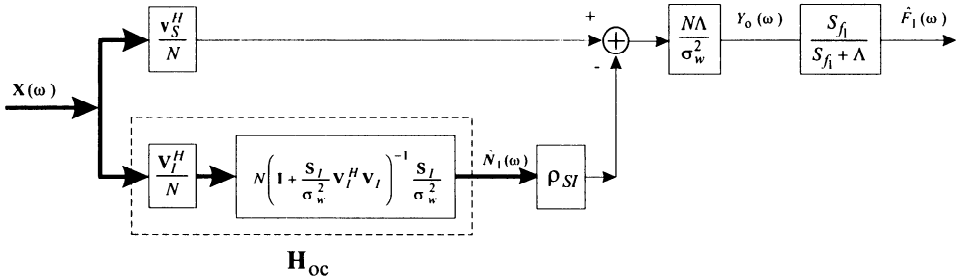


Figure 6.31 MMSE filter for single signal (temporally uncorrelated).

is generating a set of  $D$  sufficient statistics that are then multiplied by a matrix that takes into account the signal spectral matrix and generates  $\hat{\mathbf{D}}(\omega)$ . Note also that the  $i$ th output is the MMSE estimate of the corresponding source signal  $F_i(\omega)$ . In other words, minimizing  $\xi$  in (6.175) is equivalent to minimizing each  $\xi_i$ ,

$$\xi_i = E \left\{ |D_i(\omega) - \hat{D}_i(\omega)|^2 \right\}. \quad (6.182)$$

Therefore, we would expect that the multiple plane-wave signal problem is equivalent to  $D$  single plane-wave signal problems in which the other  $D - 1$  signals are treated exactly as if they were noise (see Problem 6.5.5). If the signal of interest (e.g.,  $F_1(\omega)$ ) is uncorrelated from the other  $D - 1$  signals, then,

$$\mathbf{S}_f = \begin{bmatrix} S_{f_1} & 0 \\ 0 & \mathbf{S}_I \end{bmatrix}. \quad (6.183)$$

In this case the processor in Figure 6.30 can be partitioned into the configuration shown in Figure 6.31. We observe that this is exactly the distortionless processor shown in Figure 6.10 followed by a scalar gain.

A special case of interest is when the noise is temporally and spatially uncorrelated. If, in addition, the spectral height is the same at each sensor, then

$$\mathbf{S}_n(\omega) = \sigma_w^2 \mathbf{I} \quad (6.184)$$

and  $\mathbf{H}_o(\omega)$  becomes,

$$\boxed{\mathbf{H}_o = \left( \mathbf{I} + \frac{\mathbf{S}_f}{\sigma_w^2} \mathbf{V}^H \mathbf{V} \right)^{-1} \frac{\mathbf{S}_f}{\sigma_w^2} \mathbf{V}^H.} \quad (6.185)$$

Comparing (6.181) and (6.158), we see that both the MVDR processor and the MMSE processor use the same matrix operation,  $\mathbf{V}^H \mathbf{S}_n^{-1}$ , to create the  $D$ -dimensional signal subspace. The MVDR processor then uses a  $D \times D$  matrix operation to generate a distortionless output, while the MMSE processor uses a different  $D \times D$  processor to generate the MMSE output.

Most of the behavior in the single-signal case carries over to the multiple plane-wave signal case. Several examples are given in the problems.

## 6.6 Mismatched MVDR and MPDR Beamformers

### 6.6.1 Introduction

In Section 6.2, MVDR and MPDR beamformers were derived and their performance was analyzed. In this section, their behavior is analyzed when they are mismatched. As a starting point, we repeat the formulas for the ideal MVDR and MPDR beamformers.

From (6.14),

$$\mathbf{w}_{mvdr}^H = \Lambda \mathbf{v}_m^H \mathbf{S}_n^{-1} \quad (\text{ideal MVDR}). \quad (6.186)$$

From (6.71),

$$\mathbf{w}_{mpdr}^{II} = \Lambda_1 \mathbf{v}_m^H \mathbf{S}_x^{-1} \quad (\text{ideal MPDR}), \quad (6.187)$$

where  $\Lambda_1$  is the reciprocal of the denominator in (6.71). In (6.186) and (6.187), we assume the beamformer is designed assuming the array manifold vector of the desired signal is  $\mathbf{v}_m$ . The subscript  $m$  denotes model. The  $\omega$  and  $\mathbf{k}_s$  are suppressed.

In a typical application the beamformer is scanned across the region of  $(\theta, \phi)$  space of interest by changing  $\mathbf{v}_m$  in discrete steps. For example, for a standard linear array, one might scan across  $u$ -space by changing the steering direction in  $u_\Delta = 2/N$  steps. With this step size, conventional beams pointed at different steps are orthogonal. At each step, the MVDR or MPDR beamformer is constructed, assuming the signal of interest arrives along the steering direction  $\mathbf{v}_m$ . However, all signals in the interval,  $-1/N \leq u \leq 1/N$ , must be treated for the beamformer pointed at  $u = 0$ . Therefore, the effect of this DOA mismatch must be considered.

In many applications, the step size can be reduced. This reduces the signal mismatch problem but increases the time required to scan a given area.

There are other sources of mismatch. The sources of mismatch can be divided into three cases.

### Case 1

The steering vector in (6.186) or (6.187) is unequal to  $\mathbf{v}_s$ . This can happen in two ways.

#### Case 1a

The steering vector is pointed at the wrong point in frequency-wavenumber space because

$$\mathbf{a}_s \neq \mathbf{a}_m, \quad (6.188)$$

$$\omega_s \neq \omega_m, \quad (6.189)$$

or the velocity of propagation is different from that used in the model (this difference may occur in sonar applications).

In (6.188), the steering vector is pointed at the wrong coordinates in azimuth and elevation, but the frequency is correct. In (6.189), the steering vector is pointed at the correct coordinate in azimuth and elevation, but the frequency is incorrect, so the wavenumber is incorrect.

#### Case 1b

The steering vector is pointed at the correct point in frequency-wavenumber space, but the array has been perturbed. Array perturbations could include errors in sensor gain and phase or location of sensors. Then,

$$\mathbf{v}_m(\mathbf{k}_d) \neq \mathbf{v}_s(\mathbf{k}_d). \quad (6.190)$$

Recall that we studied this problem in Chapter 2 in the context of the change in beam pattern and array gain.

A combination of Cases 1a and 1b is also possible.

### Case 2

The spatial spectral estimates will not be exact if there is a finite amount of data. Thus,

$$\hat{\mathbf{S}}_n \neq \mathbf{S}_n \quad (6.191)$$

and

$$\hat{\mathbf{S}}_x \neq \mathbf{S}_x. \quad (6.192)$$

We might expect that, depending on how the various errors are modeled, that Cases 1a, 1b, and 2 would all have a similar effect on the beamformer performance. The advantage of recognizing this similarity is that, when the MVDR or MPDR beamformer is modified to improve performance for one kind of mismatch, the modification will generally improve performance for the other types of mismatch.

In Section 6.6.2, we study the case in which the signal mismatch is due to the desired signal arriving from a different direction than the direction that was used to design the beamformer. This is referred to as DOA mismatch.

In Section 6.6.3, we consider the case in which the steering vector mismatch is due to array perturbations.

In Section 6.6.4, we introduce a technique referred to as **diagonal loading** to make the beamformer more robust in the presence of mismatch.

In Section 6.6.5, we summarize our results and discuss other techniques for improving robustness.

We defer our analysis of Case 2, the finite data problem, until Chapter 7. We will find that the techniques that we use to improve robustness in the presence of signal mismatch will usually improve robustness to spatial spectral matrix mismatch.

### 6.6.2 DOA Mismatch

In this section, we discuss the problem of signal mismatch in MVDR and MPDR beamformers. We also consider the conventional beamformer for comparison.<sup>5</sup>

The weight vectors for the three beamformers are:

$$\mathbf{w}_c^H = \frac{\mathbf{v}_m^H}{N}, \quad (6.193)$$

$$\mathbf{w}_{mvdr}^H = \frac{\mathbf{v}_m^H \mathbf{S}_n^{-1}}{\mathbf{v}_m^H \mathbf{S}_n^{-1} \mathbf{v}_m}, \quad (6.194)$$

and

$$\mathbf{w}_{mpdr}^H = \frac{\mathbf{v}_m^H \mathbf{S}_x^{-1}}{\mathbf{v}_m^H \mathbf{S}_x^{-1} \mathbf{v}_m}, \quad (6.195)$$

where

$$\mathbf{v}_m \triangleq \mathbf{v}(\omega : \mathbf{k}_m). \quad (6.196)$$

---

<sup>5</sup>Our discussion follows Cox [Cox73].

Using the frequency-domain snapshot model, the input is

$$\mathbf{X}(\omega) = \mathbf{v}_a F(\omega) + \mathbf{N}(\omega), \quad (6.197)$$

where

$$\mathbf{v}_a \triangleq \mathbf{v}(\omega : \mathbf{k}_a) \quad (6.198)$$

is the actual array manifold vector. The vector  $\mathbf{v}_a$  can be different from  $\mathbf{v}_m$  because the signal is actually arriving from a different direction than we assumed, or it could be different because the array geometry is different than our model. In this section, we initially assume that  $\mathbf{v}_a$  is deterministic.

If there are interfering plane waves, they are included in  $\mathbf{N}(\omega)$ . For simplicity, we assume that the noise power is the same at each sensor. We can define a normalized noise covariance matrix as

$$\mathbf{S}_n = S_n \rho_n. \quad (6.199)$$

The output power is,

$$\begin{aligned} P_o &= \sigma_s^2 \left| \mathbf{w}^H \mathbf{v}_a \right|^2 + \mathbf{w}^H \mathbf{S}_n \mathbf{w} \\ &= P_s + P_n. \end{aligned} \quad (6.200)$$

Therefore, the output *SNR* is

$$SNR_o \triangleq \frac{P_s}{P_n} = \frac{\sigma_s^2 \left| \mathbf{w}^H \mathbf{v}_a \right|^2}{\mathbf{w}^H \mathbf{S}_n \mathbf{w}}. \quad (6.201)$$

The signal mismatch has two negative effects: it can lower the output signal power  $P_s$ , and it can raise the output noise power  $P_n$ .

The array gain is

$$A = \frac{\left| \mathbf{w}^H \mathbf{v}_a \right|^2}{\mathbf{w}^H \rho_n \mathbf{w}}. \quad (6.202)$$

The array gain for the three beamformers in (6.193)–(6.195) in the presence of mismatch will be computed. First, consider the conventional beamformer defined by (6.193).

### 6.6.2.1 Conventional beamformer

The output *SNR* is<sup>6</sup>

$$SNR_o = \frac{\sigma_s^2 \left| \mathbf{v}_m^H \mathbf{v}_a \right|^2}{\mathbf{v}_m^H \mathbf{S}_n \mathbf{v}_m} = \frac{\sigma_s^2 N^2 |B_c(\mathbf{v}_a : \mathbf{v}_m)|^2}{\mathbf{v}_m^H \mathbf{S}_n \mathbf{v}_m}. \quad (6.203)$$

---

<sup>6</sup>The notation for  $B_c(\mathbf{v}_a : \mathbf{v}_m)$  is used to emphasize the dependence on  $\mathbf{v}$ .

As expected, the output signal power is reduced as a function of the beam pattern. The denominator is unchanged.

The array gain is

$$\boxed{A_c = \frac{N^2 |B_c(\mathbf{v}_a : \mathbf{v}_m)|^2}{\mathbf{v}_m^H \boldsymbol{\rho}_n \mathbf{v}_m}}. \quad (6.204)$$

The ratio of the mismatched array gain to matched array gain is just the power pattern of the array

$$\frac{A_c(\mathbf{v}_a)}{A_c(\mathbf{v}_m)} = |B_c(\mathbf{v}_a : \mathbf{v}_m)|^2. \quad (6.205)$$

We now consider the MVDR beamformer.

### 6.6.2.2 MVDR beamformer

In this discussion, it is useful to introduce the generalized cosine notation,

$$\begin{aligned} \cos^2(\mathbf{v}_m, \mathbf{v}_a : \boldsymbol{\rho}_n^{-1}) &= \cos^2(\mathbf{v}_a, \mathbf{v}_m : \boldsymbol{\rho}_n^{-1}) \\ &\triangleq \frac{|\mathbf{v}_m^H \boldsymbol{\rho}_n^{-1} \mathbf{v}_a|^2}{(\mathbf{v}_m^H \boldsymbol{\rho}_n^{-1} \mathbf{v}_m)(\mathbf{v}_a^H \boldsymbol{\rho}_n^{-1} \mathbf{v}_a)}, \end{aligned} \quad (6.206)$$

which is an inner product in a  $\boldsymbol{\rho}_n^{-1}$  space.

Substituting (6.194) into (6.200) gives the output signal power,

$$\begin{aligned} P_s &= \sigma_s^2 \left| \frac{\mathbf{v}_m^H \mathbf{S}_n^{-1} \mathbf{v}_a}{\mathbf{v}_m^H \mathbf{S}_n^{-1} \mathbf{v}_m} \right|^2 = \sigma_s^2 \left| \frac{\mathbf{v}_m^H \boldsymbol{\rho}_n^{-1} \mathbf{v}_a}{\mathbf{v}_m^H \boldsymbol{\rho}_n^{-1} \mathbf{v}_m} \right|^2 \\ &= \sigma_s^2 \left( \frac{\mathbf{v}_a^H \boldsymbol{\rho}_n^{-1} \mathbf{v}_a}{\mathbf{v}_m^H \boldsymbol{\rho}_n^{-1} \mathbf{v}_m} \right) \cos^2(\mathbf{v}_m, \mathbf{v}_a : \boldsymbol{\rho}_n^{-1}). \end{aligned} \quad (6.207)$$

This can also be written in terms of the beam pattern of the MVDR beamformer.

$$P_s = \sigma_s^2 |B_{mvdr}(\mathbf{v}_a : \mathbf{v}_m)|^2. \quad (6.208)$$

The output noise power is

$$P_n = \Lambda = \left[ \mathbf{v}_m^H \mathbf{S}_n^{-1} \mathbf{v}_m \right]^{-1}, \quad (6.209)$$

which is unchanged from the nominal model. The output  $SNR_o$  is

$$SNR_o = \frac{\sigma_s^2 |\mathbf{v}_m^H \mathbf{S}_n^{-1} \mathbf{v}_a|^2}{\mathbf{v}_m^H \mathbf{S}_n^{-1} \mathbf{v}_m} = \frac{\sigma_s^2 |\mathbf{v}_m^H \boldsymbol{\rho}_n^{-1} \mathbf{v}_a|^2}{\sigma_n^2 \mathbf{v}_m^H \boldsymbol{\rho}_n^{-1} \mathbf{v}_m} \quad (6.210)$$

and the mismatched array gain is

$$A_{mvdr} = \frac{\left| \mathbf{v}_m^H \boldsymbol{\rho}_{\mathbf{n}}^{-1} \mathbf{v}_a \right|^2}{\mathbf{v}_m^H \boldsymbol{\rho}_{\mathbf{n}}^{-1} \mathbf{v}_m}. \quad (6.211)$$

The array gain can also be written as

$$A_{mvdr}(\mathbf{v}_a : \mathbf{v}_m) = \frac{|B_{mvdr}(\mathbf{v}_a : \mathbf{v}_m)|^2}{(\mathbf{v}_m^H \boldsymbol{\rho}_{\mathbf{n}}^{-1} \mathbf{v}_m)^{-1}} = |B_{mvdr}(\mathbf{v}_a : \mathbf{v}_m)|^2 A_o(\mathbf{v}_m). \quad (6.212)$$

We can normalize this expression by dividing by  $A_o(\mathbf{v}_m)$ ,

$$\frac{A_{mvdr}(\mathbf{v}_a : \mathbf{v}_m)}{A_o(\mathbf{v}_m)} = |B_{mvdr}(\mathbf{v}_a : \mathbf{v}_m)|^2. \quad (6.213)$$

Thus, the mismatch degradation is completely characterized by the optimum MVDR beam pattern steered to  $\mathbf{v}_m$ . As long as the interference is in the sidelobe region, the main lobe of the beam pattern is well-behaved, so we would anticipate a gradual degradation due to mismatch.

The expression in (6.212) includes two effects: the beamformer mismatch and the different matched array gain because  $\mathbf{v}_a \neq \mathbf{v}_m$ . We can isolate the mismatch effect by dividing by  $A_o(\mathbf{v}_a)$ ,

$$\frac{A_{mvdr}(\mathbf{v}_a : \mathbf{v}_m)}{A_o(\mathbf{v}_a)} = |B_{mvdr}(\mathbf{v}_a : \mathbf{v}_m)|^2 \frac{A_o(\mathbf{v}_m)}{A_o(\mathbf{v}_a)}. \quad (6.214)$$

We can also write the expression in (6.214) as

$$\frac{A_{mvdr}(\mathbf{v}_a : \mathbf{v}_m)}{A_o(\mathbf{v}_a)} = \frac{\left| \mathbf{v}_m^H \boldsymbol{\rho}_{\mathbf{n}}^{-1} \mathbf{v}_a \right|^2}{\left( \mathbf{v}_m^H \boldsymbol{\rho}_{\mathbf{n}}^{-1} \mathbf{v}_m \right) \left( \mathbf{v}_a^H \boldsymbol{\rho}_{\mathbf{n}}^{-1} \mathbf{v}_a \right)}. \quad (6.215)$$

Using (6.206), the right side can be written as the generalized cosine,

$$\frac{A_{mvdr}|_{\mathbf{v}_m \neq \mathbf{v}_a}}{A_{mvdr}|_{\mathbf{v}_m = \mathbf{v}_a}} = \cos^2 \left( \mathbf{v}_m, \mathbf{v}_a : \boldsymbol{\rho}_{\mathbf{n}}^{-1} \right), \quad (6.216)$$

which is always less than one. Its value depends on the angular separation of  $\mathbf{v}_m$  and  $\mathbf{v}_a$  and the noise field. The effect of the noise field enters through its eigenvalues and eigenvectors.

Denoting the eigenvalues and eigenvectors of  $\rho_n$  by  $(\lambda_1, \dots, \lambda_N)$  and  $(\Phi_1, \dots, \Phi_N)$ , respectively, we have

$$\begin{aligned}\cos^2(\mathbf{v}_m, \mathbf{v}_a : \rho_n^{-1}) &= \frac{\left| \mathbf{v}_m^H \Phi \Lambda^{-1} \Phi^H \mathbf{v}_a \right|^2}{(\mathbf{v}_m^H \Phi \Lambda^{-1} \Phi^H \mathbf{v}_m)(\mathbf{v}_a^H \Phi \Lambda^{-1} \Phi^H \mathbf{v}_a)} \\ &= \frac{\left| \sum_{i=1}^N \frac{\rho_{mi}^* \rho_{si}}{\lambda_i} \right|^2}{\sum_{i=1}^N \frac{|\rho_{mi}|^2}{\lambda_i} \sum_{i=1}^N \frac{|\rho_{si}|^2}{\lambda_i}},\end{aligned}\quad (6.217)$$

where  $\rho_{mi}$  is the correlation between  $\mathbf{v}_m$  and  $\Phi_i$  and  $\rho_{si}$  is the correlation between  $\mathbf{v}_a$  and  $\Phi_i$ . (Recall that  $\sum \lambda_i = N$  because of the normalization.) Thus, the  $\cos^2$  function emphasizes the components of  $\mathbf{v}_m$  and  $\mathbf{v}_a$  corresponding to small eigenvalues and de-emphasizes those corresponding to large eigenvalues.

#### Example 6.6.1

Consider a standard 10-element linear array. The interference consists of a single plane-wave interferer plus white noise. We assume the interferer is at  $u_I = 0.30$ . We assume  $|u_a| \leq 0.1$ . In Figure 6.32, we plot the expressions in (6.213) for an  $INR = 10$  dB ( $INR \triangleq \frac{\sigma_s^2}{\sigma_w^2}$ ). The plot is insensitive to the  $INR$  value.

#### Example 6.6.2 (continuation)

Consider the same model as in Example 6.6.1 except  $u_I$  is inside the main lobe. In Figure 6.33(a), we assume  $u_I = 0.0433$  and plot the expression in (6.213) for several values of  $INR$ . In Figure 6.33(b), we assume  $u_I = 0.02$  and plot the same results.

We see that the array gain is very sensitive to mismatch for both values of  $u_I$ . If the actual signal DOA moves away from the interferer's location,  $u_I$ , the normalized array gain increases dramatically. However, if the actual signal DOA moves toward  $u_I$ , the normalized array gain approaches zero. In some applications, this variation may be acceptable. However, in most cases, we will want to impose additional constraints in order to maintain reasonably constant performance in the presence of small DOA mismatch.

#### 6.6.2.3 MPDR beamformer

In this beamformer, the spectral matrix of the *entire* input is inverted instead of the noise-only input. From the results with discrete interference in Section 6.2, we can anticipate what will happen when  $\mathbf{v}_m \neq \mathbf{v}_a$ . The processor will treat the signal along  $\mathbf{v}_a$  as a discrete interfering signal and will put a partial null in its direction. In the limit, as  $\sigma_s^2$  approaches infinity, it will become a perfect null and the signal will be completely eliminated.

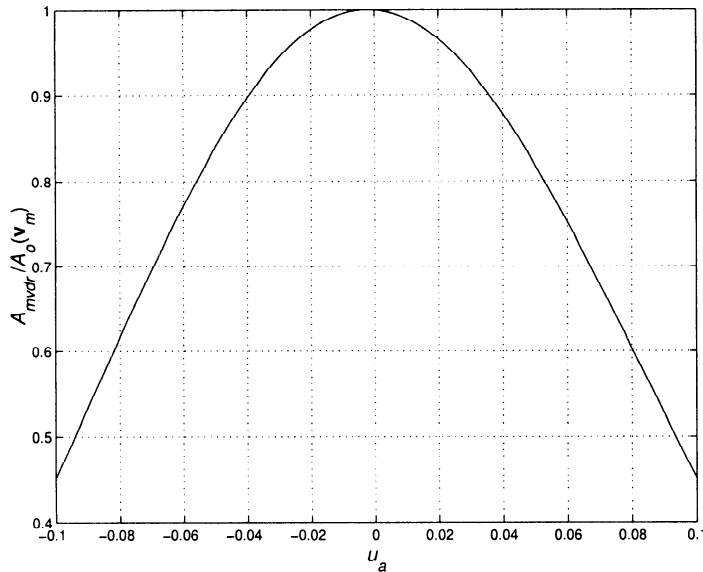


Figure 6.32 Normalized array gain of MVDR beamformer in the presence of mismatch (normalized by  $A_o(v_m)$ ) single plane-wave interferer with  $INR = 10$  dB at  $u_I = 0.3$ ,  $u_m = 0$ .

The array gain is obtained from (6.73),

$$A_{mpdr} = \frac{|\mathbf{v}_m^H \mathbf{S}_x^{-1} \mathbf{v}_a|^2}{\mathbf{v}_m^H \mathbf{S}_x^{-1} \boldsymbol{\rho}_n \mathbf{S}_x^{-1} \mathbf{v}_m}. \quad (6.218)$$

The spatial spectral matrix is

$$\mathbf{S}_x = \sigma_s^2 \mathbf{v}_a \mathbf{v}_a^H + \sigma_n^2 \boldsymbol{\rho}_n, \quad (6.219)$$

where

$$\sigma_n^2 = \sigma_w^2 + \frac{1}{N} \text{tr} [\mathbf{S}_c]. \quad (6.220)$$

In (6.220),  $\mathbf{S}_c$  denotes the non-white noise component. We use the matrix inversion lemma to obtain

$$\mathbf{S}_x^{-1} = \frac{1}{\sigma_n^2} \boldsymbol{\rho}_n^{-1} \left\{ \mathbf{I} - \mathbf{v}_a \mathbf{v}_a^H \boldsymbol{\rho}_n^{-1} \frac{\sigma_s^2}{\sigma_n^2} \left( 1 + \frac{\sigma_s^2}{\sigma_n^2} \mathbf{v}_a^H \boldsymbol{\rho}_n^{-1} \mathbf{v}_a \right)^{-1} \right\}. \quad (6.221)$$

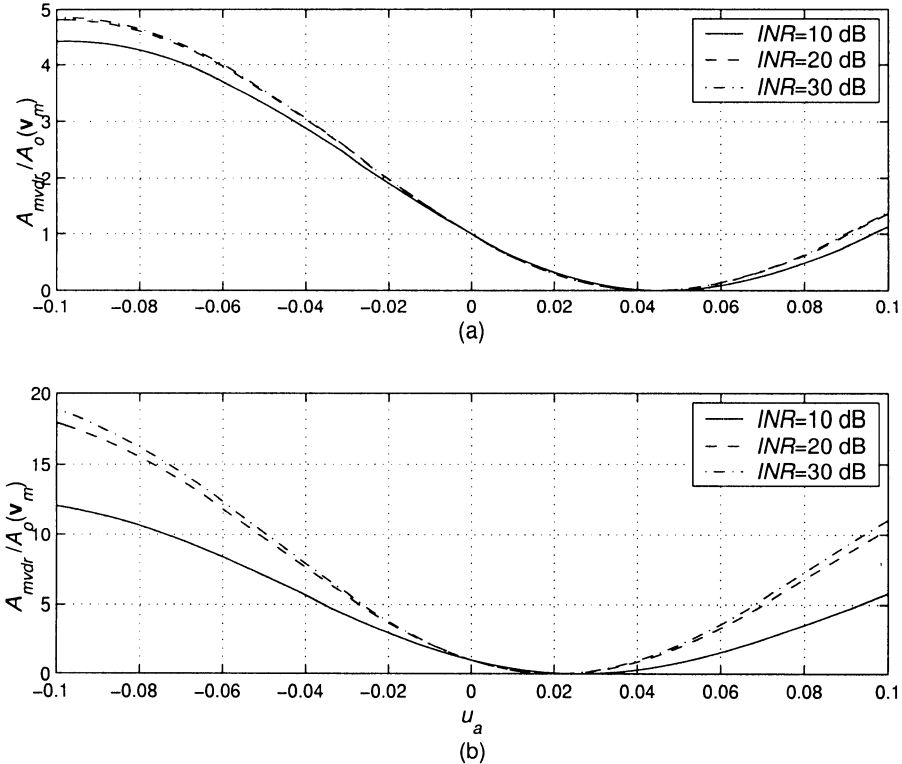


Figure 6.33 Normalized array gain,  $A_{mvdr}(\mathbf{v}_a : \mathbf{v}_m) / A_o(\mathbf{v}_m)$ , of MVDR beamformer in the presence of mismatch: (a)  $u_I = 0.0433$ ; (b)  $u_I = 0.02$ .

To evaluate the numerator in (6.218), we write

$$\mathbf{v}_m^H \mathbf{S}_{\mathbf{x}}^{-1} \mathbf{v}_a = \frac{1}{\sigma_n^2} \left\{ \mathbf{v}_m^H \boldsymbol{\rho}_{\mathbf{n}}^{-1} \mathbf{v}_a \left[ 1 - \mathbf{v}_a^H \boldsymbol{\rho}_{\mathbf{n}}^{-1} \mathbf{v}_a \frac{\sigma_s^2}{\sigma_n^2} \left( 1 + \frac{\sigma_s^2}{\sigma_n^2} \mathbf{v}_a^H \boldsymbol{\rho}_{\mathbf{n}}^{-1} \mathbf{v}_a \right)^{-1} \right] \right\}. \quad (6.222)$$

We denote the output *SNR* of an MVDR processor that is matched to  $\mathbf{v}_a$  as  $M$ ,

$$M = \frac{\sigma_s^2}{\sigma_n^2} \mathbf{v}_a^H \boldsymbol{\rho}_{\mathbf{n}}^{-1} \mathbf{v}_a. \quad (6.223)$$

Then (6.222) can be written as

$$\mathbf{v}_m^H \mathbf{S}_{\mathbf{x}}^{-1} \mathbf{v}_a = \frac{\mathbf{v}_m^H \boldsymbol{\rho}_{\mathbf{n}}^{-1} \mathbf{v}_a}{\sigma_n^2 (1 + M)}. \quad (6.224)$$

To evaluate the denominator in (6.218), we write

$$\begin{aligned} \mathbf{v}_m^H \mathbf{S}_{\mathbf{x}}^{-1} \boldsymbol{\rho}_{\mathbf{n}} \mathbf{S}_{\mathbf{x}}^{-1} \mathbf{v}_m &= \mathbf{v}_m^H \frac{1}{\sigma_n^2} \boldsymbol{\rho}_{\mathbf{n}}^{-1} \left[ \mathbf{I} - \mathbf{v}_a \mathbf{v}_a^H \boldsymbol{\rho}_{\mathbf{n}}^{-1} \frac{\sigma_s^2}{\sigma_n^2} (1+M)^{-1} \right] \\ &\quad \cdot \boldsymbol{\rho}_{\mathbf{n}} \frac{1}{\sigma_n^2} \boldsymbol{\rho}_{\mathbf{n}}^{-1} \left[ \mathbf{I} - \mathbf{v}_a \mathbf{v}_a^H \boldsymbol{\rho}_{\mathbf{n}}^{-1} \frac{\sigma_s^2}{\sigma_n^2} (1+M)^{-1} \right] \mathbf{v}_m. \end{aligned} \quad (6.225)$$

This reduces to

$$\begin{aligned} \mathbf{v}_m^H \mathbf{S}_{\mathbf{x}}^{-1} \boldsymbol{\rho}_{\mathbf{n}} \mathbf{S}_{\mathbf{x}}^{-1} \mathbf{v}_m &= \frac{1}{\sigma_n^4} \mathbf{v}_m^H \boldsymbol{\rho}_{\mathbf{n}}^{-1} \mathbf{v}_m \left[ 1 - 2|B_{mvdr}|^2 \mathbf{v}_m^H \boldsymbol{\rho}_{\mathbf{n}}^{-1} \mathbf{v}_m \frac{\sigma_s^2}{\sigma_n^2} (1+M)^{-1} \right. \\ &\quad \left. + |B_{mvdr}|^2 \mathbf{v}_m^H \boldsymbol{\rho}_{\mathbf{n}}^{-1} \mathbf{v}_m \frac{M}{(1+M)^2} \frac{\sigma_s^2}{\sigma_n^2} \right], \end{aligned} \quad (6.226)$$

where the argument of  $B_{mvdr}$  is suppressed. The form of this expression can be simplified if we use the generalized cosine notation and the relationship

$$\sin^2(\mathbf{v}_m, \mathbf{v}_a; \boldsymbol{\rho}_{\mathbf{n}}^{-1}) = 1 - \cos^2(\mathbf{v}_m, \mathbf{v}_a; \boldsymbol{\rho}_{\mathbf{n}}^{-1}). \quad (6.227)$$

Using these definitions in (6.226), the denominator becomes

$$DEN = \frac{1}{\sigma_n^4} \mathbf{v}_m^H \boldsymbol{\rho}_{\mathbf{n}}^{-1} \mathbf{v}_m (1+M)^2 \left[ 1 + (2M + M^2) \sin^2(\mathbf{v}_m, \mathbf{v}_a; \boldsymbol{\rho}_{\mathbf{n}}^{-1}) \right]. \quad (6.228)$$

Using (6.228) and the magnitude squared of (6.224) in (6.218) gives

$$A_{mpdr}(\mathbf{v}_a : \mathbf{v}_m) = \frac{\mathbf{v}_m^H \boldsymbol{\rho}_{\mathbf{n}}^{-1} \mathbf{v}_m |B_{mvdr}(\mathbf{v}_a : \mathbf{v}_m)|^2}{1 + [2M + M^2] \sin^2(\mathbf{v}_m, \mathbf{v}_a; \boldsymbol{\rho}_{\mathbf{n}}^{-1})}, \quad (6.229)$$

or equivalently,

$$A_{mpdr} = \boxed{\frac{\mathbf{v}_a^H \boldsymbol{\rho}_{\mathbf{n}}^{-1} \mathbf{v}_a \cos^2(\mathbf{v}_m, \mathbf{v}_a; \boldsymbol{\rho}_{\mathbf{n}}^{-1})}{1 + [2M + M^2] \sin^2(\mathbf{v}_m, \mathbf{v}_a; \boldsymbol{\rho}_{\mathbf{n}}^{-1})}}. \quad (6.230)$$

Note that either (6.229) or (6.230) can be written in terms of MVDR array gain in a perfectly matched environment,

$$\begin{aligned} A_{mpdr}(\mathbf{v}_a : \mathbf{v}_m) &= \left\{ \frac{A_o(\mathbf{v}_m) |B_o(\mathbf{v}_a : \mathbf{v}_m)|^2}{1 + [2M + M^2] \sin^2(\mathbf{v}_m, \mathbf{v}_a; \boldsymbol{\rho}_{\mathbf{n}}^{-1})} \right\} \\ &= \left\{ \frac{A_o(\mathbf{v}_a) \cos^2(\mathbf{v}_m, \mathbf{v}_a; \boldsymbol{\rho}_{\mathbf{n}}^{-1})}{1 + [2M + M^2] \sin^2(\mathbf{v}_m, \mathbf{v}_a; \boldsymbol{\rho}_{\mathbf{n}}^{-1})} \right\}. \end{aligned} \quad (6.231)$$

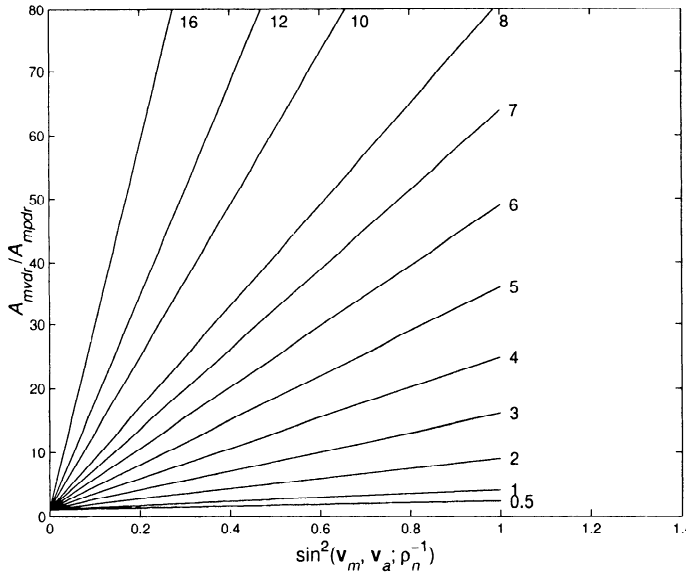


Figure 6.34 Ratio of  $A_{mvdr}$  to  $A_{mpdr}$  versus  $\sin^2(\mathbf{v}_m, \mathbf{v}_a; \rho_n^{-1})$  for various  $M$ .

The numerator of (6.231) is just the array gain of the MVDR filter in the presence of the mismatch. Thus, the denominator of (6.231) indicates the effect of including the signal in the matrix inversion. The ratio of the two array gains is

$$\frac{A_{mvdr}(\mathbf{v}_a : \mathbf{v}_m)}{A_{mpdr}(\mathbf{v}_a : \mathbf{v}_m)} = 1 + [2M + M^2] \sin^2(\mathbf{v}_m, \mathbf{v}_a; \rho_n^{-1}). \quad (6.232)$$

The result in (6.232) is due to Cox [Cox73].

In Figure 6.34, the array gain ratio is plotted versus  $\sin^2(\mathbf{v}_m, \mathbf{v}_a; \rho_n^{-1})$  for various values of the maximum *SNR*. Since the gain ratio depends on  $M^2 \sin^2(\mathbf{v}_m, \mathbf{v}_a; \rho_n^{-1})$ , large values of  $M$  can cause significant signal suppression. For example, if  $M = 10$  and  $\sin^2(\mathbf{v}_m, \mathbf{v}_a; \rho_n^{-1}) = 0.5$ , then the array gain ratio is 61. The output *SNR* of  $\mathbf{w}_o^H$  is 5.0 and the output *SNR* of  $\mathbf{w}_{mpdr}^H$  is 0.082. As we would expect from our directional noise examples, weak signals suffer less suppression than strong signals.

The results in (6.230) and (6.232) are useful general expressions. However, examining some specific array geometries will give additional insight.

Note that, for white noise, (6.230) reduces to

$$A_{mpdr}(\mathbf{v}_a : \mathbf{v}_m) = \frac{N |\rho_{ma}|^2}{1 + [2M + M^2][1 - |\rho_{ma}|^2]}, \quad (6.233)$$

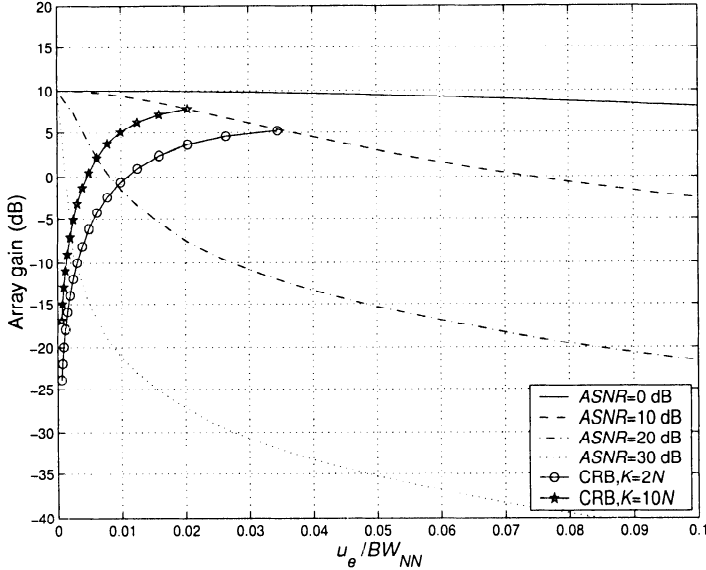


Figure 6.35 Array gain of MPDR beamformer versus  $\frac{u_e}{BW_{NN}}: N = 10$ ,  $ASNR = -10 \text{ dB}, \dots, 30 \text{ dB}$ .

where

$$|\rho_{ma}|^2 = \cos^2(\mathbf{v}_m, \mathbf{v}_a; \mathbf{I}) = |B_c(\mathbf{v}_a : \mathbf{v}_m)|^2, \quad (6.234)$$

and

$$M = N \frac{\sigma_s^2}{\sigma_w^2} \triangleq ASNR \quad (6.235)$$

is the optimum array output  $SNR$  in the presence of white noise. The actual output  $SNR$  is

$$SNR_o = \frac{\sigma_s^2}{\sigma_w^2} A_{mpdr}(\mathbf{v}_a : \mathbf{v}_m). \quad (6.236)$$

We consider an example to illustrate the behavior.

#### Example 6.6.3

Consider a standard  $N$ -element linear array where the interference is white noise. In Figure 6.35, we plot the array gain in (6.233) versus  $\Delta u/BW_{NN}$  for various values of  $M$ . The result in Figure 6.35 is valid for  $N \geq 10$ . We see that if the  $ASNR$  is high (e.g.,  $\geq 10$  dB) there is significant degradation for small  $\Delta u/BW_{NN}$ .

We see that as the  $SNR$  increases the performance degrades significantly with very small DOA mismatch. Therefore, if DOA mismatch is anticipated in the application of interest, then we need to find techniques to avoid the degradation illustrated in Figures 6.34 and 6.35.

Techniques that appear feasible include:

- (i) Impose additional constraints on the beamformer to prevent (or decrease) the signal nulling. We consider quadratic constraints in Sections 6.6.4 and 6.10. We will find that quadratic constraints lead to a technique called **diagonal loading**. This technique designs the beamformer by assuming that the white noise  $\sigma_w^2$  is higher than its actual value. We consider linear constraints in Section 6.7.
- (ii) Eliminate (or reduce) the signal component before estimating  $\mathbf{S}_x$ . If we could achieve perfect signal elimination, then the MPDR beamformer would become an MVDR beamformer. This is possible in some applications.
- (iii) The degradation relative to perfectly matched performance becomes worse as the *SNR* increases. When we study parameter estimation, we find that the accuracy with which we can estimate the DOA of a plane-wave signal increases with the *ASNR*. We show that for a single plane-wave signal impinging on a standard linear array in the presence of white Gaussian noise the root-mean-square error in estimating  $u_a$  is

$$\frac{(E[|\hat{u}_a - u_a|^2])^{\frac{1}{2}}}{BW_{NN}} = \left( \frac{3}{8K} \left[ \frac{1}{ASNR} + \frac{1}{ASNR^2} \right] \frac{1}{1 - \frac{1}{N^2}} \right)^{\frac{1}{2}} \quad (6.237)$$

for  $ASNR \geq 10$  dB. In (6.237),  $K$  denotes the number of snapshots. The estimator for this case is simple to implement. In Figure 6.35, we have superimposed the normalized version of (6.237) onto the plot in Figure 6.35 for  $ASNR \geq 10$  dB and relabeled the axis as  $u_e/BW_{NN} = (\hat{u}_a - u_a)/BW_{NN}$ . For our current purposes, it provides a guideline as to the maximum amount of mismatch that must be considered in a beamformer that includes a preliminary estimation step.

We refer to beamformers that attempt to preserve good performance in the presence of mismatch as **robust beamformers**. A minimal goal for robust beamformers is that their performance should never degrade below the performance of a conventional beamformer (or some other classical beamformer from Chapter 3 or 4) due to allowable mismatch scenarios. In the course of our development, we will see if this is a realistic goal. Note that this goal is not a useful mathematical statement because we have not identified any positive performance objective (such as maximum  $SNR_o$  in the absence of mismatch).

Before considering solutions to the DOA mismatch problem, we consider the array perturbation problem and show that it causes a similar degradation.

### 6.6.3 Array Perturbations

In this section, we discuss how array perturbations affect the performance of the MVDR beamformer and the MPDR beamformer. We recall from Chapter 2, that the effect of random errors in sensor gain and phase and sensor position was to add a constant floor to the beam pattern whose height was inversely proportional to the array gain in the presence of white noise,  $A_w$ . If the weight vector was normalized such that

$$\mathbf{w}^H \mathbf{v}_s = 1, \quad (6.238)$$

then

$$A_w = \left\{ \| \mathbf{w} \|^2 \right\}^{-1}, \quad (6.239)$$

so that, as the norm of the weight vector increased, the sensitivity to array perturbations increased.

In this section, we investigate the behavior of the output signal-to-noise ratio ( $SNR_o$ ) of MVDR and MPDR beamformers in the presence of array perturbations.

This problem has been analyzed using various perturbation models in a number of references (e.g., Nitzberg [Nit76], Kleinberg [Kle80], Mucci and Pridham [MP81], Farrier [Far83], Quazi [Qua82], Godara [God85], [God86], and Youn and Un [YU94]).

The general frequency-domain snapshot model can be written as

$$\mathbf{X}(\omega) = \mathbf{V}(\psi, \rho) \mathbf{F}(\omega) + \mathbf{W}(\omega), \quad (6.240)$$

where  $\mathbf{F}(\omega)$  is a composite source signal matrix that contains both the desired signal  $F_d(\omega)$  and the  $D$  plane-wave interfering signals  $\mathbf{F}_I(\omega)$ . The vector  $\psi$  describes the angles of arrival of the  $D+1$  signals in  $\psi$ -space. The vector  $\rho$  is a real  $M \times 1$  vector that represents the perturbations in the array parameters. The additive white noise has spectral height  $\sigma_w^2$ . For notational simplicity, we assume that the array lies along the  $x$ -axis and assume the signals lie in the  $xy$ -plane. Thus, the direction of arrival of signals can be described by a scalar variable. We return to the 3-D case later.

We first assume that  $\rho$  is a real Gaussian random vector

$$p_{\rho}(\rho) = \frac{1}{(2\pi)^{\frac{M}{2}} |\Lambda_{\rho}|^{\frac{1}{2}}} \exp \left\{ -\frac{1}{2} (\rho - \rho_0)^T \Lambda_{\rho}^{-1} (\rho - \rho_0) \right\}, \quad (6.241)$$

where  $\rho_0$  represents the nominal value of the parameter vector  $\rho$  and  $\Lambda_\rho$  is the covariance matrix. Later, we consider the case when  $\rho$  is a real unknown nonrandom vector.

We rewrite the array manifold vector to include the gain and phase of each sensor explicitly.

$$\mathbf{v}(\psi_i, \rho) = \left[ a_o e^{j\phi_0} e^{j\frac{2\pi}{\lambda} \mathbf{u}_i^T \mathbf{p}_0} \mid \dots \mid a_o e^{j\phi_{N-1}} e^{j\frac{2\pi}{\lambda} \mathbf{u}_i^T \mathbf{p}_{N-1}} \right]^T. \quad (6.242)$$

In the general case, the  $\rho$  vector is a  $5N \times 1$  vector containing a gain, phase, and position vectors. Define

$$[\mathbf{a}]_n = a_n^n(1 + \Delta a_n), \quad n = 0, \dots, N - 1, \quad (6.243)$$

$$[\phi]_n = \phi_n^n + \Delta\phi_n, \quad n = 0, \dots, N - 1, \quad (6.244)$$

$$[\mathbf{p}_x]_n = p_{xn}^n + \Delta p_{xn}, \quad n = 0, \dots, N - 1, \quad (6.245)$$

$$[\mathbf{p}_y]_n = p_{yn}^n + \Delta p_{yn}, \quad n = 0, \dots, N - 1, \quad (6.246)$$

$$[\mathbf{p}_z]_n = p_{zn}^n + \Delta p_{zn}, \quad n = 0, \dots, N - 1. \quad (6.247)$$

The superscript “ $n$ ” denotes the nominal value. This model is similar to the model in Section 2.6.3. Then,  $\rho$  is

$$\rho = \left[ \mathbf{a}^T \quad \phi^T \quad \mathbf{p}_x^T \quad \mathbf{p}_y^T \quad \mathbf{p}_z^T \right]^T. \quad (6.248)$$

In most cases we study a subset of the possible variations and  $\rho$  has a smaller dimension. The probability density of  $\rho$  is given by (6.241).

In the second perturbation model, we combine  $\mathbf{a}$  and  $\phi$  into a complex vector  $\mathbf{g}$ ,

$$g_n = a_n e^{j\phi_n}, \quad n = 0, \dots, N - 1, \quad (6.249)$$

where

$$g_n = (1 + \Delta a_n) e^{j\Delta\phi_n}, \quad n = 0, 1, \dots, N - 1, \quad (6.250)$$

where  $\Delta a_n$  and  $\Delta\phi_n$  are the amplitude and phase errors. For small errors,

$$g_n \simeq 1 + \Delta a_n + j\Delta\phi_n \triangleq 1 + \Delta g_n. \quad (6.251)$$

If the gain and phase errors are independent with equal variances  $\sigma_g^2 = \sigma_\phi^2$ , then  $\Delta g_n$  is a zero-mean circular complex random variable. Then,

$$E [\Delta g_i \Delta g_i^*] = 2\sigma_g^2. \quad (6.252)$$

Thus, for small perturbations and equal variance for the gain and phase errors, the two models are the same.

This second model is more restrictive than the first model. The advantage of the second model is that it leads to analytic results in some cases where the first model is analytically difficult.

We consider two examples to illustrate the effect of array perturbations.

#### Example 6.6.4

Consider a standard 10-element linear array along the  $x$ -axis. The signal arrives from broadside and the interferer arrives at  $u_x = 0.30$ ,  $u_y = 0$  with an  $INR = 20$  dB. Assume that the sensor positions are subject to random perturbations in the  $x$  and  $y$  directions. The perturbations are statistically independent zero-mean Gaussian random variables with standard deviation  $\sigma_p$ , where  $\sigma_p = 0, 0.05\lambda, 0.1\lambda$ , and  $0.2\lambda$ . The perturbations are constant during the snapshot sequence. Thus, the actual array manifold vector,  $\mathbf{v}_p$ , is the random vector defined by (6.246). We assume that the actual spatial spectral matrix  $\mathbf{S}_{x,p}$  is available to design the beamformer. In an actual adaptive beamformer,  $\mathbf{S}_{x,p}$  will be the matrix we estimate. We design the beamformer using  $\mathbf{v}_m$ , the nominal array manifold vector. Thus, using (6.71),

$$\mathbf{w}_{mpdr,p}^H = \frac{\mathbf{v}_m^H \mathbf{S}_{x,p}^{-1}}{\mathbf{v}_m^H \mathbf{S}_{x,p}^{-1} \mathbf{v}_m}. \quad (6.253)$$

In Figure 6.36, we plot the expected value of the array gain versus input  $SNR$  for various  $\sigma_p^2$ . We see that the array perturbations cause the array manifold vector  $\mathbf{v}_m$  to be mismatched. As the  $SNR$  increases, the beamformer attempts to null out the mismatched signal and the array gain decreases.

#### Example 6.6.5

Consider a standard 10-element linear array. We consider only gain errors and use the first perturbation model. The interference consists of white sensor noise.

The actual received spectral matrix is

$$\mathbf{S}_{xa} = \sigma_d^2 \tilde{\mathbf{v}}_d \tilde{\mathbf{v}}_d^H + \sigma_w^2 \mathbf{I}, \quad (6.254)$$

where

$$\tilde{\mathbf{v}}_d \triangleq \mathbf{v}_s(\psi, \mathbf{a}) \quad (6.255)$$

and

$$a_n = 1 + \Delta a_n, n = 0, 1, \dots, N - 1. \quad (6.256)$$

The  $\Delta a_n$  are independent zero mean, and

$$\sigma_g^2 \triangleq E[|\Delta a_n|^2], \quad n = 0, 1, \dots, N - 1. \quad (6.257)$$

The beamformer uses  $\mathbf{S}_{xa}$  to find the optimum MPDR weight vector

$$\mathbf{w}^H = \frac{\mathbf{v}_d^H \mathbf{S}_{xa}^{-1}}{\mathbf{v}_d^H \mathbf{S}_{xa}^{-1} \mathbf{v}_d}. \quad (6.258)$$

Note that (6.258) would imply perfect knowledge of  $\mathbf{S}_{xa}$ . In practice, we use  $\hat{\mathbf{S}}_{xa}$ , and (6.258) represents the limiting behavior of the weight vector. In this case, one can find the  $SNR_o$  analytically (e.g., [YU94]). The result is

$$SNR_o = SNR_{in} \left\{ \frac{N + \sigma_g^2}{(1 + (N - 1)\sigma_g^2 SNR_{in})^2 + (N - 1)(N + \sigma_g^2)\sigma_g^2 SNR_{in}^2} \right\}. \quad (6.259)$$

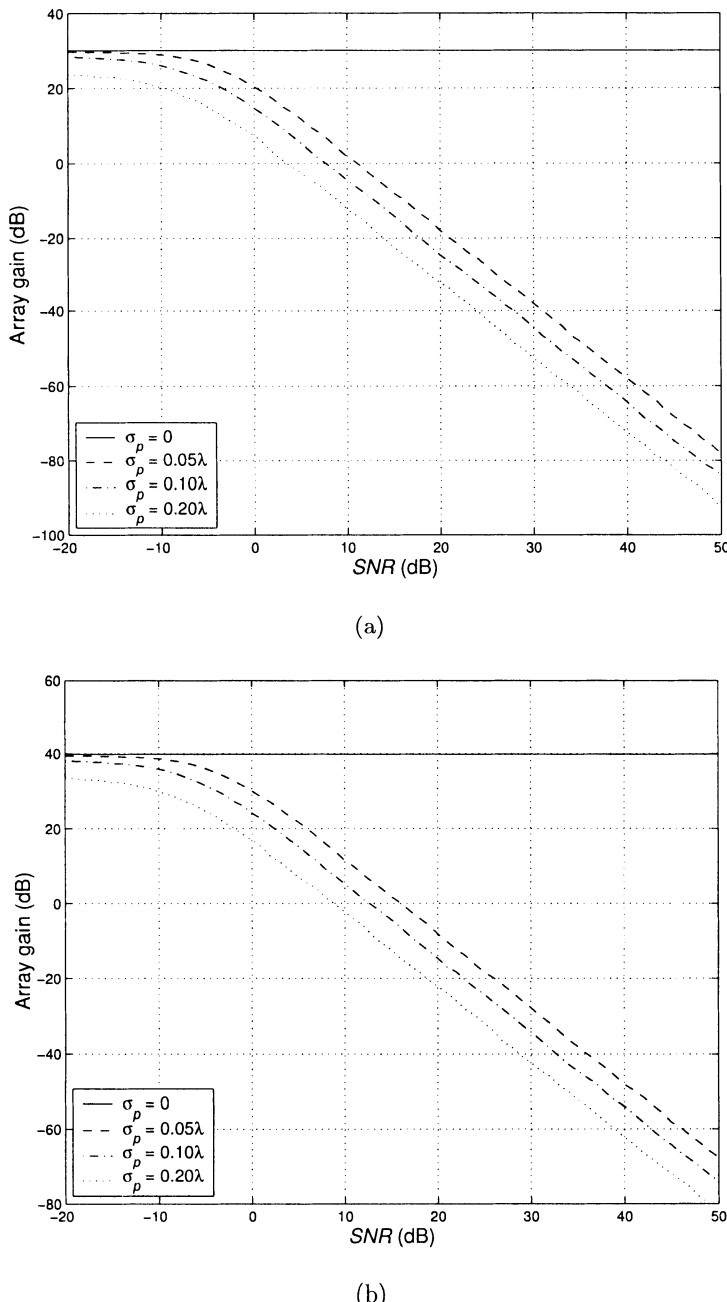
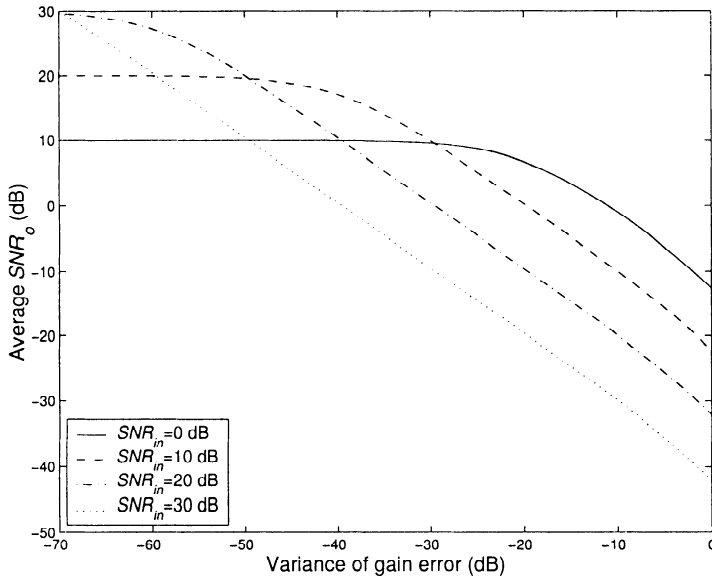


Figure 6.36 Array gain of MPDR beamformer versus  $SNR$  for various  $\sigma_p$ :  $N = 10$ ,  $u_s = 0$ ,  $u_I = 0.30$ ; 500 trials; (a)  $INR = 20$  dB; (b)  $INR = 30$  dB.

Figure 6.37  $SNR_o$  versus  $\sigma_g^2$ .

For  $N \gg 1$ ,  $N \gg \sigma_g^2$  and large  $SNR_{in}$ ,

$$SNR_o \cong \frac{1}{N\sigma_g^2(1 + \sigma_g^2)SNR_{in}}. \quad (6.260)$$

The output  $SNR_o$  is plotted versus  $\sigma_g^2$  in Figure 6.37 for  $N = 10$ . We see that if the  $SNR_{in}$  is large, there is significant degradation for small  $\sigma_g^2$  and the slope is 10 dB per decade, as indicated by (6.260).

#### 6.6.4 Diagonal Loading

We have observed that the sensitivity of the MPDR beamformer to signal DOA mismatch and array perturbations increases as  $\|\mathbf{w}\|^2$  increases. This suggests the use of a quadratic constraint,

$$\|\mathbf{w}\|^2 \leq T_o, \quad (6.261)$$

where  $T_o$  is a design parameter. From the discussion in Section 2.6.2, we know that

$$T_o \geq \frac{1}{N}. \quad (6.262)$$

We explore the choice of  $T_o$  in Section 6.10. In this section, we show how the imposition of a quadratic constraint leads to a procedure that we refer to as **diagonal loading (DL)**.

The quadratically constrained MPDR optimization problem is:

$$\text{Minimize} \quad \mathbf{w}^H \mathbf{S}_x \mathbf{w}, \quad (6.263)$$

subject to the distortionless constraint,

$$\mathbf{w}^H \mathbf{v}_m = 1, \quad (6.264)$$

and the quadratic constraint,

$$\mathbf{w}^H \mathbf{w} = T_o. \quad (6.265)$$

We have used an equality constraint for simplicity. We explore the inequality constraint in Section 6.10.

The function to minimize is

$$\begin{aligned} F &\triangleq \mathbf{w}^H \mathbf{S}_x \mathbf{w} + \lambda_1 [\mathbf{w}^H \mathbf{w} - T_o] \\ &\quad + \lambda_2 [\mathbf{w}^H \mathbf{v}_m - 1] + \lambda_2^* [\mathbf{v}_m^H \mathbf{w} - 1]. \end{aligned} \quad (6.266)$$

Differentiating with respect to  $\mathbf{w}$  and setting the result to zero gives

$$\mathbf{w}^H \mathbf{S}_x + \lambda_1 \mathbf{w}^H + \lambda_2^* \mathbf{v}_m^H = 0. \quad (6.267)$$

Solving for  $\mathbf{w}^H$  and solving for  $\lambda_2^*$  by imposing the constraint in (6.264), gives

$$\mathbf{w}^H = \frac{\mathbf{v}_m^H [\mathbf{S}_x + \lambda_1 \mathbf{I}]^{-1}}{\mathbf{v}_m^H [\mathbf{S}_x + \lambda_1 \mathbf{I}]^{-1} \mathbf{v}_m}. \quad (6.268)$$

We see that the effect of the quadratic constraint (QC) is to add a diagonal matrix to  $\mathbf{S}_x$  in the formula for  $\mathbf{w}^H$ . In effect, the MPDR-QC weight vector is designing for a higher white noise level than is actually present.

The value of  $\lambda_1$  depends on the choice of  $T_o$ . In this section, we use a simpler approach and specify  $\lambda_1$  directly. In Section 6.10, we see that this approach is not optimum. However, it is adequate in many cases and is widely used in practice. To emphasize the decoupling from  $T_o$ , we rewrite (6.268) as

$$\mathbf{w}^H = \frac{\mathbf{v}_m^H [\mathbf{S}_x + \sigma_L^2 \mathbf{I}]^{-1}}{\mathbf{v}_m^H [\mathbf{S}_x + \sigma_L^2 \mathbf{I}]^{-1} \mathbf{v}_m}. \quad (6.269)$$

Rewriting (6.269) as

$$\mathbf{w}_{mpdr,dl}^H = \frac{\mathbf{v}_m^H [\mathbf{I} + \frac{\mathbf{S}_x}{\sigma_L^2}]^{-1}}{\mathbf{v}_m^H [\mathbf{I} + \frac{\mathbf{S}_x}{\sigma_L^2}]^{-1} \mathbf{v}_m}, \quad (6.270)$$

we see that, as  $\sigma_L^2 \rightarrow \infty$ , the MPDR-DL beamformer approaches the conventional beamformer.

We can write  $\mathbf{S}_x$  as

$$\mathbf{S}_x = \sigma_s^2 \mathbf{v}_a \mathbf{v}_a^H + \mathbf{S}_c + \sigma_w^2 \mathbf{I}, \quad (6.271)$$

where  $\mathbf{v}_a$  is the actual array manifold vector,  $\mathbf{S}_c$  is the non-white interference, and  $\sigma_w^2 \mathbf{I}$  is the uncorrelated noise component. We define the load-to-white noise level (*LNR*) as

$$LNR = \frac{\sigma_L^2}{\sigma_w^2}. \quad (6.272)$$

We consider two examples to illustrate how diagonal loading affects the performance.

#### Example 6.6.6: MPDR-DL beamformer; mismatched signal

Consider a standard 10-element linear array. The array is steered to broadside ( $\mathbf{v}_m = \mathbf{1}$ ). The interference consists of two equal-power uncorrelated plane-wave signals located at  $u_I = \pm 0.30$ . Thus,

$$\mathbf{S}_x = \sigma_s^2 \mathbf{v}_a \mathbf{v}_a^H + \sum_{i=1}^2 \sigma_i^2 \mathbf{v}_i \mathbf{v}_i^H + \sigma_w^2 \mathbf{I}. \quad (6.273)$$

We utilize the beamformer in (6.269) and plot the array gain for various values of *SNR*, *INR*, and *LNR* versus  $\frac{u_a}{BW_{NN}}$ . Figure 6.38 corresponds to an *INR* = 30 dB.

In Figure 6.38(a), we plot the array gain versus  $\frac{u_a}{BW_{NN}}$  for various input *SNR* with no loading. We see that there is significant degradation for  $SNR > -10$  dB. In Figure 6.38(b), we plot the array gain versus  $\frac{u_a}{BW_{NN}}$  with 20-dB *LNR*. We see that loading provides adequate performance for  $SNR \leq 10$  dB. In Figure 6.38(c), we plot the array gain versus  $\frac{u_a}{BW_{NN}}$  with 30-dB *LNR*. The curve for high input *SNR* has improved somewhat because we are not nulling the signal as deeply. However, the *LNR* equals the *INR*, so we are not nulling the interferers adequately.

In order to compare results in a more compact manner, we model  $u_a$  as a uniform random variable between  $\pm 0.1$ ,

$$p_{u_a} = \begin{cases} 5 & |u_a| \leq 0.1 \\ 0 & \text{elsewhere.} \end{cases} \quad (6.274)$$

The motivation for choosing an uncertainty range of  $\pm 0.1$  ( $= \frac{1}{N}$  for a 10-element array) is the following scenario. We want to scan over  $u$ -space ( $-1 \leq u \leq 1$ ) by forming optimal beams whose steering directions are spaced by  $\frac{2}{N}$ . This spacing leads to orthogonal conventional beams whose main lobes intersect at  $\pm \frac{1}{N}, \pm \frac{3}{N}, \dots$ . Therefore, any signal with  $|u_a - u_m| \leq \frac{1}{N}$  would be processed by the beamformer. Signals with  $\frac{1}{N} < |u_a - u_m| < \frac{3}{N}$  would be processed by the adjacent beamformers.

There are cases in which the uncertainty in  $u_a$  may be much less than this. We could use closer beam spacing or we could do preliminary processing to estimate  $\hat{u}_a$ . If we estimate  $u_a$ , we would use a Gaussian probability density for  $u_a$  instead of the uniform density in (6.274). We discuss these cases later.

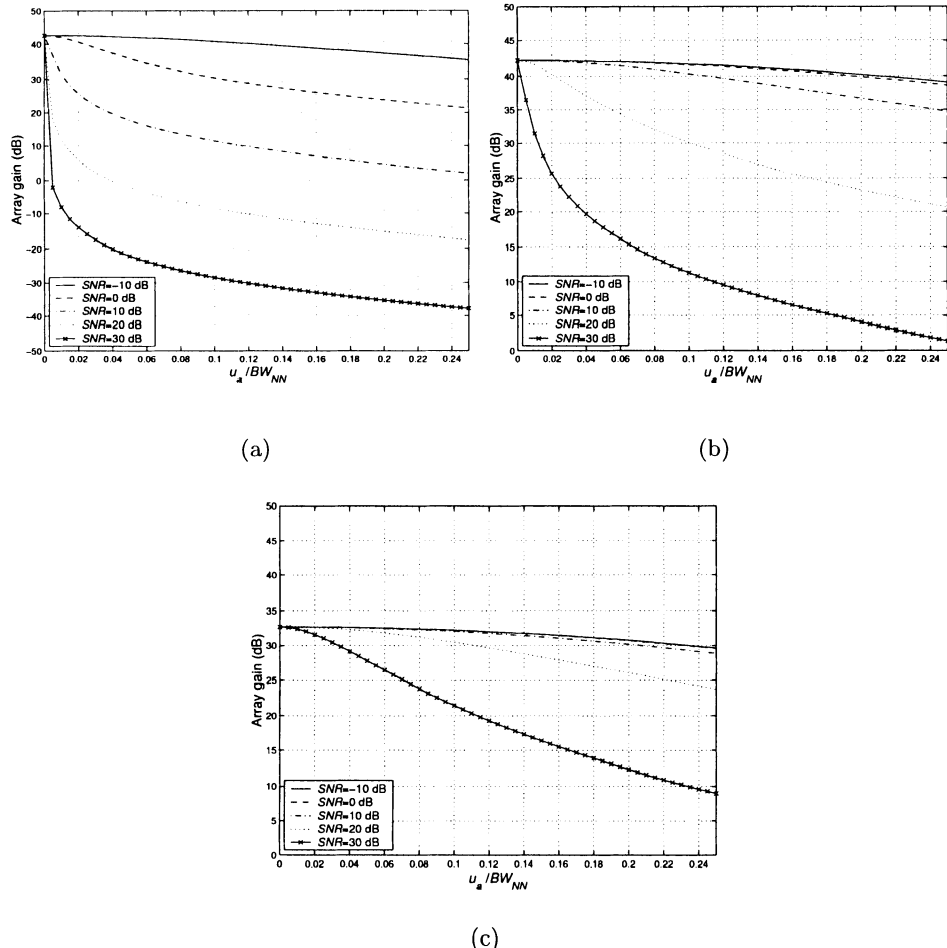


Figure 6.38 MPDR-DL beamformer, array gain versus  $\frac{u_a}{BW_{NN}}$  for various SNR:  $N = 10$ ,  $u_m = 0$ ,  $u_I = \pm 0.30$ ,  $INR = 30$  dB. (a)  $\sigma_L^2 = 0$ ; (b)  $LNR = 20$  dB; (c)  $LNR = 30$  dB.

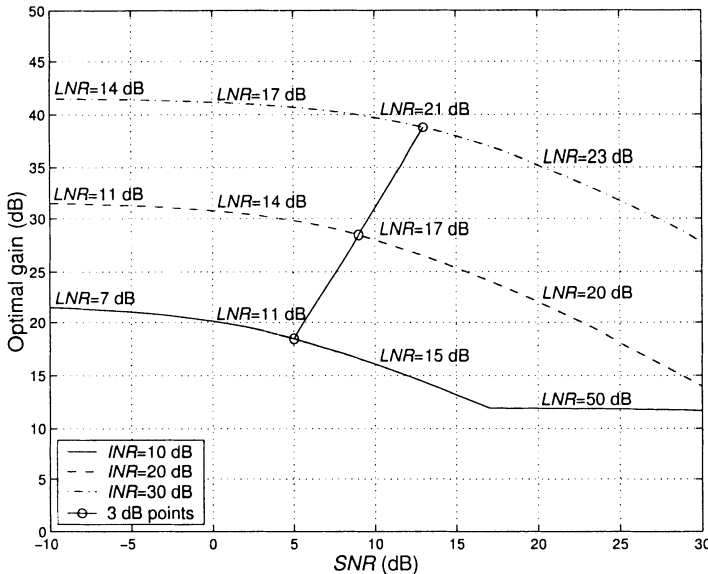


Figure 6.39 MPDR-DL beamformer, array gain, and optimal loading versus  $SNR$  for various  $INR$ ;  $N=10$ ,  $u_m=0$ ,  $u_I = \pm 0.3$ .

We then compute  $E[A_{mpdr,dL}]$  as a function of  $INR$  and  $SNR$  and choose the  $LNR$  to maximize  $E[A_{mpdr,dL}]$ . In Figure 6.39, we plot  $E[A_{mpdr,dL}]$  versus  $SNR$  for various  $INR$ . We also show the optimum  $LNR$  values. Comparing the results in Figure 6.39 with the results in Figure 6.35, we see that diagonal loading provides a significant gain in performance.

This leads to our approximate rule of thumb,

$$SNR + 10 \text{ dB} \leq LNR \leq INR, \quad (6.275)$$

if the  $SNR$  and  $INR$  allow these inequalities. The worst case for this technique is when the  $SNR \geq INR$  and both are large ( $\geq 10$  dB). We shall find that many of our beamforming algorithms have difficulty in this region. Although a particular algorithm may have trouble, the  $SNR > INR$  case is a desirable one.

In the next example, we consider the use of diagonal loading to provide robustness in the presence of array perturbations.

#### Example 6.6.7: MPDR-DL beamformer; array perturbations (continuation)

Consider a standard 10-element linear array along the  $x$ -axis. The array is steered to broadside. The interference model is given in (6.273). In this example, the signal is matched ( $\mathbf{v}_a = \mathbf{v}_m$ ) but the sensor positions are perturbed in the  $x$  and  $y$  directions. The perturbations are statistically independent zero-mean Gaussian random variables with standard deviation  $\sigma_\rho$ , where  $\sigma_\rho = 0.02\lambda, 0.05\lambda$ , and  $0.1\lambda$ . The perturbations are constant during the snapshot sequence. The actual array manifold vector  $\mathbf{v}_p$  is given by (6.246).

We assume that  $\mathbf{S}_{\mathbf{x},p}$  is available to design the beamformer,

$$\mathbf{S}_{\mathbf{x},p} = \sigma_s^2 \mathbf{v}_p \mathbf{v}_p^H + \sum_{i=1}^2 \sigma_i^2 \mathbf{v}_i \mathbf{v}_i^H + \sigma_w^2 \mathbf{I}. \quad (6.276)$$

The weight vector is

$$\mathbf{w}^H \triangleq \mathbf{w}_{mpdr,dl}^H = \frac{\mathbf{v}_m^H [\mathbf{S}_{\mathbf{x},p} + \sigma_L^2 \mathbf{I}]^{-1}}{\mathbf{v}_m^H [\mathbf{S}_{\mathbf{x},p} + \sigma_L^2 \mathbf{I}]^{-1} \mathbf{v}_m}. \quad (6.277)$$

We examine the behavior as a function of the  $SNR$ ,  $INR$ , and  $LNR$  for various  $\sigma_p$ .

In Figure 6.40 we plot the array gain versus  $SNR$  for the case in which each interferer has an  $INR = 30$  dB. In part (a),  $\sigma_p = 0.02\lambda$ . We see that an  $LNR = 10$  dB keeps the array gain above 40 dB for  $SNR \leq 10$  dB. An  $LNR = 20$  dB keeps the array gain above 40 dB for  $SNR \leq 18$  dB. In Part (b),  $\sigma_p = 0.05\lambda$ . An  $LNR = 10$  dB keeps the array gain above 40 dB for  $SNR \leq 5$  dB. An  $LNR = 20$  dB keeps the array gain above 40 dB for  $SNR \leq 13$  dB. In part (c),  $\sigma_p = 0.10\lambda$ . An  $LNR = 10$  dB keeps the array gain above 40 dB for  $SNR \leq -3$  dB. An  $LNR = 20$  dB keeps the array gain above 40 dB for an  $SNR \leq 3$  dB. In all cases, an  $LNR = 30$  dB degrades the nulling performance of the beamformer and reduces the array gain significantly.

In Figure 6.41, we plot the optimum loading versus  $\frac{\sigma_p}{\lambda}$  for various  $SNR$ . We also show the corresponding array gain. In this case we assume that  $\sigma_p/\lambda$  and  $SNR$  are known and we choose the optimum  $LNR$  based on that knowledge.

In this section, we have seen that diagonal loading offers a significant improvement in performance in the presence of mismatch. If we have reasonably good information on the expected  $SNR$  and  $INR$  levels we can select the appropriate amount of fixed diagonal loading.

The disadvantage of this approach is that we may not have enough prior information to determine the correct fixed loading level or the environment may change over time. In Section 6.10, we re-examine the MPDR-QC beamformer in (6.268) and study the choice of  $T_o$ . In Chapter 7, we study the finite data problem and develop variable loading algorithms that determine the loading level from the observed data.

We will find that diagonal loading plays a central role in most robust beamformers.

### 6.6.5 Summary

In this section, we have studied the behavior of MVDR and MPDR beamformers in the presence of various types of differences between the model and the actual environment.

In Section 6.6.2, we studied the case of DOA mismatch. We found that the behavior of the conventional beamformer and the MVDR beamformer was characterized by their beam patterns in the absence of mismatch (see

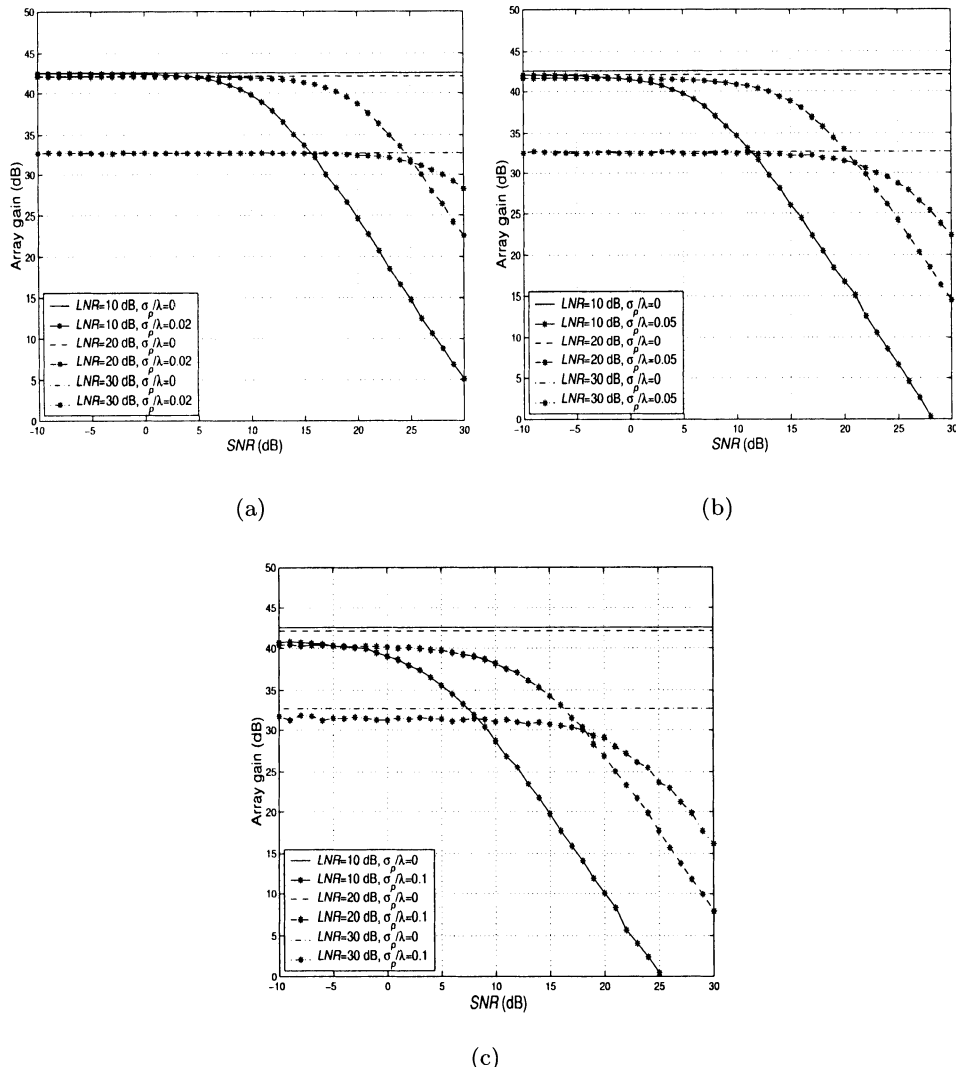
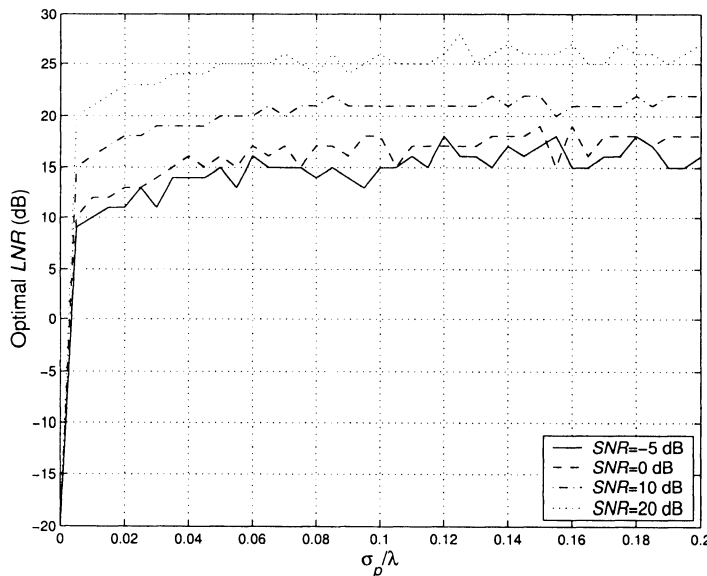
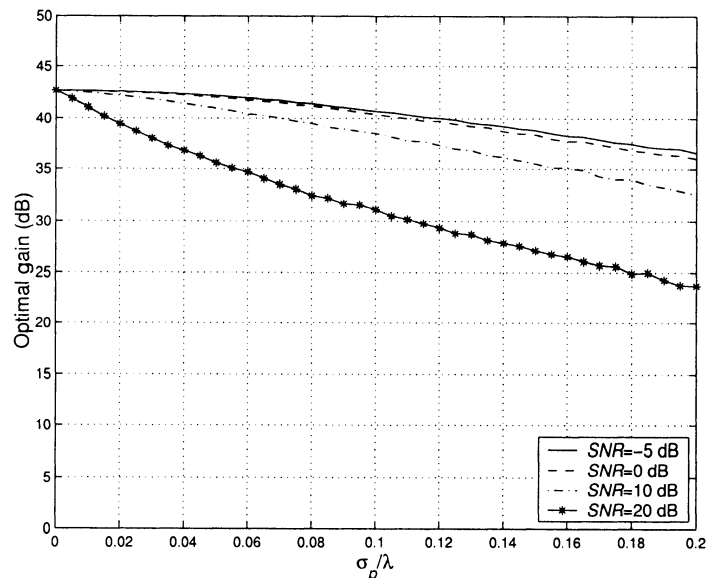


Figure 6.40 MPDR-DL beamformer with array perturbations, array gain versus  $SNR$  for various  $LNR$ ;  $u_I = \pm 0.3$ ,  $INR = 30$  dB, 500 trials (a)  $\sigma_p = 0.02\lambda$ ; (b)  $\sigma_p = 0.05\lambda$ ; (c)  $\sigma_p = 0.1\lambda$ .



(a)



(b)

Figure 6.41 MPDR-DL beamformer with array perturbations; 500 trials: (a) optimal *LNR* versus  $\sigma_p/\lambda$ ; (b) array gain versus  $\sigma_p/\lambda$ .

(6.205) and (6.213)). Therefore, as long as the MVDR beam pattern is well-behaved, the performance degrades gradually in the presence of DOA mismatch. However, the MPDR beamformer treats the mismatched signal as an interferer and attempts to null it. As the *SNR* increases, the degradation due to mismatch increases and small mismatches lead to unacceptable performance.

In Section 6.6.3, we studied the case of array perturbations. We found that the array perturbations caused a performance degradation similar to that in the DOA mismatch case.

In Section 6.6.4, we introduced a quadratic constraint in order to inhibit main-lobe nulling. The quadratic constraint leads to diagonal loading. We found that, if the *INRs* were 15–20 dB larger than the *SNR*, we could use DL and obtain adequate performance for both the DOA mismatch and the array perturbation case.

In the next section, we develop other constraint techniques in order to provide main-lobe protection and increased robustness in the presence of mismatch.

## 6.7 LCMV and LCMP Beamformers

In Section 6.2, we derived the minimum variance distortionless beamformer by imposing a linear constraint,

$$\mathbf{w}^H \mathbf{v}_m = 1. \quad (6.278)$$

In Section 6.6, we saw that the performance of the resulting MPDR beamformers was not particularly robust to various changes in the environment. In this section, we develop beamformers in which additional linear constraints are imposed to make the beamformer more robust. We refer to beamformers using  $\mathbf{S}_n$  as linear constrained minimum variance (LCMV) beamformers. In many cases, we must use  $\mathbf{S}_x$  instead of  $\mathbf{S}_n$ . We refer to these beamformers as linear constrained minimum power (LCMP) beamformers. The majority of the literature uses the LCMV descriptor for both types of beamformers.

In this section, we develop the two beamforming algorithms. We define a set of linear constraints by the  $N \times M_c$  constraint matrix,  $\mathbf{C}$ , whose columns are linearly independent. We require that

$$\mathbf{w}^H \mathbf{C} = \mathbf{g}^H \quad (6.279)$$

or equivalently,

$$\mathbf{C}^H \mathbf{w} = \mathbf{g}. \quad (6.280)$$

Subject to the constraint in (6.279) we derive two beamformers. The LCMV beamformer minimizes

$$\mathbf{P}_n = \mathbf{w}^H \mathbf{S}_n \mathbf{w}, \quad (6.281)$$

subject to the constraint in (6.279). The LCMP beamformer minimizes

$$\mathbf{P}_o = \mathbf{w}^H \mathbf{S}_x \mathbf{w}, \quad (6.282)$$

subject to the constraint in (6.279).

In Section 6.7.1, we discuss typical linear constraints that are useful and discuss various choices of  $\mathbf{C}$  and  $\mathbf{g}$ . In Section 6.7.2, we derive the optimum LCMV and LCMP beamformers. In Section 6.7.3, we develop the generalized sidelobe canceller implementation of the LCMV and LCMP beamformers.

In Section 6.7.4, we study the performance of the LCMV and LCMP beamformers. We first consider their performance in a nominal environment. We then consider the various mismatch problems such as steering vector mismatch and array imperfections, and see how the constraints improve robustness.

The constraints in Sections 6.7.1–6.7.4 focus on constraining the beam pattern at specific points in frequency-wavenumber space and impose a hard constraint at those points. In Section 6.7.5, we study a different type of linear constraint called **quiescent pattern constraints**. We use the adjective “quiescent” to describe the beam pattern of the optimum beamformer in the presence of white noise. This beamformer utilizes the classical beam patterns that we developed in Chapters 3 and 4 as a basis for the design. By using these constraints (such as mean-square deviation from the quiescent pattern) we can obtain improved performance in some cases.

In Section 6.7.6, we develop a technique called covariance augmentation to combat moving or broadband interferers. In Section 6.7.7, we summarize our results.

### 6.7.1 Typical Constraints

We use the frequency domain snapshot model. The input signal is modeled as,

$$\mathbf{X}(\omega) = \mathbf{V}\mathbf{F}(\omega) + \mathbf{N}(\omega). \quad (6.283)$$

The output is

$$Y(\omega) = \mathbf{w}^H \mathbf{X}(\omega). \quad (6.284)$$

We now discuss typical constraints on  $\mathbf{w}$ .

### 6.7.1.1 Distortionless constraint

We introduced this constraint in Section 6.2. If the signal of interest corresponds to an array manifold vector  $\mathbf{v}_m$ , then we require

$$\mathbf{w}^H \mathbf{v}_m = 1, \quad (6.285)$$

which guarantees that any signal propagating along  $\mathbf{k}_m$  will pass through the filter undistorted. The subscript “ $m$ ” denotes model. We would like

$$\mathbf{v}_m = \mathbf{v}_s,$$

where  $\mathbf{v}_s$  is the desired signal’s array manifold vector. We use  $\mathbf{v}_m$  to allow for mismatch.

We use an  $N \times 1$  vector  $\mathbf{c}_i$  to denote the  $i$ th constraint. Unless noted, we always assume that the first constraint is the distortionless constraint. Thus,

$$\mathbf{c}_1 = \mathbf{v}_m. \quad (6.286)$$

We have seen that this constraint will be inadequate to ensure adequate performance in the presence of various mismatches. One possible improvement is to use multiple directional constraints.

### 6.7.1.2 Directional constraints

The general directional constraint is

$$\mathbf{w}^H \mathbf{v}(\mathbf{k}_i) = g_i, \quad i = 1, 2, \dots, M_0, \quad (6.287)$$

where  $\mathbf{k}_i$  denotes the wave number along which we want to impose the constraint and  $g_i$  is a complex number denoting the value of the constraint.

To illustrate a special case of these constraints that could be used to make the beamformer robust against steering errors, we consider a uniform linear array. Then, the distortionless constraint can be written as

$$\mathbf{w}^H \mathbf{v}(\psi_m) = 1. \quad (6.288)$$

We can try to force a flatter beam pattern near the signal direction by adding two constraints,

$$\mathbf{w}^H \mathbf{v}(\psi_m + \Delta\psi) = 1, \quad (6.289)$$

$$\mathbf{w}^H \mathbf{v}(\psi_m - \Delta\psi) = 1. \quad (6.290)$$

In matrix notation, the constraint matrix is an  $N \times 3$  matrix,

$$\mathbf{C} = \left[ \begin{array}{c|c|c} \mathbf{v}(\psi_m) & \mathbf{v}(\psi_m + \Delta\psi) & \mathbf{v}(\psi_m - \Delta\psi) \end{array} \right], \quad (6.291)$$

$$\mathbf{g} = \begin{bmatrix} 1 \\ 1 \\ 1 \end{bmatrix}, \quad (6.292)$$

and

$$\mathbf{w}^H \mathbf{C} = \mathbf{g}^H. \quad (6.293)$$

In later examples, we see that this type of constraint can degrade the noise rejection performance significantly. A second possibility is to choose the  $g_i$  to match the conventional beamformer shape. Thus,

$$\mathbf{g} = \begin{bmatrix} 1 \\ B_c(\psi_m + \Delta\psi : \psi_m) \\ B_c(\psi_m - \Delta\psi : \psi_m) \end{bmatrix}. \quad (6.294)$$

Depending on the extent of signal mismatch, other values of  $g_2$  and  $g_3$  may be appropriate. For symmetric mismatch, we use

$$\mathbf{g} = \begin{bmatrix} 1 \\ g_c \\ g_c \end{bmatrix}, \quad (6.295)$$

where

$$B_c(\psi_m + \Delta\psi : \psi_m) \leq g_c \leq 1. \quad (6.296)$$

### Example 6.7.1

Consider a standard  $N$ -element linear array. Assume we impose the distortionless constraint plus a constraint at the HPBW points of the conventional beam pattern,  $u = \pm 0.891/N$ . Assume the array is pointed at broadside,  $\mathbf{C}$  is an  $N \times 3$  matrix,

$$\mathbf{C} = \left[ \begin{array}{c|c|c} 1 & \mathbf{v}_u \left( \frac{0.891}{N} \right) & \mathbf{v}_u \left( \frac{-0.891}{N} \right) \end{array} \right], \quad (6.297)$$

where  $\mathbf{v}_u(\cdot)$  is the array manifold vector in  $u$ -space.

The value of  $\mathbf{g}$  is given by either (6.292), (6.294), or (6.295).

When we impose the constraints, we assume that the columns of  $\mathbf{C}$  are linearly independent so that its rank is  $M_0$ , the number of constraints. However, we will find that if the wavenumbers are too close together, the matrix that we must invert will be ill-conditioned.

### 6.7.1.3 Null constraints

We encountered null constraints in Section 3.7. This type of constraint is appropriate if there is an interfering signal (jammer) coming from a known direction. In this case,

$$\mathbf{w}^H \mathbf{v}(\mathbf{k}_i) = 0, \quad i = 2, \dots, M_0. \quad (6.298)$$

Thus,

$$\mathbf{C} = \left[ \begin{array}{c|c|c|c|c} \mathbf{v}_m & \mathbf{v}_2 & \mathbf{v}_3 & \cdots & \mathbf{v}_{M_0} \end{array} \right] \quad (6.299)$$

and

$$\mathbf{g}^T = \left[ \begin{array}{ccccc} 1 & 0 & 0 & \cdots & 0 \end{array} \right]. \quad (6.300)$$

We recall from Section 6.3 that the MVDR beamformer only puts a perfect null on a directional noise when  $\sigma_I^2/\sigma_w^2$  is infinite.

Thus, a constraint such as

$$\mathbf{w}^H \mathbf{v}(\mathbf{k}_i) = \varepsilon_i, \quad i = 2, \dots, M_0, \quad (6.301)$$

where  $\varepsilon_i$  is related to  $\sigma_I^2/\sigma_w^2$ , may be used.

We also recall that the performance of the beamformer was sensitive to interferer mismatch. Thus, we may want to use multiple point constraints in the vicinity of the interferer. For example, in the single interferer and a linear array case, we might impose three constraints

$$\mathbf{C}_I = \left[ \begin{array}{c|c|c} \mathbf{v}(\psi_I) & \mathbf{v}(\psi_I + \Delta\psi) & \mathbf{v}(\psi_I - \Delta\psi) \end{array} \right], \quad (6.302)$$

where  $\mathbf{C}_I$  is the null part of the constraint matrix, and

$$\mathbf{g}^T = \left[ \begin{array}{ccc} 0 & B & B \end{array} \right]. \quad (6.303)$$

Once again, we do not want to put the columns of  $\mathbf{C}_I$  too close together. This not only gives an ill-conditioned matrix but it also unnecessarily uses degrees of freedom.

### 6.7.1.4 Derivative constraints

Another method of controlling the shape of the beam pattern near the peak or a null is to utilize derivative constraints. The complex beam pattern is

$$B(\mathbf{k} : \mathbf{k}_m) = \mathbf{w}^H \mathbf{v}(\mathbf{k}), \quad (6.304)$$

and the corresponding power pattern is

$$P(\mathbf{k} : \mathbf{k}_m) = |B(\mathbf{k} : \mathbf{k}_m)|^2. \quad (6.305)$$

We can also write the above pattern using  $\theta$  and  $\phi$  as variables. For example,

$$P(\omega, \theta, \phi) = |B(\omega, \theta, \phi)|^2. \quad (6.306)$$

The reason for writing the alternative forms is that we impose derivative constraints in a different manner in the various forms. Three representative choices are:

### (i) Beam pattern derivatives

Set the derivatives of  $B(\mathbf{k} : \mathbf{k}_s)$  with respect to  $k_x$ ,  $k_y$ ,  $k_z$  equal to a specified value at some point  $\mathbf{k}_c$ . Alternatively, we can use derivatives with respect to  $\theta$  and  $\phi$ .

### (ii) Power pattern derivatives

Set the derivatives of  $P(\omega, \theta, \phi)$  with respect to  $\theta$  and  $\phi$  equal to a specified value at some point  $(\theta_c, \phi_c)$ . Alternatively, we can use derivatives with respect to  $\mathbf{k}$ .

### (iii) Frequency derivatives

Set the derivatives of either  $B(\omega, \theta, \phi)$  or  $P(\omega, \theta, \phi)$  with respect to  $\omega$  equal to a specified value at some point  $\omega_L$ .

We explore these cases briefly. First, consider a standard linear array. Then,

$$B(\psi) = \mathbf{w}^H \mathbf{v}(\psi) \quad (6.307)$$

and

$$\frac{dB(\psi)}{d\psi} = \mathbf{w}^H \frac{d\mathbf{v}(\psi)}{d\psi} \triangleq \mathbf{w}^H \mathbf{d}(\psi), \quad (6.308)$$

where, using symmetric indexing,

$$[\mathbf{d}(\psi)]_n \triangleq \begin{cases} jne^{jn\psi}, & -\frac{N-1}{2} \leq n \leq \frac{N-1}{2}, \quad N \text{ odd}, \\ \begin{cases} j(n - \frac{1}{2})e^{j(n-\frac{1}{2})\psi}, & n = 1, \dots, \frac{N}{2}, \\ j(n + \frac{1}{2})e^{j(n+\frac{1}{2})\psi}, & n = -1, \dots, -\frac{N}{2}, \end{cases} & N \text{ even}. \end{cases} \quad (6.309)$$

Note that  $\mathbf{d}(\psi)$  is conjugate asymmetric.

The second derivative is

$$\frac{d^2 B(\psi)}{d\psi^2} = \mathbf{w}^H \frac{\partial}{\partial \psi} \mathbf{d}(\psi) = \mathbf{w}^H \dot{\mathbf{d}}(\psi), \quad (6.310)$$

where, using symmetric indexing,

$$[\dot{\mathbf{d}}(\psi)]_n = \begin{cases} -n^2 e^{jn\psi}, & -\frac{N-1}{2} \leq n \leq \frac{N-1}{2}, \quad N \text{ odd}, \\ \begin{cases} -(n - \frac{1}{2})^2 e^{j(n-\frac{1}{2})\psi}, & n = 1, \dots, \frac{N}{2}, \\ -(n + \frac{1}{2})^2 e^{j(n+\frac{1}{2})\psi}, & n = -1, \dots, -\frac{N}{2}, \end{cases} & N \text{ even}, \end{cases} \quad (6.311)$$

is conjugate symmetric.

A typical application is to impose constraints on the derivatives of the main lobe evaluated at its steering direction. A simple example illustrates this application.

### Example 6.7.2

We utilize an  $N \times 3$  constraint matrix. We assume the array is pointed at broadside.

$$\mathbf{C} = [ \mathbf{1} \mid \mathbf{d}(0) \mid \dot{\mathbf{d}}(0) ]. \quad (6.312)$$

There are several logical choices for the  $\mathbf{g}$  vector. The first choice sets the first and second derivatives equal to zero. Thus,

$$\mathbf{g}^H = [ 1 \mid 0 \mid 0 ]. \quad (6.313)$$

The second choice matches the behavior of the conventional beam pattern. Thus,

$$\mathbf{g}^H = [ 1 \mid 0 \mid \ddot{B}_C(\psi) \Big|_{\psi=0} ]. \quad (6.314)$$

The third choice uses an intermediate value for  $g_3$ ,

$$\mathbf{g}^T = [ 1 \mid 0 \mid g_3 ], \quad (6.315)$$

where

$$\ddot{B}_C(\psi) \Big|_{\psi=0} \leq g_3 \leq 0. \quad (6.316)$$

We could also express the beam pattern in  $\theta$ -space. Then

$$B(\theta) = \mathbf{w}^H \mathbf{v}_\theta(\theta) \quad (6.317)$$

and

$$\frac{dB(\theta)}{d\theta} = \mathbf{w}^H \frac{d\mathbf{v}_\theta(\theta)}{d\theta} = \mathbf{w}^H \mathbf{d}_\theta(\theta), \quad (6.318)$$

where, using symmetric indexing,

$$[\mathbf{d}_\theta(\theta)]_n \triangleq \begin{cases} jn\pi \sin \theta e^{jn\pi \cos \theta}, & -\frac{N-1}{2} \leq n \leq \frac{N-1}{2}, \quad N \text{ odd}, \\ \begin{cases} j(n - \frac{1}{2}) \sin \theta e^{j(n - \frac{1}{2})\pi \cos \theta}, & n = 1, \dots, \frac{N}{2}, \\ j(n + \frac{1}{2}) \sin \theta e^{j(n + \frac{1}{2})\pi \cos \theta}, & n = -1, \dots, -\frac{N}{2}, \end{cases} & N \text{ even}, \end{cases} \quad (6.319)$$

with similar expressions for the second derivative.

The constraints in (6.312)–(6.314) have been used by a number of authors (e.g., Cox [Cox73], Applebaum and Chapman [AC76], Vural [Vur77], [Vur79], Er and Cantoni [EC83], Steele [Ste83], Buckley and Griffiths [BG86]).

In [BG86], it is pointed out that if one constrains the phase of the derivative by setting (6.319) or (6.309) equal to zero, then the resulting beam pattern will be affected by the choice of the spatial reference point (the origin of coordinates).

Tseng [Tse92] shows this dependency in a straightforward manner. Assume that  $\bar{\mathbf{v}}$  is a steering vector defined at a reference point other than  $\mathbf{v}$ . Then,

$$\bar{\mathbf{v}} = \mathbf{v} e^{j\omega \Delta\tau(\theta)}, \quad (6.320)$$

where  $\Delta\tau(\theta)$  is the time delay corresponding to the difference in the two reference points. Thus, if we impose a gain constraint, changing the reference point changes the phase of the beam pattern by a fixed amount, but does not affect the magnitude response.

Imposing a derivative constraint has a different effect. Differentiating (6.320) with respect to  $\theta$  gives

$$\bar{\mathbf{d}}_\theta \triangleq \frac{\partial \bar{\mathbf{v}}}{\partial \theta} = \mathbf{v}_\theta e^{j\omega \Delta\tau(\theta)} + \mathbf{v} \cdot j\omega \frac{\partial \Delta\tau(\theta)}{\partial \theta} e^{j\omega \Delta\tau(\theta)}. \quad (6.321)$$

Because of the second term,  $\bar{\mathbf{v}}_\theta$  is not just a phase-shifted replica of  $\mathbf{v}_\theta$ . Therefore, both the magnitude and phase responses will be affected by the choice of spatial reference point.

If we differentiate the power pattern, the problem of reference point sensitivity is eliminated. This approach is utilized by Tseng [Tse92], Tseng and Griffiths [TG92a], Thng et al. [TCL95], and others. This leads to a set of nonlinear constraints. However, [Tse92] shows how to transform them to a set of linear constraints.

For a planar array, the best notation will depend on the array geometry.

For a standard rectangular array, using symmetric indexing,

$$B(\psi_x, \psi_y) = \sum_{n=-\frac{N-1}{2}}^{\frac{N-1}{2}} \sum_{m=-\frac{M-1}{2}}^{\frac{M-1}{2}} w_{nm} e^{j[n\psi_x + m\psi_y]}, \quad N \text{ odd.} \quad (6.322)$$

Then,

$$\frac{dB(\psi_x, \psi_y)}{d\psi_x} = \sum_{n=-\frac{N-1}{2}}^{\frac{N-1}{2}} \sum_{m=-\frac{M-1}{2}}^{\frac{M-1}{2}} w_{nm} j n e^{j[n\psi_x + m\psi_y]}, \quad N \text{ odd,} \quad (6.323)$$

$$\frac{dB(\psi_x, \psi_y)}{d\psi_y} = \sum_{n=-\frac{N-1}{2}}^{\frac{N-1}{2}} \sum_{m=-\frac{M-1}{2}}^{\frac{M-1}{2}} w_{nm} j m e^{j[n\psi_x + m\psi_y]}, \quad N \text{ odd,} \quad (6.324)$$

are the first derivatives. The second derivatives are

$$\frac{d^2 B(\psi_x, \psi_y)}{d\psi_x^2} = \sum_{n=-\frac{N-1}{2}}^{\frac{N-1}{2}} \sum_{m=-\frac{M-1}{2}}^{\frac{M-1}{2}} w_{nm} (-n^2) e^{j[n\psi_x + m\psi_y]}, \quad N \text{ odd,} \quad (6.325)$$

$$\frac{d^2 B(\psi_x, \psi_y)}{d\psi_y^2} = \sum_{n=-\frac{N-1}{2}}^{\frac{N-1}{2}} \sum_{m=-\frac{M-1}{2}}^{\frac{M-1}{2}} w_{nm} (-m^2) e^{j[n\psi_x + m\psi_y]}, \quad N \text{ odd,} \quad (6.326)$$

$$\frac{d^2 B(\psi_x, \psi_y)}{d\psi_x d\psi_x} = \sum_{n=-\frac{N-1}{2}}^{\frac{N-1}{2}} \sum_{m=-\frac{M-1}{2}}^{\frac{M-1}{2}} w_{nm} (-mn) e^{j[n\psi_x + m\psi_y]}, \quad N \text{ odd.} \quad (6.327)$$

Thus, to control the first and second derivatives in addition to the distortionless constraint will require six constraints.

When dealing with derivative constraints in either linear or planar arrays it is important to check the columns of  $\mathbf{C}$  for linear independence and remove any dependent constraint vectors (or use the SVD approach discussed in Chapter 3, e.g., discussion after (3.296)).

The third case corresponds to frequency derivatives and can be illustrated with a simple example.

### Example 6.7.3

Consider a uniform linear array. Then,

$$B(\omega, u) = \sum_{n=-\frac{N-1}{2}}^{\frac{N-1}{2}} w_n e^{j \frac{\omega}{c} u n d}, \quad (6.328)$$

$$\frac{dB(\omega, u)}{d\omega} = \sum_{n=-\frac{N-1}{2}}^{\frac{N-1}{2}} w_n j n \frac{ud}{c} e^{j \frac{\omega}{c} und}, \quad (6.329)$$

$$\frac{d^2B(\omega, u)}{d\omega^2} = \sum_{n=-\frac{N-1}{2}}^{\frac{N-1}{2}} w_n \left( -n^2 \frac{u^2 d^2}{c^2} \right) e^{j \frac{\omega}{c} und}. \quad (6.330)$$

For a uniform linear array, the behavior versus frequency is the dual of the behavior versus  $u$ . This duality does not necessarily apply to other array geometries.

Before leaving derivative constraints, it is useful to revisit null constraints. As discussed in Section 6.7.1.3, a null constraint can be used if there is an interferer coming from a specific direction. The performance is very sensitive to mismatch in the interferer direction. In order to improve robustness, derivative constraints in the vicinity of the null can be imposed. For a single interferer arriving from  $\psi_I$ , a constraint matrix whose null component is

$$\mathbf{C}_I = \begin{bmatrix} \mathbf{v}(\psi_I) & \dot{\mathbf{v}}(\psi_I) & \ddot{\mathbf{v}}(\psi_I) \end{bmatrix}, \quad (6.331)$$

where

$$\mathbf{g}_I^T = \begin{bmatrix} 0 & 0 & g_3 \end{bmatrix}, \quad (6.332)$$

can be used. These constraints will create a broader null. It is an alternative to (6.301) and (6.302) that may be more useful.

We see from this brief discussion that derivative constraints offer a wide range of choices. After the optimum LCMV and LCMP beamformers are derived, we will explore how the derivative constraints affect the beam pattern and array gain.

### 6.7.1.5 Eigenvector constraints

A different type of constraint was introduced by Er and Cantoni [EC85] in order to achieve effective control of the beam pattern over a region of  $\omega\text{-k}$  space. The technique was further developed by Buckley [Buc87] and Van Veen [VV91]. (e.g., Chapter 4 of [HS92]).<sup>7</sup> These constraints are referred to as eigenvector constraints for reasons that will be clear when they are derived.

The basic model assumes that there is a desired response over a specified region in the  $\omega\text{-k}$  space. We want to define a set of constraints that will minimize the total squared error between the desired response and the actual response. This is analogous to the least squared error approach in Chapter

---

<sup>7</sup>Our discussion is similar to [EC85].

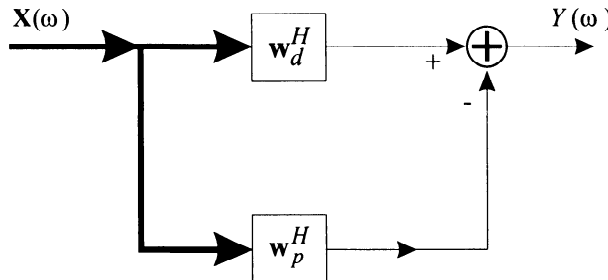


Figure 6.42 Partition of beamformer.

3, except we only specify the desired response over a segment of the  $\omega\text{-k}$  space.

The desired beam pattern can be written as

$$B_d(w, \mathbf{k}) = \mathbf{w}_d^H \mathbf{v}(w : \mathbf{k}), \quad (6.333)$$

where we have suppressed the  $w$  dependence in the weight vector. The squared error is

$$e^2 = \int_{\mathbf{k} \in \mathbf{K}} \int_{\omega \in \Omega} \left| \mathbf{w}_d^H \mathbf{v}(\omega, \mathbf{k}) - \mathbf{w}^H \mathbf{v}(\omega : \mathbf{k}) \right|^2 d\mathbf{k} d\omega. \quad (6.334)$$

It is convenient to partition the beamformers as shown in Figure 6.42. Then,

$$\mathbf{w} = \mathbf{w}_d - \mathbf{w}_p. \quad (6.335)$$

Substituting (6.333) into (6.334) gives

$$e^2 = \mathbf{w}_p^H \mathbf{Q} \mathbf{w}_p \quad (6.336)$$

where

$$\mathbf{Q} = \int_{\mathbf{k} \in \mathbf{K}} \int_{\omega \in \Omega} \mathbf{v}(\omega : \mathbf{k}) \mathbf{v}^H(\omega : \mathbf{k}) d\mathbf{k} d\omega. \quad (6.337)$$

Note that  $\mathbf{Q}$  is just the correlation matrix at the array from a distributed source  $S_o(\omega : \mathbf{k}) = 2\pi$  over  $\mathbf{K}$  and  $\Omega$ . It does not depend on the desired pattern shape, but only the constraint region and the array manifold vector. It is a non-negative definite Hermitian matrix.

We use the error expression in (6.336) in two different ways. In this section, we use the principal eigenvectors of  $\mathbf{Q}$  to form the linear constraint matrix  $\mathbf{C}$ . In Section 6.11, we impose a constraint on  $e^2$  (i.e.,  $e^2 \leq e_0$ ) and find the resultant beamformer. This leads to a generalized form of diagonal

loading called soft constraint beamforming. In this section, we impose a set of linear constraints on  $\mathbf{w}_p$  to reduce  $e^2$ .

The eigendecomposition of  $\mathbf{Q}$  can be written as

$$\mathbf{Q} = \mathbf{U}_Q \Lambda_Q \mathbf{U}_Q^H = \sum_{i=1}^N \lambda_i \Phi_i \Phi_i^H, \quad (6.338)$$

where  $N$  is the number of sensors. The matrix  $\mathbf{U}_Q$  is an  $N \times N$  matrix of the eigenvectors,

$$\mathbf{U}_Q = \begin{bmatrix} \Phi_1 & \Phi_2 & \cdots & \Phi_N \end{bmatrix}, \quad (6.339)$$

and

$$\Lambda_Q = \text{diag} \left\{ \lambda_1 \quad \lambda_2 \quad \cdots \quad \lambda_N \right\}, \quad (6.340)$$

is a diagonal matrix of the ordered eigenvalues.

We impose  $N_e$  linear constraints on  $\mathbf{w}_p$ ,

$$\Phi_i^H \mathbf{w}_p = 0, \quad i = 1, \dots, N_e. \quad (6.341)$$

We normally choose  $N_e$  to correspond to the number of significant eigenvalues of  $\mathbf{Q}$ . The eigenvalue behavior in Figure 5.14 is typical of many problems of interest. As we increase  $N_e$ , we reduce the number of degrees of freedom available for adaptation. However, we reduce the error in (6.336). Using (6.338) and (6.341) in (6.336) gives,

$$e^2 = \sum_{N_e+1}^N \lambda |\Phi_i^H \mathbf{w}_p|^2. \quad (6.342)$$

The choice of  $N_e$  is a trade-off between generating a beam pattern that is close to  $B_d$  over a desired region and retaining adequate degrees of freedom. For most  $\mathbf{Q}$  matrices, the eigenvalues drop off sharply, so the choice of  $N_e$  is clear.

Note that the constraint in (6.341) is on the weight vector in the bottom path in Figure 6.42. In some cases, this model is the easiest to work with. In other cases, we want to impose the constraint directly on  $\mathbf{w}$ .

To rewrite the constraints, we expand the three weight vectors in terms of their eigenvectors and match the coefficients. The resulting constraint on  $\mathbf{w}$  is

$$\Phi_i^H \mathbf{w} = \Phi_i^H \mathbf{w}_d, \quad i = 1, \dots, N_e. \quad (6.343)$$

To put (6.343) in the same notation as (6.279)–(6.280), define

$$\mathbf{C} = \begin{bmatrix} \Phi_1 & \Phi_2 & \cdots & \Phi_{N_e} \end{bmatrix} \quad (6.344)$$

and

$$[\mathbf{g}^H]_i = \mathbf{w}_d^H \Phi_i, \quad i = 1, 2, \dots, N_e. \quad (6.345)$$

The resulting constraint equation is

$$\mathbf{w}^H \mathbf{C} = \mathbf{g}^H. \quad (6.346)$$

Note that we do not include a distortionless constraint because it will be almost linearly dependent on  $\Phi_1$  in most cases.

We consider a simple example to illustrate the behavior.

#### Example 6.7.4: Narrowband main-lobe constraint

Consider a standard 10-element narrowband linear array. We assume that the desired beam pattern is the conventional beam pattern

$$B_d(u) = B_c(u), \quad -u_d \leq u \leq u_d. \quad (6.347)$$

Then,

$$\mathbf{Q} = \int_{-u_d}^{u_d} \mathbf{v}(u) \mathbf{v}^H(u) du. \quad (6.348)$$

The  $mn$  element of  $\mathbf{Q}$  is

$$\begin{aligned} [\mathbf{Q}]_{mn} &= \int_{-u_d}^{u_d} e^{j\pi u[m-n]} du \\ &= \frac{2 \sin[\pi u_d(m-n)]}{\pi(m-n)}, \end{aligned} \quad (6.349)$$

so  $\mathbf{Q}$  is a Toeplitz matrix. The eigenvectors are the discrete prolate spheroidal sequences. Note that  $\mathbf{Q}$  is completely determined by the array manifold vectors and does not depend on  $B_d(u)$ . This  $\mathbf{Q}$  matrix is the same as the matrix we encountered in Example 5.5.1. The number of significant eigenvalues will depend on  $u_d$ . In many cases, we choose  $u_d = 1/N$  (or  $u_d = 0.1$  for  $N = 10$ ). From Figure 5.14, we see that there are three significant eigenvalues.

This simple example does not illustrate the real value of eigenvector constraints. We encounter more interesting examples when we study broadband beamforming.

##### 6.7.1.6 Quiescent pattern constraints

There are other types of constraints that will prove useful. The eigenvector constraint matched a desired response over a certain region. An alternative approach would be to specify the pattern over the entire  $\omega\text{-k}$  plane and try to approximate it in a least squares sense while minimizing the output power (or variance). We explore this approach in Section 6.7.5.

### 6.7.1.7 Summary

At this point, we have developed a large menu of possible constraints. The next step is to develop the optimum LCMV and LCMP beamformers and then see how the various constraints affect the array gain, the beam pattern, and the robustness to model variations.

## 6.7.2 Optimum LCMV and LCMP Beamformers

In this section, we find the optimum LCMV and LCMP beamformers for the narrowband case. For  $M_c$  linear constraints, the constraint equation can be written as,

$$\mathbf{w}^H \mathbf{C} = \mathbf{g}^H, \quad (6.350)$$

where  $\mathbf{w}^H$  is  $1 \times N$ ,  $\mathbf{C}$  is  $N \times M_c$ ,  $\mathbf{g}^H$  is  $1 \times M_c$ , and  $N$  is the number of sensors. We require that the columns of  $\mathbf{C}$  be linearly independent.

We will assume that the first column of  $\mathbf{C}$  is  $\mathbf{v}_m$  and that the first element of  $\mathbf{g}$  is 1 so that the processor is distortionless.

We consider two related optimization problems. In the first case, we assume that  $\mathbf{S}_n$  is known or that we will be able to estimate it. In the second case, we assume that  $\mathbf{S}_x$  is known or that we will be able to estimate it. These two cases correspond to the MVDR and MPDR beamformers in Section 6.2.

In the first case, we minimize the output due to noise subject to the constraint in (6.350)

$$\sigma_{no}^2 = \mathbf{w}^H \mathbf{S}_n \mathbf{w}. \quad (6.351)$$

We refer to this case as the linear constraint minimum variance (LCMV) beamformer.

In the second case, we minimize the output power subject to the constraint in (6.350)

$$E[y^2] = \mathbf{w}^H \mathbf{S}_x \mathbf{w}. \quad (6.352)$$

We refer to this case as the linear constraint minimum power beamformer (LCMP).

The minimization procedure is identical for the two cases, so we will solve the first case and indicate the answer for the second case.

We minimize the function

$$J \triangleq \mathbf{w}^H \mathbf{S}_n \mathbf{w} + [\mathbf{w}^H \mathbf{C} - \mathbf{g}^H] \boldsymbol{\lambda} + \boldsymbol{\lambda}^H [\mathbf{C}^H \mathbf{w} - \mathbf{g}]. \quad (6.353)$$

The Lagrange multiplier  $\lambda$  is an  $M_c \times 1$  vector because of the  $M_c$  constraints. Taking the complex gradient of  $\mathbf{J}$  with respect to  $\mathbf{w}^H$  and setting it equal to zero gives

$$\mathbf{S}_n \mathbf{w} + \mathbf{C} \lambda = \mathbf{0}, \quad (6.354)$$

or

$$\mathbf{w} = -\mathbf{S}_n^{-1} \mathbf{C} \lambda. \quad (6.355)$$

Substituting (6.355) into (6.350) gives

$$-\lambda^H \mathbf{C}^H \mathbf{S}_n^{-1} \mathbf{C} = \mathbf{g}^H. \quad (6.356)$$

Solving for  $\lambda^H$  and substituting into (6.355) gives

$$\boxed{\mathbf{w}_{lcmv}^H = \mathbf{g}^H [\mathbf{C}^H \mathbf{S}_n^{-1} \mathbf{C}]^{-1} \mathbf{C}^H \mathbf{S}_n^{-1}}, \quad (6.357)$$

as the optimum constrained processor for Case 1. The existence of the inverse is guaranteed because  $\mathbf{S}_n$  is full rank and the columns of  $\mathbf{C}$  are linearly independent.

Similarly, for Case 2,

$$\boxed{\mathbf{w}_{lcmp}^H = \mathbf{g}^H [\mathbf{C}^H \mathbf{S}_x^{-1} \mathbf{C}]^{-1} \mathbf{C}^H \mathbf{S}_x^{-1}} \quad (6.358)$$

is optimum processor for the second case.<sup>8</sup>

One interpretation of the optimum processor in (6.357) is shown in Figure 6.43. The beamformer first forms a set of  $M_c$  constraint beams and then combines them to form  $Y(\omega)$ . Note that the processor can be viewed as operating in a  $M_c$ -dimensional constraint subspace.

The combiner utilizes the inverse of the matrix  $[\mathbf{C}^H \mathbf{S}_n^{-1} \mathbf{C}]$ . One of the issues in the practical implementation of constrained processors is the condition number of this matrix,

$$r = \frac{\lambda_{\max}}{\lambda_{\min}}. \quad (6.359)$$

As this number increases there may be a problem with the numerical accuracy of the results. The  $r$  will increase as the columns of  $\mathbf{C}$  become more correlated in a space defined by  $\mathbf{S}_n^{-1}$  (or  $\mathbf{S}_x^{-1}$ ).

---

<sup>8</sup>This result is contained in Frost [Fro72] in the context of a tapped delay line implementation of a closed-loop adaptive array processor.

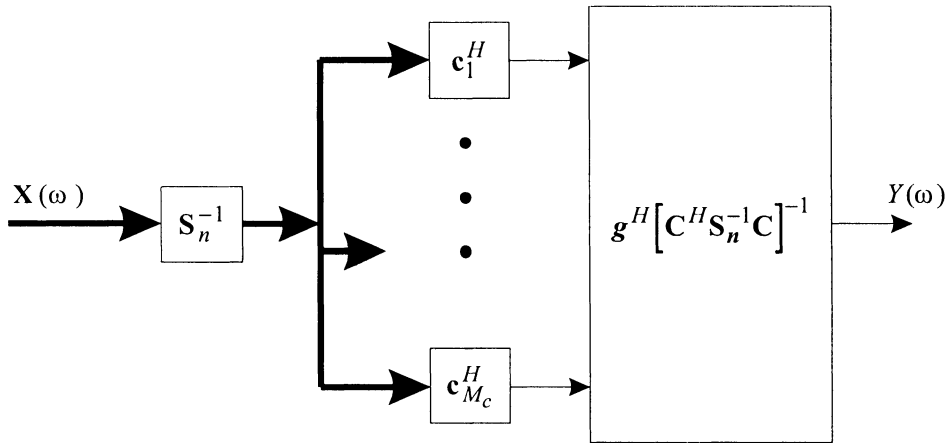


Figure 6.43 Optimum constrained receiver.

If the noise is white, then (6.357) reduces to

$$\boxed{\mathbf{w}_q^H = \mathbf{g}^H [\mathbf{C}^H \mathbf{C}]^{-1} \mathbf{C}^H}, \quad (6.360)$$

which is referred to as the **quiescent** weight vector (the idea of  $\mathbf{w}_q$  was introduced by Applebaum and Chapman [AC76] and utilized by Gabriel [Gab76a], [Gab76b]). We will find that it plays an important role in some of our subsequent discussions.

In the next section, we interpret the optimum LCMV beamformer as a generalized sidelobe canceller.

### 6.7.3 Generalized Sidelobe Cancelers

A useful implementation of the LCMV (or LCMP) beamformer is obtained by dividing the  $N$ -dimensional space into two subspaces, a **constraint** subspace and an **orthogonal** subspace. The constraint subspace is defined by the columns of  $\mathbf{C}$ , an  $N \times M_c$  matrix. The orthogonal subspace is defined by the columns of  $\mathbf{B}$ , an  $N \times (N - M_c)$  matrix. The columns in  $\mathbf{B}$  are linearly independent and each column is orthogonal to each column in  $\mathbf{C}$ . Thus,

$$\mathbf{C}^H \mathbf{B} = \mathbf{0}, \quad (6.361)$$

where  $\mathbf{0}$  is a  $M_c \times (N - M_c)$  matrix of zeros.

First, we assume that  $\mathbf{w}_o$  is known. From (6.358)

$$\mathbf{w}_o^H \triangleq \mathbf{w}_{lcmv}^H = \mathbf{g}^H [\mathbf{C}^H \mathbf{S}_x^{-1} \mathbf{C}]^{-1} \mathbf{C}^H \mathbf{S}_x^{-1}. \quad (6.362)$$

We partition the processor into two orthogonal components,

$$\mathbf{w}_o^H = \mathbf{w}_c^H - \mathbf{w}_p^H, \quad (6.363)$$

where  $\mathbf{w}_c^H$  is defined to be the projection of  $\mathbf{w}_o^H$  onto the constraint subspace and  $\mathbf{w}_p^H$  is the projection of  $\mathbf{w}_o^H$  onto  $\mathbf{B}$ . The projection matrix onto the constraint subspace is

$$\mathbf{P}_C = \mathbf{C} [\mathbf{C}^H \mathbf{C}]^{-1} \mathbf{C}^H, \quad (6.364)$$

and

$$\mathbf{w}_c^H = \mathbf{w}_o^H \mathbf{P}_C. \quad (6.365)$$

Substituting (6.362)) and (6.364) into (6.365),

$$\mathbf{w}_c^H = \mathbf{w}_o^H \mathbf{P}_C = \mathbf{g}^H [\mathbf{C}^H \mathbf{S}_x^{-1} \mathbf{C}]^{-1} \mathbf{C}^H \mathbf{S}_x^{-1} \left\{ \mathbf{C} [\mathbf{C}^H \mathbf{C}]^{-1} \mathbf{C}^H \right\} \quad (6.366)$$

or

$$\boxed{\mathbf{w}_c^H = \mathbf{g}^H [\mathbf{C}^H \mathbf{C}]^{-1} \mathbf{C}^H = \mathbf{w}_q^H}, \quad (6.367)$$

which does not depend on  $\mathbf{S}_x$ . The weight vector in the upper path,  $\mathbf{w}_q^H$ , is the quiescent component of  $\mathbf{w}_o^H$ . If the input is white noise,

$$\mathbf{w}_o^H = \mathbf{w}_q^H. \quad (6.368)$$

The second component of  $\mathbf{w}_o^H$  is  $\mathbf{w}_p^H$ , which can be written as

$$\mathbf{w}_p = -\mathbf{B} [\mathbf{B}^H \mathbf{B}]^{-1} \mathbf{B}^H \mathbf{w}_o = -\mathbf{P}_C^\perp \mathbf{w}_o. \quad (6.369)$$

Thus,

$$\mathbf{w}_p^H = \mathbf{g}^H [\mathbf{C}^H \mathbf{S}_x^{-1} \mathbf{C}]^{-1} \mathbf{C}^H \mathbf{S}_x^{-1} \cdot \mathbf{B} [\mathbf{B}^H \mathbf{B}]^{-1} \mathbf{B}^H. \quad (6.370)$$

This leads to the processor shown in Figure 6.44. This is a correct, but not particularly useful, implementation.

Note that

$$Y_b(\omega) = \mathbf{w}_p^H \mathbf{X}(\omega) \quad (6.371)$$

is obtained by multiplying  $\mathbf{X}(\omega)$  by a matrix completely contained in the  $\mathbf{B}$  subspace. This suggests dividing the processor in the lower path into two parts, as shown in Figure 6.45. The first processor operates on  $\mathbf{X}(\omega)$  to obtain an  $(N - M_c) \times 1$  vector. Note that the output of  $\mathbf{B}$  cannot contain

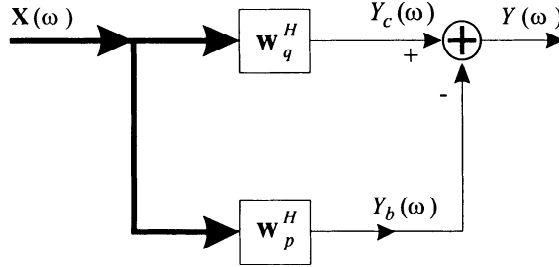


Figure 6.44 Partitioned processor.

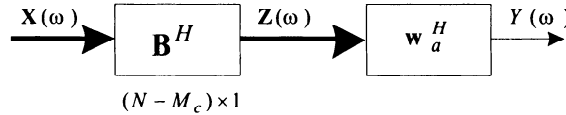


Figure 6.45 Cascade of blocking matrix and adaptive matrix.

any components in the **C** space because of (6.361). We refer to **B** as the **blocking matrix**. The second matrix operates on the  $(N - M_c) \times 1$  vector to produce  $Y_b(\omega)$ . The formula for  $\mathbf{w}_a^H$  follows directly from  $\mathbf{w}_p^H$ . It is the matrix that will adapt as a function of the data when adaptive beamformers are discussed in Chapter 7. Combining Figures 6.44 and 6.45 gives the realization shown in Figure 6.46. This realization is referred to as a generalized sidelobe canceller because of its similarity to classical sidelobe cancellers. Generalized sidelobe cancellers were utilized by Owsley [Ows71] and Applebaum and Chapman [AC76]. Griffiths and Jim [GJ82] analyzed them and introduced the “generalized sidelobe canceller” name. Other references include Er and Cantoni [EC83] and Cox et al. [CZO87].

We now recall the criterion by which the overall filter was designed. It was to minimize the output power subject to the constraint

$$\mathbf{w}^H \mathbf{C} = \mathbf{g}^H. \quad (6.372)$$

The top processor satisfies the constraint exactly and the bottom path is orthogonal to **C** so it cannot impact the constraint. The output power is

$$P_o = [\mathbf{w}_q - \mathbf{B}\mathbf{w}_a]^H \mathbf{S_x} [\mathbf{w}_q - \mathbf{B}\mathbf{w}_a]. \quad (6.373)$$

Taking the gradient with respect to  $\mathbf{w}_a$  and setting the result equal to zero gives

$$[\mathbf{w}_q^H - \mathbf{w}_a^H \mathbf{B}^H] \mathbf{S_x} \mathbf{B} = \mathbf{0}, \quad (6.374)$$

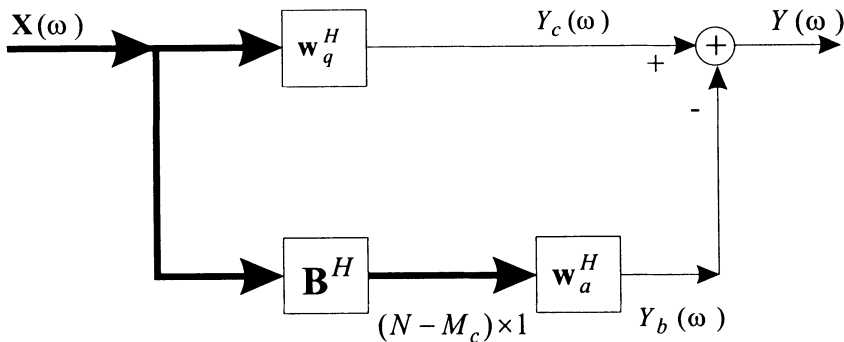


Figure 6.46 Generalized sidelobe canceller.

or<sup>9</sup>

$$\hat{\mathbf{w}}_a^H = \mathbf{w}_q^H \mathbf{S}_x \mathbf{B} [\mathbf{B}^H \mathbf{S}_x \mathbf{B}]^{-1}. \quad (6.375)$$

For a single plane-wave signal input,

$$\mathbf{S}_x = \sigma_s^2 \mathbf{v}_m \mathbf{v}_m^H + \mathbf{S}_n. \quad (6.376)$$

The first column of  $\mathbf{C}$  is  $\mathbf{v}_m$ , so

$$\mathbf{v}_m^H \mathbf{B} = 0, \quad (6.377)$$

and

$$\mathbf{S}_x \mathbf{B} = \mathbf{S}_n \mathbf{B}. \quad (6.378)$$

Then, (6.375) reduces to

$$\hat{\mathbf{w}}_a^H = \mathbf{w}_q^H \mathbf{S}_n \mathbf{B} [\mathbf{B}^H \mathbf{S}_n \mathbf{B}]^{-1}. \quad (6.379)$$

Note that (6.377)–(6.379) assume that there is no signal mismatch ( $\mathbf{v}_a = \mathbf{v}_m$ ) and that  $\mathbf{S}_x$  and  $\mathbf{S}_n$  are known. In this case, the LCMV and LCMP beamformers are identical. More generally, as long as the signal is completely contained in the constraint subspace, the two beamformers will be the same. The formula in (6.375) is used to implement the beamformer because the model assumes that only  $\mathbf{S}_x$  is available. In practice, an estimate  $\hat{\mathbf{S}}_x$  is used.

When the noise is white, the left matrix product in (6.379),

$$\mathbf{w}_q^H [\sigma_\omega^2 \mathbf{I}] \mathbf{B} = \mathbf{0}, \quad (6.380)$$

---

<sup>9</sup>The result in (6.375) can also be written as  $\hat{\mathbf{w}}_a^H = \mathbf{S}_{d\mathbf{z}^H} \mathbf{S}_z^{-1}$ . We exploit this interpretation in Chapter 7.

so  $\hat{\mathbf{w}}_a^H = \mathbf{0}$ , which is the result in (6.368). For this case, the output noise is

$$P_n = \sigma_w^2 \mathbf{w}_q^H \mathbf{w}_q = \sigma_w^2 \|\mathbf{w}_q\|^2, \quad (6.381)$$

the square of the magnitude of  $\mathbf{w}_q$ . If the columns of  $\mathbf{C}$  approach linear dependency and the  $\mathbf{g}$  elements belonging to those columns are very different, then  $\|\mathbf{w}_q\|^2$  becomes large.

This is the same phenomenon we observed with the MVDR filter when we moved the interferer inside the main lobe. Here, if we move a null constraint inside the main lobe, we obtain a beamformer that is sensitive to model mismatch.

Note that  $\mathbf{B}$  is not unique. It must satisfy (6.361) and have rank equal to  $(N - M_c)$ . One method for constructing  $\mathbf{B}$  is to find  $\mathbf{P}_{\mathbf{C}}^\perp$ ,

$$\mathbf{P}_{\mathbf{C}}^\perp = \mathbf{I} - \mathbf{C} \left( \mathbf{C}^H \mathbf{C} \right)^{-1} \mathbf{C}^H, \quad (6.382)$$

which is an  $N \times N$  matrix. Then orthonormalize  $\mathbf{P}_{\mathbf{C}}^\perp$  and choose the first  $(N - M_c)$  columns of the orthonormalized matrix. The resulting  $\mathbf{B}$  matrix has the property that

$$\mathbf{B}^H \mathbf{B} = \mathbf{I}. \quad (6.383)$$

Note that (6.383) implies that the component of  $\mathbf{S}_z$  due to the white noise component of  $\mathbf{S}_x$  is white noise with variance  $\sigma_w^2$ . In subsequent discussions, we will always choose  $\mathbf{B}$  to satisfy (6.383).

#### 6.7.4 Performance of LCMV and LCMP Beamformers

In this section, we analyze the performance of LCMV and LCMP beamformers with directional, derivative, or eigenvector constraints. In this chapter, we assume the ensemble spatial spectral matrix is available. In Chapter 7, we analyze the behavior when we estimate  $\mathbf{S}_n$  or  $\mathbf{S}_x$  from the input data.

The purpose of introducing the linear constraints is to provide main-lobe protection in the case of a main-lobe interferer and to prevent performance degradation in the presence of DOA mismatch and/or array perturbations. Our performance discussion in the text emphasizes the DOA mismatch problem. The results for the array perturbation problem are similar and are developed in the problems. Diagonal loading is used in most cases in order to obtain satisfactory performance.

A large number of examples are included in order to adequately explore the utility of the various constraints.

### 6.7.4.1 Array gain

The expressions for the array gain of LCMV and LCMP beamformers are straightforward. For the LCMV beamformer,  $\mathbf{w}$  is given by (6.357). For the LCMP beamformer,  $\mathbf{w}$  is given by (6.358).

The output signal power is

$$P_s = \sigma_s^2 |\mathbf{w}^H \mathbf{v}_s|^2. \quad (6.384)$$

The output noise power is,

$$P_n = \sigma_n^2 |\mathbf{w}^H \boldsymbol{\rho}_n \mathbf{w}|, \quad (6.385)$$

where  $\boldsymbol{\rho}_n$  is the normalized spatial spectral matrix and includes both the white noise and any additional interference (see (6.106)). The array gain is,

$$A_o = \frac{|\mathbf{w}^H \mathbf{v}_s|^2}{|\mathbf{w}^H \boldsymbol{\rho}_n \mathbf{w}|}, \quad (6.386)$$

where  $\mathbf{w}$  is given by either (6.357) or (6.358). If we include a distortionless constraint, then the numerator in (6.385) is unity and the array gain is

$$A_o = [\mathbf{w}^H \boldsymbol{\rho}_n \mathbf{w}]^{-1}. \quad (6.387)$$

The output  $SNR_o$  is<sup>10</sup>

$$SNR_o = \left( \frac{\sigma_s^2}{\sigma_n^2} \right) A_o. \quad (6.388)$$

Since we have included the interference in the noise spectral matrix, we refer to the result in (6.388) as the output  $SNR$ .

The array gain for the LCMV beamformer is obtained by substituting (6.357) into (6.387). The result is

$$A_{lcmv} = \frac{1}{\mathbf{g}^H [\mathbf{C}^H \boldsymbol{\rho}_n^{-1} \mathbf{C}]^{-1} \mathbf{g}}. \quad (6.389)$$

In order to find the array gain for the LCMP beamformer, we substitute (6.358) into (6.387) and obtain

$$A_{lcmp} = \left\{ \mathbf{g}^H [\mathbf{C}^H \mathbf{S}_x^{-1} \mathbf{C}]^{-1} \mathbf{C}^H \mathbf{S}_x^{-1} \boldsymbol{\rho}_n \mathbf{S}_x^{-1} \mathbf{C} [\mathbf{C}^H \mathbf{S}_x^{-1} \mathbf{C}]^{-1} \mathbf{g} \right\}^{-1}. \quad (6.390)$$

---

<sup>10</sup>The subscript “o” on the left side of (6.387) denotes output. On the right-hand side it denotes optimum. The meaning should be clear from the context.

From (6.379), the array gain for the LCMP case is equal to the array gain for the LCMV case when the distortionless constraint is imposed and the signal is perfectly matched. Thus,

$$A_{lcmv} = \frac{1}{\mathbf{g}^H [\mathbf{C}^H \boldsymbol{\rho}_n^{-1} \mathbf{C}]^{-1} \mathbf{g}}. \quad (6.391)$$

In order to study the effects of mismatch, (6.390) must be used.

The array gain or  $SNR_o$  when there is no model mismatch is one performance measure of interest. The second measure is the array gain or  $SNR_o$  under mismatched conditions, which was one of the primary reasons for introducing constraints.

In order to analyze the effect of signal mismatch, use  $\mathbf{C}_m$  and  $\mathbf{v}_m$  in (6.358),

$$\mathbf{w}^H = \mathbf{g}^H [\mathbf{C}_m^H \mathbf{S}_x^{-1} \mathbf{C}_m]^{-1} \mathbf{C}_m^H \mathbf{S}_x^{-1}, \quad (6.392)$$

where  $\mathbf{C}_m$  and  $\mathbf{g}_m$  are constructed assuming  $\mathbf{v}_m$  is correct. Substitute  $\mathbf{w}^H$  from (6.392) and  $\mathbf{v}_a$  into (6.385). Carrying out the substitution and simplifying gives

$$A_{lcmv}(\mathbf{v}_a : \mathbf{v}_m) = \frac{\left| \mathbf{g}^H (\mathbf{C}_m^H \boldsymbol{\rho}_n^{-1} \mathbf{C}_m)^{-1} \mathbf{C}_m^H \boldsymbol{\rho}_n^{-1} \mathbf{v}_a \right|^2}{\left( 1 + \frac{\sigma_s^2}{\sigma_w^2} \gamma \right)^2 \mathbf{g}^H (\mathbf{C}_m^H \boldsymbol{\rho}_n^{-1} \mathbf{C}_m) \mathbf{g} + \frac{\sigma_s^4}{\sigma_w^4} \gamma \left| \mathbf{g}^H (\mathbf{C}_m^H \boldsymbol{\rho}_n^{-1} \mathbf{C}_m)^{-1} \mathbf{C}_m^H \boldsymbol{\rho}_n^{-1} \mathbf{v}_a \right|^2}, \quad (6.393)$$

where

$$\gamma = \mathbf{v}_a^H \boldsymbol{\rho}_n^{-1} \mathbf{v}_a - \mathbf{v}_a^H \boldsymbol{\rho}_n^{-1} \mathbf{C}_m \left( \mathbf{C}_m^H \boldsymbol{\rho}_n^{-1} \mathbf{C}_m \right)^{-1} \mathbf{C}_m^H \boldsymbol{\rho}_n^{-1} \mathbf{v}_a, \quad (6.394)$$

and  $\mathbf{v}_a$  is the actual signal manifold vector. The results in (6.393) and (6.394) are due to Steele [Ste83].

We consider a series of examples to illustrate the behavior using various constraints. In all of the examples, we consider a standard linear array and assume the array is steered to broadside. We assume  $u_a$ , the actual arrival direction varies between  $-0.25BW_{NN}$  and  $0.25BW_{NN}$ . This assumption corresponds to a model in which we search  $u$ -space with beams spaced at  $0.5BW_{NN}$ .

We can also search  $u$ -space using a finer grid. This technique would reduce the mismatch problem at the cost of increased computational complexity.

### 6.7.4.2 Directional constraints

In this section, we study the behavior using directional constraints.

**Example 6.7.5: Directional main-lobe constraints; LCMV beamformer**

Consider a standard 10-element linear array. We use the three main-lobe constraints in (6.291),

$$\mathbf{C} = \begin{bmatrix} \mathbf{v}_u(0) & \mathbf{v}_u(-0.0866) & \mathbf{v}_u(0.0866) \end{bmatrix}, \quad (6.395)$$

where the array manifold vector is specified in  $u$ -space. We consider four  $\mathbf{g}$  matrices,

$$\mathbf{g} = \begin{bmatrix} 1 & g_{ci} & g_{ci} \end{bmatrix}, \quad i = 1, \dots, 4, \quad (6.396)$$

where

$$g_{c1} = 1, \quad (6.397)$$

$$g_{c2} = B_c(0.0866), \quad (6.398)$$

$$g_{c3} = \frac{1 + B_c(0.0866)}{2}, \quad (6.399)$$

$$g_{c4} = \frac{2 + B_c(0.0866)}{3}. \quad (6.400)$$

We assume the array is pointed at broadside ( $u_m = 0$ ) and the only interference is white noise. The actual signal arrival angle is  $u_a$ , and we examine the output  $SNR_o$  as a function of  $\frac{u_a}{BW_{NN}}$ . We assume that the actual value of  $\mathbf{S}_n$  (in this case  $\sigma_w^2 \mathbf{I}$ ) is used to design the beamformer.

In Figure 6.47, we plot the array gain versus  $\frac{u_a}{BW_{NN}}$  for an input  $SNR$  of 20 dB for the four choices of  $g_c$ . We also show the MVDR beamformer as a reference. For LCMV beamformers, the array gain is not a function of the input  $SNR$ . We use this input  $SNR$  as a reference level in the next example.

We see that the best choice for  $g_c$  depends on the range of mismatch that we expect in a particular application. As  $g_c$  is increased from  $B_c(0.0866)$  to 1, the array gain at  $u_a = 0$  decreases, but the slope of the array gain curve versus  $\frac{u_a}{BW_{NN}}$  also decreases. For our case in which the maximum mismatch is  $0.25BW_{NN}$ , we would use  $g_{c2}$ .

In the next example, we use the same model but assume that the actual  $\mathbf{S}_x$ , rather than  $\mathbf{S}_n$ , is available to design the LCMP beamformer,

$$\mathbf{S}_x = \sigma_s^2 \mathbf{v}_a \mathbf{v}_a^H + \sigma_w^2 \mathbf{I}. \quad (6.401)$$

We will see that there is a dramatic difference in performance.

**Example 6.7.6: Directional main-lobe constraints; LCMP beamformers (continuation)**

Consider the same model as in Example 6.7.5. We use the actual  $\mathbf{S}_x$  to design the beamformer. We use the  $\mathbf{C}$  matrix in (6.395) and use  $g_{c2}$  (6.398) in the  $\mathbf{g}$  matrix. We plot the array gain versus  $\frac{u_a}{BW_{NN}}$  for various input  $SNR$  (from -20 dB to 30 dB in 10-dB increments). The results are in Figure 6.48.

We see that there is a significant decrease in array gain for  $SNR \geq 10$  dB. We could reduce this loss by adding more directional constraints, but this

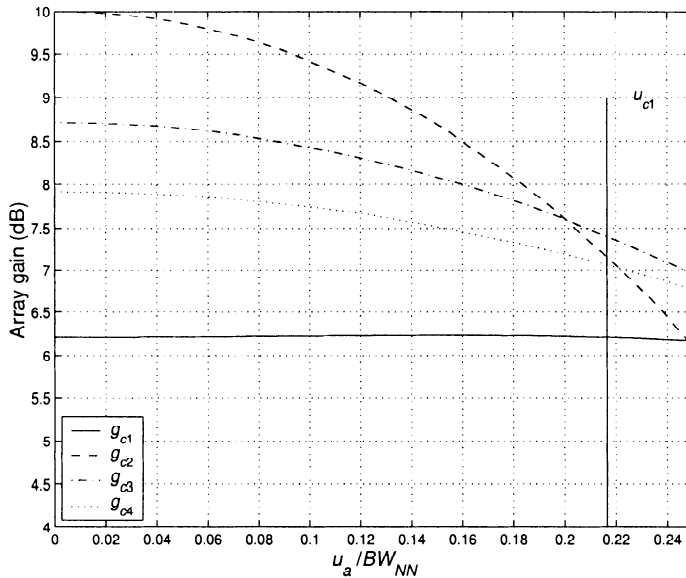


Figure 6.47 LCMV beamformer using directional constraints in white noise environment,  $SNR = 20$  dB,  $u_c = \pm 0.866$ ; array gain versus  $u_a/BW_{NN}$ .

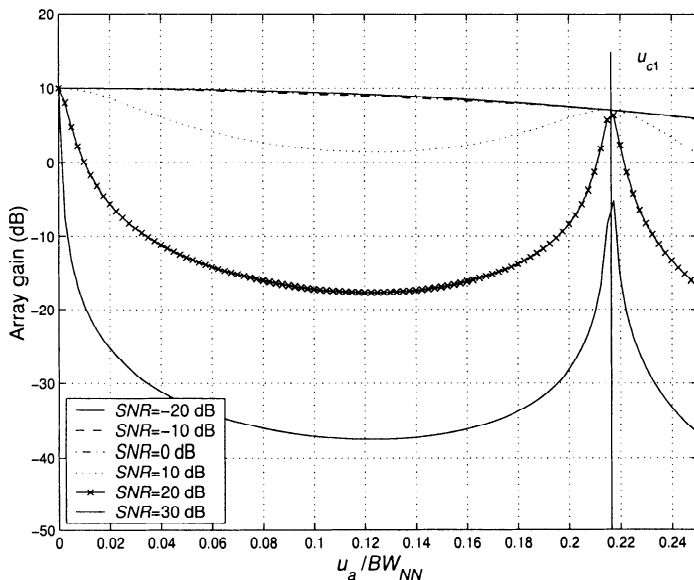


Figure 6.48 LCMP beamformer using directional constraints in white noise environment;  $u_c = \pm 0.0866$ ,  $g_c = B_c$ ; array gain versus  $u_a/BW_{NN}$ .

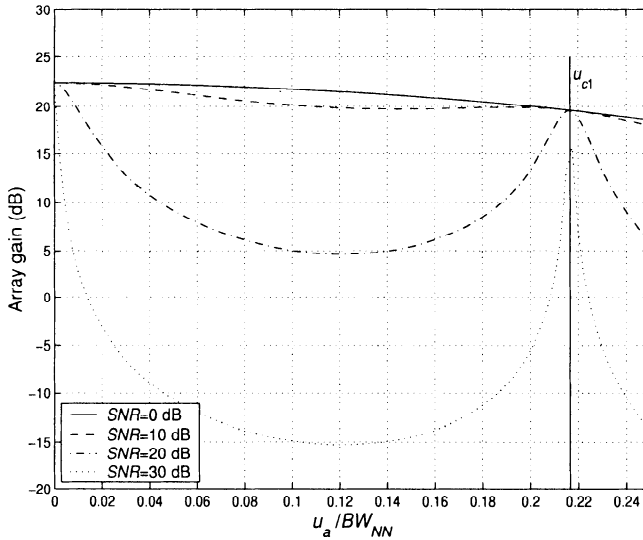


Figure 6.49 LCMP beamformer using directional constraints with two plane-wave interferers ( $\pm 0.30$ ) and white noise.  $INR = 10$  dB for each interferer; array gain versus  $u_a/BW_{NN}$ .

would reduce the degrees of freedom available to null interferers or reduce spatially spread noise.

In order to avoid the signal nulling behavior, we utilize diagonal loading as developed in Section 6.6.4. The appropriate level of diagonal loading depends on the interference environment. Before introducing diagonal loading, we consider an example with multiple plane-wave interferers to provide a baseline case.

**Example 6.7.7: Directional main-lobe constraints; LCMP beamformers (continuation)**

Consider the same model as in Example 6.7.5. In addition to the white noise interference, we assume that there are two equal-power, uncorrelated plane-wave interferers located at  $u_I = \pm 0.30$ . Thus,

$$\mathbf{S}_x = \sigma_s^2 \mathbf{v}_a \mathbf{v}_a^H + \sum_{i=1}^2 \sigma_i^2 \mathbf{v}_i \mathbf{v}_i^H + \sigma_w^2 \mathbf{I}. \quad (6.402)$$

We use the  $\mathbf{C}$  matrix in (6.395) and let  $g_c = B_c(0.0866)$ . We plot the array gain versus  $u_a/BW_{NN}$  for various  $SNR$  and  $INR$ . In Figure 6.49, the  $INR$  of each interferer is 10 dB. In Figure 6.50, the  $INR$  of each interferer is 30 dB. As in the white noise case, there is significant degradation for higher  $SNR$ .

We now introduce diagonal loading.

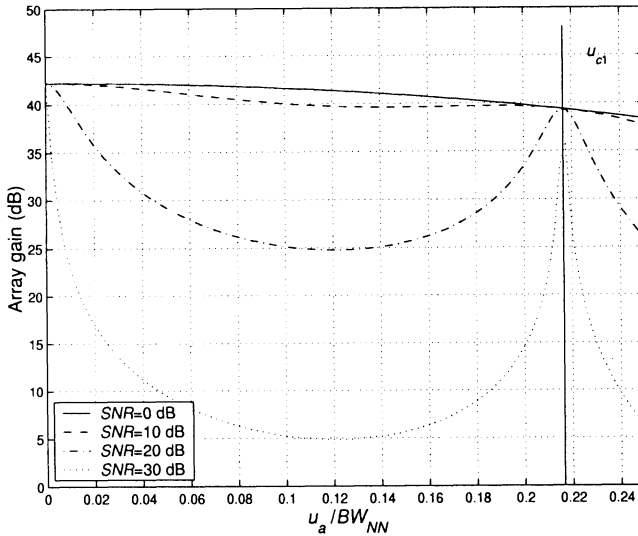


Figure 6.50 LCMP beamformer using directional constraints with two plane-wave interferers ( $\pm 0.30$ ) and white noise,  $INR = 30$  dB for each interferer; array gain versus  $u_a/BW_{NN}$ .

**Example 6.7.8: Directional main-lobe constraints; LCMP beamformers with diagonal loading (continuation)**

Consider the same model as in Example 6.7.7. The actual  $\mathbf{S}_x$  is given by (6.402). The weight vector is given by (6.358) modified to include diagonal loading,

$$\mathbf{w}_o^H \triangleq \mathbf{w}_{lcmp,dl}^H = \mathbf{g}^H \left[ \mathbf{C}^H \left[ \mathbf{S}_x + \sigma_L^2 \mathbf{I} \right]^{-1} \mathbf{C} \right]^{-1} \mathbf{C}^H \left[ \mathbf{S}_x + \sigma_L^2 \mathbf{I} \right]^{-1}. \quad (6.403)$$

The appropriate value of  $\sigma_L^2$  will depend on the  $SNR$  and  $INR$ . We define

$$LNR = \frac{\sigma_L^2}{\sigma_w^2}.$$

In order to decrease the signal nulling effect, we would like

$$LNR \geq SNR + 10 \text{ dB}. \quad (6.404)$$

However, to obtain adequate nulling of the interferers, we would like

$$INR(\text{dB}) - (LNR)(\text{dB}) \geq 10 \text{ dB}. \quad (6.405)$$

In some scenarios the two requirements conflict. In Figures 6.51–6.54, we plot the array gain versus  $u_a/BW_{NN}$  for various  $SNR$ ,  $INR$ , and  $LNR$  combinations.

In Figure 6.51, the  $INR$  is 30 dB. We plot the array gain with 15 dB loading versus  $u_a/BW_{NN}$ . We see that for  $SNR \leq 20$  dB, the array gain decreases monotonically to about 38 dB at  $u_a = 0.25BW_{NN}$ . In Figure 6.52, the  $INR$  is 30 dB. We plot the array gain with 20-dB loading versus  $u_a/BW_{NN}$ . The higher loading moves the curve for low  $SNR$  down

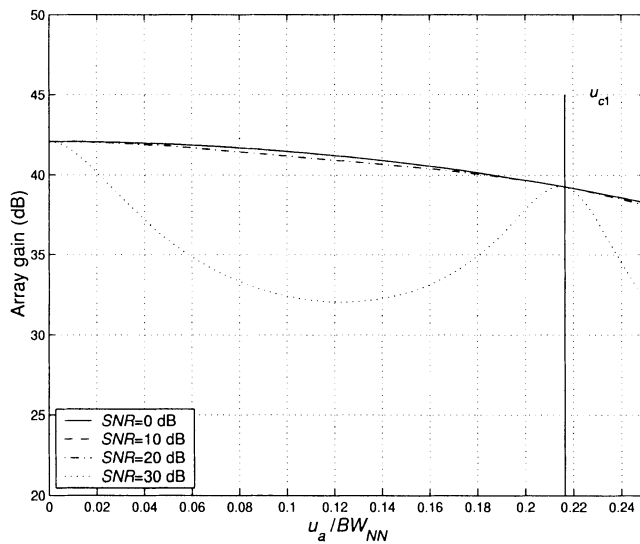


Figure 6.51 LCMP-DL beamformer using directional constraints with two plane-wave interferers ( $\pm 0.30$ ) and white noise,  $INR = 30$  dB,  $LNR = 15$  dB; array gain versus  $u_a/BW_{NN}$ .

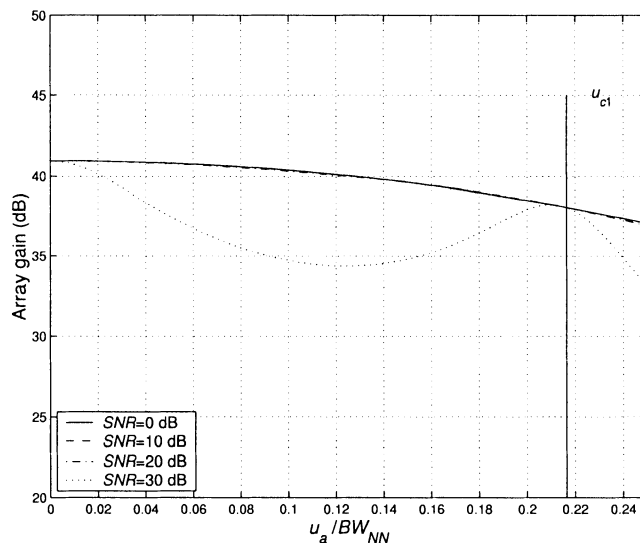


Figure 6.52 LCMP-DL beamformer using directional constraints with two plane-wave interferers ( $\pm 0.30$ ) and white noise,  $INR = 30$  dB,  $LNR = 20$  dB, array gain versus  $u_a/BW_{NN}$ .

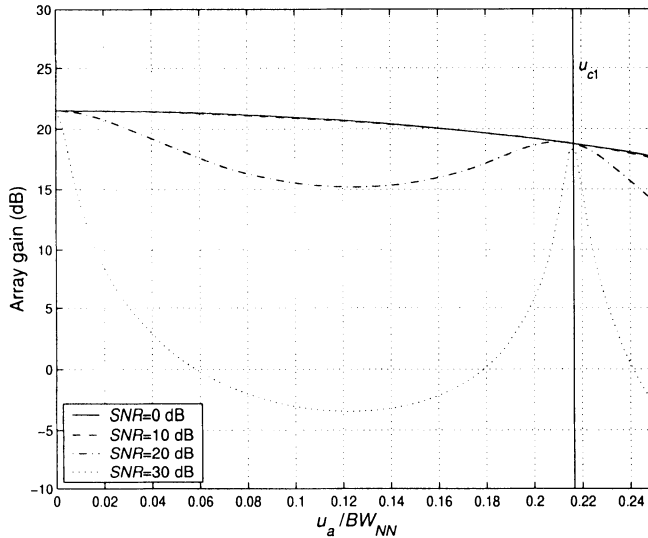


Figure 6.53 LCMP-DL beamformer using directional constraints with two plane-wave interferers ( $\pm 0.30$ ) and white noise,  $INR = 10$  dB,  $LNR = 10$  dB, array gain versus  $u_a/BW_{NN}$ .

about 1 dB but raises the minimum value of the curve for  $SNR = 30$  dB.

In Figures 6.53 and 6.54, the  $INR$  is 10 dB. Now we cannot add enough loading to prevent nulling of the 30-dB signal.

The plots in Figures 6.51–6.54 are useful to understand the beamformer behavior. However, a single metric is helpful to compare various techniques. We let  $u_a$  be a uniform random variable ranging from  $-0.25BW_{NN}$  to  $0.25BW_{NN}$  and compute the expected value of the array gain:

$$E[A] = \frac{1}{0.2} \int_{-0.1}^{+0.1} A(u_a : u_m) du_a. \quad (6.406)$$

We can then compute the diagonal loading that maximizes  $E[A]$  for a given interferer scenario ( $u_I$  and  $INR$ ) as a function of  $SNR$ . In Figure 6.55,  $E[A]$  is plotted versus  $SNR$  for several values of  $INR$ . We show the  $LNR$  values at several points on the curves.

It is important to note that, in practical applications, we will generally not have the information necessary to find an optimum  $LNR$ . However, these examples give us general guidelines. Later we will introduce variable diagonal loading based on data measurements.

In general, the  $E[A]$  is not sensitive to the exact value of  $LNR$ . In Figures 6.56 and 6.57, we plot  $E[A]$  versus  $LNR$  for various  $SNR$ . In Figure 6.56, the  $INR$  is 30 dB. In Figure 6.57, the  $INR$  is 20 dB.

We see that, even for an  $SNR = 30$  dB, the range of  $LNR$ , which results in a 3-dB loss from the optimum  $LNR$  exceeds 10 dB.

This sequence of examples illustrates typical performance for LCMP-DL algorithms using directional constraints. As long as the  $INR$  is sufficiently larger than the  $SNR$ , we can achieve satisfactory performance by adding appropriate diagonal loading. For higher

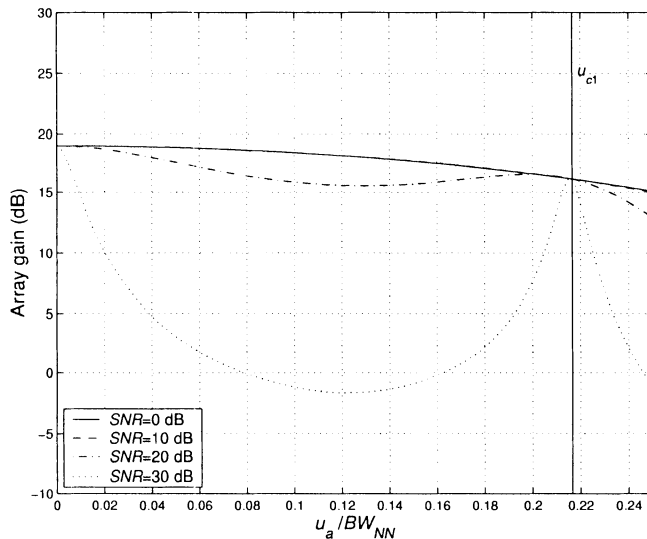


Figure 6.54 LCMP-DL beamformer using directional constraints with two plane-wave interferers ( $\pm 0.30$ ) and white noise,  $INR = 10$  dB,  $LNR = 15$  dB, array gain versus  $u_a/BW_{NN}$ .

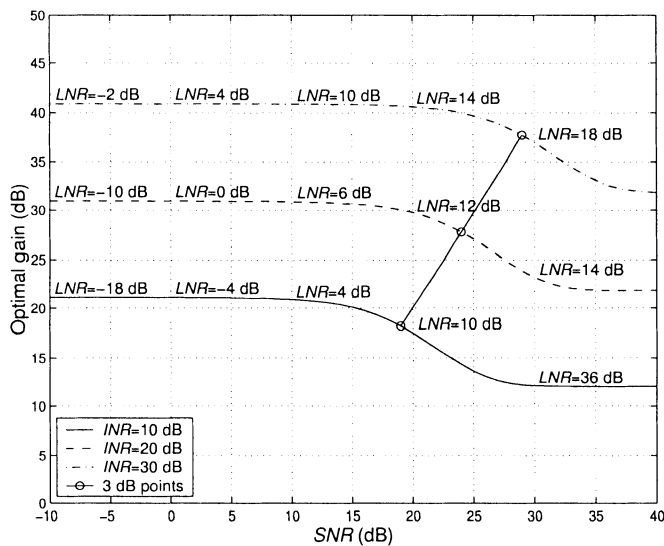


Figure 6.55 LCMP-DL beamformer using directional constraints, various  $INR$  and  $LNR$ ,  $E[\text{array gain}]$  versus  $SNR$ .

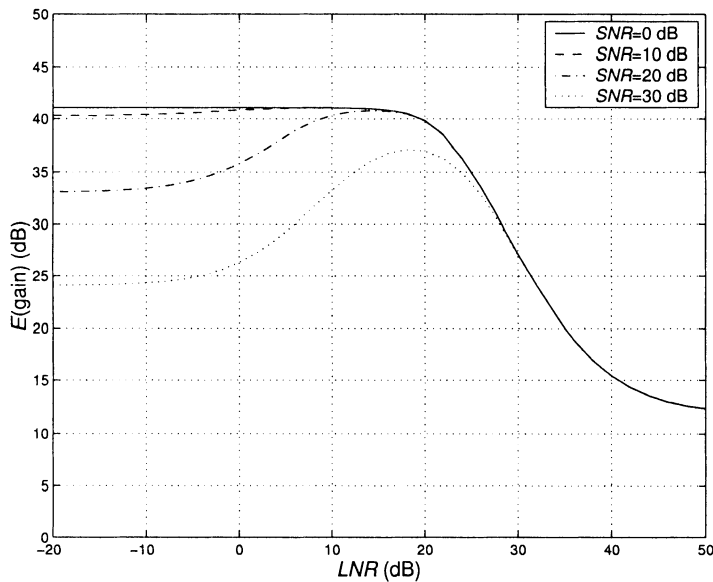


Figure 6.56 LCMP-DL beamformer using directional constraints,  $INR = 30$  dB, various  $SNR$ ,  $E[\text{array gain}]$  versus  $LNR$ .

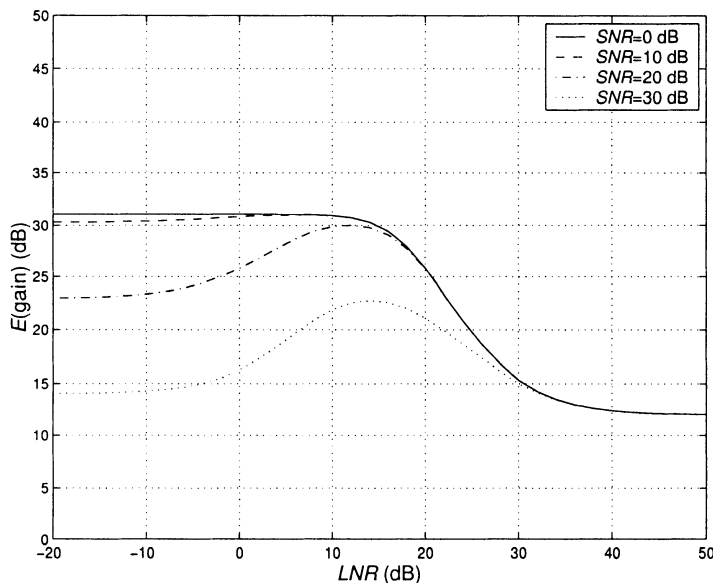


Figure 6.57 LCMP-DL beamformer using directional constraints,  $INR = 20$  dB, various  $SNR$ ,  $E[\text{array gain}]$  versus  $LNR$ .

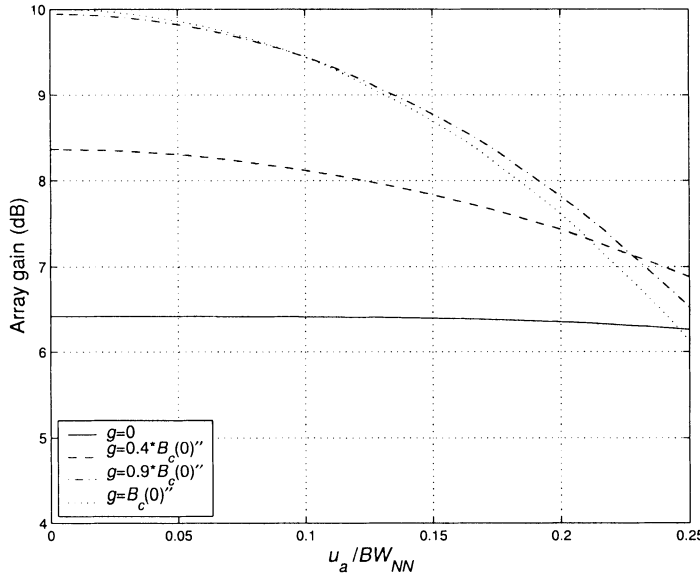


Figure 6.58 LCMP beamformer with second derivative constraints:  $SNR = 20$  dB, white noise environment, array gain versus  $u_a/BW_{NN}$ .

$SNR$ , we can reduce the range of mismatch by estimating  $u_a$ . We can then move the directional constraints to the steering direction.

#### 6.7.4.3 Derivative constraints

In this section, we consider derivative constraints.

##### Example 6.7.9: Derivative main-lobe constraints; LCMV beamformer

Consider a standard 10-element linear array. We use distortionless, first derivative, and second derivative constraints evaluated at the origin. From (6.312),

$$\mathbf{C} = \begin{bmatrix} 1 & d(0) & \dot{d}(0) \end{bmatrix}. \quad (6.407)$$

We consider four  $\mathbf{g}$  matrices: (6.313), (6.314), and (6.315) with  $g_3 = 0.4 \left( \frac{1-N^2}{12} \right)$  and  $0.9 \left( \frac{1-N^2}{12} \right)$ .

We assume that the array is pointed at broadside ( $u_m = 0$ ) and that the interference consists of white noise. The actual signal arrival angle is  $u_a$ , and we examine the array gain as a function of  $u_a/BW_{NN}$ . We assume that the actual value of  $\mathbf{S}_x$  (in this case,  $\sigma_w^2 \mathbf{I}$ ) is used to design the beamformer.

In Figure 6.58, we plot the array gain versus  $u_a/BW_{NN}$  for the LCMV beamformer. Using  $g_3$  equal to  $0.9\dot{B}_c(o)$  gives the best results for this scenario.

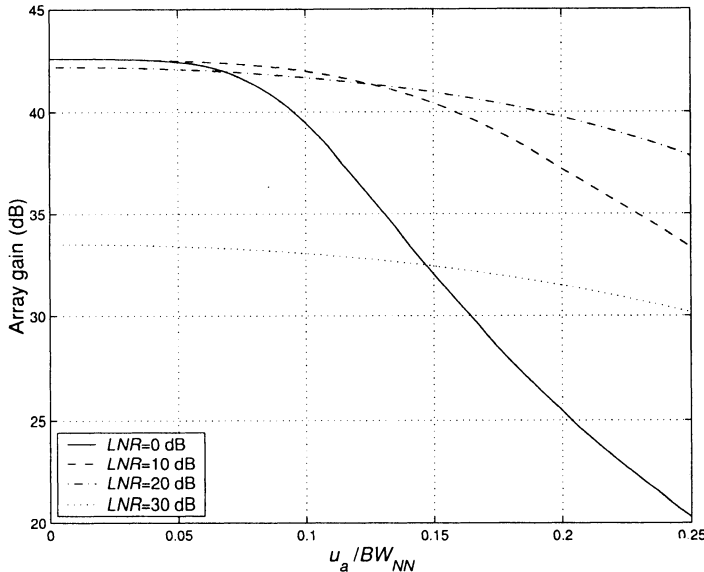


Figure 6.59 LCMV beamformer with second derivative constraints,  $SNR = 20$  dB,  $INR = 30$  dB,  $u_I = \pm 0.3$ ,  $g_3 = 0.8\ddot{B}_c(0)$ , array gain versus  $\frac{u_a}{BW_{NN}}$ .

We now consider the LCMP case. Based on the results of the directional constraints, we go directly to the diagonally loaded model and include  $\sigma_L^2 = 0$  as a special case.

**Example 6.7.10: Derivative main-lobe constraints; diagonally loaded LCMP beamformer (continuation)**

We utilize the interference plus noise model given in (6.402), and the  $\mathbf{C}$  matrix in (6.407), and the  $\mathbf{g}$  matrix in (6.315) with  $g_3 = 0.8\ddot{B}_c(0)$ . We consider various combinations of  $SNR$ ,  $INR$ , and  $LNR$ .

In Figure 6.59, we plot the array gain versus  $u_a / BW_{NN}$  for an  $INR = 30$  dB and an  $SNR = 20$  dB. We see that, with an  $LNR = 20$  dB, the array gain goes from 42 dB at  $u_a = 0$  to 38 dB at  $u_a = 0.25BW_{NN}$ . In Figure 6.60, we plot  $E[A]$  versus  $SNR$  for various values of  $INR$ .

Comparing Figures 6.55 and 6.60, we see that directional and derivative constraints provide essentially the same performance when optimal DL is used. Comparing these results to Figure 6.39, we see that the two additional constraints allow us to increase the  $SNR$  by about 15 dB and maintain the same  $E[\text{array gain}]$ .

#### 6.7.4.4 Eigenvector constraints

In this section, we consider eigenvector constraints.

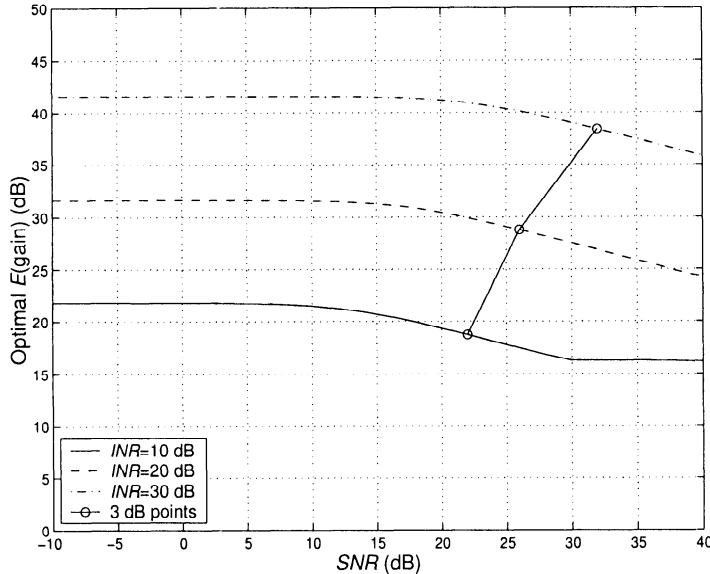


Figure 6.60 LCMP-DL beamformer with second derivative constraints and optimal loading,  $u_a$  is uniform  $[-0.1, 0.1]$ ,  $u_I = \pm 0.3$ ,  $g_3 = 0.8\ddot{B}_c(0)$ ,  $INR = 10, 20$ , and  $30$  dB,  $E[\text{array gain}]$  versus  $SNR$ .

#### Example 6.7.11: Eigenvector constraints; LCMP beamformer

Consider a standard 10-element linear array. In (6.347), we assumed that

$$B_d(u) = B_c(u), \quad -u_d \leq u \leq u_d.$$

We let  $u_d = 0.1$ . Since  $\mathbf{Q}$  in (6.348) does not depend on  $B_d(u)$ , the eigenvectors and columns of  $\mathbf{C}$  are the discrete prolate spheroidal functions. The vector  $\mathbf{g}^H$  is given by (6.345).

In Figure 6.61, we plot the array gain versus  $u_a/BW_{NN}$  for the case in which the  $SNR$  is 20 dB and the  $INR$  of each interferer is 30 dB. As we would expect, the behavior is very similar to the behavior using directional constraints because, in the narrowband case, they are essentially equivalent.

In Figure 6.62, we plot the expected value of the array gain versus  $SNR$  for various  $INR$ .

#### 6.7.4.5 Summary

In Section 6.7.4, we have studied the performance of LCMV and LCMP beamformers in the presence of a DOA mismatch. This range of uncertainty  $|u_a| \leq \frac{1}{N}$  is among the most stressful for testing array robustness. In the problems, we consider array perturbations in the form of sensor position perturbations.

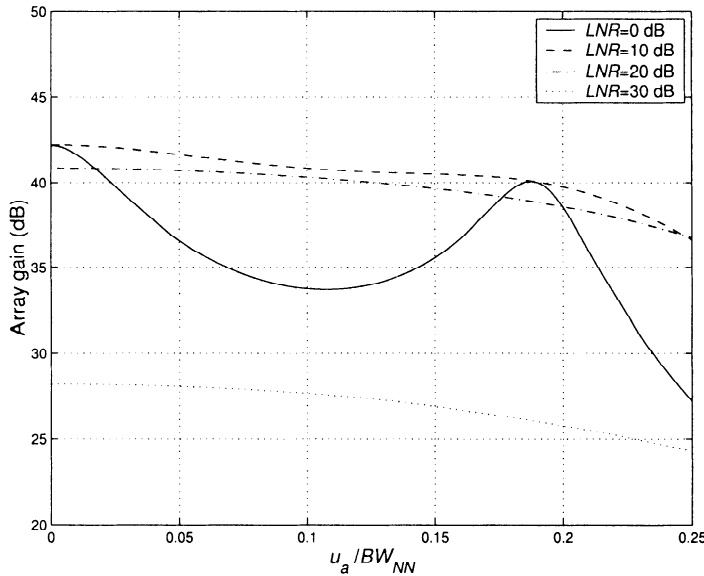


Figure 6.61 LCMP-DL beamformer with three eigenvector constraints,  $SNR = 20$  dB,  $INR = 30$  dB,  $u_I = \pm 0.3$ ,  $B_d(u) = B_c(u)$ ,  $u_d = 0.1$ ; array gain versus  $u_a / BW_{NN}$ .

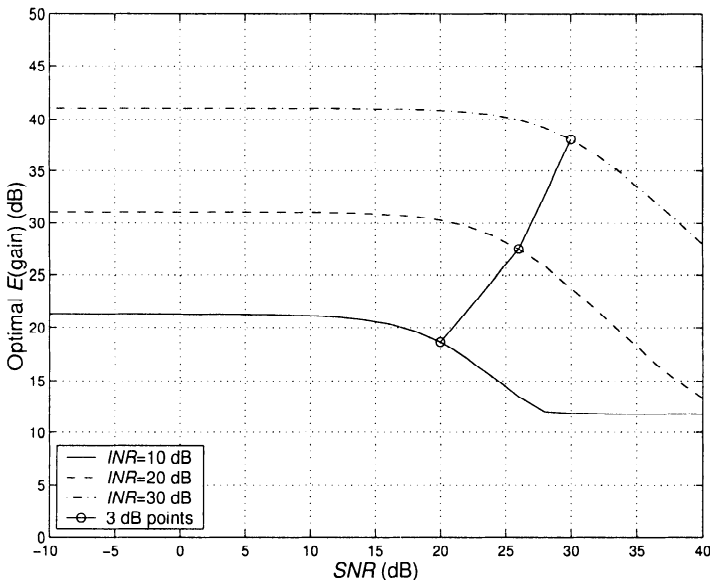


Figure 6.62 LCMP-DL beamformer with eigenvector constraints;  $E[\text{array gain}]$  versus  $SNR$  for various  $INR$ .

In the problems, we analyze a wide range of array configurations and interference scenarios. We find the results for the linear array with discrete interference are characteristic of the general case. The key element in the beamformer performance is an appropriate level of diagonal loading. In Section 6.10, we revisit the diagonal loading question. In Chapter 7, we develop variable loading algorithms that depend on the data input.

We found that the case of high *SNR* compared to *INR* led to significantly degraded performance in the presence of DOA mismatch. A logical step would be to perform a preprocessing to estimate the DOA prior to beamforming. We look at this approach briefly in Chapter 7 and in more detail in Chapter 9 when we study parameter estimation.

### 6.7.5 Quiescent Pattern (QP) Constraints

The constraints that we have discussed up to this point have focused on constraining the beam pattern at specific points in frequency-wavenumber space or in small regions of the space. The eigenvector constraints in Section 6.7.1.5 can control arbitrary regions of the frequency-wavenumber space, but as the region grows more degrees of freedom are required.

In this section, an algorithm is developed that first specifies a desired quiescent pattern (QP). We then specify a region in  $\omega\text{-}\mathbf{k}$  space in which we expect the desired signal to arrive. Constraints are introduced to avoid signal degradation. These constraints are in a space that is orthogonal to the space defined by the quiescent pattern.

Applebaum [AC76], in his early work on adaptive arrays recognized the importance of including desirable quiescent patterns in his adaption procedure. In [AC76], examples are given for a 32-element linear array in which the quiescent pattern utilizes Dolph-Chebyshev weighting with  $-30$ -dB side-lobes. Distortionless, first-order derivative, and second-order derivative constraints are imposed and the optimum pattern is found for a single directional interferer and white noise.

Gabriel [Gab87] also discusses the importance of a good quiescent pattern and gives examples. Subsequently, Griffiths and Buckley [GB87] developed a solution in the context of the generalized sidelobe canceller in Figure 6.46. A different approach was developed by Tseng and Griffiths [TG92b]. Our discussion follows [TG92b].

We denote the weight vector of desired quiescent pattern by  $\mathbf{w}_{dq}$ . In order to specify the constraint, we recall that the quiescent pattern is

$$\mathbf{w}_q = \mathbf{C}(\mathbf{C}^H \mathbf{C})^{-1} \mathbf{g}. \quad (6.408)$$

Therefore, if we define

$$\bar{\mathbf{w}}_{dq} = \frac{\mathbf{w}_{dq}}{\|\mathbf{w}_{dq}\|^2}, \quad (6.409)$$

and use the constraint

$$\bar{\mathbf{w}}_{dq}^H \mathbf{w} = 1, \quad (6.410)$$

then the resulting quiescent pattern is, from (6.408),

$$\mathbf{w}_q = \frac{\mathbf{w}_{dq}}{\|\mathbf{w}_{dq}\|^2} \left( \frac{\mathbf{w}_{dq}^H \mathbf{w}_{dq}}{\|\mathbf{w}_{dq}\|^4} \right)^{-1} = \mathbf{w}_{dq}. \quad (6.411)$$

However, we must impose other constraints to prevent the desired signal from being cancelled by the adaptive weights. We assume there is a response region from which the signal will arrive. We specify that region in a  $(\theta, \phi, f)$  space and define

$$\mathbf{Q} = \int_F \int_\Theta \int_\Phi \mathbf{v}(\theta, \phi, f) \mathbf{v}^H(\theta, \phi, f) d\theta d\phi df. \quad (6.412)$$

Note that this is same  $\mathbf{Q}$  that we defined in the eigenvector constraint discussion in (6.337).

Instead of using this matrix directly, we define a modified matrix,

$$\bar{\mathbf{R}}_s = \mathbf{P}_{\bar{\mathbf{w}}_{dq}}^\perp \mathbf{Q} \mathbf{P}_{\bar{\mathbf{w}}_{dq}}^\perp, \quad (6.413)$$

where

$$\mathbf{P}_{\bar{\mathbf{w}}_{dq}} = \bar{\mathbf{w}}_{dq} \left( \bar{\mathbf{w}}_{dq}^H \bar{\mathbf{w}}_{dq} \right)^{-1} \bar{\mathbf{w}}_{dq}^H \quad (6.414)$$

is the projection matrix with respect to  $\bar{\mathbf{w}}_{dq}$ . We then construct a matrix  $\bar{\mathbf{C}}_s$  whose columns are the principal eigenvectors of  $\bar{\mathbf{R}}_s$  and require, in addition to the constraint in (6.410), that

$$\bar{\mathbf{C}}_s^H \mathbf{w} = \mathbf{0}. \quad (6.415)$$

Thus, the quiescent response is unchanged because  $\bar{\mathbf{C}}_s$  is orthogonal to  $\bar{\mathbf{w}}_{dq}$  and the corresponding constraint values are zero. For example, if we use two eigenvectors:

$$\mathbf{C} = \begin{bmatrix} \bar{\mathbf{w}}_{dq} & \bar{\mathbf{C}}_s \end{bmatrix} = \begin{bmatrix} \bar{\mathbf{w}}_{dq} & \psi_{s1} & \psi_{s2} \end{bmatrix}, \quad (6.416)$$

where  $\psi_{s1}$  and  $\psi_{s2}$  are the principal eigenvectors of  $\bar{\mathbf{R}}_s$ . The algorithm relies on the eigenvectors in (6.416) for main-lobe protection.

In a similar manner, we can specify behavior in other regions of interest. For example, consider a particular area in  $\omega\text{-}\mathbf{k}$  space where we expect interference (or jamming). Denoting this region as  $\mathbf{R}_J$ , we add additional constraints,

$$\bar{\mathbf{C}}_J \mathbf{w}^H = \mathbf{0}, \quad (6.417)$$

where  $\bar{\mathbf{C}}_J$  are the principal eigenvectors of  $\bar{\mathbf{R}}_J$ , which is defined as

$$\bar{\mathbf{R}}_J = \mathbf{P}_{\bar{\mathbf{C}}_s}^\perp \mathbf{P}_{\bar{\mathbf{w}}_{dq}}^\perp \mathbf{R}_J \mathbf{P}_{\bar{\mathbf{w}}_{dq}}^\perp \mathbf{P}_{\bar{\mathbf{C}}_s}^\perp. \quad (6.418)$$

Once again, the additional constraints do not change the quiescent response.

The total constraint matrix is

$$\begin{aligned} \mathbf{C} &= \left[ \begin{array}{ccc} \bar{\mathbf{w}}_{dq} & \bar{\mathbf{C}}_s & \bar{\mathbf{C}}_J \end{array} \right] \\ &= \left[ \begin{array}{ccccc} \bar{\mathbf{w}}_{dq} & \psi_{s1} & \psi_{s2} & \psi_{J1} & \psi_{J2} \end{array} \right], \end{aligned} \quad (6.419)$$

and

$$\mathbf{g}^H = \left[ \begin{array}{c|c|c|c|c} 1 & 0 & \cdots & 0 \end{array} \right]. \quad (6.420)$$

Then, the optimum beamformer is given by (6.358),

$$\mathbf{w}_o^H = \mathbf{g}^H \left[ \mathbf{C}^H \mathbf{S}_x^{-1} \mathbf{C} \right]^{-1} \mathbf{C}^H \mathbf{S}_x^{-1}. \quad (6.421)$$

To illustrate the algorithm, we first consider an example with the same signal and interference model that we have used in previous examples.

#### Example 6.7.12

Consider a standard 10-element linear array. The nominal signal arrival angle is  $u_s = 0$ . The actual signal arrival angle is  $u_a$ , where  $0 \leq |u_a| \leq 0.1$ . We first consider the case in which  $\mathbf{w}_{dq}$  corresponds to the conventional beam pattern.

Then

$$\bar{\mathbf{w}}_{dq} = \mathbf{1}/N, \quad (6.422)$$

and

$$\mathbf{P}_{\bar{\mathbf{w}}_{dq}}^\perp = \mathbf{I} - \mathbf{1}\mathbf{1}^H/N. \quad (6.423)$$

The region of interest is  $|u_a| \leq 0.1$ . Then

$$\mathbf{Q} = \int_{-u_d}^{u_d} \mathbf{v}(u) \mathbf{v}^H(u) du, \quad (6.424)$$

which is the same  $\mathbf{Q}$  as in (6.348) and  $u_d = 0.1$ . Thus,

$$[\mathbf{Q}]_{mn} = \frac{2 \sin[\pi u_d(m-n)]}{\pi(m-n)}. \quad (6.425)$$

We use (6.423) and (6.424) in (6.413) to find  $\bar{\mathbf{R}}_s$ . We find the eigenvectors of  $\bar{\mathbf{R}}_s$  and use the  $N_e$  eigenvectors with the largest eigenvalues to construct  $\bar{\mathbf{C}}_s$ .

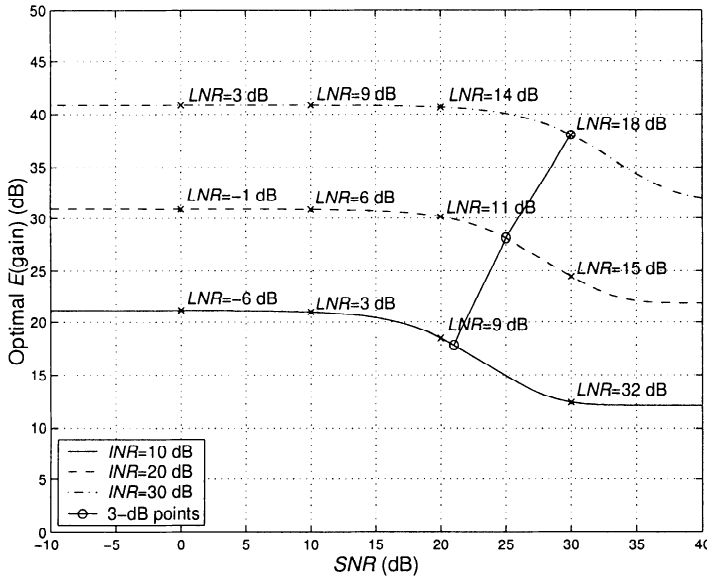


Figure 6.63 LCMP beamformer with quiescent pattern constraints; conventional QP,  $N_e = 2$ ,  $u_d = 0.1$ ,  $E[\text{array gain}]$  versus  $SNR$  for various  $INR$ .

The interference model is given by (6.402). There are two plane-wave interferers at  $\pm 0.30$ .

$$\mathbf{S}_x = \sigma_s^2 \mathbf{v}_a \mathbf{v}_a^H + \sum_{i=1}^2 \sigma_i^2 \mathbf{v}_i \mathbf{v}_i^H + \sigma_w^2 \mathbf{I}. \quad (6.426)$$

The weight vector is given by (6.358) with the  $N \times (N_e + 1)$  constraint matrix,

$$\mathbf{C} = [\bar{\mathbf{w}}_{dq} \mid \boldsymbol{\psi}_1 \mid \cdots \mid \boldsymbol{\psi}_{N_e}], \quad (6.427)$$

and the  $\mathbf{g}$  matrix,

$$\mathbf{g}^H = [1 \ 0 \ \cdots \ 0]. \quad (6.428)$$

In order to provide a comparison with our previous examples, we let  $N_e = 2$  so that there are three constraints. We also add diagonal loading.

In Figure 6.63, we plot the expected value of array gain versus  $SNR$  for various  $INR$ . We see that with appropriate  $LNR$ , we can maintain the array gain over values of  $SNR \leq INR$ .

#### Example 6.7.13 (continuation)

The model is identical to Example 6.7.12. We use a desired quiescent weighting corresponding to a Taylor-Villenueve weighting with  $-20$  dB maximum sidelobe and  $\bar{n} = 2$ .

In Figure 6.64, we plot the expected value of the array gain versus  $SNR$  for various  $INR$ . We also show the results from Example 6.7.12.

We see that the results for the two choices of quiescent beam patterns

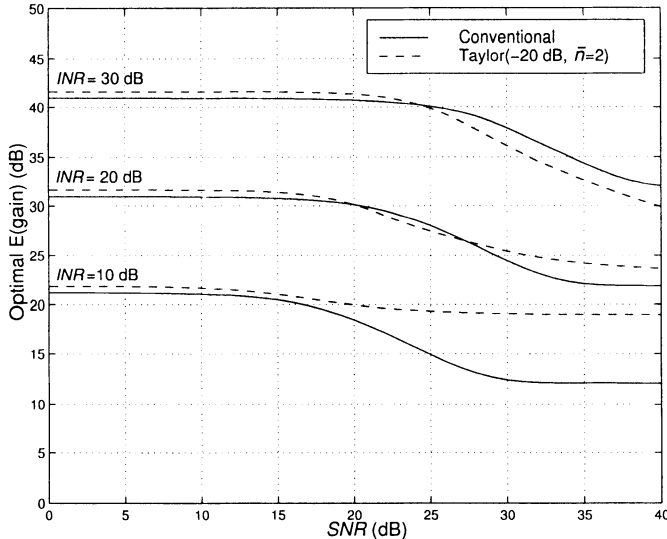


Figure 6.64 LCMP beamformer with quiescent pattern constraints, Taylor QP,  $N_e = 2$ ,  $u_d = 0.1$ ,  $E[\text{array gain}]$  versus  $\text{SNR}$  for various  $\text{INR}$ .

are similar for  $\text{SNR} \leq 20 - 25$  dB. For higher  $\text{SNR}$ , a higher  $\text{LNR}$  is required to prevent signal cancellation, and the quiescent sidelobe structure provides the array gain.

To illustrate a different application of the QP technique, we consider a simple example from [TG92b].

#### Example 6.7.14 [TG92b]

Consider a standard 21-element linear array. The desired signal direction is broadside and the anticipated jammer region is  $40^\circ \leq \bar{\theta} \leq 50^\circ$ , where  $\bar{\theta}$  is the broadside angle.

The desired quiescent pattern is shown in Figure 6.65. It has unit gain in signal direction,  $-50$ -dB sidelobes in the anticipated jamming region ( $40^\circ \leq \bar{\theta} \leq 50^\circ$ ) and  $-30$ -dB sidelobes elsewhere. It is designed using the techniques in Section 3.9.3. By having lower sidelobes in the area of the anticipated jammer, the adaptive beamformer will converge more rapidly if the jammer arrives in that area.

The first two constraints are

$$\bar{\mathbf{w}}_{dq}^H \mathbf{w} = 1, \quad (6.429)$$

and

$$\mathbf{c}_2^H \mathbf{w} = 0, \quad (6.430)$$

where

$$\mathbf{c}_2 = \mathbf{P}_{\bar{\mathbf{w}}_{dq}}^\perp \mathbf{v}(0). \quad (6.431)$$

We refer to (6.429) and (6.430) as constraint set 1.

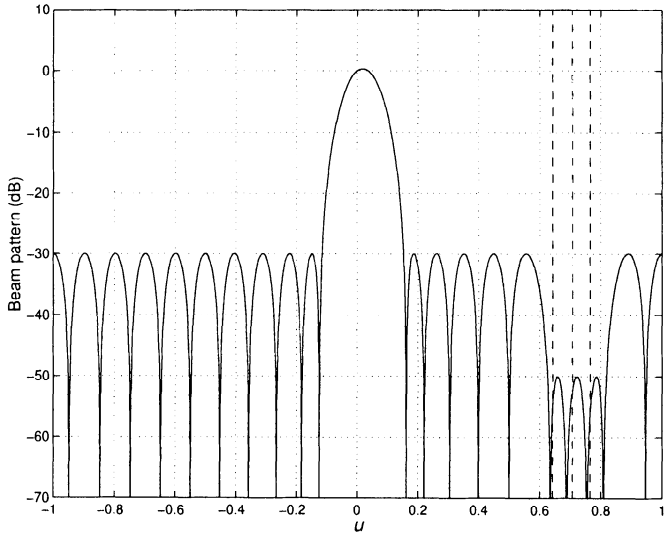


Figure 6.65 Desired quiescent pattern:  $N = 21$ ,  $u_s = 0$ .

A second constraint set is constructed by constraining the four nulls in the -50-dB sidelobe region (at  $38.1^\circ$ ,  $42.1^\circ$ ,  $47.5^\circ$ , and  $52.3^\circ$ ) to remain nulls. Thus,

$$\mathbf{R}_J = \frac{1}{4} \sum_{i=1}^4 \mathbf{v}(\bar{\theta}_i) \mathbf{v}^H(\bar{\theta}_i). \quad (6.432)$$

This step leads to four additional constraints,  $\psi_i$ , where the  $\psi_i$  are the eigenvectors of

$$\tilde{\mathbf{R}}_J = \mathbf{P}_{\mathbf{C}_2}^\perp \mathbf{P}_{\bar{\mathbf{w}}_{dq}}^\perp \mathbf{R}_J \mathbf{P}_{\bar{\mathbf{w}}_{dq}}^\perp \mathbf{P}_{\mathbf{C}_2}^\perp. \quad (6.433)$$

There are a total of six constraints,

$$\mathbf{C} = [ \bar{\mathbf{w}}_{dq} \quad \mathbf{c}_2 \quad \psi_1 \quad \psi_2 \quad \psi_3 \quad \psi_4 ], \quad (6.434)$$

where the  $\psi_i$  are the four principal eigenvectors of  $\tilde{\mathbf{R}}_J$ .

We now assume that a jammer with a 30-dB *INR* arrives at  $45^\circ$ . The resulting adapted beam pattern is shown in Figure 6.66. We see that the constraint set preserves the desired quiescent pattern reasonably well and creates a null in the direction of the jammer. The array gain is 42.19 dB for this case.

We also consider the case in which only the first two constraints are used. The resulting adapted beam pattern is shown in Figure 6.67. The array gain is 42.21 dB.

We see that the QP approach provides a great deal of design flexibility and allows us to tailor our optimum beamformer to different anticipated scenarios.

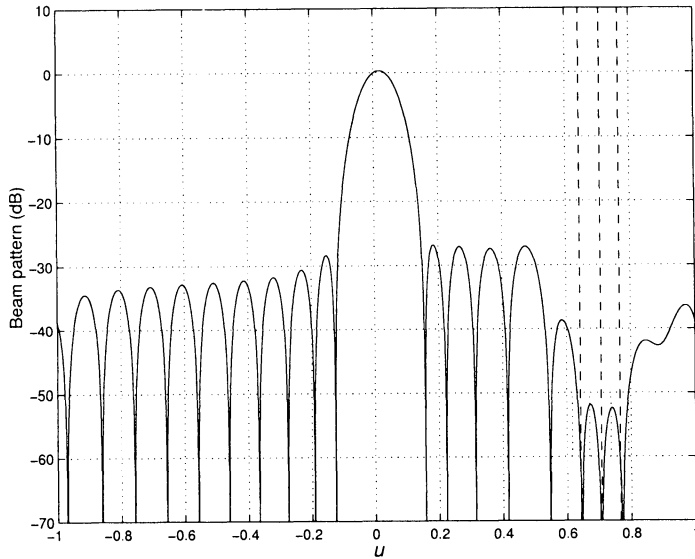


Figure 6.66 Optimum beam pattern: six constraints;  $N = 21$ ,  $u_s = 0$ ,  $u_I = 0.707$ ,  $SNR = 0$  dB,  $INR = 30$  dB.

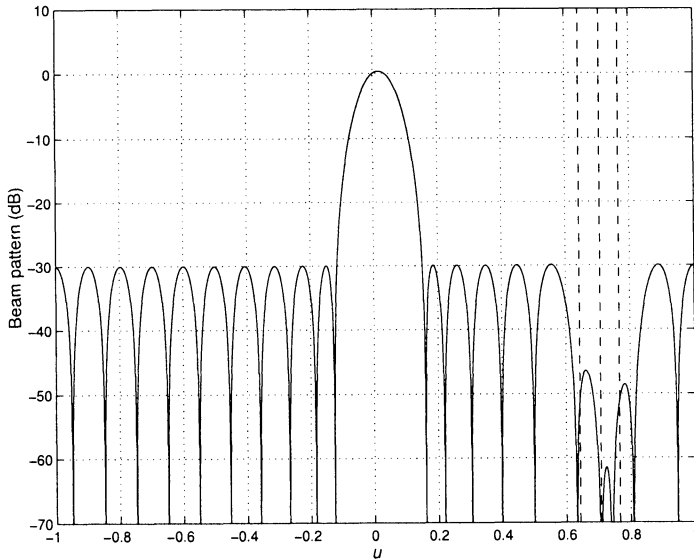


Figure 6.67 Optimum beam pattern: constraint set 1 (2 constraints);  $N = 21$ ,  $u_s = 0$ ,  $u_I = 0.707$ ,  $SNR = 0$  dB,  $INR = 30$  dB.

### 6.7.6 Covariance Augmentation

Diagonal loading is a useful tool to control signal mismatch. In many applications, we also encounter interferer mismatch. This behavior can occur because our measurement of  $\mathbf{S}_x$  is poor due to small sample support, the interferers may move, or the interferer may be spread in either space or frequency. In order to deal with this problem, we want to broaden the nulls that the beamformer is placing on the interferers.

One approach to broadening the nulls is to impose derivative constraints on the nulls of the adapted beam pattern, as discussed in (6.331) and (6.332). Gershman and Ermolaev [GE91] and Gershman et al. [GSB96] have developed adaptive algorithms to accomplish this.

A second approach was developed independently by Mailloux [Mai95] and Zatman [Zat95] that augments the spatial spectral matrix. A discussion of this technique that is referred as **covariance matrix tapers** (CMT) is given by Guerci [Gue99]. The relationship between the two techniques is derived by Zatman [Zat99] [Zat00].<sup>11</sup> We discuss the second approach in this section.

Assume that the MPDR beamformer is designed under the assumption that

$$\mathbf{S}_{x,m} = \sigma_s^2 \mathbf{v}_s \mathbf{v}_s^H + \sum_{i=1}^D \sigma_i^2 \mathbf{v}_i(u_i) \mathbf{v}_i^H(u_i) + \sigma_w^2 \mathbf{I}. \quad (6.435)$$

The actual interferers arrive from  $u_{ai} = u_i + \Delta u_i$ .

We construct an augmented spatial spectral matrix to account for the uncertainty in the interferer locations. We first define a matrix  $\mathbf{T}$ ,

$$\mathbf{T}_{ij} = \text{sinc}(|i - j|\gamma), \quad (6.436)$$

where  $\gamma$  is a design parameter that is matched to the uncertainty in the  $u_i$ .

From Section 5.5.2, we recall that this is the spatial spectral matrix for a narrowband spatially spread signal whose power is constant over an interval  $-\gamma \leq \psi \leq \gamma$ .

We define an augmented spatial spectral matrix as a Hadamard product of  $\mathbf{S}_{x,m}$  and  $\mathbf{T}$ ,

$$\mathbf{S}_{x,au} \triangleq \mathbf{S}_{x,m} \odot \mathbf{T}. \quad (6.437)$$

We design the beamformer using  $\mathbf{S}_{x,au}$  instead of  $\mathbf{S}_x$ . This augmentation broadens the nulls. We consider an example to illustrate the behavior.

---

<sup>11</sup>We are using  $\mathbf{S}_x$ , so a more appropriate title is spatial matrix tapers. We use CMT to be consistent with the literature.

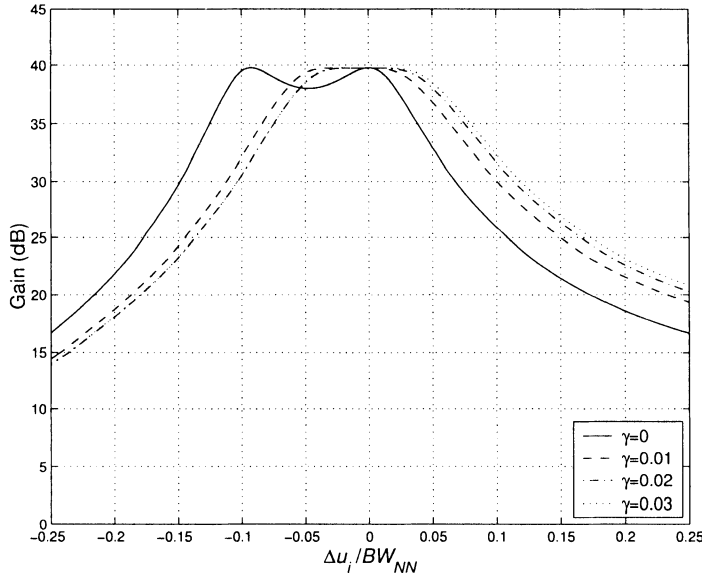


Figure 6.68 Array gain versus  $\Delta u_I/BW_{NN}$ :  $N=10$ ,  $u_a=0$ ,  $u_I=0.3$ ,  $INR = 30$  dB, covariance matrix taper with various  $\gamma$ .

#### Example 6.7.15

Consider a standard 10-element array. The MPDR beamformer is designed under the assumption that

$$\mathbf{S}_{\mathbf{x},m} = \sigma_s^2 \mathbf{v}_s \mathbf{v}_s^H + \sigma_I^2 \mathbf{v}_I(u_I) \mathbf{v}_I^H(u_I) + \sigma_w^2 \mathbf{I}. \quad (6.438)$$

The array is steered to broadside. The actual interferer arrives from  $u_{Ia} = u_I + \Delta u$ .

We consider two beamformers. The first is the MPDR beamformer. The second is a beamformer that is constructed using the augmented  $\mathbf{S}_{\mathbf{x}}$  matrix defined in (6.437). We first consider the case with no signal mismatch and  $u_I = 0.30$  with an  $INR = 30$  dB. We vary  $\gamma$  from 0 to 0.05 in 0.01 steps.

In Figure 6.68, we plot the array gain versus  $\Delta u_I/BW_{NN}$  for the various  $\gamma$ . In Figure 6.69, we plot the beam pattern in the vicinity of  $u_I = 0.3$  for  $\gamma = 0, 0.01, 0.02$  and  $0.03$ . We see that the null has been broadened with negligible loss in array gain.

#### 6.7.7 Summary

We have explored five types of linear constraints in Section 6.7.4 and 6.7.5. In Figure 6.70, we plot their performance for the signal and interference model that we analyzed in a sequence of examples. We see that the five LCMP-DL beamformers have similar performance for  $SNRs$  that are less than the 3-dB loss value. They are all significantly better than MPDR-DL. It is important to recognize the contribution of diagonal loading to the

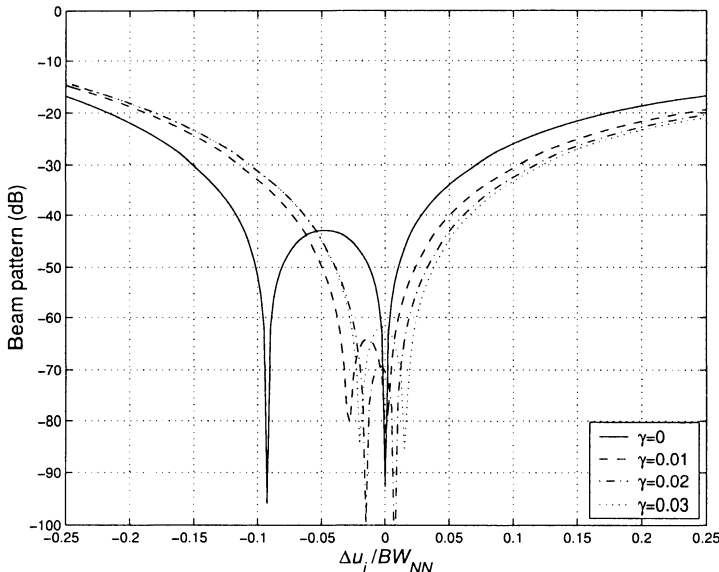


Figure 6.69 Beam pattern around  $u_I = 0.30$ : covariance matrix taper with various  $\gamma$ .

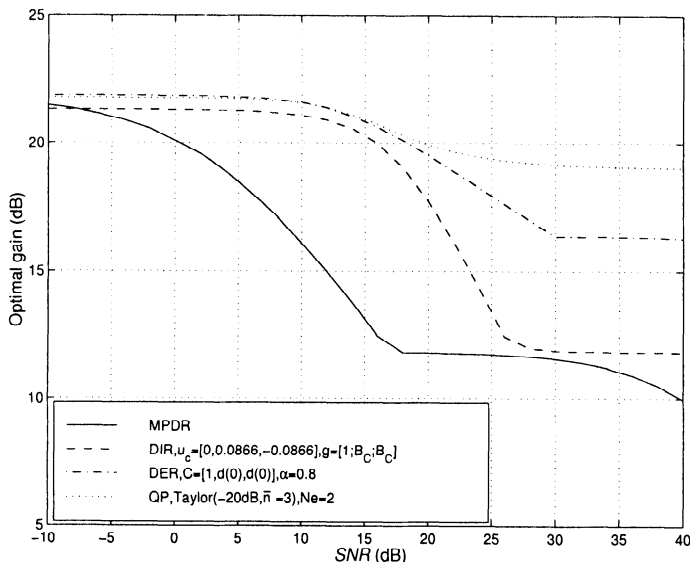
robust behavior. In most scenarios, it will be a necessary component of the optimum beamformer. Note that, although diagonal loading was introduced as the solution to a well-posed optimization problem (6.261)–(6.268), it is usually applied in a more ad hoc manner. When diagonal loading is used in this manner, it can provide good performance, but it is not optimum in any formal sense.

In the problems, we discuss a number of signal and interference scenarios for DOA mismatch. We also study the array perturbation problem. We find similar results to the above examples.

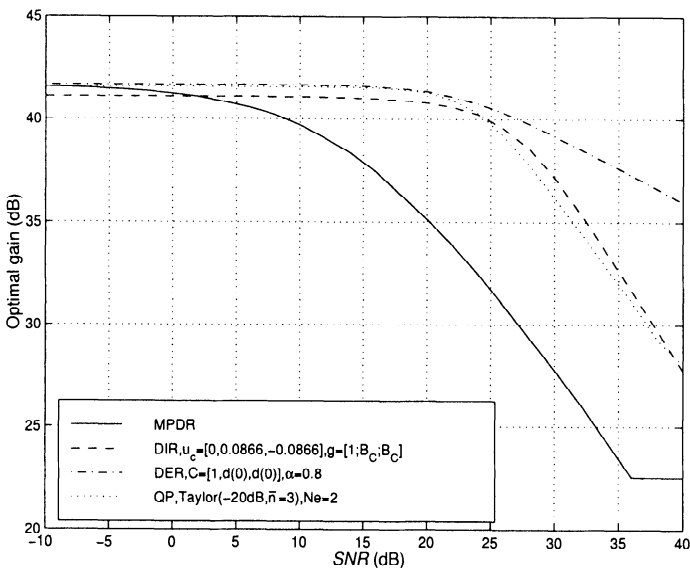
All of the optimum beamformers that we have discussed up to this point are operating in an  $N$ -dimensional space. In the next two sections, we develop algorithms that operate in a reduced-dimension space. We find that this reduced-dimension operation offers significant advantages.

## 6.8 Eigenvector Beamformers

In the first part of this chapter we found that MVDR and MPDR beamformers are the optimum processors for waveform estimation under a variety



(a)



(b)

Figure 6.70 Performance comparison using various constraints and optimum DL:  $N = 10$ ,  $u_I = \pm 0.3$ . (a)  $INR = 10$  dB; (b)  $INR = 30$  dB.

of criteria. In Section 6.6, we studied the problem of signal or interference mismatch and found that the optimum processors, particularly the MPDR beamformer, could suffer significant performance degradation in the presence of mismatch. In Section 6.7, we found that by introducing linear constraints and DL, we can obtain robust performance.

All of beamformers assumed  $\mathbf{S}_x$ , the spatial spectral matrix (or  $\mathbf{S}_n$ ), was known and required computation of  $\mathbf{S}_x^{-1}$  (or  $\mathbf{S}_n^{-1}$ ) to find the weight vector.

In practice, we must estimate  $\mathbf{S}_x$  from a finite amount of data. Specifically, we will have  $K$  independent samples of  $\mathbf{X}$  available. In Chapter 7, we encounter several problems:

- (i) The accuracy of the estimate of  $\mathbf{S}_x$  depends on  $K/N$ ; the ratio of the number of samples,  $K$ , to the number of sensors,  $N$ . With our assumption of additive uncorrelated noise ( $\sigma_w^2 \mathbf{I}$ ) always being present,  $N$  is the rank of  $\mathbf{S}_x$ .
- (ii) We define the performance using known statistics as the **steady state** performance. We find that the ratio of the performance using estimated statistics to the steady state performance depends on  $K/N$ .
- (iii) In some applications, the environment is stationary over a long period of time and we can solve the problem by taking more samples so  $K/N$  increases. In other applications, the environment is only stationary over a short period (e.g., interfering signals arrive and depart) and we must work with a low  $K/N$  restriction.
- (iv) We also find that, in the low  $K/N$  environment, the noise eigenvectors cause significant degradation to the beam pattern.

In addition to the problems of estimation accuracy, we encounter the problems of computational complexity:

- (i) The number of operations to compute  $\mathbf{S}_x^{-1}$  is of  $O(N^3)$ .
- (ii) More efficient algorithms can be developed but their complexity still increases with  $N$ .

All of these problems motivate us to find algorithms in which we are doing our optimization in a smaller dimensional space. We consider two approaches to the problem.

In this section, we utilize the eigenvectors to construct the optimization space. Since the eigenvectors and eigenvalues depend on  $\mathbf{S}_x$  (in practice, they depend on  $\hat{\mathbf{S}}_x$ ) the subspace construction will be data dependent (or

adaptive) in actual applications. In Section 6.9, we construct the subspace by preprocessing the input with a set of conventional beams that span the region of  $(\omega, \mathbf{k})$  space of interest.

Many of the advantages of eigenspace (ES) and beamspace (BS) processing will not become apparent until we study their adaptive realizations. However, the steady state performance provides the foundation for these analyses.

In this section, we develop beamformers that compute the eigenvalues and eigenvectors of  $\mathbf{S}_x$  and use them to construct the beamformer. In this chapter, we assume  $\mathbf{S}_x$  is available.

In many of the eigenvector beamformers that we develop, we only need to compute the eigenvectors corresponding to the largest eigenvalues. This requirement means that we can exploit various efficient computation techniques in lieu of performing a complete eigendecomposition.

We consider two types of beamformers. They both utilize an eigendecomposition, but they use the results in algorithms that are significantly different. The first type of beamformer projects the input onto a reduced-rank subspace called the eigenspace containing the signal and interference.<sup>12</sup> They then process the projected input in the subspace to form the beam. In the presence of signal mismatch, this technique provides significant performance improvement even in the case of known statistics. It will also provide a reduction in computational complexity. We refer to these beamformers as **eigenspace (ES) beamformers**.

In Section 6.8.1, we develop an algorithm that uses the principal components of  $\mathbf{S}_x$  as a basis for a subspace. In Section 6.8.2, we develop an algorithm that uses the cross-correlation between the eigenvectors and  $\mathbf{v}_m$  as a criterion for selecting the subspace.

The second type of beamformer uses the eigendecomposition to construct a subspace called the **dominant-mode** (DM) subspace. The algorithm is designed to reject the modes in the DM subspace and is referred to as a dominant-mode rejection (DMR) beamformer. When there is no mismatch and the statistics are known, the DMR and ES beamformers are identical. However, in the presence of signal mismatch, array mismatch, or estimated statistics, their performance can be dramatically different. We develop and analyze this beamformer in Section 6.8.3. We summarize our results in Section 6.8.4.

---

<sup>12</sup>This statement is true for the cases of discrete interference, known statistics, and no model mismatch. We discuss the general case in Sections 6.8.1 and 6.8.2.

### 6.8.1 Principal-component (PC) Beamformers

The general approach has been studied under a number of different names. Under the eigendecomposition label, there are algorithms proposed by Hung and Turner [HT83], Citron and Kailath [CK84], Owsley [Ows85], Gabriel [Gab86], Friedlander [Fri88], Haimovich and Bar-Ness [HBN88], [HBN91], Van Veen [VV88], Chang and Yeh [CY92], Youn and Un [YU94], and Yu and Yeh [YY95].

Under the reduced covariance matrix or principal-components (PC) label, the problem has been studied by Kirstein and Tufts [KT85].

Under the projection label, algorithms have been developed by Feldman and Griffiths [FG91], [FG94].

Related work includes that of Er and Cantoni [EC85], Zunich and Griffiths [ZG91], and Bull et al. [BAB90].

The first step in the design is to perform an eigendecomposition of  $\mathbf{S}_x$ ,

$$\mathbf{S}_x = \sum_{i=1}^N \lambda_i \Phi_i \Phi_i^H = \mathbf{U} \Lambda \mathbf{U}^H, \quad (6.439)$$

where  $\mathbf{U}$  is an  $N \times N$  matrix of eigenvectors,

$$\mathbf{U} \triangleq \begin{bmatrix} \Phi_1 & \Phi_2 & \cdots & \Phi_N \end{bmatrix}, \quad (6.440)$$

and  $\Lambda$  is a diagonal matrix of the ordered eigenvalues,

$$\Lambda = \text{diag} \begin{bmatrix} \lambda_1 & \lambda_2 & \cdots & \lambda_N \end{bmatrix}. \quad (6.441)$$

In practice, we would use  $\hat{\mathbf{S}}_x$ , the sample covariance matrix, to generate the eigendecomposition. We now select  $D_r$  of these eigenvectors to form a  $N \times D_r$  matrix  $\mathbf{U}_r$ . The subscript  $r$  denotes “reduced.”

There are several ways to select the eigenvectors to be used in  $\mathbf{U}_r$ . The first model assumes there is a single plane-wave signal,  $D$  plane-wave interferers, and additive white noise. We select the eigenvectors corresponding to the  $D + 1$  largest eigenvalues. We refer to these as the principal components. We define

$$\mathbf{U}_{S+I} = \begin{bmatrix} \Phi_1 & \Phi_2 & \cdots & \Phi_{D+1} \end{bmatrix} \quad (6.442)$$

to be the signal-plus-interference subspace. In this model, we must estimate the number of plane waves present. We develop techniques for estimating the value of  $D + 1$  in Chapter 7 (e.g., the discussion of AIC and MDL in Section 7.9.3).

The second model does not assume any structure for the interference (e.g., it could include a spatially spread component). We perform the eigen-decomposition in (6.439) and select the  $D_r$  largest eigenvalues. There are various tests for determining if an eigenvalue is large:

$$(i) \quad \frac{\lambda_i}{\text{tr}[\mathbf{S}_x]} > n_1, \quad (6.443)$$

the percent of the total power is contained in  $\lambda_i$ ,

$$(ii) \quad \frac{\lambda_{i+1}}{\lambda_i} > n_2, \quad (6.444)$$

the ratio of the  $(i + 1)$ th eigenvalue to the  $i$ th eigenvalue which has been declared to be large.

After we have selected an appropriate value of  $D_r$ , we define a  $N \times D_r$  matrix,

$$\mathbf{U}_r = \begin{bmatrix} \Phi_1 & \Phi_2 & \cdots & \Phi_{D_r} \end{bmatrix}, \quad (6.445)$$

which defines the reduced subspace and the  $D_r \times D_r$  diagonal matrix,

$$\Lambda_r = \text{diag} \left\{ \lambda_1 \quad \lambda_2 \quad \cdots \quad \lambda_{D_r} \right\}. \quad (6.446)$$

Using the model in (6.442), we can write

$$\mathbf{S}_x = \mathbf{U}_{S+I} \Lambda_{S+I} \mathbf{U}_{S+I}^H + \mathbf{U}_N \Lambda_N \mathbf{U}_N^H, \quad (6.447)$$

where  $\mathbf{U}_N$  is orthogonal to  $\mathbf{U}_{S+I}$ . We can write  $\mathbf{S}_x^{-1}$  as

$$\mathbf{S}_x^{-1} = \mathbf{U}_{S+I} \Lambda_{S+I}^{-1} \mathbf{U}_{S+I}^H + \mathbf{U}_N \Lambda_N^{-1} \mathbf{U}_N^H. \quad (6.448)$$

Because  $\mathbf{v}_m$  is in  $\mathbf{U}_{S+I}$ , it is orthogonal to  $\mathbf{U}_N$ . Therefore the MPDR beamformer reduces to

$\mathbf{w}_{mpdr,es}^H = \gamma_{es} \mathbf{v}_m^H \mathbf{U}_{S+I} \Lambda_{S+I}^{-1} \mathbf{U}_{S+I}^H,$

(6.449)

where

$\gamma_{es} = \left( \mathbf{v}_m^H \mathbf{U}_{S+I} \Lambda_{S+I}^{-1} \mathbf{U}_{S+I}^H \mathbf{v}_m \right)^{-1}.$

(6.450)

We use the symbol  $\gamma_{es}$  instead of our previous symbol  $\Lambda$  to avoid confusion with the eigenvalue matrix. The resulting beamformer is shown in Figure 6.71. We refer to it as a principal component or eigenspace beamformer.

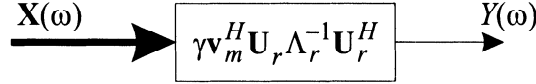


Figure 6.71 Principal component beamformer.

The result in (6.449) can also be written in terms of the individual eigenvalues and eigenvectors,

$$\mathbf{w}_{mpdr,es}^H = \frac{\sum_{i=1}^{D_r} \frac{1}{\lambda_i} (\mathbf{v}_m^H \Phi_i) \Phi_i^H}{\sum_{i=1}^{D_r} \frac{1}{\lambda_i} |\mathbf{v}_m^H \Phi_i|^2}. \quad (6.451)$$

If we use the model in (6.445), then

$$\mathbf{w}_{mpdr,es}^H = \gamma_{es} \mathbf{v}_m^H \mathbf{U}_r \Lambda_r^{-1} \mathbf{U}_r^H. \quad (6.452)$$

The algorithm in this form is referred to in the literature as the eigenspace beamformer (e.g., [HBN91],[CY92]) or the **signal-plus-interference** subspace beamformer (e.g., [Fri88]).

We can also interpret (6.452) as a projection beamformer (e.g., Feldman and Griffiths [FG91], [FG94]).

We define a projected steering vector as

$$\mathbf{v}_p \triangleq \mathbf{P}_{\mathbf{U}_r} \mathbf{v}_m = \mathbf{U}_r \mathbf{U}_r^H \mathbf{v}_m, \quad (6.453)$$

because

$$\mathbf{U}_r^H \mathbf{U}_r = \mathbf{I}. \quad (6.454)$$

The projection beamformer is

$$\mathbf{w}_p = \gamma_p \mathbf{S}_{\mathbf{x}}^{-1} \mathbf{v}_p = \gamma_p \mathbf{S}_{\mathbf{x}}^{-1} \mathbf{U}_r \mathbf{U}_r^H \mathbf{v}_m. \quad (6.455)$$

Expanding  $\mathbf{S}_{\mathbf{x}}^{-1}$  gives

$$\mathbf{w}_p = \gamma_p \left[ \mathbf{U}_r \Lambda_r^{-1} \mathbf{U}_r^H + \mathbf{U}_N \Lambda_N^{-1} \mathbf{U}_N^H \right] \mathbf{U}_r \mathbf{U}_r^H \mathbf{v}_m, \quad (6.456)$$

where  $\mathbf{U}_N$  is the  $N \times (N - D_r)$  noise subspace that is orthogonal to  $\mathbf{U}_r$ . Then (6.456) reduces to

$$\mathbf{w}_p = \gamma_p \left[ \mathbf{U}_r \Lambda_r^{-1} \mathbf{U}_r^H \right] \mathbf{v}_m, \quad (6.457)$$

which is the same as (6.452) if we choose  $\gamma_p = \gamma_{es}$ .

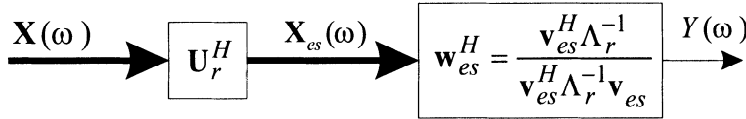


Figure 6.72 Eigenspace beamformer.

We see that we can interpret the PC beamformer as a beamformer that uses the projection of the model array manifold vector onto the principal component subspace in  $\mathbf{w}_{mpdr,es}$ . We would expect that this projection approach should provide robustness against model signal mismatch.

A third interpretation of the beamformer is also useful. We can define

$$\mathbf{X}_{es} = \mathbf{U}_r^H \mathbf{X}, \quad (6.458)$$

and

$$\mathbf{v}_{es} = \mathbf{U}_r^H \mathbf{v}_m. \quad (6.459)$$

This leads to the processor shown in Figure 6.72. Here

$$\mathbf{w}_{mpdr,es}^H = \frac{\mathbf{v}_{es}^H \Lambda_r^{-1}}{\mathbf{v}_{es}^H \Lambda_r^{-1} \mathbf{v}_{es}}. \quad (6.460)$$

The advantage of this representation is that it highlights that the beamformer is operating in the eigenspace.

If we include diagonal loading,

$$\mathbf{w}_{es,mpdr,dl} = \frac{\mathbf{v}_{es}^H [\Lambda_r + \sigma_L^2 \mathbf{I}_{D_r}]^{-1}}{\mathbf{v}_{es}^H [\Lambda_r + \sigma_L^2 \mathbf{I}_{D_r}]^{-1} \mathbf{v}_{es}}. \quad (6.461)$$

Note that the diagonal loading is in the eigenspace. When  $\mathbf{S}_x$  is known, diagonal loading is not useful to combat DOA mismatch. However, it is useful to protect the main lobe against main-lobe interferers.

For an LCMP beamformer, we define the constraints in the original  $N$ -dimensional space.

$$\mathbf{C}^H \mathbf{w} = \mathbf{C}^H [\mathbf{U}_r \mathbf{w}_{es}] = \mathbf{C}_{es}^H \mathbf{w}_{es} = \mathbf{g}^H, \quad (6.462)$$

where

$$\mathbf{C}_{es}^H \triangleq \mathbf{C}^H \mathbf{U}_r. \quad (6.463)$$

Then, using (6.358),

$$\boxed{\mathbf{w}_{lcmp,es}^H = \mathbf{g}^H [\mathbf{C}_{es}^H \Lambda_r^{-1} \mathbf{C}_{es}]^{-1} \mathbf{C}_{es}^H \Lambda_r^{-1}.} \quad (6.464)$$

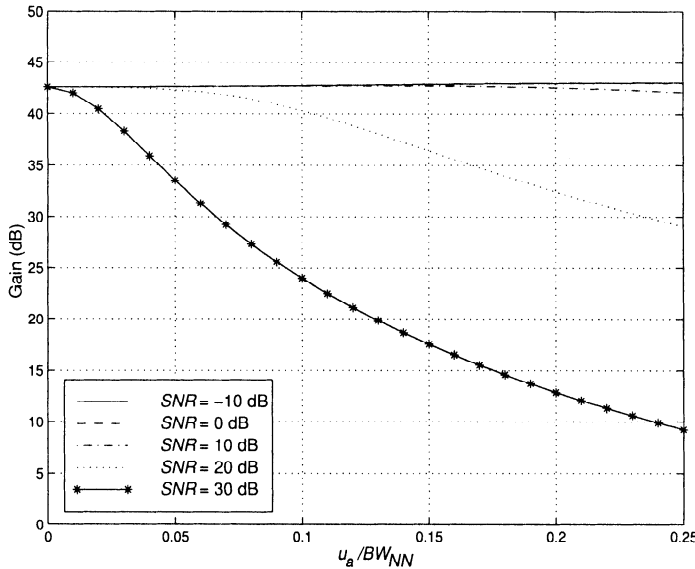


Figure 6.73 MPDR eigenspace beamformer with  $D_r = 3$ ,  $u_I = \pm 0.3$ ,  $INR = 30$  dB, various  $SNR$ ; array gain versus  $u_a/BW_{NN}$ .

We consider an example to illustrate a typical result.

#### Example 6.8.1

Consider a standard 10-element linear array. The nominal signal arrival angle is  $u_m = 0$ . The input spatial spectral matrix is

$$\mathbf{S}_x = \sigma_s^2 \mathbf{v}_a \mathbf{v}_a^H + \sum_{i=1}^2 \sigma_i^2 \mathbf{v}_i \mathbf{v}_i^H + \sigma_w^2 \mathbf{I}. \quad (6.465)$$

We assume the interfering plane waves are at  $\pm 0.30$ . We perform an eigendecomposition of  $\mathbf{S}_x$  and construct a 3-D subspace using the eigenvectors corresponding to the three largest eigenvalues. We use the eigenspace beamformer in (6.460)

In Figure 6.73, we plot the array gain versus  $u_a/BW_{NN}$  for an  $INR = 30$  dB. Comparing these results to the MPDR-DL results in Figure 6.38(b), we see that the eigenspace beamformer is better for all of the  $SNR$  considered. The eigenspace beamformer partially compensates for the DOA mismatch by projecting  $\mathbf{v}_m$  into the actual subspace.

The result in Example 6.8.1 for low  $SNR$  is correct but misleading. In practice, we have to estimate  $D_r$  and use  $\hat{\mathbf{S}}_x$  for the eigendecomposition. In Section 7.9.2, we find that for low  $SNR$  we frequently underestimate  $D_r$  and lose the eigenvalue that is most closely correlated with the signal. To investigate this effect we repeat Example 6.8.1 with  $D_r = 2$  instead of 3.

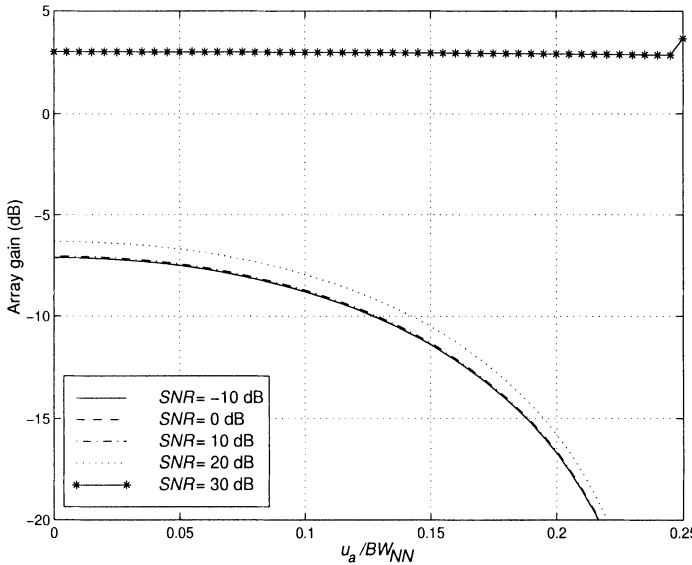


Figure 6.74 MPDR eigenspace beamformer with  $D_r = 2$ ,  $u_I = \pm 0.3$ ,  $INR = 30 \text{ dB}$ , various  $SNR$ ; array gain versus  $u_a/BW_{NN}$ .

#### Example 6.8.2 (continuation)

Consider the same model as in Example 6.8.1. We use the beamformer in (6.451) with  $D_r = 2$ . In Figure 6.74, we plot the array gain versus  $u_a/BW_{NN}$ .

We see that the performance is significantly degraded. This is because there is very little signal content in the eigenspace. Thus, it is important that the dimension of the eigenspace is chosen properly.

We can also implement the eigenspace beamformer in a generalized side-lobe canceller (GSC) format, as shown in Figure 6.75. The adaptive matrix,  $\mathbf{w}_a^H$ , in Figure 6.46 has been divided into a cascade of two matrices. These matrices are defined in the next several equations. In this case, the eigendecomposition of the spatial spectral matrix of  $\mathbf{X}_b(\omega)$  is used (e.g., [VV88]).

The overall weight vector is

$$\mathbf{w} = \mathbf{w}_q - \mathbf{B}\mathbf{w}_a, \quad (6.466)$$

where

$$\mathbf{w}_q = \mathbf{C}[(\mathbf{C}^H \mathbf{C})]^{-1} \mathbf{g}. \quad (6.467)$$

From Section 6.7.3, the optimum adaptive component in Figure 6.46 is

$$\mathbf{w}_{ao}^H = \mathbf{S}_{d\mathbf{z}^H} \mathbf{S}_{\mathbf{z}}^{-1}, \quad (6.468)$$

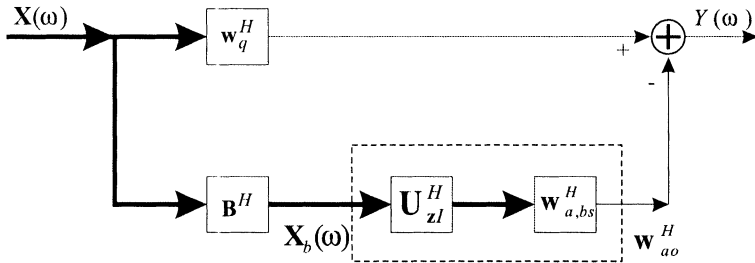


Figure 6.75 Generalized sidelobe canceller implementation of eigenspace beamformer.

where

$$\mathbf{S}_z = \mathbf{B}^H \mathbf{S}_x \mathbf{B} \quad (6.469)$$

is the spectral matrix at the output of the blocking matrix  $\mathbf{B}$ , and

$$\mathbf{S}_{d\mathbf{z}^H} = \mathbf{w}_q^H \mathbf{S}_x \mathbf{B}. \quad (6.470)$$

We now utilize an eigendecomposition of  $\mathbf{S}_z$ :

$$\mathbf{S}_z = \mathbf{U}_{zI} \Lambda_{zI} \mathbf{U}_{zI}^H + \mathbf{U}_{zN} \Lambda_{zN} \mathbf{U}_{zN}^H. \quad (6.471)$$

If the signal arrives from the direction that the blocking matrix assumed, then the first subspace in (6.471) is an interference subspace, because the blocking matrix  $\mathbf{B}$  has removed all signal components. If there is signal mismatch, then some signal component will leak into the lower path. We refer to  $\mathbf{U}_{zI}$  as an interference subspace even though it may contain leaked signal.  $\mathbf{U}_{zN}$  is orthogonal to the interference subspace. We can also show that  $\mathbf{S}_{d\mathbf{z}^H}$  contains the component due to interference only (e.g., [Jab86a]) and  $\mathbf{U}_{zN}$  is orthogonal to  $\mathbf{S}_{d\mathbf{z}^H}$ .

Therefore,

$$\mathbf{w}_{ao}^H = \mathbf{w}_q^H \mathbf{S}_x \mathbf{B} [\mathbf{U}_{zI} \Lambda_{zI}^{-1} \mathbf{U}_{zI}^H]. \quad (6.472)$$

and

$$\mathbf{w}_{a,es}^H = \mathbf{w}_q^H \mathbf{S}_x \mathbf{B} \mathbf{U}_{zI} \Lambda_{zI}^{-1}. \quad (6.473)$$

The results in (6.468) and (6.473) specify the GSC version of the eigenspace beamformer.

We should observe that some of the important issues concerning eigenspace beamformers will not appear until we study the finite data problem and adaptive implementations in Chapter 7. Specifically:

- (i) We have to estimate  $D_r$  and compute the eigenvalues and eigenvectors. It is important that a significant part of the signal energy is contained in the resulting eigenspace. When the *SNR* is low, we may include a “noise” eigenvector instead of a “signal” eigenvector. This error causes a dramatic decrease in performance.
- (ii) It is important to observe that we do not have to compute all of the eigenvalues. We can use the techniques discussed in Golub and Van Loan [GVL89] to compute the eigenvalues in descending order.

### 6.8.2 Cross-spectral Eigenspace Beamformers

In Section 6.8.1, we performed an eigendecomposition of  $\mathbf{S}_x$  and formed a reduced-rank beamformer by choosing the eigenvectors with the  $D_r$  largest eigenvalues. In this section, we use a different choice of eigenvectors to form the subspace.<sup>13</sup>

The MPDR beamformer was designed to minimize the output power subject to the distortionless constraint,

$$\mathbf{w}^H \mathbf{v}_m = 1. \quad (6.474)$$

The resulting weight vector is

$$\mathbf{w}^H = \frac{\mathbf{v}_m^H \mathbf{S}_x^{-1}}{\mathbf{v}_m^H \mathbf{S}_x^{-1} \mathbf{v}_m}, \quad (6.475)$$

and the output power is

$$P_o = \left( \mathbf{v}_m^H \mathbf{S}_x^{-1} \mathbf{v}_m \right)^{-1}. \quad (6.476)$$

The eigendecomposition of  $\mathbf{S}_x$  is

$$\mathbf{S}_x = \sum_{i=1}^N \lambda_i \Phi_i \Phi_i^H \quad (6.477)$$

and

$$\mathbf{S}_x^{-1} = \sum_{i=1}^N \frac{\Phi_i \Phi_i^H}{\lambda_i}. \quad (6.478)$$

---

<sup>13</sup>This approach is discussed in Goldstein and Reed (e.g., [GR97a],[GR97b],[GR97c]). The ideas were discussed earlier in Byerly and Roberts [BR89].

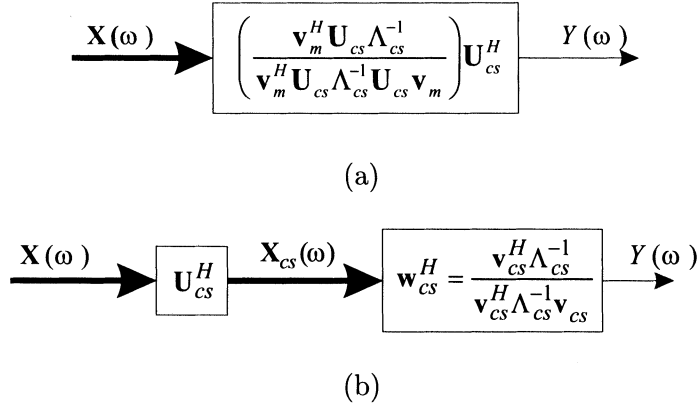


Figure 6.76 Cross-spectral beamformer.

Using (6.478) in (6.476), we have

$$P_o = \left( \mathbf{v}_m^H \sum_{i=1}^N \frac{\Phi_i \Phi_i^H}{\lambda_i} \mathbf{v}_m \right)^{-1} = \left( \sum_{i=1}^N \frac{|\mathbf{v}_m^H \Phi_i|^2}{\lambda_i} \right)^{-1}. \quad (6.479)$$

To retain  $D_c$  eigenvectors as the basis for the reduced-rank subspace, we choose the  $D_c$  largest terms in the summation,

$$\lambda_{(n)}, \Phi_{(n)} = \arg \max_{\lambda_i, \Phi_i} \left\{ \frac{|\mathbf{v}_m^H \Phi_i|^2}{\lambda_i} \right\}, \quad (n) = 1, \dots, D_c. \quad (6.480)$$

We use the subscript “ $(n)$ ” on this set of eigenvectors because the subscript  $n$  has been associated with eigenvectors ordered according to the size of the corresponding eigenvalue.

We define an  $N \times D_c$  matrix,  $\mathbf{U}_{cs}$ , whose columns are the  $D_c$  eigenvectors chosen in (6.480). We then use the MPDR beamformer in the reduced-rank space

$$\mathbf{w}_{cs}^H = \frac{\mathbf{v}_m^H \mathbf{U}_{cs} \Lambda_{cs}^{-1} \mathbf{U}_{cs}^H}{\mathbf{v}_m^H \mathbf{U}_{cs} \Lambda_{cs}^{-1} \mathbf{U}_{cs}^H \mathbf{v}_m}. \quad (6.481)$$

The **cross-spectral** (CS) beamformer is shown in Figure 6.76(a). An equivalent implementation is shown in Figure 6.76(b). A generalized sidelobe canceller version is shown in Figure 6.77.

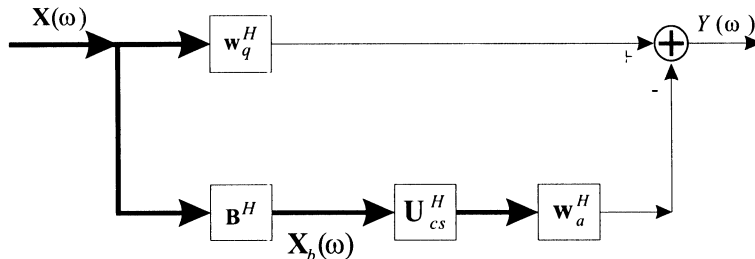


Figure 6.77 Generalized sidelobe canceller implementation of cross-spectral beamformer.

If we try to implement the cross-spectral beamformer for the model in Example 6.8.1, we find that it does not work in the presence of DOA mismatch. For  $u_a = 0$ , the steering vector is matched to the model steering vector  $\mathbf{v}_m$  and the eigenvectors that we pick correspond to the ones with the three largest eigenvalues. The resulting beamformer is the same as in Example 6.8.1. However, when  $u_a \neq 0$ , we start picking eigenvectors corresponding to the noise subspace and the performance deteriorates rapidly. Adding diagonal loading does not help.

We would anticipate that the cross-spectral beamformer would offer a performance advantage when the dimension of eigenspace was less than the rank of the signal-plus-interference subspace. Goldstein and Reed [GR97b] have an example that demonstrates a performance improvement, but the interference model is tailored to the algorithm. We were able to construct scenarios in which the CS beamformer was better than the PC beamformer under nominal conditions, but it degraded rapidly with mismatch. Another scenario that should offer an advantage is spatially spread interference where the eigenvalues roll off gradually. We consider this case in the problems and find very little performance improvement over the PC beamformer. The computational disadvantage of the CS beamformer is that we must compute all of the eigenvalues in order to find the terms in (6.480).

### 6.8.3 Dominant-mode Rejection Beamformers

In this section, we develop a class of beamformers referred to as **dominant mode rejection** (DMR) beamformers. The reason for the name will be clear after we derive the beamformer. The DMR beamformer is a special case of an enhanced MPDR beamformer that was derived by Abraham and Owsley [AO90].

We perform an eigendecomposition of  $\mathbf{S}_x$  and divide the result into two terms,

$$\mathbf{S}_x = \sum_{i=1}^{D_m} \lambda_i \Phi_i \Phi_i^H + \sum_{i=D_m+1}^N \lambda_i \Phi_i \Phi_i^H, \quad (6.482)$$

where the eigenvalues are ordered,  $\lambda_1 \geq \lambda_2 \cdots \geq \lambda_N$ , and  $D_m$  is a parameter that we will discuss shortly.

We form a modified spectral matrix by replacing the  $(N - D_m)$  smallest eigenvalues by their average,

$$\alpha \triangleq \frac{1}{N - D_m} \sum_{i=D_m+1}^N \lambda_i. \quad (6.483)$$

We can also find  $\alpha$  from the expression,

$$\alpha = \frac{1}{N - D_m} \left\{ \text{tr} [\mathbf{S}_x] - \sum_{i=1}^{D_m} \lambda_i \right\}. \quad (6.484)$$

The advantage of (6.484) is that we only have to compute the  $D_m$  largest eigenvalues.

Note that, if the model consists of a plane-wave signal plus  $(D_m - 1)$  plane-wave interferers in the presence of spatially uncorrelated noise ( $\sigma_w^2 \mathbf{I}$ ), then

$$\alpha = \sigma_w^2, \quad (6.485)$$

when the statistics are known. However when we estimate  $\mathbf{S}_x$  using finite data or have spatially correlated background noise, then  $\alpha \neq \sigma_w^2$ .

The modified spectral matrix is

$$\tilde{\mathbf{S}}_x \triangleq \sum_{i=1}^{D_m} \lambda_i \Phi_i \Phi_i^H + \alpha \sum_{i=D_m+1}^N \Phi_i \Phi_i^H. \quad (6.486)$$

We can denote the dominant mode subspace by the  $N \times D_m$  matrix

$$\mathbf{U}_{dm} \triangleq \begin{bmatrix} \Phi_1 & \Phi_2 & \cdots & \Phi_{dm} \end{bmatrix}. \quad (6.487)$$

The orthogonal noise subspace is

$$\mathbf{U}_{dm}^\perp \triangleq \begin{bmatrix} \Phi_{dm+1} & \Phi_{dm+2} & \cdots & \Phi_N \end{bmatrix}. \quad (6.488)$$

Then (6.486) can be written as

$$\tilde{\mathbf{S}}_x = \sum_{i=1}^{D_m} \lambda_i \Phi_i \Phi_i^H + \alpha \mathbf{U}_{dm}^\perp [\mathbf{U}_{dm}^\perp]^H. \quad (6.489)$$

We refer to the  $D_m$  eigenvectors with the largest eigenvalues as the **dominant modes**. They are due to the signal, plane-wave interferers, and spatially spread interference.

Note that  $\tilde{\mathbf{S}}_{\mathbf{x}}$  is a full-rank matrix in contrast to the reduced-rank matrices in Sections 6.8.1 and 6.8.2.

The inverse of  $\tilde{\mathbf{S}}_{\mathbf{x}}$  is,

$$\begin{aligned}\tilde{\mathbf{S}}_{\mathbf{x}}^{-1} &= \sum_{i=1}^{D_m} \frac{1}{\lambda_i} \Phi_i \Phi_i^H + \frac{1}{\alpha} \mathbf{U}_{dm}^\perp [\mathbf{U}_{dm}^\perp]^H \\ &= \frac{1}{\alpha} \left[ \sum_{i=1}^{D_m} \frac{\alpha}{\lambda_i} \Phi_i \Phi_i^H + \mathbf{P}_{dm}^\perp \right],\end{aligned}\quad (6.490)$$

where  $\mathbf{P}_{dm}^\perp$  is the projection matrix onto the subspace orthogonal to  $\mathbf{U}_{dm}$ . The weight vector is

$$\mathbf{w}_{dm}^H = \frac{\mathbf{v}_m^H \tilde{\mathbf{S}}_{\mathbf{x}}^{-1}}{\mathbf{v}_m^H \tilde{\mathbf{S}}_{\mathbf{x}}^{-1} \mathbf{v}_m} = \frac{\alpha \sum_{i=1}^{D_m} \frac{1}{\lambda_i} (\mathbf{v}_m^H \Phi_i) \Phi_i^H + \mathbf{v}_m^H \mathbf{P}_{dm}^\perp}{\alpha \sum_{i=1}^{D_m} \frac{1}{\lambda_i} |\mathbf{v}_m^H \Phi_i|^2 + \mathbf{v}_m^H \mathbf{P}_{dm}^\perp \mathbf{v}_m}. \quad (6.491)$$

In the first case of interest,  $\mathbf{v}_m$  is completed contained in the DM subspace. For the case of known statistics with no signal mismatch this will occur if  $D_m$  is chosen correctly. Then,

$$\mathbf{v}_m^H \mathbf{P}_{dm}^\perp = 0, \quad (6.492)$$

and (6.491) reduces to

$$\mathbf{w}_{dm}^H = \frac{\sum_{i=1}^{D_m} \frac{1}{\lambda_i} (\mathbf{v}_m^H \Phi_i) \Phi_i^H}{\sum_{i=1}^{D_m} \frac{1}{\lambda_i} |\mathbf{v}_m^H \Phi_i|^2}. \quad (6.493)$$

Comparing (6.493) and (6.451), we see that the eigenspace beamformer and the DMR beamformer are identical for this case. The DMR beamformer in (6.493) is distortionless in the absence of mismatch.

To investigate the response due to an eigenvector (or mode), we first divide  $\lambda_i$  into a signal and noise component,

$$\lambda_i = \lambda_i^s + \alpha, \quad i = 1, 2, \dots, D_m. \quad (6.494)$$

The power output when the input spectral matrix is  $\lambda_k \Phi_k \Phi_k^H$  is

$$P_{\Phi_k} = \frac{\frac{1}{(\lambda_k^s/\alpha+1)} |\mathbf{v}_m^H \Phi_k|^2}{\left[ \sum_{i=1}^{D_m} \frac{1}{(\lambda_i^s/\alpha+1)} |\mathbf{v}_m^H \Phi_i|^2 \right]^2}. \quad (6.495)$$

If  $\lambda_k^s/\alpha \gg 1$ , then the output due to the  $k$ th mode will be small and that particular mode will be rejected. Hence, the dominant mode rejection (DMR) beamformer name. The second term is a measure of the correlation between the  $k$ th eigenvector and  $\mathbf{v}_m$ . As this correlation increases, the depth of the null on the  $k$ th mode decreases. Note that  $\mathbf{v}_m$  is not normalized, so that the maximum value of the second term is  $N^2$ .

In practice there will be some mismatch in the model. We will have to estimate  $\mathbf{S}_x$ . The eigendecomposition of  $\hat{\mathbf{S}}_x$  will lead to mismatch in the eigenvalues and eigenvectors. In addition, we will have to estimate  $D_{dm}$ , the dimension of the dominant-mode eigenspace. This estimate,  $\hat{D}_{dm}$ , may be in error. There can also be mismatch in the signal DOA, so that  $\mathbf{v}_a \neq \mathbf{v}_m$ .

In the next two examples, we discuss the behavior of the DMR beamformer under two types of mismatch. In Example 6.8.3, we consider the case of DOA mismatch. In Example 6.8.4, we choose  $\hat{D}_{dm} = D_{dm} - 1$  in order to simulate underestimating the dimension of the dominant-mode eigenspace. Both examples use the same scenarios as in Examples 6.8.1 and 6.8.2.

#### Example 6.8.3

Consider a standard 10-element linear array. The nominal signal arrival direction is  $u_m = 0$ . The actual input spectral matrix is

$$\mathbf{S}_x = \sigma_s^2 \mathbf{v}_a \mathbf{v}_a^H + \sum_{i=1}^2 \sigma_i^2 \mathbf{v}_i \mathbf{v}_i^H + \sigma_w^2 \mathbf{I}. \quad (6.496)$$

We assume the interfering plane waves are at  $\pm 0.30$ . We perform an eigendecomposition<sup>14</sup> of  $\mathbf{S}_x$  and construct a 3-D subspace using the eigenvectors corresponding to the three largest eigenvalues. We use the weight vector in (6.491) with  $\alpha$  replaced by  $\sigma_w^2$ ,

$$\mathbf{w}_{dm}^H = \frac{\sigma_w^2 \sum_{i=1}^{D_{dm}} \frac{1}{\lambda_i} (\mathbf{v}_m^H \Phi_i) \Phi_i^H + \mathbf{v}_m^H \mathbf{P}_{dm}^\perp}{\sigma_w^2 \sum_{i=1}^{D_{dm}} \frac{1}{\lambda_i} |\mathbf{v}_m^H \Phi_i|^2 + \mathbf{v}_m^H \mathbf{P}_{dm}^\perp \mathbf{v}_m}. \quad (6.497)$$

In Figure 6.78, we plot the array gain versus  $u_a/BW_{NN}$ . When the  $SNR = -10$  dB, there is very gradual degradation. When the  $SNR = 0$  dB, the degradation is still gradual; by  $u_a = 0.1/BW_{NN} = 0.25$ , the array gain has decreased by 13 dB. For higher  $SNR$ , the decrease in array gain is significant.

Other scenarios with different  $u_i$  and  $\sigma_i^2$  give similar results. It appears that, when  $D_m = D + 1$ , the  $SNR$  must be at least 10 dB below the weaker interferer in the two interferer case.

#### Example 6.8.4 (continuation)

Consider the same model as in Example 6.8.3. We use (6.491) with  $D_m = 2$  to test the effects of underestimation. Now  $\alpha$  includes the third eigenvalue,

$$\alpha = \frac{1}{8}(\lambda_3 + 7\sigma_w^2). \quad (6.498)$$

---

<sup>14</sup>Note that this is exactly the same eigendecomposition as in Example 6.8.1.

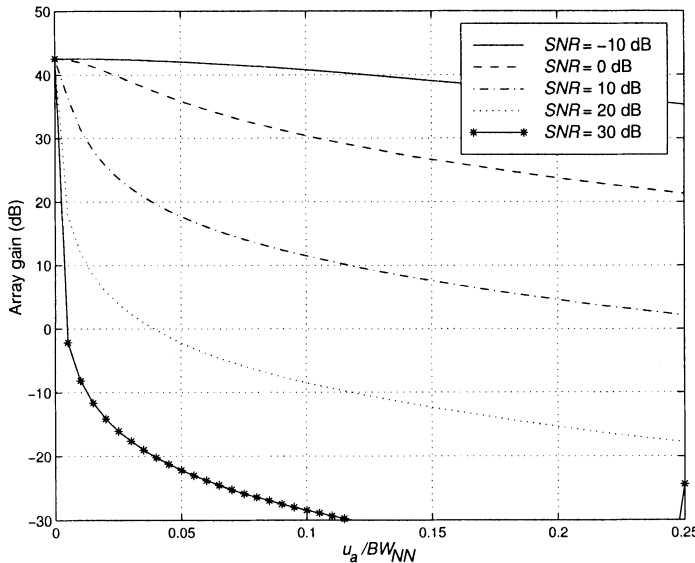


Figure 6.78 DMR beamformer with  $D_m = 3$ ,  $u_I = \pm 0.3$ ,  $INR = 30$  dB, various  $SNR$ ; array gain versus  $u_a/BW_{NN}$ .

In Figure 6.79, we plot the array gain versus  $u_a/BW_{NN}$ . We see that for an  $SNR = -10$  dB, 0 dB, and 10 dB, there is minimal degradation. This is because there is almost no signal content in the two DM eigenvectors. For  $SNR = 20$  dB, there is some signal component in the two DM eigenvectors. As  $u_a$  increases the geometry causes this signal content to decrease and the array gain goes up. For  $SNR = 30$  dB, there is significant signal content and the array gain is very low. Other scenarios give similar results.

This result suggests that the dimension of the dominant mode subspace should equal  $D$ , the number of interferers when the  $SNR \ll INR$ .

The performance of DMR beamformer degrades when  $\mathbf{v}_a$  is in the dominant mode subspace. Cox and Pitre [CP97] (e.g., [CPL98] or [Cox00]) have developed a robust DMR beamformer that improves performance under certain scenarios. The reader is referred to those references for a description of the algorithm.

#### 6.8.4 Summary

In this section we have developed two beamformers that utilize the eigendecomposition in a different manner.

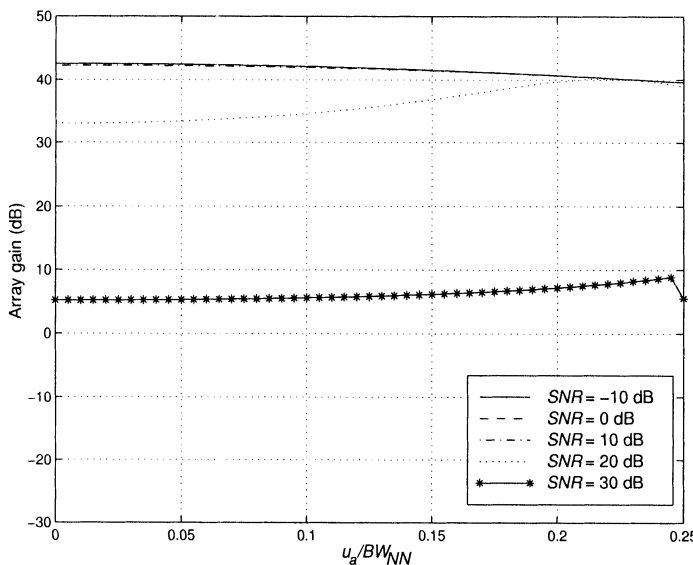


Figure 6.79 DMR beamformer with  $D_m = 2$ ,  $u_I = \pm 0.3$ ,  $INR = 30$  dB, various  $SNR$ ; array gain versus  $u_a/BW_{NN}$ .

The principal component (or eigenspace) beamformer forms an eigenspace using the eigenvectors with largest eigenvalues. All of the subsequent processing is done in this reduced-dimension eigenspace. In order to have good performance, the desired signal must have a significant component in the eigenspace. In order to accomplish this, the  $SNR$  must be large enough to cause this inclusion. The exact value required will depend on the signal and interference geometry, the accuracy of the  $\hat{\mathbf{S}}_x$  estimator, and other mismatches. In practice, we must also estimate  $D_r$  from the data and we will find that it is important not to underestimate  $D_r$ .

The dominant mode rejection beamformer performs the same eigendecomposition, but uses it in a different manner. The DMR beamformer averages the smallest eigenvalues and uses the average value in place of  $\lambda_i$ ,  $i = D_{dm} + 1, \dots, N$ . The result is a modified version of the MPDR beamformer. The eigenvectors that are not in DM subspace only appear in  $\mathbf{P}_{dm}^\perp$ , which can be calculated using the DM eigenvectors. If the model is perfectly matched, then the DMR and PC beamformers are the same. In the presence of mismatch, their behavior is different. In the DMR beamformer we would like to remove the signal from the DM subspace. This result will happen in a low  $SNR$  environment. The exact value required will depend on

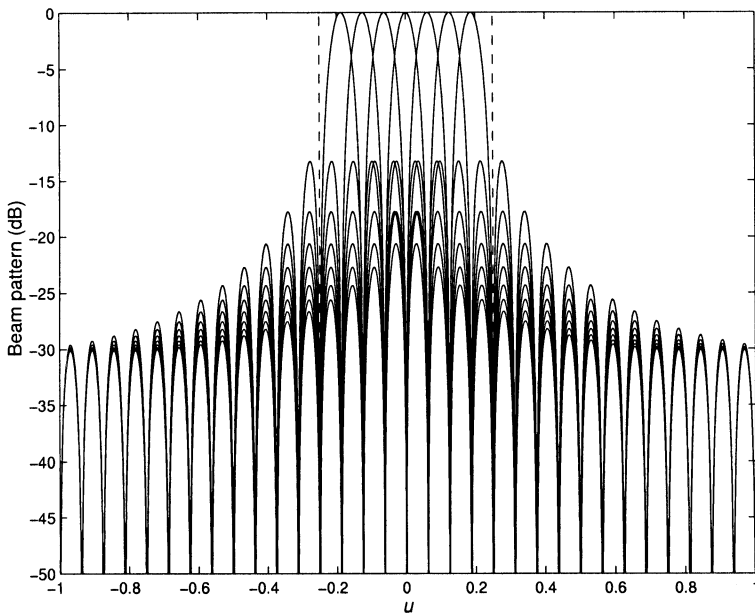


Figure 6.80 Orthogonal beams for beamspace processor.

the signal and interference geometry, the accuracy of the  $\hat{\mathbf{S}}_x$  estimator, and other mismatches. When we estimate  $D_r$  from the data, an underestimate  $\hat{D}_r = D_r - 1$  may improve the performance.

In Chapter 7 (Section 7.9) we look at the behavior when the necessary quantities must be estimated from a data set. Our tentative conclusion is that we can improve on the MPDR performance by using eigendecomposition. For high  $SNR$ , we would use the eigenspace beamformer. For low  $SNR$ , we would use the DMR beamformer.

## 6.9 Beamspace Beamformers

A second approach to reducing the rank of the processor is to perform a preliminary preprocessing with a set of non-adaptive beamformers. We then process the beamformer outputs in an optimum manner. We refer to the space spanned by the output of the beamformers as the beamspace and the overall processor as a **beamspace** beamformer.

A typical example is shown in Figure 6.80. The array is a standard 32-element linear array. We use seven orthogonal conventional beams spaced symmetrically about  $u_s = 0$ . We denote the weight vector associated with

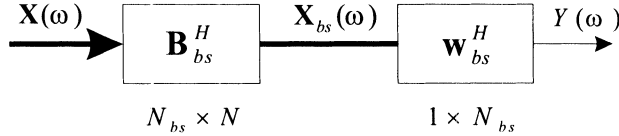


Figure 6.81 Beamspace processing.

the  $m$ th beam as  $\mathbf{b}_{bs,m}^H, m = 1, \dots, 7$ . In this case,

$$\mathbf{b}_{bs,m}^H = \frac{1}{\sqrt{N}} \mathbf{v}_u^H \left( u - (m-4) \frac{2}{N} \right), \quad m = 1, \dots, 7, \quad (6.499)$$

where  $\mathbf{v}_u(u)$  is the array manifold vector in  $u$ -space. We define an  $N \times 7$  matrix  $\mathbf{B}_{bs}$  whose columns are the  $\mathbf{b}_{bs}$  vectors in (6.499). In the general case,  $\mathbf{B}_{bs}$  is an  $N \times N_{bs}$  matrix.

We refer to the seven beams as a **beam fan**. We denote the interval between the first left null of the left beam and the first right null of the right beam as the **beamspace sector**.

In Section 6.9.1, we consider beamspace MPDR beamformers with diagonal loading. In Section 6.9.2, we consider beamspace LCMP with diagonal loading. In Section 6.9.3, we summarize our results.

### 6.9.1 Beamspace MPDR

The model is shown in Figure 6.81. The output of the beamspace matrix is,

$$\mathbf{X}_{bs} = \mathbf{B}_{bs}^H \mathbf{X}, \quad (6.500)$$

and we require

$$\mathbf{B}_{bs}^H \mathbf{B}_{bs} = \mathbf{I}. \quad (6.501)$$

The beamspace array manifold vector is defined as

$$\mathbf{v}_{bs} = \mathbf{B}_{bs}^H \mathbf{v}_s. \quad (6.502)$$

If we use orthogonal conventional beams as in Figure 6.80, then, as discussed in Section 3.10,

$$\left[ \mathbf{b}_{bs,i}^H \right]_n = \frac{1}{\sqrt{N}} \left[ e^{-j(n-\frac{N-1}{2})(\psi_c - (m-4)\frac{2\pi}{N})} \right], \quad n = 0, \dots, N-1, \\ m = 1, \dots, 7, \quad (6.503)$$

where  $\psi_c$  is the MRA of the center beam, and

$$[\mathbf{v}_s]_n = e^{j(n-\frac{N-1}{2})\psi}, \quad n = 0, \dots, N-1, \quad (6.504)$$

so, for  $\psi_c = 0$ ,

$$\mathbf{v}_{bs}(\psi) = \sqrt{N} \begin{bmatrix} \frac{\sin(\frac{N}{2}(\psi+3\frac{2\pi}{N}))}{\sin(\frac{1}{2}(\psi+3\frac{2\pi}{N}))} \\ \vdots \\ \frac{\sin(\frac{N}{2}(\psi-(m-4)\frac{2\pi}{N}))}{\sin(\frac{1}{2}(\psi-(m-4)\frac{2\pi}{N}))} \\ \vdots \\ \frac{\sin(\frac{N}{2}(\psi-3\frac{2\pi}{N}))}{\sin(\frac{1}{2}(\psi-3\frac{2\pi}{N}))} \end{bmatrix}. \quad (6.505)$$

If we use other weightings such as Chebychev or Taylor to form the beamspace, then

$$\left[ \mathbf{b}_{bs,i}^H \right]_n = w_n^* e^{-j(n-\frac{N-1}{2})(\psi_c-(m-4)\frac{2\pi}{N})}, \quad n = 0, \dots, N-1, \\ m = 1, \dots, 7. \quad (6.506)$$

The output of the beamspace matrix,  $\mathbf{X}_{bs}$ , is processed with a  $1 \times N_{bs}$  matrix,  $\mathbf{w}_{bs}^H$  to obtain a scalar output  $Y$ . Thus,

$$Y = \mathbf{w}_{bs}^H \mathbf{X}_{bs} = \mathbf{w}_{bs}^H \mathbf{B}_{bs}^H \mathbf{X}. \quad (6.507)$$

The resulting beam pattern is

$$B_\psi(\psi) = \mathbf{w}_{bs}^H \mathbf{v}_{bs}(\psi). \quad (6.508)$$

The spatial spectral matrix in beamspace is

$$\mathbf{S}_{\mathbf{x}_{bs}} = \mathbf{B}_{bs}^H \mathbf{S}_{\mathbf{x}} \mathbf{B}_{bs}. \quad (6.509)$$

For a single plane-wave signal plus spatially correlated interference and white noise,

$$\mathbf{S}_{\mathbf{x}} = \sigma_s^2 \mathbf{v}_s \mathbf{v}_s^H + \mathbf{S}_c + \sigma_w^2 \mathbf{I}. \quad (6.510)$$

Then,

$$\mathbf{S}_{\mathbf{x}_{bs}} = \sigma_s^2 \mathbf{B}_{bs}^H \mathbf{v}_s \mathbf{v}_s^H \mathbf{B}_{bs} + \mathbf{B}_{bs}^H \mathbf{S}_c \mathbf{B}_{bs} + \sigma_w^2 \mathbf{B}_{bs}^H \mathbf{B}_{bs}. \quad (6.511)$$

Using (6.501) and (6.502) gives

$$\mathbf{S}_{\mathbf{x}_{bs}} = \sigma_s^2 \mathbf{v}_{bs} \mathbf{v}_{bs}^H + \mathbf{B}_{bs}^H \mathbf{S}_c \mathbf{B}_{bs} + \sigma_w^2 \mathbf{I}. \quad (6.512)$$

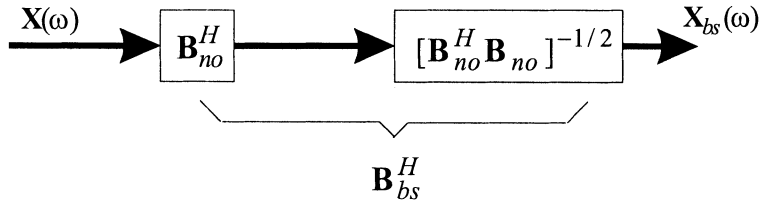


Figure 6.82 Beamspace processing using non-orthogonal beams.

For the special case in which the spatially correlated interference consists of  $D$  plane waves

$$\mathbf{S}_c = \mathbf{V}\mathbf{S}_I\mathbf{V}^H, \quad (6.513)$$

and the second term can be written as

$$\mathbf{B}_{bs}^H \mathbf{S}_c \mathbf{B}_{bs} = \mathbf{V}_{bs} \mathbf{S}_I \mathbf{V}_{bs}^H, \quad (6.514)$$

where

$$\mathbf{V}_{bs} \triangleq \mathbf{B}_{bs}^H \mathbf{V}. \quad (6.515)$$

We can now use one of our optimum beamforming algorithms on  $\mathbf{X}_{bs}$ . Note that the beamspace beamformer has a reduced number of degrees of freedom so that the number of interferers or eigenvectors that we can suppress is reduced.

One way to compensate for this reduction is to use shaped beams to form the beamspace. For example, we can use a set of shifted Dolph-Chebychev or Taylor-Villenueve beams to reduce the sidelobes significantly. Then the beamspace processor can focus on interference within the beamspace sector.

In the shaped beam case, the original beam set may not satisfy (6.501). We denote a non-orthogonal  $\mathbf{B}$  as  $\mathbf{B}_{no}$ . Then (6.512) becomes

$$\mathbf{S}_{\mathbf{x}_{bs}} = \sigma_s^2 \mathbf{v}_{bs} \mathbf{v}_{bs}^H + \mathbf{B}_{no}^H \mathbf{S}_c \mathbf{B}_{no} + \sigma_w^2 \mathbf{B}_{no}^H \mathbf{B}_{no}. \quad (6.516)$$

Most of our beamforming algorithms assume a white noise component so we pass  $\mathbf{X}_{bs}$  through a whitening matrix, as shown in Figure 6.82:

$$\mathbf{H}_w = [\mathbf{B}_{no}^H \mathbf{B}_{no}]^{-\frac{1}{2}}. \quad (6.517)$$

The overall matrix filter is

$$\mathbf{B}_{bs}^H = [\mathbf{B}_{no}^H \mathbf{B}_{no}]^{-\frac{1}{2}} \mathbf{B}_{no}^H. \quad (6.518)$$

We then use  $\mathbf{B}_{bs}^H$  as the matrix to form the beamspace. The sidelobes in the component beams of  $\mathbf{B}_{bs}$  are several dB higher than the original Dolph-Chebychev or Taylor beams.

We consider several examples to illustrate beamspace beamforming. In Examples 6.9.1 through 6.9.5, we consider a standard 32-element linear array. The beamspace sector is centered around  $u = 0$ .

### Example 6.9.1

In this example, we use the seven conventional beams shown in Figure 6.80 to form the beamspace. We then form the beamspace MPDR beamformer,

$$\mathbf{w}_{mpdr,bs}^H = \frac{\mathbf{v}_{bs}^H \mathbf{S}_{\mathbf{x}_{bs}}^{-1}}{\mathbf{v}_{bs}^H \mathbf{S}_{\mathbf{x}_{bs}}^{-1} \mathbf{v}_{bs}}. \quad (6.519)$$

We steer the array to broadside. Using (6.499) in (6.502), we have

$$\mathbf{v}_{bs}^H = [ \begin{array}{ccccccc} 0 & 0 & 0 & \sqrt{N} & 0 & 0 & 0 \end{array} ], \quad (6.520)$$

so that

$$\mathbf{w}_{mpdr,bs}^H = \frac{\mathbf{e}_4^T \mathbf{S}_{\mathbf{x}_{bs}}^{-1}}{\sqrt{N} \mathbf{e}_4^T \mathbf{S}_{\mathbf{x}_{bs}}^{-1} \mathbf{e}_4}. \quad (6.521)$$

We assume that the interference consists of two equal-power uncorrelated plane-wave interferers at  $\frac{3}{32}$  and  $\frac{5}{32}$ . We assume that the signal direction is perfectly matched so the *SNR* does not affect the array gain or beam pattern.

For  $INR \geq 10$  dB the beam patterns have essentially the same shape. In Figure 6.83, we show the beam patterns for an  $INR = 20$  dB (each interferer) for the beamspace MPDR. The two array gains are essentially the same: for element-space MPDR,  $A = 37.806$  and for beamspace MPDR,  $A = 37.753$ .

The advantage of beamspace is that the dimension of the optimum beamformers is 7 instead of the 32-dimensional element-space beamformer, so the computational complexity is reduced. In Chapter 7, we find that the number of snapshots needed to obtain a required accuracy will decrease as the dimension of the space decreases.

In the next example, we investigate the performance in the case of DOA mismatch. As in the element-space beamformer, we use diagonal loading to improve robustness.

### Example 6.9.2 (continuation)

We use the same model as in Example 6.9.1 and examine the behavior when  $u_a \neq 0$ . There are two plane-wave interferers at  $u_I = 3/32$  and  $u_I = 5/32$ . Each interferer has an  $INR = 20$  dB. We consider  $SNR = 0$  dB and 10 dB and use fixed loading of 10 dB and 15 dB. In Figure 6.84, we plot the array gain versus  $u_a/BW_{NN}$  for beamspace MPDR.

The loading provides some robustness against signal mismatch, but an LCMP beamformer may be necessary.

In the next example, we investigate the performance in the case of array perturbations.

### Example 6.9.3 (continuation)

We use the same model as in Example 6.9.2 and assume  $u_a = 0$ . We use the array perturbation model in Example 6.6.4. We use a beamspace MPDR algorithm with diagonal

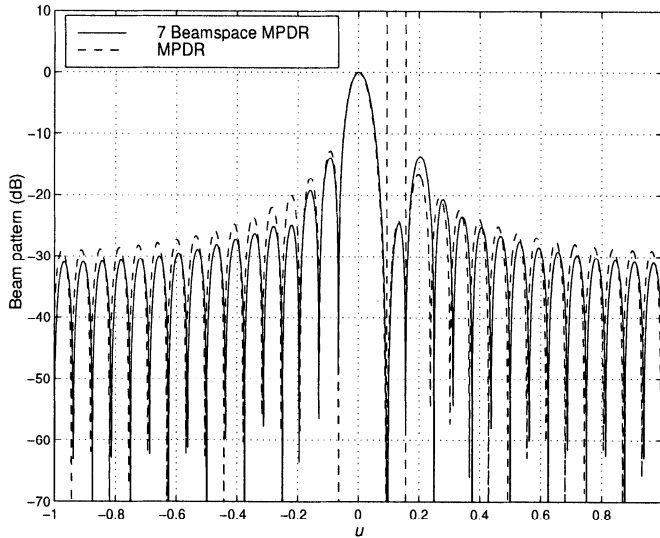


Figure 6.83 Beamspace MPDR;  $N=32$ ,  $N_{bs} = 7$ ,  $u_s = 0$ ,  $SNR = 0$  dB,  $u_I = 0.094, 0.16$ ,  $INR = 20$  dB: beam patterns.

loading. In Figure 6.85, we plot the array gain versus  $\frac{\sigma_p}{\lambda}$  when appropriate diagonal loading is used. We also include the results for element-space MPDR with diagonal loading.

We use the same  $INR$  and  $LNR$  values as in Example 6.9.2. In Figure 6.85(a), the  $SNR$  is 0 dB. In Figure 6.85(b), the  $SNR$  is 10 dB.

We see that the beamspace algorithm is always better than the element-space algorithm. For higher  $SNR$ , the performance difference is significant.

In the next example, we modify the beam patterns of the fixed beams in order to further suppress out-of-sector interference.

#### Example 6.9.4

Consider a standard 32-element linear array. We form a 7-dimensional beamspace using beams whose steering direction is shifted by  $\frac{2}{N}$ . Each beam utilizes Taylor (Villeneuve) weighting with  $-30$  dB sidelobes and  $\bar{n} = 6$ . We use (6.518) to generate the orthonormal rows in  $\mathbf{B}_{bs}^H$ . The interference consists of eight statistically independent plane-wave interferers with DOA in  $u$ -space of  $\pm \frac{3}{32}, \pm \frac{9}{32}, \pm \frac{11}{32}$ , and  $\pm \frac{13}{32}$ . Note that six of the interferers are outside the sector ( $\pm 7/32$ ) of the beamspace and there are more interferers than beamspace degrees-of-freedom. Each interferer has the same  $INR$ . We use an MPDR beamformer in beamspace.

In Figure 6.86, we show the resulting beam pattern for the case when the  $INR = 30$  dB. The array gain is the same as the element-space MPDR beamformer. We see that the beamspace processor has put a “perfect” null on the interferer inside the beamspace sector and reduces the beam pattern to less than  $-59$  dB in the direction of the out-of-sector interferers.

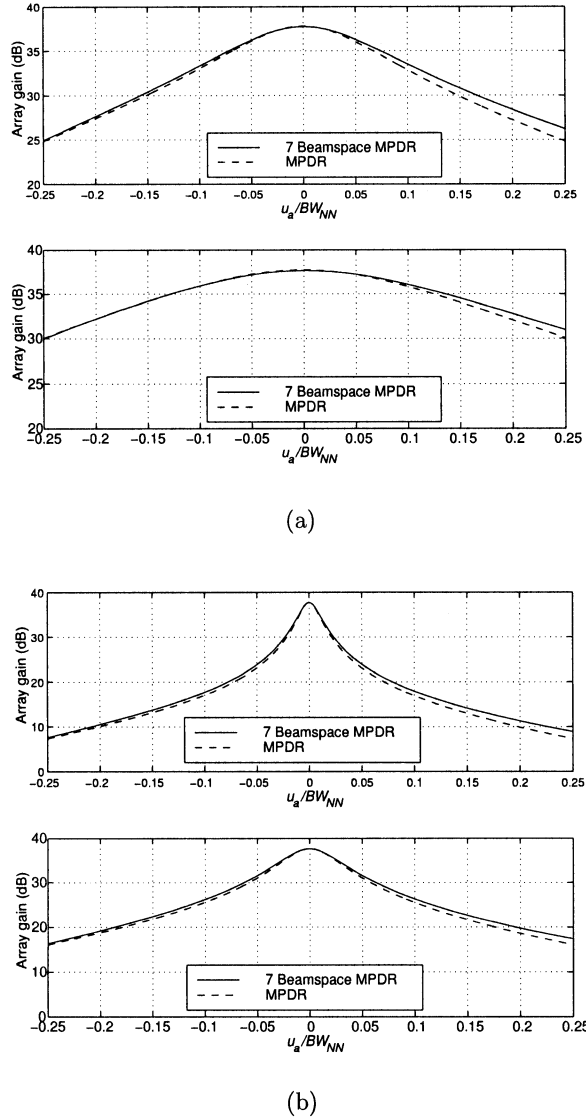
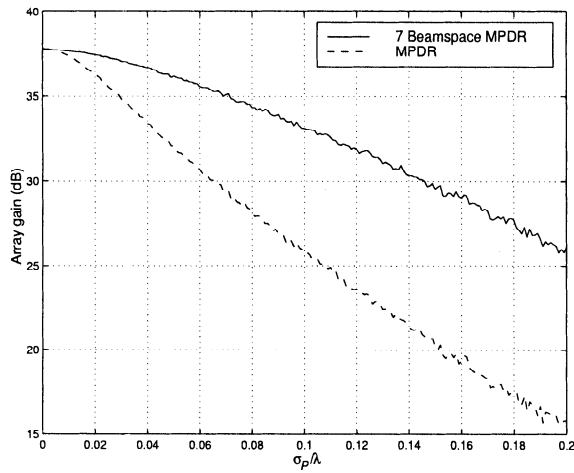
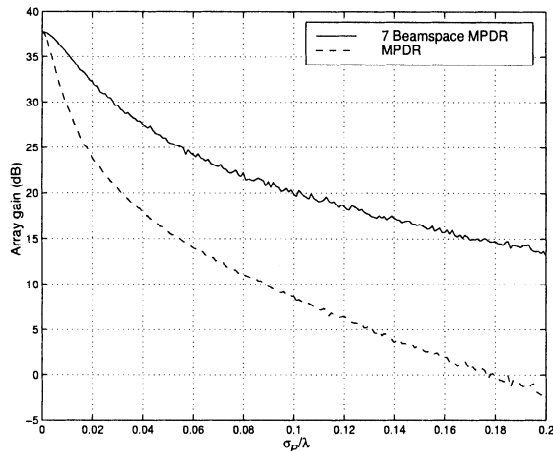


Figure 6.84 Signal mismatch, beamspace MPDR with fixed DL;  $N=32$ ,  $N_{bs}=7$ ,  $u_m=0$ ,  $SNR=0$  dB,  $u_{I1}=3/32$ ,  $u_{I2}=5/32$ ,  $INR_1=INR_2=20$  dB, array gain versus  $u_a/BW_{NN}$ : (a)  $SNR=0$  dB,  $LNR=10$  dB and 15 dB; (b)  $SNR=10$  dB,  $LNR=15$  dB and 20 dB.



(a)



(b)

Figure 6.85 Array position perturbations, beamspace MPDR with fixed DL;  $N=32$ ,  $N_{bs}=7$ ,  $u_m = 0$ ,  $u_{I1}=3/32$ ,  $u_{I2}=5/32$ ,  $INR_1=INR_2= 20$  dB, array gain versus  $\sigma_p/\lambda$ , 200 trials: (a)  $SNR = 0$  dB,  $LNR = 10$  dB; (b)  $SNR = 10$  dB,  $LNR = 20$  dB.

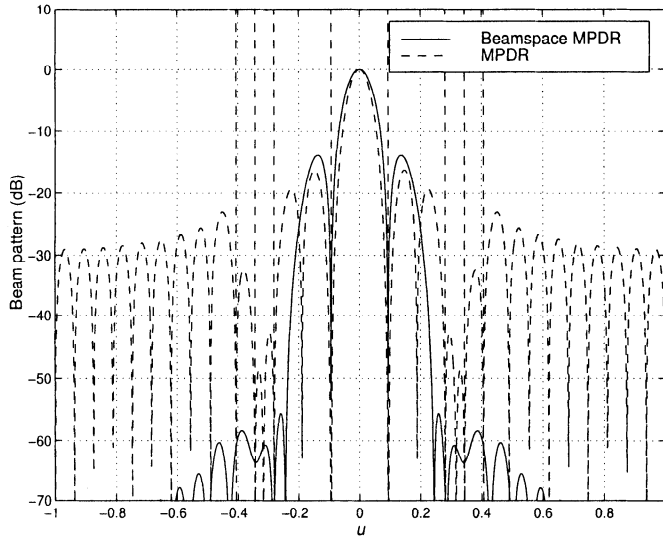


Figure 6.86 Beamspace MPDR beamformer with Taylor weighted beams;  $N=32$ ,  $N_{bs}=7$ ,  $u_s = 0$ ,  $SNR = 20$  dB, eight interferers with  $INR = 30$  dB; beam pattern.

### 6.9.2 Beamspace LCMP

We can also implement LCMV and LCMP beamformers in beamspace. We first formulate the constraints in element space. From (6.350),

$$\mathbf{w}^H \mathbf{C} = \mathbf{g}^H, \quad (6.522)$$

where  $\mathbf{w}^H$  is  $1 \times N$ ,  $\mathbf{C}$  is  $N \times M_c$ , and  $\mathbf{g}^H$  is  $1 \times M_c$ . From Figure 6.81,

$$\mathbf{w}^H = \mathbf{w}_{bs}^H \mathbf{B}_{bs}^H. \quad (6.523)$$

Using (6.523) in (6.522) gives

$$\mathbf{w}_{bs}^H (\mathbf{B}_{bs}^H \mathbf{C}) = \mathbf{g}^H. \quad (6.524)$$

Defining

$$\mathbf{C}_{bs} \triangleq \mathbf{B}_{bs}^H \mathbf{C}, \quad (6.525)$$

(6.524) can be written as

$$\mathbf{w}_{bs}^H \mathbf{C}_{bs} = \mathbf{g}^H. \quad (6.526)$$

Following the steps as in (6.350)–(6.358), the optimum beamspace LCMV and LCMP processors are:

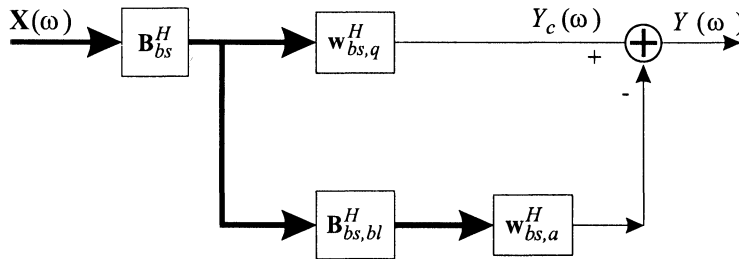


Figure 6.87 Beamspace generalized sidelobe canceller.

$$\mathbf{w}_{lcmv,bs}^H = \mathbf{g}^H \left[ \mathbf{C}_{bs}^H \mathbf{S}_{\mathbf{n},bs}^{-1} \mathbf{C}_{bs} \right]^{-1} \mathbf{C}_{bs}^H \mathbf{S}_{\mathbf{n},bs}^{-1}, \quad (6.527)$$

and

$$\mathbf{w}_{lcmp,bs}^H = \mathbf{g}^H \left[ \mathbf{C}_{bs}^H \mathbf{S}_{\mathbf{x},bs}^{-1} \mathbf{C}_{bs} \right]^{-1} \mathbf{C}_{bs}^H \mathbf{S}_{\mathbf{x},bs}^{-1}. \quad (6.528)$$

Note that, because the beamspace processor has fewer degrees of freedom, the impact of  $M_c$  constraints on the ability to null multiple interferers is increased.

The generalized sidelobe canceller implementation follows in the same manner as Section 6.7.3 and is shown in Figure 6.87.

The quiescent weight vector is

$$\mathbf{w}_{bs,q}^H = \mathbf{g}^H \left[ \mathbf{C}_{bs}^H \mathbf{C}_{bs} \right]^{-1} \mathbf{C}_{bs}^H. \quad (6.529)$$

The beamspace blocking matrix is defined by the constraint,

$$\mathbf{C}_{bs}^H \mathbf{B}_{bsbl} = \mathbf{0}, \quad (6.530)$$

and

$$\mathbf{B}_{bsbl}^H \mathbf{B}_{bsbl} = \mathbf{I}. \quad (6.531)$$

The second processor in the lower path is

$$\hat{\mathbf{w}}_{bs,a}^H = \mathbf{w}_{bs,q}^H \mathbf{S}_{\mathbf{x},bs} \mathbf{B}_{bsbl} \left[ \mathbf{B}_{bsbl}^H \mathbf{S}_{\mathbf{x},bs} \mathbf{B}_{bsbl} \right]^{-1}. \quad (6.532)$$

The various constraints that were developed in element space can be used in these two configurations. A summary of appropriate constraints is given in Table 6.2.

Table 6.2 Constraint References

Constraint	Section
Directional	6.7.4.1
Derivative	6.7.4.2
Eigenvector	6.7.4.3
Quiescent pattern	6.7.5

In most applications, diagonal loading is also added. In general, beamspace processing works well when the rank of the interference is less than the degrees of freedom available in beamspace. When, the interference rank is too large, the performance of the beamspace algorithm can be much poorer than an element-space algorithm.

### 6.9.3 Summary: Beamspace Optimum Processors

In this section, we have observed several advantages of beamspace processing:

- (i) The computational complexity is reduced from  $O(N^3)$  to  $O(N_{bs}^3)$ .
- (ii) The beamspace processor is more robust to array perturbations.
- (iii) By using low sidelobe beams to construct the beamspace, the subsequent beamspace beamformer emphasizes the sector of interest in its optimization.

In Chapter 7, we see another important advantage when we estimate  $\mathbf{S}_{\mathbf{x},bs}$ . The number of snapshots (samples),  $K$ , required to obtain an adequate estimate of  $\mathbf{S}_{\mathbf{x}}$  is a function of  $K/N$ . However, the number of snapshots required to get a comparable estimate of  $\mathbf{S}_{\mathbf{x},bs}$  is a function of  $K/N_{bs}$ , which may be significantly larger.

One disadvantage of beamspace processing is its loss of available degrees of freedom to combat interference.

In the next section, we revisit the issue of diagonal loading.

## 6.10 Quadratically Constrained Beamformers

In Section 6.6.4, the technique of constraining  $\|\mathbf{w}\|^2$  in order to improve the robustness of MPDR beamformers to signal mismatch and array perturbations was introduced. It resulted in diagonal loading. The level of loading was chosen without coupling it to the original constraint on the norm of the weight vector. Diagonal loading was also used in Section 6.7 to improve the robustness of LCMV and LCMP to mismatch.

In this section, we revisit the quadratic constraint problem and solve for the optimum loading as a function of  $T_o$ . First, the derivation in Section 6.6.4 is modified to include linear constraints. Then, a LCMV (or LCMP) beamformer is designed that minimizes the output noise variance subject to the constraint that<sup>15</sup>

$$\mathbf{w}^H \mathbf{w} = T \leq T_o. \quad (6.533)$$

The constraints  $T_o$  can only be set within a certain range of values. This range will be discussed shortly.

The LCMP optimization problem is:

$$\text{Minimize} \quad P_o = \mathbf{w}^H \mathbf{S}_x \mathbf{w}, \quad (6.534)$$

subject to the linear constraints,

$$\mathbf{C}^H \mathbf{w} = \mathbf{g}, \quad (6.535)$$

and the quadratic constraint,

$$\mathbf{w}^H \mathbf{w} \leq T_o. \quad (6.536)$$

Note that, when the signal is mismatched, minimizing  $P_o$  in (6.534) is not equivalent to maximizing the array gain. To maximize the array gain we would need  $\mathbf{S}_n$  (or an estimate of it). In our model we have assumed that only  $\mathbf{S}_x$  or its estimate is available.

We first solve the problem for the equality constraint,

$$\mathbf{w}^H \mathbf{w} = T_o. \quad (6.537)$$

In order to explore the allowable range of  $T_o$ , we denote the optimum solution by  $\tilde{\mathbf{w}}_o$ . We write  $\tilde{\mathbf{w}}_o$  as a generalized sidelobe canceller,

$$\begin{aligned} \tilde{\mathbf{w}}_o &= \mathbf{P}_C \tilde{\mathbf{w}}_o + \mathbf{P}_C^\perp \tilde{\mathbf{w}}_o \\ &= \mathbf{w}_q + \mathbf{P}_C^\perp \tilde{\mathbf{w}}_o. \end{aligned} \quad (6.538)$$

Therefore

$$\tilde{\mathbf{w}}_o^H \tilde{\mathbf{w}}_o = \mathbf{w}_q^H \mathbf{w}_q + \tilde{\mathbf{w}}_o^H \mathbf{P}_C^\perp \tilde{\mathbf{w}}_o \geq \mathbf{w}_q^H \mathbf{w}_q. \quad (6.539)$$

So,

$$\min \left\{ \tilde{\mathbf{w}}_o^H \tilde{\mathbf{w}}_o \right\} = \mathbf{w}_q^H \mathbf{w}_q. \quad (6.540)$$

---

<sup>15</sup>The first approach to the design of optimum array with a robustness constraint was published in 1955 (Gilbert and Morgan [GM55]) and 1956 (Uzsoky and Solymár [US56]). The specific problem formulation used here was published by Cox et al. [CZO87] and Owlsley [Ows73].

Therefore

$$T_o \geq \mathbf{w}_q^H \mathbf{w}_q = \mathbf{g}^H (\mathbf{C}^H \mathbf{C})^{-1} \mathbf{C}^H \mathbf{C} (\mathbf{C}^H \mathbf{C})^{-1} \mathbf{g}, \quad (6.541)$$

or

$$T_o \geq \mathbf{g}^H (\mathbf{C}^H \mathbf{C})^{-1} \mathbf{g}. \quad (6.542)$$

So we cannot set the constraint to be less than  $\mathbf{g}^H (\mathbf{C}^H \mathbf{C})^{-1} \mathbf{g}$ .

We now solve the optimization problem. Initially, we use an equality constraint. The function to minimize is

$$\begin{aligned} F &\triangleq \mathbf{w}^H \mathbf{S}_x \mathbf{w} + \lambda_1 [\mathbf{w}^H \mathbf{w} - T_o] \\ &\quad + \lambda_2 [\mathbf{C}^H \mathbf{w} - \mathbf{g}] + [\mathbf{w}^H \mathbf{C} - \mathbf{g}^H] \boldsymbol{\lambda}_2^H. \end{aligned} \quad (6.543)$$

Taking the gradient with respect to  $\mathbf{w}$  and setting the result to zero gives

$$\mathbf{w}^H \mathbf{S}_x + \lambda_1 \mathbf{w}^H + \lambda_2 \mathbf{C}^H = \mathbf{0}, \quad (6.544)$$

or

$$\mathbf{w}^H = -\lambda_2 \mathbf{C}^H [\lambda_1 \mathbf{I} + \mathbf{S}_x]^{-1}. \quad (6.545)$$

Solving for  $\boldsymbol{\lambda}_2$  gives

$$\tilde{\mathbf{w}}_o^H = \mathbf{g}^H [\mathbf{C}^H [\mathbf{S}_x + \lambda_1 \mathbf{I}]^{-1} \mathbf{C}]^{-1} \mathbf{C}^H [\mathbf{S}_x + \lambda_1 \mathbf{I}]^{-1}. \quad (6.546)$$

To emphasize that we are really using an inequality constraint, we change notation, letting

$$\tilde{\mathbf{w}}_o = \tilde{\mathbf{w}}_{oqc} \quad (6.547)$$

and

$$\beta = \lambda_1. \quad (6.548)$$

The solution in (6.546) can be written as

$$\tilde{\mathbf{w}}_{oqc} = (\mathbf{S}_x + \beta \mathbf{I})^{-1} \mathbf{C} [\mathbf{C}^H (\mathbf{S}_x + \beta \mathbf{I})^{-1} \mathbf{C}]^{-1} \mathbf{g}. \quad (6.549)$$

We can solve for  $\beta$  numerically using (6.549). As in Section 6.6.4, the effect of a positive  $\beta$  is to add a diagonal term to the actual  $\mathbf{S}_x$  in the expression defining the optimum beamformer. This technique is the diagonal loading used in Sections 6.6 and 6.7. In those cases, we picked a value of  $\beta$  based on the *SNR* and *INR*. We now want to find the optimum value of  $\beta$ . The beamformer is implemented in a generalized sidelobe canceller configuration.

Assume

$$\mathbf{B}^H \mathbf{B} = \mathbf{I}, \quad (6.550)$$

and write the LCMP as

$$\tilde{\mathbf{w}}_{oqc} = \tilde{\mathbf{S}}_{\mathbf{x}}^{-1} \mathbf{C} \left( \mathbf{C}^H \tilde{\mathbf{S}}_{\mathbf{x}}^{-1} \mathbf{C} \right)^{-1} \mathbf{g}, \quad (6.551)$$

where

$$\tilde{\mathbf{S}}_{\mathbf{x}} = \mathbf{S}_{\mathbf{x}} + \beta \mathbf{I}. \quad (6.552)$$

Then

$$\tilde{\mathbf{w}}_{gsc} = \mathbf{w}_q - \mathbf{B} \tilde{\mathbf{w}}_a \quad (6.553)$$

and

$$\begin{aligned} \tilde{\mathbf{w}}_a &= \left[ \mathbf{B}^H \tilde{\mathbf{S}}_{\mathbf{x}} \mathbf{B} \right]^{-1} \mathbf{B}^H \tilde{\mathbf{S}}_{\mathbf{x}} \mathbf{w}_q \\ &= \left[ \mathbf{B}^H \mathbf{S}_{\mathbf{x}} \mathbf{B} + \beta \mathbf{B}^H \mathbf{B} \right]^{-1} \left( \mathbf{B}^H \mathbf{S}_{\mathbf{x}} \mathbf{w}_q + \beta \mathbf{B}^H \mathbf{w}_q \right), \end{aligned} \quad (6.554)$$

which reduces to

$$\boxed{\tilde{\mathbf{w}}_a = \left[ \mathbf{B}^H \mathbf{S}_{\mathbf{x}} \mathbf{B} + \beta \mathbf{I} \right]^{-1} \mathbf{B}^H \mathbf{S}_{\mathbf{x}} \mathbf{w}_q.} \quad (6.555)$$

Now find  $\beta$  to satisfy

$$\begin{aligned} T_o &\geq \tilde{\mathbf{w}}_{gsc}^H \tilde{\mathbf{w}}_{gsc} \\ &= \mathbf{w}_q^H \mathbf{w}_q + \tilde{\mathbf{w}}_a^H \mathbf{B}^H \mathbf{B} \tilde{\mathbf{w}}_a \\ &= \mathbf{w}_q^H \mathbf{w}_q + \tilde{\mathbf{w}}_a^H \tilde{\mathbf{w}}_a, \end{aligned} \quad (6.556)$$

or

$$\boxed{T_o - \mathbf{w}_q^H \mathbf{w}_q \geq \tilde{\mathbf{w}}_a^H \tilde{\mathbf{w}}_a.} \quad (6.557)$$

Replacing the left side by  $\alpha^2$  gives

$$\boxed{\alpha^2 \geq \tilde{\mathbf{w}}_a^H \tilde{\mathbf{w}}_a,} \quad (6.558)$$

where  $\alpha^2 \geq 0$ .

When  $\beta = 0$ , the standard LCMP solution is obtained. When  $\beta \rightarrow \infty$ , the quiescent beamformer is obtained.

As  $\beta$  increases, the norm of  $\tilde{\mathbf{w}}_a$  decreases. To see this, we first rewrite (6.555) as

$$\tilde{\mathbf{w}}_a = [\mathbf{S}_{\mathbf{z}} + \beta \mathbf{I}]^{-1} \mathbf{p}_{\mathbf{z}}, \quad (6.559)$$

where

$$\mathbf{S}_z = \mathbf{B}^H \mathbf{S}_x \mathbf{B}, \quad (6.560)$$

is the spectral matrix of  $\mathbf{z}$ , the output from the blocking matrix, and

$$\mathbf{p}_z = \mathbf{B}^H \mathbf{S}_x \mathbf{w}_q, \quad (6.561)$$

is the cross-spectral term.

The squared norm of the weight vector  $\tilde{\mathbf{w}}_a$  can be written as

$$\tilde{\mathbf{w}}_a^H \tilde{\mathbf{w}}_a = \mathbf{p}_z^H (\mathbf{S}_z + \beta \mathbf{I})^{-2} \mathbf{p}_z. \quad (6.562)$$

Taking the derivative with respect to  $\beta$  gives

$$\frac{d}{d\beta} \tilde{\mathbf{w}}_a^H \tilde{\mathbf{w}}_a = -2 \mathbf{p}_z^H (\mathbf{S}_z + \beta \mathbf{I})^{-3} \mathbf{p}_z. \quad (6.563)$$

Since the diagonally loaded data matrix  $[\mathbf{S}_z + \beta \mathbf{I}]$  is positive definite when  $\beta \geq 0$ , the derivative value in (6.563) is negative. Therefore, the weight vector norm is decreasing in  $\beta$  for  $\beta > 0$ .

The amount of diagonal loading is adjusted to satisfy the quadratic constraint, however, the optimal loading level cannot be directly expressed as a function of the constraint and has to be solved for numerically (Tian et al. [TBV98]).

Assuming  $\tilde{\mathbf{w}}_a^H \tilde{\mathbf{w}}_a > \alpha^2$ , when  $\beta=0$ , an iterative procedure can be used to solve the constraint equation,

$$\tilde{\mathbf{w}}_a^H \tilde{\mathbf{w}}_a = \mathbf{w}_q^H \mathbf{S}_x \mathbf{B} (\mathbf{B}^H \mathbf{S}_x \mathbf{B} + \beta \mathbf{I})^{-2} \mathbf{B}^H \mathbf{S}_x \mathbf{w}_q = \alpha^2. \quad (6.564)$$

Starting with  $\beta^{(0)} = 0$ , let

$$\beta^{(1)} = \beta^{(0)} + \Delta\beta, \quad (6.565)$$

and

$$\beta^{(k)} = \beta^{(k-1)} + \Delta\beta. \quad (6.566)$$

At each step, compute  $\tilde{\mathbf{w}}_a^H \tilde{\mathbf{w}}_a$ . Continue the iteration until (6.564) is satisfied.

We consider two examples to illustrate typical behavior.

#### Example 6.10.1

Consider a standard 10-element linear array. The array is steered to broadside. The interference consists of two uncorrelated equal-power interferers each with an  $INR = 20$  dB. The interferers are located at  $u = 0.29$  and  $u = 0.45$ . The signal arrives  $u_a$  with an  $SNR = 10$  dB. An MPDR-QC beamformer is implemented with  $T_o = 0.12$ . Note that, whenever a

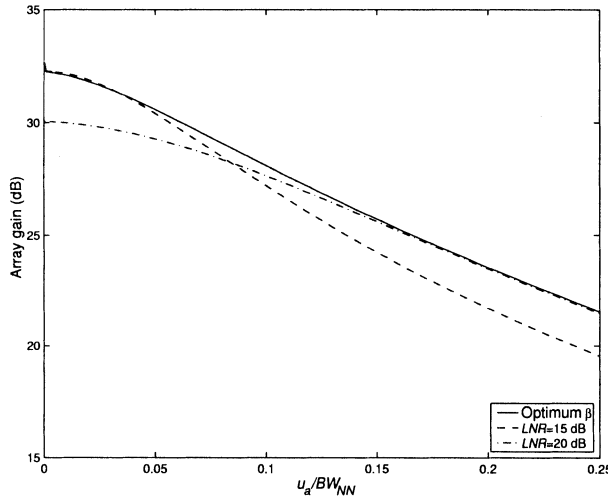


Figure 6.88 MPDR-QC beamformer with  $T_o = 0.12$ ; MPDR-DL beamformer with  $LNR = 15$  dB and  $20$  dB;  $SNR = 10$  dB,  $INR = 20$  dB,  $u_I = 0.29$  and  $0.45$ ; array gain versus  $u_a/BW_{NN}$ ,  $200$  trials.

distortionless constraint is included,  $T_o \geq 1/N = 0.1$ . An MPDR-DL beamformer is also implemented with fixed loading of  $15$  dB and  $20$  dB.

In Figure 6.88, the array gain for the three beamformers is plotted versus  $u_a/BW_{NN}$ . In Figure 6.89, the value of  $\beta$  is plotted versus  $u_a/BW_{NN}$ . In Figure 6.90, the value of  $\|w\|^2$  is plotted versus  $u_a/BW_{NN}$ .

In terms of array gain, there is only a moderate advantage in using the optimum  $\beta$ . However, the fixed loading levels were chosen based on knowledge of the  $SNR$  and  $INR$ . The constraint  $T_o$  was chosen based on a desired white noise gain level and the loading was derived to meet the constraint. This approach is more flexible and will lead to a useful adaptive loading technique.

#### Example 6.10.2 (continuation)

Consider the same model as in Example 6.10.1. In this example, there is no signal mismatch, but there are array perturbations. The signal arrives at  $u_s = 0$ . The array lies along the  $x$ -axis and the sensor positions are perturbed randomly in the  $x$  and  $y$  directions. The perturbations of each sensor in the  $x$  and  $y$  directions are statistically independent zero-mean Gaussian random variables with standard derivation  $\sigma_p$ . The  $SNR$  is  $10$  dB and the  $INR$  of each interferer is  $20$  dB.

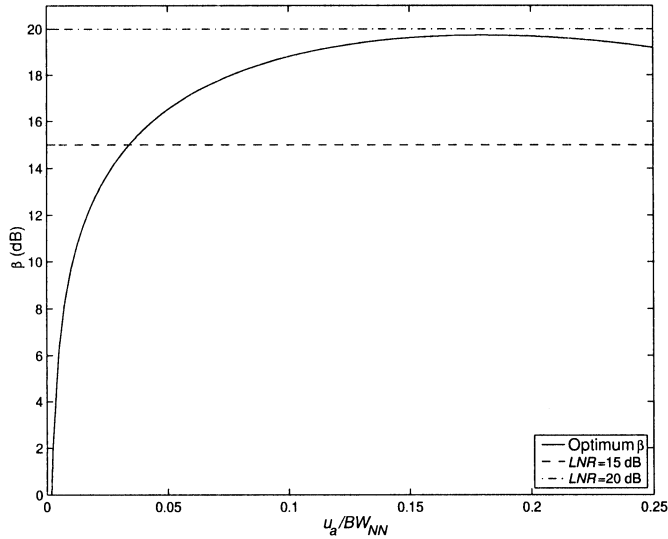
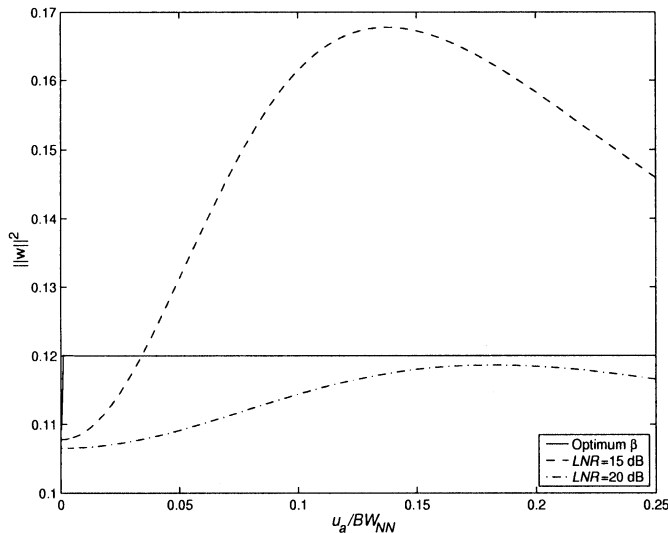
In Figure 6.91, the expected value of the array gain versus  $\frac{\sigma_p}{\lambda}$  is plotted for two cases:

- (i) MPDR-QC with  $T_o = 0.12$ .

- (ii) MPDR-DL with  $LNR = 15$  dB and  $20$  dB.

In Figure 6.92, the value of  $\beta$  is plotted versus  $\sigma_p/\lambda$ .

The use of the optimum  $\beta$  provides a  $1\text{--}2$  dB improvement over the fixed loading performance.

Figure 6.89  $\beta$  versus  $u_a/BW_{NN}$ .Figure 6.90  $\|w\|^2$  versus  $u_a/BW_{NN}$ .

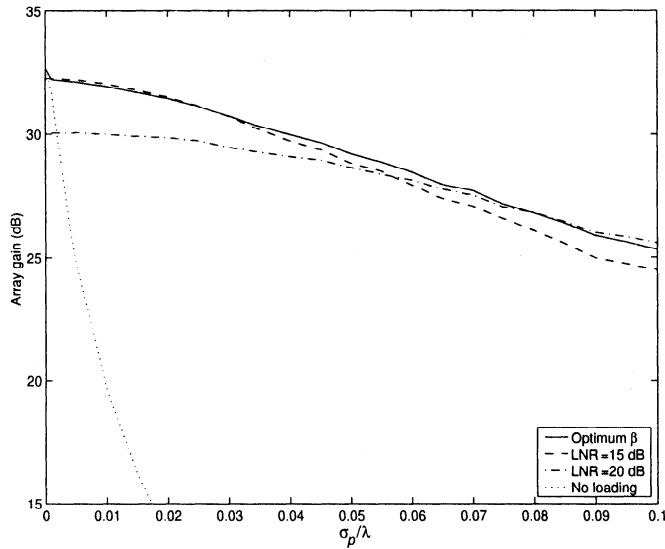


Figure 6.91 Array perturbations: MPDR-QC beamformer with  $T_o = 0.12$  and MPDR-DL beamformer with  $LNR = 15$  dB and  $20$  dB, average array gain versus  $\sigma_p/\lambda$ , 100 trials.

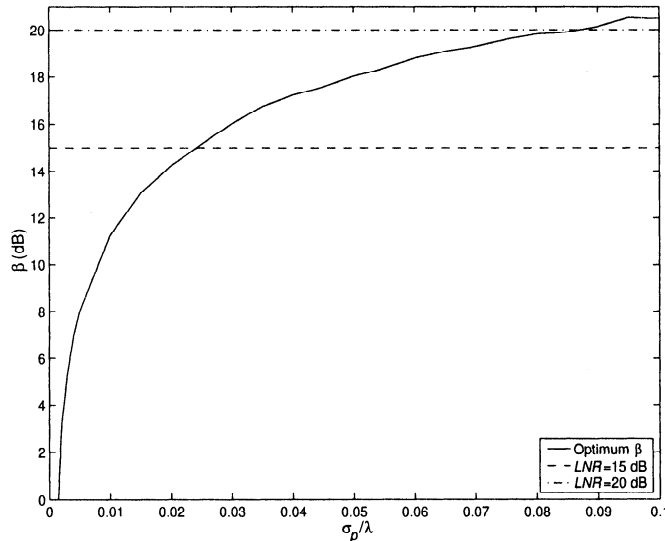


Figure 6.92  $\beta$  versus  $\sigma_p/\lambda$ , 100 trials.

In this section, quadratic constraints were introduced as a technique to make the optimum algorithm more robust in the presence of signal mismatch or array perturbations. It also provides main-lobe protection when a strong interferer moves into the main-lobe region. In Chapter 7, we find that it also provides robust behavior when the spatial spectral matrix is estimated from a limited amount of data.

An iterative technique was used to find the value of  $\beta$  required to satisfy the constraint. This technique has an advantage over fixed loading, because it only employs enough loading to meet the constraint. In the examples in this section, an appropriate level of fixed loading was chosen using knowledge of the signal and interference environment. In practice, this may be an unrealistic assumption. However, a suitable value of  $T_o$  can be chosen based on the entire range of signal and interference scenarios that are expected.

Quadratic constraints and diagonal loading will be revisited in Chapter 7. They will be a necessary component of most practical algorithms. In the next section, an algorithm is developed that turns out to be a generalization of diagonal loading.

## 6.11 Soft-constraint Beamformers

In this section, a quadratic constraint technique is developed that is referred to in the literature as a **soft-constraint beamformer**. This type of constraint was introduced by Er and Cantoni [EC85] and developed in detail by Van Veen [VV91]. Er and Cantoni consider the narrowband case and use a planar array as an example. Van Veen considers a broadband case using a tapped delay-line implementation. To simplify the notation, we consider a narrowband standard linear array in the text and develop the generalizations in the problems. The initial discussion is the same as Section 6.7.1.5.

The first step is to specify a desired beam pattern  $B_d(\psi)$ . We want the beam pattern to approximate it over some region in  $\psi$ -space. The desired beam pattern is

$$B_d(\psi) = \mathbf{w}_d^H \mathbf{v}(\psi). \quad (6.567)$$

In some cases  $B_d(\psi)$  might not be realizable with an  $N$ -element array. In that case,  $\mathbf{w}_d$  is the weight vector that minimizes the squared error (see Section 3.7.2).

We define a weighted least squares response error between the desired beam pattern and the actual beam pattern over a region in  $\psi$ -space as

$$e^2 = \int_{\Psi_0} f(\psi) \left| \mathbf{w}_d^H \mathbf{v}(\psi) - \mathbf{w}^H \mathbf{v}(\psi) \right|^2 d\psi, \quad (6.568)$$

where  $\Psi_0$  is the region of interest and  $f(\psi)$  is a weighting function that allows for emphasis of different regions in  $\psi$ -space. The error weight vector is defined as

$$\mathbf{w}_p = \mathbf{w}_d - \mathbf{w}. \quad (6.569)$$

Using (6.569) in (6.568) gives

$$e^2 = \mathbf{w}_p^H \mathbf{Q} \mathbf{w}_p, \quad (6.570)$$

where

$$\mathbf{Q} \triangleq \int_{\Psi_0} f(\psi) \mathbf{v}(\psi) \mathbf{v}^H(\psi) d\psi. \quad (6.571)$$

For the special case of a standard linear array and a constant  $f(\psi)$ ,

$$[\mathbf{Q}]_{mn} = \int_{\Psi_0} e^{j\psi(m-n)} d\psi. \quad (6.572)$$

If  $\Psi_0$  is a symmetric interval  $[-\psi_0, \psi_0]$ , then (6.572) reduces to

$$[\mathbf{Q}]_{mn} = \int_{-\psi_0}^{\psi_0} e^{j\psi(m-n)} d\psi = \frac{2 \sin(\psi_0(m-n))}{(m-n)}. \quad (6.573)$$

Note that, if  $\psi_0 = \pi$ , then we are attempting to approximate the desired beam pattern over the entire visible region and  $\mathbf{Q}$  is a diagonal matrix. As  $\psi_0$  decreases, the off-diagonal terms increase.

There are several approaches to introducing the constraint. The first ([EC85] or [VV91]) is to minimize the output  $P_o$ ,

$$P_o = \mathbf{w}^H \mathbf{S}_x \mathbf{w}, \quad (6.574)$$

subject to the constraint

$$e^2 \leq e_0^2, \quad (6.575)$$

where the value of  $e_0^2$  depends on the application.

Using a Lagrange multiplier, we define

$$F = (\mathbf{w}_d^H - \mathbf{w}_p^H) \mathbf{S}_x (\mathbf{w}_d - \mathbf{w}_p) + \lambda (\mathbf{w}_p^H \mathbf{Q} \mathbf{w}_p - e_0^2). \quad (6.576)$$

Minimizing gives

$$\boxed{\hat{\mathbf{w}}_p = [\mathbf{S}_x + \lambda \mathbf{Q}]^{-1} \mathbf{S}_x \mathbf{w}_d}, \quad (6.577)$$

and  $\lambda$  is chosen as large as possible subject to the constraint,

$$\boxed{\hat{\mathbf{w}}_p^H \mathbf{Q} \hat{\mathbf{w}}_p \leq e_0^2.} \quad (6.578)$$

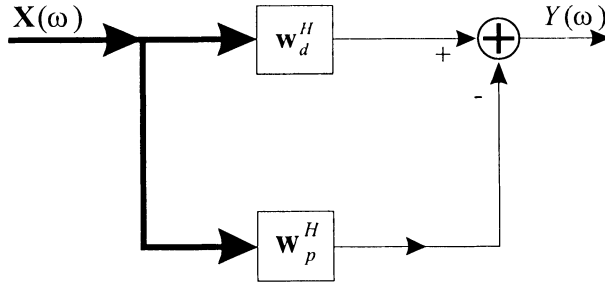


Figure 6.93 Partitioned processor.

We refer to the resulting beamformer as the MPSC beamformer. Van Veen [VV91] refers to it as soft-constrained minimum variance beamformer (SCMV). Note that the result in (6.577) corresponds to a partitioned processor as shown in Figure 6.93. This is the same partitioned processor that we saw in Figure 6.42. We see that MPSC is a generalization of diagonal loading that provides freedom to emphasize different areas of the beam pattern.

Just as in the diagonal loading case, we must solve for  $\lambda$  as a function of  $e_0^2$  using numerical procedures. As  $e_0^2 \rightarrow \infty$ ,  $\lambda \rightarrow 0$ , and we have an unconstrained beamformer. In this case,  $\mathbf{w}_p \rightarrow \mathbf{w}_d$ , and the output goes to zero. This result happens because of the absence of a distortionless constraint. As  $e_0^2 \rightarrow 0$ ,  $\mathbf{w}_p \rightarrow 0$ , and the beamformer is  $\mathbf{w}_d^H$ .

To obtain useful results,  $e_0^2$  must be small enough to avoid a zero output, but large enough to allow some adaptation. It is convenient to rewrite  $e_0$  as

$$e_0^2 = \alpha \mathbf{w}_d^H \mathbf{Q} \mathbf{w}_d, \quad 0 \leq \alpha \leq 1. \quad (6.579)$$

If  $\alpha = 1$ ,  $\hat{\mathbf{w}}_p = \mathbf{w}_d$  satisfies (6.577) and (6.578) with  $\lambda = 0$ , so we do not need to consider larger values of  $e_0^2$ . To avoid notational confusion between  $\lambda$  and eigenvalues, we replace  $\lambda$  with  $\beta$  and rewrite (6.577) as

$$\hat{\mathbf{w}}_{mpsc,p} = [\mathbf{S}_x + \beta \mathbf{Q}]^{-1} \mathbf{S}_x \mathbf{w}_d, \quad (6.580)$$

subject to the constraint

$$\hat{\mathbf{w}}_{mpsc,p}^H \mathbf{Q} \hat{\mathbf{w}}_{mpsc,p} \leq \alpha \hat{\mathbf{w}}_d^H \mathbf{Q} \mathbf{w}_d, \quad 0 \leq \alpha \leq 1. \quad (6.581)$$

The parameter  $\alpha$  plays a similar role to  $T_o$  in the diagonal loading model. As an alternative to solving for  $\beta$  as a function of  $\alpha$ , we can choose  $\beta$  based on expected scenarios. This is analogous to fixed diagonal loading.

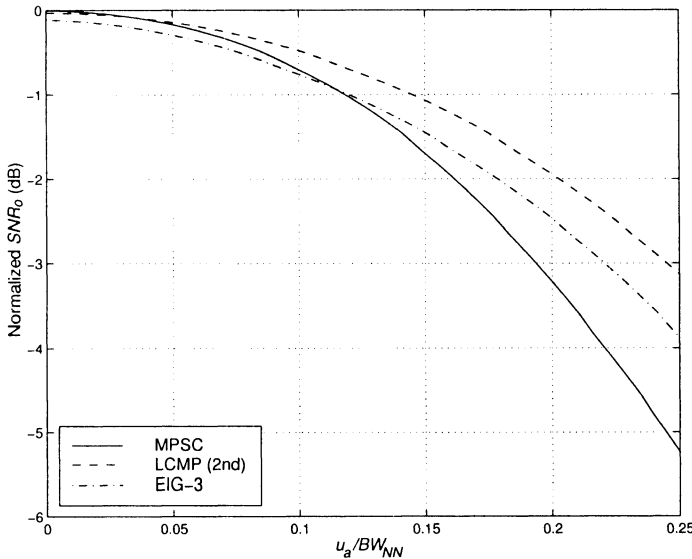


Figure 6.94 MPSC beamformer: normalized  $SNR_o$  versus  $u_a/BW_{NN}$ ,  $w_d = 1/N$ ,  $\psi_0 = 0.1\pi$ ,  $\alpha = 0.001$ ,  $u_I = 0.3$  and  $0.5$ ,  $INR = 20$  dB,  $SNR = 0$  dB.

We consider an example to illustrate typical performance of soft constraint beamformers.

#### Example 6.11.1

Consider a standard 10-element linear array. The desired beam pattern corresponds to a conventional beam and  $\psi_0 = 0.1\pi$ . There are two uncorrelated plane-wave interferers at  $u = 0.3$  and  $0.5$  with an  $INR = 20$  dB each. The performance of the MPSC beamformer specified by (6.580) with  $\alpha = 0.001$  is analyzed.

For comparison, the LCMP beamformer using three eigenvector constraints (Example 6.7.11), and an LCMP beamformer with second derivative constraints (Example 6.7.10) is also analyzed.

In Figure 6.94, the normalized  $SNR_o$  is plotted versus  $u_a/BW_{NN}$  for an  $SNR = 0$  dB. In Figure 6.95, the normalized  $SNR_o$  is plotted for an  $SNR = 10$  dB. Note that the vertical scale is different in the two Figures.

For the  $SNR = 0$ -dB case, the eigenvector-constraint beamformer is slightly worse for  $u_a/BW_{NN} \leq 0.1$  and better for larger  $u_a$ . The LCMP beamformer is better over the entire range, but the difference is small for  $u_a/BW_{NN} \leq 0.1$ .

For the  $SNR = 10$ -dB case, there is a wider difference in performance. The eigenvector-constraint algorithm is slightly worse for small  $u_a$  and slightly better for larger  $u_a$ . The LCMP algorithm drops off for  $u_a/BW_{NN}$ , but this could be improved by diagonal loading.

Small values of  $\alpha$  are used so the soft constraint is very tight. As  $\alpha$  is decreased, the MPSC beamformer acts very much like an eigenvector-constraint algorithm that uses all of the principal eigenvalues. Thus, as  $\alpha$  decreases, effective degrees of freedom are being lost.

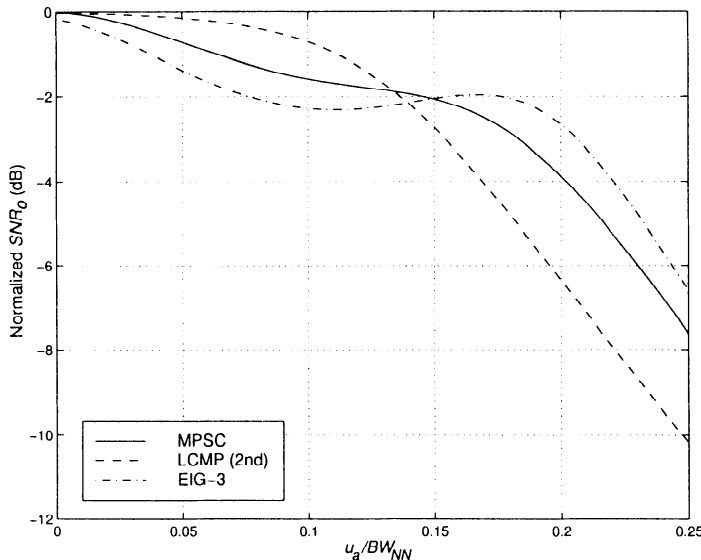


Figure 6.95 MPSC beamformer: normalized  $SNR_o$  versus  $u_a/BW_{NN}$ ,  $\mathbf{w}_d = \mathbf{1}/N$ ,  $\psi_0 = 0.1\pi$ ,  $\alpha = 0.001$ ,  $u_I = 0.3$  and  $0.5$ ,  $INR = 20$  dB,  $SNR = 10$  dB.

In order to improve the soft-constraint performance at  $u_a = 0$ , a linear distortionless constraint can be added. In the general case, a set of linear constraints defined by  $\mathbf{C}$  and  $\mathbf{g}$  can be added. If we try to implement the beamformer in a direct form, there are two Lagrange multipliers and the solution is complicated. However, a GSC solution is straightforward.

The GSC configuration in Figure 6.46 is used. We minimize

$$[\mathbf{w}_q - \mathbf{B}\mathbf{w}_a]^H \mathbf{S}_{\mathbf{x}} [\mathbf{w}_q - \mathbf{B}\mathbf{w}_a], \quad (6.582)$$

subject to the constraint

$$[\mathbf{w}_q - \mathbf{B}\mathbf{w}_a - \mathbf{w}_d]^H \mathbf{Q} [\mathbf{w}_q - \mathbf{B}\mathbf{w}_a - \mathbf{w}_d] \leq e_0^2 = \alpha \mathbf{w}_d^H \mathbf{Q} \mathbf{w}_d. \quad (6.583)$$

The constraint in (6.583) can also be written as

$$[(\mathbf{w}_q - \mathbf{w}_d) - \mathbf{B}\mathbf{w}_a]^H \mathbf{Q} [(\mathbf{w}_q - \mathbf{w}_d) - \mathbf{B}\mathbf{w}_a] \leq e_0^2. \quad (6.584)$$

Minimizing using a Lagrange multiplier gives

$$\hat{\mathbf{w}}_a = \left[ \mathbf{B}^H (\mathbf{S}_{\mathbf{x}} + \beta \mathbf{Q}) \mathbf{B} \right]^{-1} \mathbf{B}^H [\mathbf{S}_{\mathbf{x}} \mathbf{w}_q + \beta \mathbf{Q} (\mathbf{w}_q - \mathbf{w}_d)], \quad (6.585)$$

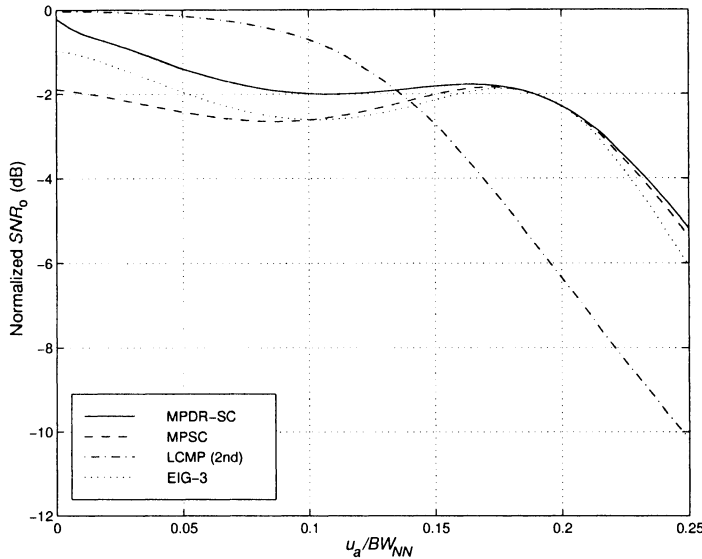


Figure 6.96 MPSC beamformer: normalized  $SNR_o$  versus  $u_a/BW_{NN}$ , desired pattern is Dolph-Chebychev ( $-40$ -dB SLL),  $u_I = 0.3$  and  $0.5$  ( $20$ -dB), distortionless constraint plus soft constraint with  $\alpha = 10^{-3}$ .

where  $\beta$  is chosen to satisfy (6.584). To find  $\beta$ , an iterative procedure similar to the procedure in (6.564)–(6.566) is used.

We consider a simple example to illustrate the behavior.

#### Example 6.11.2 (continuation)

Consider the same model as in Example 6.11.1 except the desired beam pattern is Dolph-Chebychev with  $-40$ -dB SLL. A single distortionless constraint is added. In Figure 6.96, the normalized  $SNR_o$  versus  $u_a/BW_{NN}$  for four beamformers is plotted. The  $SNR = 10$  dB and  $\alpha = 10^{-3}$ . As expected, the distortionless constraint improves the performance for small  $u_a$  without degrading the performance for large  $u_a$ . In Figure 6.97,  $\alpha$  is decreased to  $10^{-4}$ . This decrease degrades the performances of MPSC and MPDR-SC for small  $u_a$ , but improves them for larger  $u_a$ .

The LCMP-SC beamformer provides another technique for improving the robustness of an LCMP beamformer. In some signal, interference, and mismatch scenarios it can provide improved performance over other techniques.

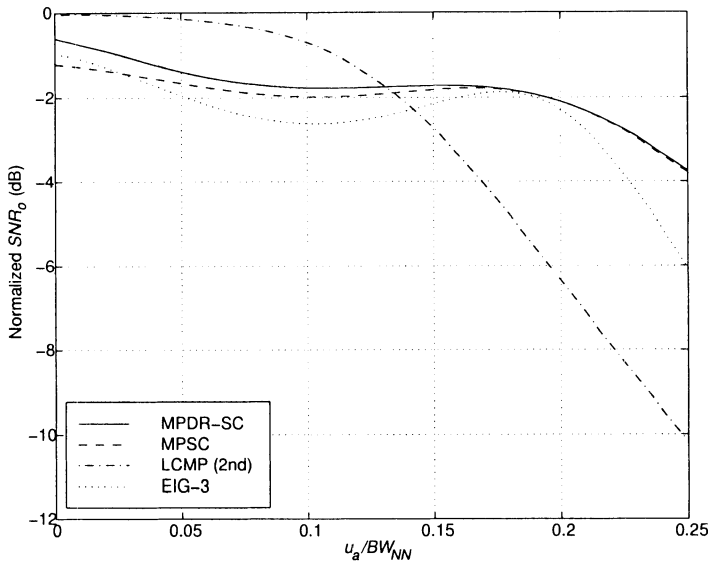


Figure 6.97 MPDR-SC beamformer: normalized  $SNR_o$  versus  $u_a/BW_{NN}$ , desired pattern is Dolph-Chebychev (-40-dB SLL),  $u_I = 0.3$  and  $0.5$  (20-dB) distortionless constraint plus soft constraint with  $\alpha = 10^{-4}$ .

## 6.12 Beamforming for Correlated Signal and Interferences

### 6.12.1 Introduction

In our discussion up to this point, we have assumed that the desired signal and the interference were uncorrelated. In many applications, the desired signal and interfering signals are correlated ( $|\rho| \neq 0$ ) or coherent ( $|\rho| = 1$ ). This situation can occur in a multipath environment or in a “smart” jamming scenario (i.e., the jamming signal is derived from the transmitted signal).

We consider two approaches to the problem. In the first approach, we implement an MPDR or LCMP beamformer and analyze the effects of correlation between the desired signal and the interference. We then develop a pre-processing technique called **spatial smoothing** that reduces the correlation. The output of this pre-processing step is the input to the MPDR or LCMP beamformer.

In the second approach, we implement a MMSE beamformer. When the desired signal and the interference are uncorrelated, the MMSE and the MPDR processor have the same matrix processing (6.44). However, when

the desired signal and interference are correlated, the MMSE processor is given by (6.42), which does not reduce to the MPDR processor.

In Section 6.12.2, we analyze the effects of correlation on the performance on an MPDR beamformer. In Section 6.12.3, we analyze the performance of an MMSE beamformer. In Section 6.12.3, we develop a technique called spatial smoothing to improve the beamformer performance. In Section 6.12.4, we summarize our results.

### 6.12.2 MPDR Beamformer: Correlated Signals and Interference

In this section, we analyze the effect of correlation between the signal and the interferers. We assume that the interference consists of  $(D - 1)$  plane-wave interferers and that one or more of these interferers are correlated with the desired signal. We use the frequency-domain snapshot model.

In this case,

$$\mathbf{X}(\omega) = \mathbf{V}\mathbf{F}(\omega) + \mathbf{W}(\omega), \quad (6.586)$$

and the vector  $\mathbf{F}(\omega)$  is a  $D$ -dimensional zero-mean random vector that contains both the desired signal and the interfering signals,

$$\mathbf{S}_x = \mathbf{V}\mathbf{S}_f\mathbf{V}^H + \sigma_w^2\mathbf{I}. \quad (6.587)$$

The source spectral matrix,  $\mathbf{S}_f$ , is not diagonal. The  $N \times D$  matrix,  $\mathbf{V}$ , is the array manifold matrix. The additive spatially white noise  $\mathbf{W}(\omega)$  is uncorrelated with the signal and interference. If there is a single interfering signal,  $\mathbf{S}_f$  can be written as

$$\mathbf{S}_f = \begin{bmatrix} \sigma_s^2 & \sigma_s\sigma_I\rho \\ \sigma_s\sigma_I\rho^* & \sigma_I^2 \end{bmatrix}. \quad (6.588)$$

For  $|\rho| = 1$ , the source covariance matrix is singular. We want to examine the behavior of the MPDR beamformer as a function of  $\rho$ . This problem (or models with similar beamformers) has been analyzed by a number of references. References include: Owsley [Ows74], [Ows80], Cattani and Godara [CG80], Widrow et al. [WDGN82], [Ows85], Kesler et al. [KBK85], Paulraj and Kailath [PK85], Shahmirian and Kesler [SK85b], Shan and Kailath [SK85a], Su et al. [SSW86], Luthra [Lut86], Takao et al. [TKY86], Reddy et al. [RPK87a], [RPK87b], Paulraj et al. [PRK87], Bresler et al. [BRK88], Zoltowski [Zol88], Godara [God90], Raghunath and Reddy [RR92b], [RR92a], and Tsai et al. [TYS95]. We utilize results from [TYS95]. In this section, we analyze the performance.

To understand the behavior, it is useful to write  $\mathbf{X}(\omega)$  as

$$\mathbf{X}(\omega) = \sigma_s F_d(\omega) \mathbf{v}_s + \sigma_I \left[ \rho^* F_d(\omega) + \sqrt{1 - |\rho|^2} F_u(\omega) \right] \mathbf{v}_I + \mathbf{W}(\omega). \quad (6.589)$$

The form in (6.589) separates  $F_I(\omega)$  into a component that is correlated with the desired signal  $F_d(\omega)$  and the remaining uncorrelated term  $F_u(\omega)$ .

The MPDR beamformer  $\mathbf{w}_{mpdr}^H$  uses a distortionless constraint,

$$\mathbf{w}^H \mathbf{v}_s = 1, \quad (6.590)$$

and minimizes the total output power  $P_o$ . Intuitively, we would anticipate that the optimum  $\mathbf{w}$  would constrain the output from  $\mathbf{v}_s$  as required by (6.590), but would add in enough of  $F_d(\omega)$  arriving from  $\mathbf{v}_I$  to partially cancel the desired signal. The output is

$$\begin{aligned} Y(\omega) &= \mathbf{w}^H \sigma_s F_d(\omega) \mathbf{v}_s + \mathbf{w}^H \sigma_I [\rho^* F_d(\omega) \\ &\quad + \sqrt{1 - |\rho|^2} F_u(\omega)] \mathbf{v}_I + \mathbf{w}^H \mathbf{W}(\omega), \end{aligned} \quad (6.591)$$

or

$$\begin{aligned} Y(\omega) &= \left[ \mathbf{w}^H \mathbf{v}_s \sigma_s + \mathbf{w}^H \mathbf{v}_I \sigma_I \rho^* \right] F_d(\omega) \\ &\quad + \mathbf{w}^H \mathbf{v}_I \left[ \sigma_I \sqrt{1 - |\rho|^2} F_u(\omega) + \mathbf{w}^H \mathbf{W}(\omega) \right] \\ &\stackrel{\triangle}{=} Y_d(\omega) + Y_I(\omega) + Y_n(\omega), \end{aligned} \quad (6.592)$$

where the three terms are uncorrelated.

The output power in the desired signal is

$$\begin{aligned} P_{do} &= E [Y_d(\omega) Y_d^*(\omega)] \\ &= \left[ \mathbf{w}^H \mathbf{v}_s \sigma_s + \mathbf{w}^H \mathbf{v}_I \sigma_I \rho^* \right] \left[ \mathbf{v}_s^H \mathbf{w} \sigma_s + \mathbf{v}_I^H \mathbf{w} \sigma_I \rho \right] \\ &= \sigma_s^2 \left| \alpha_s + \alpha_I \frac{\sigma_I \rho^*}{\sigma_s} \right|^2, \end{aligned} \quad (6.593)$$

where

$$\alpha_s \triangleq \mathbf{w}^H \mathbf{v}_s, \quad (6.594)$$

and

$$\alpha_I \triangleq \mathbf{w}^H \mathbf{v}_I. \quad (6.595)$$

For an MPDR beamformer,  $\alpha_s = 1$  and (6.593) reduces to

$$P_{do} = \sigma_s^2 \left| 1 + \alpha_I \frac{\sigma_I \rho^*}{\sigma_s} \right|^2. \quad (6.596)$$

The output power of the interference is

$$P_{Io} = E \left[ Y_I(\omega) Y_I^H(\omega) \right] = |\alpha_I|^2 (1 - |\rho|^2) \sigma_I^2, \quad (6.597)$$

and the output power due to noise is

$$P_{no} = \sigma_w^2 \| \mathbf{w} \|^2. \quad (6.598)$$

The output  $SNR_o$  is

$$SNR_o = \frac{P_{do}}{P_{Io} + P_{no}}. \quad (6.599)$$

To evaluate the  $SNR_o$ , we use  $\mathbf{w}^H$  from (6.14) in (6.593), (6.597), and (6.598). The result is (e.g., [TYS95])

$$SNR_o = \frac{A}{B}, \quad (6.600)$$

where

$$A = \left| \sigma_s \sigma_I^2 \Gamma \Delta + \sigma_w^2 (N \sigma_s + \rho^* N B_{dI}^* \sigma_I) \right|^2, \quad (6.601)$$

and

$$\begin{aligned} B = & \sigma_s^2 \sigma_I^4 \Gamma |\rho|^2 \Delta^2 + \sigma_I^2 \sigma_w^2 \Delta \left[ N \sigma_s^2 |\rho|^2 \right. \\ & \left. + N \sigma_I^2 + |\rho|^2 \sigma_s \sigma_I N (\rho^* B_{dI}^* + \rho B_{dI}) + 2 \sigma_w^2 \right] \\ & + N^2 \sigma_I^2 \sigma_w^4 |B_{dI}|^2 \Gamma + N \sigma_w^6. \end{aligned} \quad (6.602)$$

Parameters in (6.601) and (6.602) include:

$$\Gamma = 1 - |\rho|^2, \quad (6.603)$$

and

$$B_{dI} = \frac{1}{N} \mathbf{v}_I^H \mathbf{v}_s, \quad (6.604)$$

and

$$\Delta = N^2 \left( 1 - |B_{dI}|^2 \right). \quad (6.605)$$

Several limiting cases are of interest:

(i)  $\sigma_w^2 = 0, |\rho| = 1$ . In this case, we use L'Hopital's rule on (6.600) to obtain  $SNR_o = 0$ .

(ii) High  $SNR$  and  $INR$  and a sidelobe interferer. Then (6.600) reduces to

$$SNR_o \simeq \frac{\Gamma^2 \sigma_s^2}{\Gamma |\rho|^2 \sigma_s^2 + \frac{\sigma_w^2}{N}}, \quad (6.606)$$

which indicates the importance of  $|\rho|$ .

(iii) For main-lobe interference,  $|B_{dI}| \simeq 1$ ,

$$SNR_o \simeq \frac{\sigma_d^2 \left| 1 + \rho^* \frac{\sigma_I}{\sigma_s} \right|^2}{\sigma_I^2 (1 - |\rho|^2) + \frac{\sigma_w^2}{N}}. \quad (6.607)$$

The numerator depends on  $\rho$ , and the interfering signal can have either a constructive or destructive effect.

We consider an example to illustrate the behavior.

#### Example 6.12.1

Consider a standard 10-element linear array. In Figure 6.98, the  $SNR_o$  versus  $|\rho|$  for  $u_I = 0.30$  is plotted. The phase,  $\phi_\rho$ , equals 0. The  $SNR$  is 0 dB and the  $INR/SNR$  ratio is varied from 0.1 to 10.0. In Figure 6.99, the  $SNR_o$  for an  $SNR = 10$  dB is plotted.

For  $|\rho| > 0.5$ , there is significant degradation in the performance. This result is typical for a correlated interferer arriving in the sidelobe region.

An alternative approach to the MPDR beamformer is an MMSE beamformer. When the signal and interference are uncorrelated the matrix processing is the same. However, for correlated signals and interference, they are different.

### 6.12.3 MMSE Beamformer: Correlated Signals and Interference

In this section, we analyze the performance of a MMSE beamformer for the correlated signal and interference model in (6.586)–(6.588).

From (6.42),

$$\mathbf{W}_{mmse}^H = \mathbf{S}_{d\mathbf{x}^H} \mathbf{S}_{\mathbf{x}}^{-1}. \quad (6.608)$$

For the case of a single interferer,

$$S_{d\mathbf{x}^H} = \left[ \sigma_s^2 \mathbf{v}_s^H + \sigma_s \sigma_I \rho \mathbf{v}_I^H \right] \quad (6.609)$$

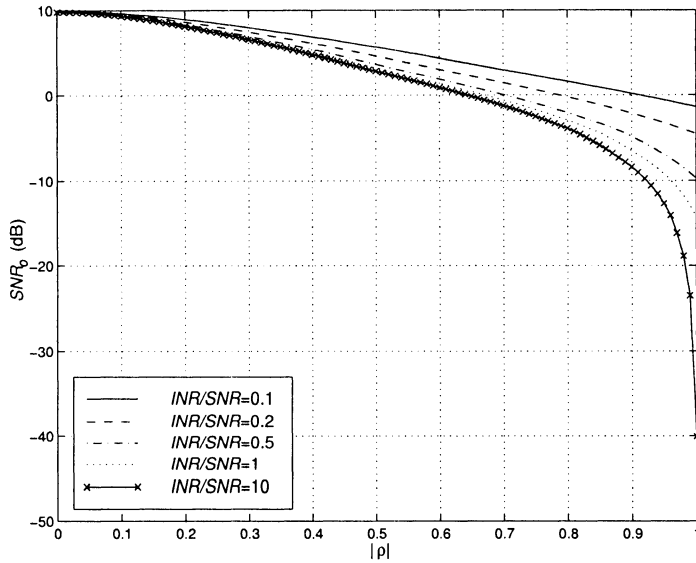


Figure 6.98 MPDR beamformer with correlated signal and interferer,  $SNR_o$  versus  $|\rho|$ ;  $u_s = 0$ ,  $SNR = 0$  dB, single plane-wave interferer at  $u_I = 0.3$ , various  $INR/SNR$  ratios.

and

$$\mathbf{S}_x^{-1} = \left[ \sigma_s^2 \mathbf{v}_s \mathbf{v}_s^H + \sigma_s \sigma_I \rho \mathbf{v}_s \mathbf{v}_I^H + \sigma_s \sigma_I \rho^* \mathbf{v}_I \mathbf{v}_s^H + \sigma_I^2 \mathbf{v}_I \mathbf{v}_I^H + \sigma_\omega^2 \mathbf{I} \right]^{-1}. \quad (6.610)$$

The expressions in (6.593) and (6.597)–(6.599) are valid with

$$\mathbf{w}^H = \mathbf{w}_{mmse}^H. \quad (6.611)$$

Note that  $\alpha_s \neq 1$  for  $\mathbf{w}_{mmse}^H$ .

#### Example 6.12.2 (continuation)

Consider the same model as in Example 6.12.1. The MMSE weight vector is specified by (6.608)–(6.610). Substituting into (6.593) and (6.597)–(6.599) gives the output  $SNR_o$ .

In Figure 6.100, the  $SNR_o$  is plotted versus  $|\rho|$  for the case when  $\rho = |\rho| \exp(j\pi/4)$  and  $\sigma_s^2 = 0$  dB. The range  $0.7 \leq |\rho| \leq 1.0$  is plotted. For  $|\rho| \leq 0.7$ , the curve is almost flat. As  $|\rho|$  increases, the correlated component of this signal from  $\mathbf{v}_I$  adds constructively. In Figure 6.101, the  $SNR_o$  is plotted for the case when  $\rho = |\rho| \exp(j\pi/4)$  and  $\sigma_s^2 = 10$  dB. The range  $0.9 \leq |\rho| \leq 1.0$  is plotted. For  $|\rho| \leq 0.9$ , the curve is almost flat. Once again, the correlated component of this signal from  $\mathbf{v}_I$  adds constructively.

In order to achieve this performance, the values of  $\mathbf{S}_{d\mathbf{x}^H}$  and  $\mathbf{S}_x$  must be known or the beamformer must estimate them. Alternatively, the beamformer can set  $\mathbf{v}_s = \mathbf{v}_m$  and estimate  $\sigma_s^2, \sigma_I^2, \rho, \mathbf{v}_I$ , and  $\mathbf{S}_x$ . We find that

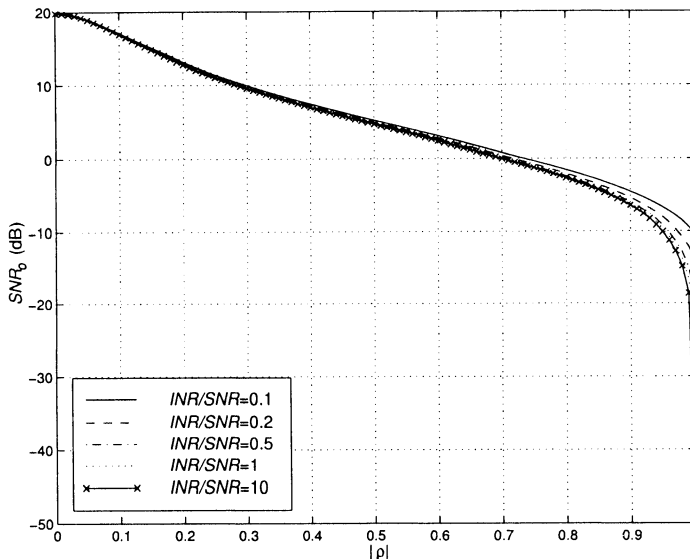


Figure 6.99 MPDR beamformer with correlated signal and interferer,  $SNR_o$  versus  $|\rho|$ ;  $u_s = 0$ ,  $SNR = 10$  dB, single plane-wave interferer at  $u_I = 0.3$ , various  $INR/SNR$  ratios.

this estimation is more difficult than the estimation of  $\mathbf{S}_x$  required for the MPDR beamformer.

One can think of the MPDR beamformer as a matched spatial processor where the beamformer is matched to  $\mathbf{v}_m$ . The MMSE beamformer is matched to the multipath environment.

#### 6.12.4 Spatial Smoothing and Forward–Backward Averaging

In this section, we introduce a technique referred to as **spatial smoothing (SS)** to remove the singularity in the input signal and interference correlation matrix, which is caused by the coherence between the desired signal and the interference. The original use of spatial smoothing was by Evans et al. [EJS82] in the direction-finding problem. We discuss this application in Chapter 9. The modification to the beamforming problem was done by Shan and Kailath ([SK85b]).

Our discussion is an adaption of [EJS82] and [PK89] to the beamformer problem. If we do not incorporate forward–backward (FB), averaging it reduces to the result in [SK85b], which was analyzed in [RPK87a] and [RR92b].

Spatial smoothing requires a regular array geometry, such as a uniform

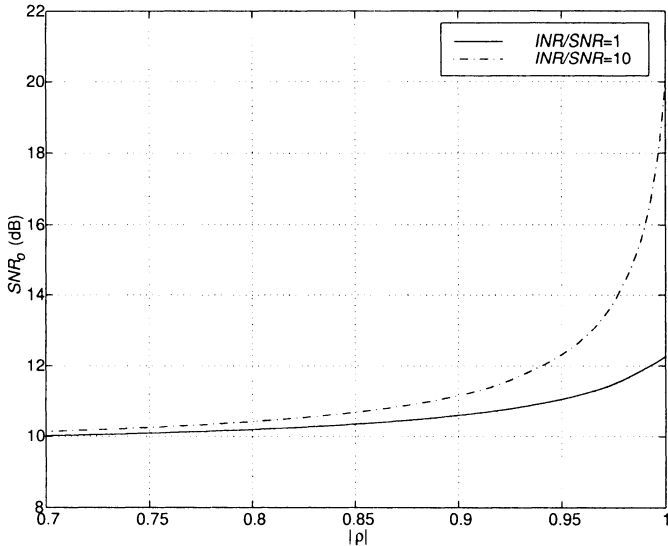


Figure 6.100 MMSE beamformer:  $SNR_o$  versus  $|\rho|$ ;  $u_a = 0$ ,  $SNR = 0$  dB, single correlated plane-wave interferer at  $u_I = 0.0866$ ,  $\rho = |\rho| \exp(j\pi/4)$ ,  $SNR = 0$  dB, various  $INR/SNR$  ratios.

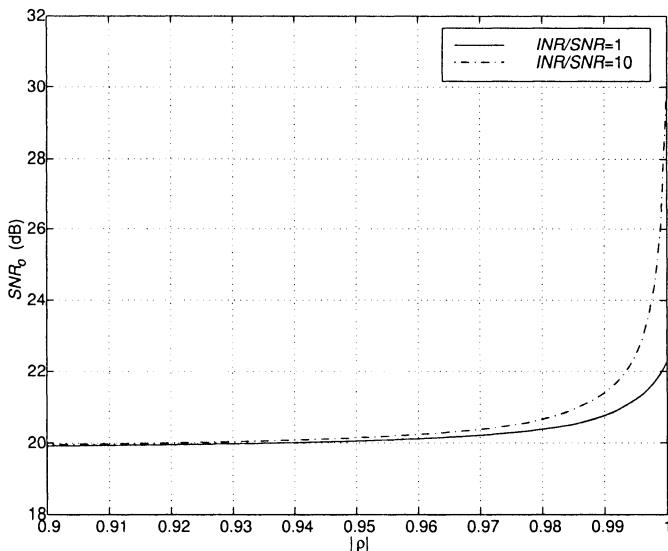


Figure 6.101 MMSE beamformer:  $SNR_o$  versus  $|\rho|$ ;  $u_a = 0$ ,  $SNR = 0$  dB, single correlated plane-wave interferer at  $u_I = 0.02$ ,  $\rho = |\rho| \exp(j\pi/4)$ .

linear array or a uniform rectangular array. We restrict our attention to a standard linear array in this section. We put the center of the array at the origin in order to eliminate some artifacts in FB smoothing. Because of this choice, the equations will be different from some of the above references.

We restrict our attention to a standard linear array. The received signal is

$$\mathbf{X}(\omega) = \mathbf{V}\mathbf{F}(\omega) + \mathbf{W}(\omega), \quad (6.612)$$

and the covariance matrix is

$$\mathbf{S}_X = \mathbf{V}\mathbf{S}_f\mathbf{V}^H + \sigma_w^2\mathbf{I}, \quad (6.613)$$

where  $\mathbf{S}_f$  is the source-signal spectral matrix and is assumed to be singular. We assume that  $D$ , the number of signals, is known or has been estimated. We use a frequency-domain snapshot model.

The linear array of interest is shown in Figure 6.102(a). Note that the array elements are indexed from 1 to  $N$ . We construct a set of  $L$  subarrays of length  $M \geq D + 1$ , as shown in Figure 6.102(b). Each subarray is shifted by one from the preceding subarray. The  $i$ th subarray has the  $i$ th element as its initial element. We use an  $M$ -element subarray centered at the origin as the reference subarray.

Let

$$\mathbf{V}_M = \left[ \mathbf{v}_M(\psi_1) \mid \mathbf{v}_M(\psi_2) \mid \cdots \mid \mathbf{v}_M(\psi_D) \right] \quad (6.614)$$

denote the set of steering vectors for the reference subarray of length  $M$ , where

$$\mathbf{v}_M(\psi) = \left[ e^{-j\frac{M-1}{2}\psi} \quad e^{-j\frac{M-3}{2}\psi} \quad \dots \quad e^{j\frac{M-1}{2}\psi} \right]. \quad (6.615)$$

We define

$$\mathbf{D} = \text{diag} \left[ e^{j\psi_1} \mid e^{j\psi_2} \mid \cdots \mid e^{j\psi_D} \right]. \quad (6.616)$$

Then the spectral matrix of the received signal at the  $i$ th subarray can be written as

$$\mathbf{S}_M^{(i)} = \mathbf{V}_M \mathbf{D}^{\frac{M-N}{2}+(i-1)} \mathbf{S}_f \left[ \mathbf{D}^{\frac{M-N}{2}+(i-1)} \right]^H \mathbf{V}_M^H + \sigma_w^2 \mathbf{I}. \quad (6.617)$$

We refer to  $\mathbf{S}_M^{(i)}$  as the forward spectral matrix of the  $i$ th subarray.

The backward spectral matrix is

$$\mathbf{S}_{MB}^{(i)} = \mathbf{J} \left[ \mathbf{S}_M^{(i)} \right]^* \mathbf{J}, \quad (6.618)$$

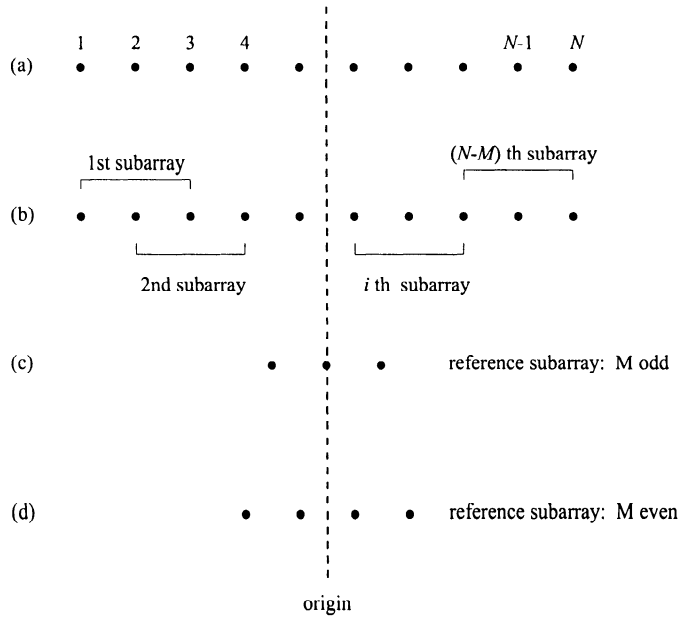


Figure 6.102 (a) Linear array; (b) subarrays; (c) reference subarray:  $M$  odd; (d) reference subarray:  $M$  even.

where  $\mathbf{J}$  is the exchange matrix. The backward spectral matrix can be written as<sup>16</sup>

$$\mathbf{S}_{MB}^{(i)} = \mathbf{J} \mathbf{V}_M^* \left[ \mathbf{D}^{\frac{M-N}{2} + (i-1)} \right]^* \mathbf{S}_f^* \left[ \mathbf{D}^{\frac{M-N}{2} + (i-1)} \right]^{*H} \mathbf{V}_M^{*H} \mathbf{J} + \sigma_w^2 \mathbf{I}. \quad (6.619)$$

Observing that

$$\mathbf{J} \mathbf{V}_M^* = \mathbf{V}_M, \quad (6.620)$$

(7.548) reduces to

$$\mathbf{S}_{MB}^{(i)} = \mathbf{V}_M \left( \mathbf{D}^{\frac{M-N}{2} + (i-1)} \right)^* \mathbf{S}_f^* \left[ \left( \mathbf{D}^{\frac{M-N}{2} + (i-1)} \right)^* \right]^H \mathbf{V}_M^H + \sigma_w^2 \mathbf{I}. \quad (6.621)$$

We now perform a weighted average across the subarrays and obtain a smoothed spectral matrix  $\mathbf{S}_{SSFB}$ :

$$\mathbf{S}_{SSFB} = \sum_{i=1}^L w_i \left\{ \frac{1}{2} \left( \mathbf{S}_M^{(i)} + \mathbf{S}_{MB}^{(i)} \right) \right\}. \quad (6.622)$$

---

<sup>16</sup>In Section 7.2.3, we develop FB averaging in more detail. Readers who have not encountered it previously may want to read that section at this point.

In most references (e.g., [RR92a], [SK85b]) the weighting is uniform. Takao et al. [TKY86] introduced the idea of non-uniform weighting.

For uniform weighting,

$$\mathbf{S}_{SSFB} = \frac{1}{2L} \sum_{i=1}^L \left( \mathbf{S}_M^{(i)} + \mathbf{S}_{MB}^{(i)} \right). \quad (6.623)$$

We derive the basic result using uniform weighting and then examine the possible advantages of non-uniform weighting.

Since  $\mathbf{D}^* = \mathbf{D}^{-1}$ , we can write  $\mathbf{S}_{SSFB}$  as

$$\begin{aligned} \mathbf{S}_{SSFB} &= \mathbf{V}_M \left[ \frac{1}{2L} \sum_{i=1}^L \left\{ \mathbf{D}^{\frac{M-N}{2}+(i-1)} \mathbf{S}_f \left[ \mathbf{D}^{\frac{M-N}{2}+(i-1)} \right]^H \right. \right. \\ &\quad \left. \left. + \left[ \mathbf{D}^{\frac{M-N}{2}+(i-1)} \right]^* \mathbf{S}_f^* \left[ \mathbf{D}^{\frac{M-N}{2}+(i-1)} \right]^{*H} \right\} \right] \mathbf{V}_M^H + \sigma_w^2 \mathbf{I}. \end{aligned} \quad (6.624)$$

We define the smoothed signal as the term in brackets,

$$\begin{aligned} \mathbf{S}_{f,SSFB} &= \frac{1}{2L} \sum_{i=1}^L \left( \mathbf{D}^{\frac{M-N}{2}+(i-1)} \mathbf{S}_f \left[ \mathbf{D}^{\frac{M-N}{2}+(i-1)} \right]^H \right. \\ &\quad \left. + \left[ \mathbf{D}^{\frac{M-N}{2}+(i-1)} \right]^* \mathbf{S}_f^* \left[ \mathbf{D}^{\frac{M-N}{2}+(i-1)} \right]^{*H} \right) \\ &= \frac{1}{L} \sum_{i=1}^L \operatorname{Re} \left[ \mathbf{D}^{\frac{M-N}{2}+(i-1)} \mathbf{S}_f \left[ \mathbf{D}^{\frac{M-N}{2}+(i-1)} \right]^H \right]. \end{aligned} \quad (6.625)$$

Then we can write

$$\mathbf{S}_{SSFB} = \mathbf{V}_M \mathbf{S}_{f,SSFB} \mathbf{V}_M^H + \sigma_w^2 \mathbf{I}. \quad (6.626)$$

Note that , if we did not use FB averaging,<sup>17</sup>

$$\mathbf{S}_{f,SS} = \frac{1}{L} \sum_{i=1}^L \mathbf{D}^{\frac{M-N}{2}+(i-1)} \mathbf{S}_f \left[ \mathbf{D}^{\frac{M-N}{2}+(i-1)} \right]^H, \quad (6.627)$$

and

$$\mathbf{S}_{SS} = \mathbf{V}_M \mathbf{S}_{f,SS} \mathbf{V}_M^H + \sigma_\omega^2 \mathbf{I}. \quad (6.628)$$

The first issue is to determine the number of subarrays need in order for the smoothed-signal covariance matrix to be non-singular. Evans et al.

---

<sup>17</sup>This is the model used in [SK85a], [SK85b], and [RPK87a].

[EJS82] indicated that  $L$  must be greater than  $D/2$ , but did not prove it. Williams et al. [WPMS88] and Pillai and Kwon [PK89] (apparently independently) have shown that, under mild conditions, that  $L \geq D/2$  guarantees that  $\mathbf{S}_{f,SSFB}$  will be non-singular. The reader is referred to either of these references for the proof. For the case when  $D = 2$ , the proof requires that the phase of  $[\mathbf{S}_f]_{12} \neq 0$ . We will use this criterion. However, if the phase of  $[\mathbf{S}_f]_{12}$  is near zero, the FB averaging will provide a matrix that is close to singular. As  $M \geq D + 1$ , and

$$N = L + M - 1, \quad (6.629)$$

we require

$$N \geq \frac{D}{2} + D, \quad (6.630)$$

or

$$N \geq \frac{3D}{2}, \quad (6.631)$$

in order to have a nonsingular  $\mathbf{S}_{f,SSFB}$ .

Note that the nonsingularity of  $\mathbf{S}_{f,SSFB}$  allows us to use various algorithms, such as the MPDR beamformer. However, if  $|\rho|$  is close to unity, the resulting performance will still be degraded.

The second issue is how rapidly do  $\mathbf{S}_{f,SSFB}$  and  $\mathbf{S}_{f,SS}$  approach diagonal matrices as a function of  $L$ . This rate will depend on the phase of  $\rho$ , the separation in wavenumber space of the correlated plane waves, and the *SNR*.

First, consider forward-only SS with uniform weighting. From (6.627),

$$[\mathbf{S}_{f,SS}^{(L)}]_{ij} = \mathbf{S}_{ij} \frac{1}{L} \sum_{l=1}^L \mathbf{D}_{ii}^{\frac{M-N}{2}+(l-1)} \left[ \mathbf{D}_{jj}^{\frac{M-N}{2}+(l-1)} \right]^*. \quad (6.632)$$

For  $i = j$ ,

$$[\mathbf{S}_{f,SS}^{(L)}]_{ii} = \mathbf{S}_{ii}. \quad (6.633)$$

However, for  $i \neq j$ ,

$$\begin{aligned} \frac{1}{L} \sum_{l=1}^L \mathbf{D}_{ii}^{\frac{M-N}{2}+(l-1)} \left[ \mathbf{D}_{jj}^{\frac{M-N}{2}+(l-1)} \right]^* &= \frac{1}{L} \sum_{l=1}^L e^{j\frac{M-N}{2}(\psi_i - \psi_j)} \cdot e^{-j(l-1)(\psi_i - \psi_j)} \\ &= e^{j\frac{M-N}{2}\Delta\psi_{ij}} \frac{1}{L} \sum_{m=0}^{L-1} e^{jm\Delta\psi_{ij}}. \end{aligned} \quad (6.634)$$

The sum on the right side of (6.634) is familiar as the conventional beam pattern for a standard  $L$ -element linear array.

Although it is convenient to recognize the right side of (6.634) as a beam pattern, there is no actual  $L$ -element array involved in the beamformer. The parameter  $L$  is the number of  $M$ -element subarrays used to construct the smoothed spectral matrix.

For the case of two sources,

$$\rho_F^{(L)} = \frac{[\mathbf{S}_{\mathbf{f},SS}^{(L)}]_{12}}{\sqrt{\mathbf{S}_{11}\mathbf{S}_{22}}}. \quad (6.635)$$

Using (6.634) for the two-source case gives

$$\begin{aligned} \rho_F^{(L)} &= \frac{\rho}{L} \frac{\sin\left(\frac{L\Delta\psi}{2}\right)}{\sin\left(\frac{\Delta\psi}{2}\right)} e^{-j\frac{L-1}{2}\Delta\psi} e^{-j\frac{M-N}{2}\Delta\psi} \\ &= \frac{\rho}{L} \frac{\sin\left(\frac{L\Delta\psi}{2}\right)}{\sin\left(\frac{\Delta\psi}{2}\right)}, \end{aligned} \quad (6.636)$$

where  $\Delta\psi = \Delta\psi_{12}$ .

In Figure 6.103(a), the magnitude of  $\rho_F^{(L)}$  is plotted versus  $L$  for various values of  $\Delta\psi$ . In practice, the value of  $L$  is constrained by  $N$  and  $D$  ( $N = M + L - 1$  and  $M \geq D + 1$ ). Thus, for  $N = 10$  and  $D = 2$ , the maximum value of  $L$  is 8. In Figure 6.103(b), the magnitude of  $\rho_F^{(L)}$  is plotted versus  $M$  for  $N = 10$  and  $D = 2$ .

A similar result can be obtained for  $\mathbf{S}_{\mathbf{f},SSFB}$  in (6.625). For the two-signal case and  $i \neq j$ , (6.625) can be written as,

$$[\mathbf{S}_{\mathbf{f},SSFB}]_{ij} = \frac{1}{L} \sum_{l=1}^L \operatorname{Re} \left[ [\mathbf{S}_{\mathbf{f}}]_{ij} e^{j(\frac{M+N}{2}+(l-1))\Delta\psi_{ij}} \right], \quad (6.637)$$

where

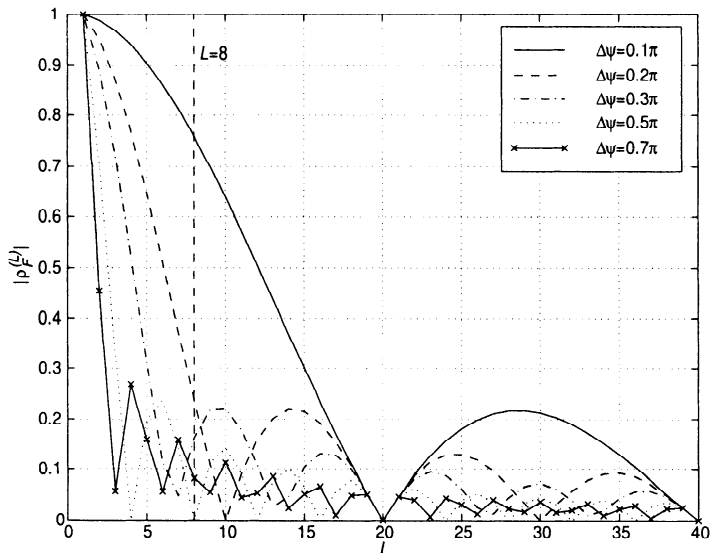
$$\Delta\psi_{ij} = \psi_i - \psi_j. \quad (6.638)$$

For the two-signal case, (6.637) reduces to

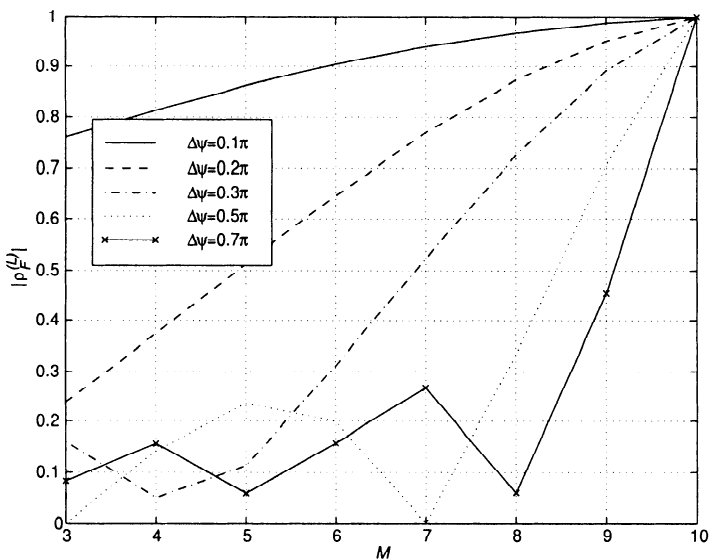
$$\rho_{FB}^{(L)} = \frac{\operatorname{Re}[\rho]}{L} \frac{(\sin \frac{L\Delta\psi}{2})}{\sin(\frac{\Delta\psi}{2})}. \quad (6.639)$$

Thus, the effect of FB smoothing is to replace  $\rho$  with  $\operatorname{Re}[\rho]$  in (6.636). Writing

$$\rho = |\rho|e^{j\phi}, \quad (6.640)$$



(a)



(b)

Figure 6.103 Magnitude of smoothed correlation coefficient for various  $\Delta\psi$ , forward-only smoothing; (a)  $|\rho_F^{(L)}|$  versus  $L$ ; (b)  $|\rho_F^{(L)}|$  versus  $M$  for  $N=10$ .

we see that the phase of  $\phi$  determines the difference between the effect of FB smoothing and forward-only smoothing. If  $\phi = \pi/2$  or  $3\pi/2$ , the correlation is completely removed by the FB averaging and no smoothing is needed. If  $\phi = 0$  or  $\pi$ , there is no difference between FB and forward-only smoothing.

The output of the spatial smoothing processing is the  $M \times M$  spectral matrix in (6.626) or (6.628). The array manifold vector for the reference subarray is given by (6.614). The weight vector for the MPDR algorithm is

$$\mathbf{w}_{SFB}^H = \frac{\mathbf{v}_M^H \mathbf{S}_{SSFB}^{-1}}{\mathbf{v}_M^H \mathbf{S}_{SSFB}^{-1} \mathbf{v}_M}, \quad (6.641)$$

if (6.626) is used, or

$$\mathbf{w}_S^H = \frac{\mathbf{v}_M^H \mathbf{S}_{SS}^{-1}}{\mathbf{v}_M^H \mathbf{S}_{SS}^{-1} \mathbf{v}_M}, \quad (6.642)$$

if (6.628) is used.

The behavior of the beamformer in (6.642) has been analyzed for the case of two correlated sources by Reddy et al. [RPK87a]. The result is identical to (6.600)–(6.605) with  $\rho$  replaced with  $\rho_F^{(L)}$  or  $\rho_{FB}^{(L)}$ ,  $N$  replaced by  $M$ , and  $B_{dI}$  defined for an  $M$ -element array. The modified equations are:

$$SNR_o = \frac{A_{SS}}{B_{SS}}, \quad (6.643)$$

where

$$A_{SS} = \left| \sigma_1 \sigma_2^2 \Gamma_s \Delta_s + \sigma_w^2 (M \sigma_1 + \rho_s^* M B_{12}^* \sigma_2) \right|^2, \quad (6.644)$$

$$\begin{aligned} B_{SS} &= \sigma_1^2 \sigma_2^2 \Gamma_s |\rho_s|^2 \Delta_s^2 + \sigma_2^2 \sigma_w^2 \Delta_s \\ &\quad \left[ M \sigma_1^2 |\rho_s|^2 + M \sigma_2^2 + |\rho_s|^2 \sigma_1 \sigma_2 M (\rho_s B_{12} + \rho_s^* B_{12}^*) + 2 \sigma_w^2 \right] \\ &\quad + M^2 \sigma_2^2 \sigma_w^4 |B_{12}|^2 \Gamma_s + M \sigma_w^6. \end{aligned} \quad (6.645)$$

Parameters in (6.644) and (6.645) include

$$\Gamma_s = 1 - |\rho_s|^2, \quad (6.646)$$

$$B_{12} = \frac{1}{M} \mathbf{v}_M^H(\psi_d) \mathbf{v}_M(\psi_I), \quad (6.647)$$

and

$$\Delta_s = M^2 (1 - |B_{12}|^2). \quad (6.648)$$

The correlation coefficient,  $\rho_s$ , denotes either  $\rho_F^{(L)}$  or  $\rho_{FB}^{(L)}$ .

If  $N$  is fixed, there are two opposing effects. As  $M$  decreases,  $L$  increases and the correlation coefficient decreases. However, as  $M$  decreases, the array gain for the subarray decreases and its resolution capability decreases. Thus, for a given value of  $\rho$ , there will a value of  $M$  that maximizes the output  $SNR$ .

We consider two examples to illustrate the behavior.

### Example 6.12.3

Consider a standard 10-element linear array. The input consists of two equal-power correlated plane-wave signals with  $\mathbf{S}_f$  given by (6.588) with

$$\rho = |\rho| e^{j\phi}. \quad (6.649)$$

The desired signal arrives from  $u_s = 0$ . The interfering signal arrives from  $u_I = 0.30$ . The  $SNR$  and  $INR$  are both 20 dB. We let

$$L = 11 - M. \quad (6.650)$$

We construct a smoothed spectral matrix using (6.626) or (6.628). We then use an MPDR beamformer with a symmetric  $M$ -element array manifold vector. We plot the array gain versus  $M$ .

In Figure 6.104, we let  $\phi = 0$  and plot the array gain versus  $M$  for  $|\rho| = 0, 0.1, 0.5, 0.95$ , and 1.0. We use forward SS.

We see that the optimum  $M$  is 4 for  $\rho \geq 0.50$ . For  $\rho = 0.10$ ,  $M_o$  is 5. For  $\rho = 0$ , we do not need SS, so  $M_o = 10$  and  $L = 1$ . For the case when  $\phi = 0$ , FB smoothing produces the same result.

In Figure 6.105, we let  $\phi = \frac{\pi}{4}$  and plot the array gain versus  $M$  for  $|\rho| = 0, 0.1, 0.5, 0.95$ , and 1.0 for FBSS.

For forward SS, the performance does not depend on  $\phi$ , so Figure 6.104 applies. For  $\rho \geq 0.5$ , the optimum  $M$  is 5 and the array gain is 26 dB, compared to 30 dB when  $\rho = 0$ .

In Figure 6.106, we let  $\phi = \frac{\pi}{2}$  and plot the array gain versus  $M$  for the same values as in Figure 6.98. FB smoothing decorrelates the signal for  $L = 1$ , so the optimum  $M$  for any value of  $|\rho|$  is 10.

The smoothed correlation coefficient is sensitive to the value of  $\Delta\psi$  (see Figure 6.103). In Figure 6.107,  $\Delta\psi$  is treated as a uniform random variable of  $0.2\pi \leq \Delta\psi \leq \pi$ . For each realization, the array gain using FB smoothing is plotted versus  $M$ . Then the result is averaged over 10,000 trials. For  $M = 4, 5$ , or 6, the array gain is slightly above 21 dB.

We now revisit the case of non-uniform weighting in the subarray averaging and consider two possible techniques. First consider the case in which we do not use FB averaging. Repeating the steps in (6.632)–(6.636), we obtain

$$\begin{aligned} [\mathbf{S}_{f,ss}^{(L)}]_{ij} &= \mathbf{S}_{ij} \left\{ e^{j\frac{M-N}{2}\Delta\psi_{ij}} \sum_{m=0}^{L-1} w_m e^{jm\Delta\psi_{ij}} \right\} \\ &= \mathbf{S}_{ij} \left\{ e^{j\frac{M-N}{2}\Delta\psi_{ij}} e^{j\frac{L-1}{2}\Delta\psi_{ij}} \left( e^{-j\frac{L-1}{2}\Delta\psi_{ij}} \sum_{m=0}^{L-1} w_m e^{jm\Delta\psi_{ij}} \right) \right\} \end{aligned}$$

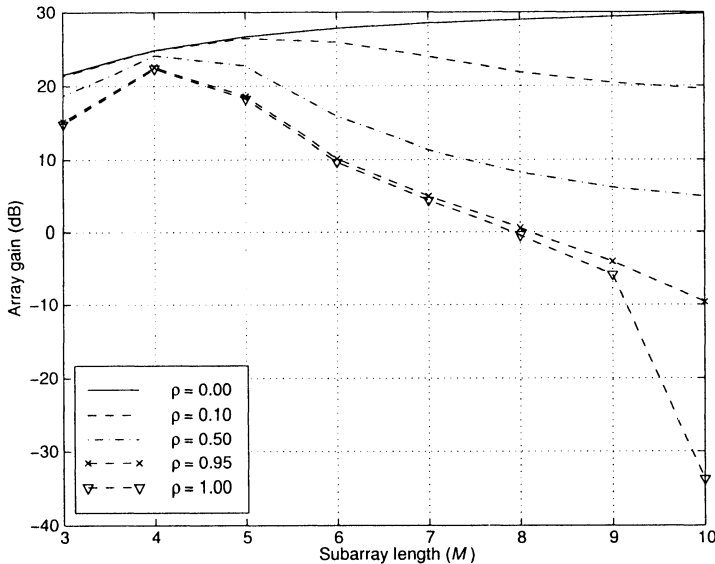


Figure 6.104 MPDR beamformer with forward spatial smoothing,  $u_s = 0$ ,  $SNR = 20$  dB,  $u_I = 0.3$ ,  $INR = 20$  dB,  $\phi = 0$ ; array gain versus  $M$  (subarray length).

$$= \mathbf{S}_{ij} \left\{ e^{-j\frac{L-1}{2}\Delta\psi_{ij}} \sum_{m=0}^{L-1} w_m^* e^{jm\Delta\psi_{ij}} \right\}. \quad (6.651)$$

The sum is just the beam pattern of a standard  $L$ -element linear array with non-uniform weighting. Then, for the two-source case

$$\rho^{(L)} = \rho B_w(\Delta\psi), \quad (6.652)$$

where  $B_w(\Delta\psi)$  is the beam pattern associated with the weights. For example, we might use a Hamming or Dolph-Chebychev weighting to lower the sidelobes in the function in Figure 6.103. A similar result can be obtained for FBSS.

This technique will be most effective when  $\Delta\psi$  and  $L$  are such that the interferer is the sidelobe region of an  $L$ -element standard linear array.

#### Example 6.12.4 (continuation)

Consider a standard 10-element array. The input consists of two equal-power coherent plane-wave signals with  $\mathbf{S}_f$  given by (6.588) with

$$\rho = \exp(j\pi/4).$$

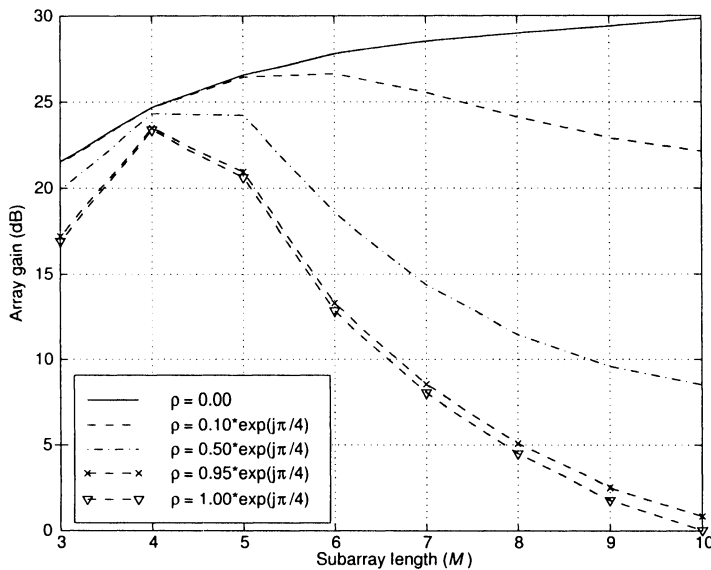


Figure 6.105 MPDR beamformer with forward spatial smoothing,  $u_s = 0$ ,  $SNR = 20$  dB,  $u_I = 0.3$ ,  $INR = 20$  dB,  $\phi = \frac{\pi}{4}$ ; array gain versus  $M$  (subarray length).

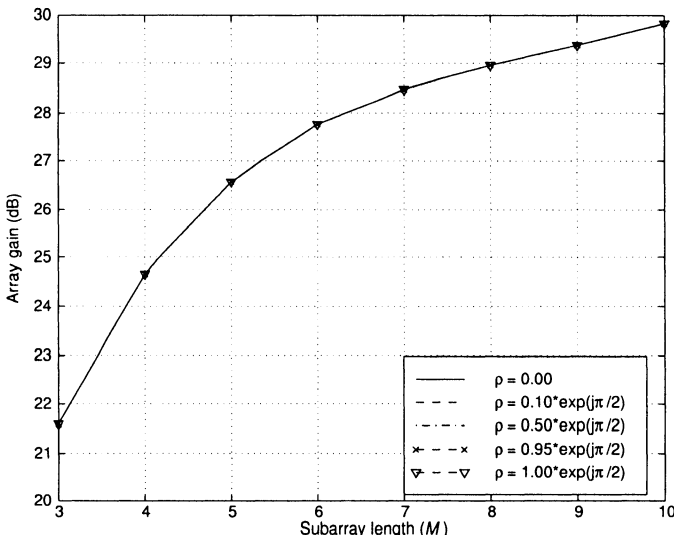


Figure 6.106 MPDR beamformer with FBSS,  $u_s = 0$ ,  $SNR = 20$  dB,  $u_I = 0.3$ ,  $INR = 20$  dB,  $\phi = \frac{\pi}{2}$ ; array gain versus  $M$  (subarray length).

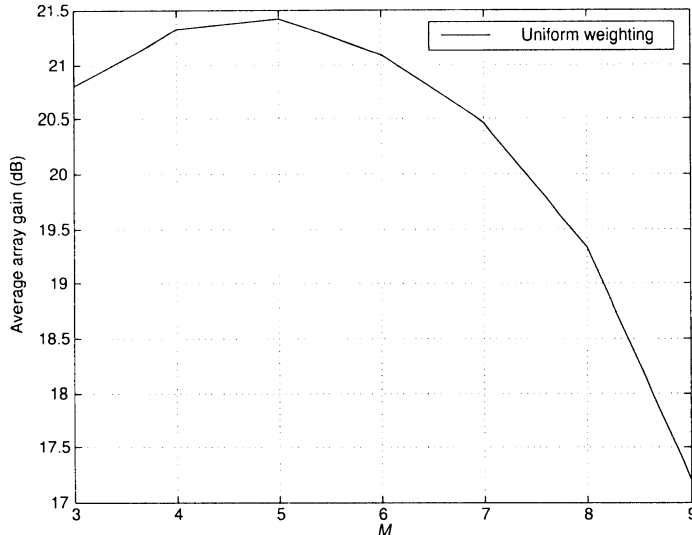


Figure 6.107 MPDR-FBSS beamformer: average array gain versus  $M$ ,  $\rho = \exp(j\pi/4)$ ,  $u_s = 0$ ,  $u_I$  is a uniform random variable (0.2, 1),  $SNR = INR = 20$  dB, 10,000 trials.

The desired signal arrives from  $u_s = 0$ . The interfering signal arrives from  $u_I$ , where  $u_I$  is a uniform random variable (0.2, 1.0). The  $SNR = INR = 20$  dB. A FB-smoothed spectral matrix is constructed using a Dolph-Chebychev weighting with -30-dB sidelobe level. The smoothed output is processed using an MPDR beamformer with a symmetric  $M$ -element array manifold vector. In Figure 6.108, the average array gain is plotted versus  $M$ . The result from Figure 6.107 is shown for comparison. The Dolph-Chebychev weighting provides about a 3-dB improvement for  $M = 4, 5, 6$ , and 7 and gives an average array gain about 24.5–25 dB.

A different approach suggested by Takao and Kikuma [TK87] is to choose the  $w_m$  to make the resulting smoothed matrix as close to Toeplitz as possible. We rewrite (6.622) as

$$\mathbf{S}_{SSFB} = \sum_{k=1}^L w_k \mathbf{H}_k \triangleq \mathbf{B}, \quad (6.653)$$

where

$$\mathbf{H}_k \triangleq \frac{1}{2} \left[ \mathbf{S}_M^{(k)} + \mathbf{S}_{MB}^{(k)} \right]. \quad (6.654)$$

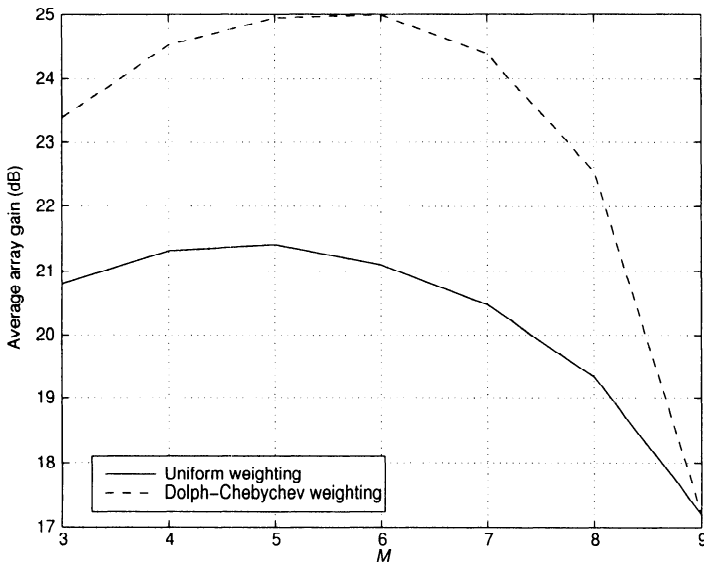


Figure 6.108 MPDR-FBSS beamformer with Dolph-Chebychev and uniform weighting: average array gain versus  $M$ ,  $\rho = \exp(j\pi/4)$ ,  $u_s = 0$ ,  $u_I$  is a uniform random variable (0.2, 1),  $SNR = INR = 20$  dB, 10,000 trials.

We test how close  $\mathbf{B}$  is to a Toeplitz matrix by defining

$$F = \sum_{i=0}^{M-2} \sum_{k=1}^{M-1} |b_{k+i,k} - b_{(i)}|^2, \quad (6.655)$$

where

$$b_{(i)} \triangleq \frac{1}{M-i} \sum_{k=1}^{M-i} b_{k+i,k}. \quad (6.656)$$

Then,

$$\begin{aligned} b_{k+i,k} - b_{(i)} &= b_{k+i,k} - \frac{1}{M-i} \sum_{k=1}^{M-i} b_{k+i,k} \\ &= \left[ \sum_{l=1}^L w_l \mathbf{H}_l \right]_{k+i,k} - \frac{1}{M-i} \sum_{k=1}^{M-i} \left[ \sum_{l=1}^L w_l \mathbf{H}_l \right]_{k+i,k} \\ &= \sum_{l=1}^L w_l \left[ [\mathbf{H}_l]_{k+i,k} - \frac{1}{M-i} \sum_{k=1}^{M-i} [\mathbf{H}_l]_{k+i,k} \right] \end{aligned}$$

$$= \sum_{l=1}^L w_l [\mathbf{e}_l]_{k+i,k}, \quad (6.657)$$

where

$$[\mathbf{e}_l]_{k+i,k} \triangleq [\mathbf{H}_l]_{k+i,k} - \frac{1}{M-i} \sum_{k=1}^{M-i} [\mathbf{H}_l]_{k+i,k}. \quad (6.658)$$

Now define the vectors,

$$\mathbf{w} = \begin{bmatrix} w_1 & w_2 & \cdots & w_L \end{bmatrix}^T \quad (6.659)$$

$$\mathbf{e}_{k+i,k} = \begin{bmatrix} [\mathbf{e}_1]_{k+i,k} & \cdots & [\mathbf{e}_L]_{k+i,k} \end{bmatrix}^T. \quad (6.660)$$

Then,

$$b_{k+i,k} - b_{(i)} = \mathbf{w}^T \mathbf{e}_{k+i,k}, \quad (6.661)$$

and

$$F = \sum_{i=0}^{M-2} \sum_{k=1}^{M-i} \mathbf{w}^T \mathbf{e}_{k+i,k} \mathbf{e}_{k+i,k}^T \mathbf{w}. \quad (6.662)$$

Defining,

$$\begin{aligned} \mathbf{R}_{\mathbf{ee}} &= \sum_{i=0}^{M-2} \sum_{k=1}^{M-i} \mathbf{e}_{k+i,k} \mathbf{e}_{k+i,k}^T \\ &= Re \left\{ \sum_{i=0}^{M-2} \sum_{k=1}^{M-i} \mathbf{e}_{k+i,k} \mathbf{e}_{k+i,k}^T \right\}, \end{aligned} \quad (6.663)$$

we can write (6.662) as

$$F = \mathbf{w}^T \mathbf{R}_{\mathbf{ee}} \mathbf{w}. \quad (6.664)$$

Minimizing  $F$  subject to the constraint

$$\mathbf{w}^T \mathbf{1} = 1, \quad (6.665)$$

gives

$$\hat{\mathbf{w}} = \frac{\mathbf{R}_{\mathbf{ee}}^{-1} \mathbf{1}}{\mathbf{1}^T \mathbf{R}_{\mathbf{ee}}^{-1} \mathbf{1}}. \quad (6.666)$$

In an actual application,  $\mathbf{S}_M^{(k)}$  and  $\mathbf{S}_{MB}^{(k)}$  will be estimated from the data so the weight in (6.666) will be data dependent. We refer to this technique as **Toeplitz weighting**. It is called **adaptive spatial averaging** in the literature [TK87].

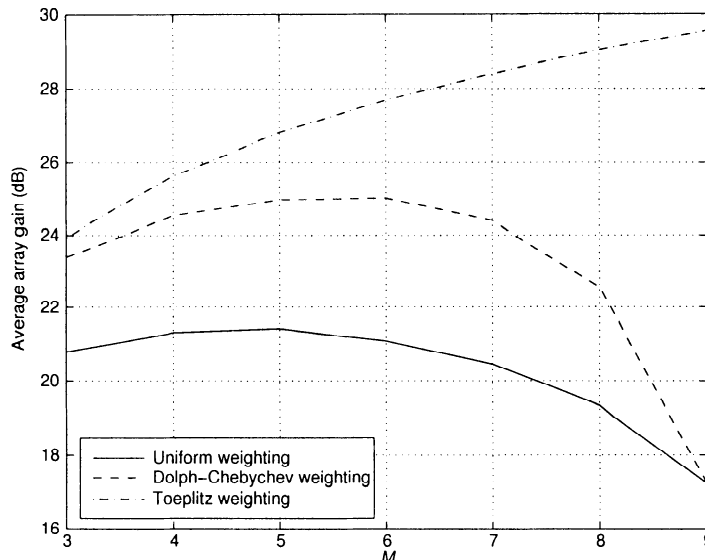


Figure 6.109 Average array gain using FBSS with Toeplitz weighting,  $\rho = \exp(j\pi/4)$ ,  $u_s = 0$ ,  $u_I$  uniform (0.2-1.0),  $SNR = INR = 20$  dB,  $N = 10$ , 10,000 trials.

We consider the models in examples 6.12.3 and 6.12.4 to see the impact on this weighting.

#### Example 6.12.5 (continuation; Example 6.12.4)

We use the same model as in Example 6.12.4 and consider the case when  $\phi = \pi/4$ . The result is shown in Figure 6.109. We see that, in the case of known spectral matrices, there is significant improvement.

### 6.12.5 Summary

In this section, we have considered the case in which the signal and interference are correlated ( $|\rho_{ij}| \neq 0$ ) or coherent ( $|\rho_{ij}| = 1$ ). We utilized a technique called spatial smoothing to reduce the correlation. After constructing a smoothed spectral matrix, we could use any of the beamforming algorithms developed in earlier sections of the chapter. We used MPDR beamformers as examples, but similar results follow for other beamformers.

We used a standard linear array as an example. Similar results hold for planar arrays that exhibit regularity under 2-D shifts.

## 6.13 Broadband Beamformers

### 6.13.1 Introduction

In this section we consider beamformers in which either the signal or the interference do not satisfy the narrowband assumption. The initial model of interest is shown in Figure 6.110(a) and (c). The signals and interferers are bandlimited around the carrier frequency  $\omega_c$  (or  $2\pi f_c$ ), which we refer to as the **center frequency** of the array. The dotted lines denote the spectral boundaries.

As indicated in Figure 6.110(c), the spectrum does not have to be symmetric around  $\omega_c$ . In some applications,  $\omega_c$  corresponds to an actual carrier frequency generated at some place in the environment. In other applications, it is chosen for analysis purposes.

We use a quadrature demodulator at each sensor output so the input to the beamformer is a complex waveform that is bandlimited to  $|\omega| \leq 2\pi B_s/2$ , as shown in Figure 6.110(b) and (d). We process the sensor outputs with a set of linear filters, as shown in Figure 6.111. The notation  $W_{f,n}(\omega)$  denotes the frequency-domain transfer function of the  $n$ th linear filter. The model in Figure 6.111 is the same model that we introduced in Chapter 2. However, in most of our subsequent discussion, we assumed  $\omega = \omega_c$  and suppressed the frequency variable in our discussion. We now reexamine our results for frequencies in the region shown in Figure 6.110(b).

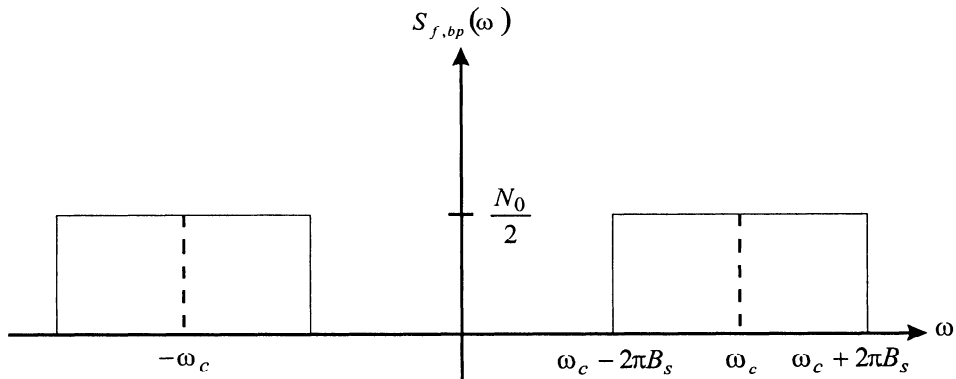
We should observe at this point that we will not actually implement the beamformer as shown in Figure 6.111. We will either use frequency-domain snapshots and operate on discrete frequency bins or we will approximate the  $W_{f,n}(\omega)$  using FIR filters. However, the structure in Figure 6.111 provide a useful reference.

In the next several figures, we illustrate some cases in which a broadband beamformer may be useful. For simplicity, we assume a linear array so that we can represent the spatial dependence in  $u$ -space. We define

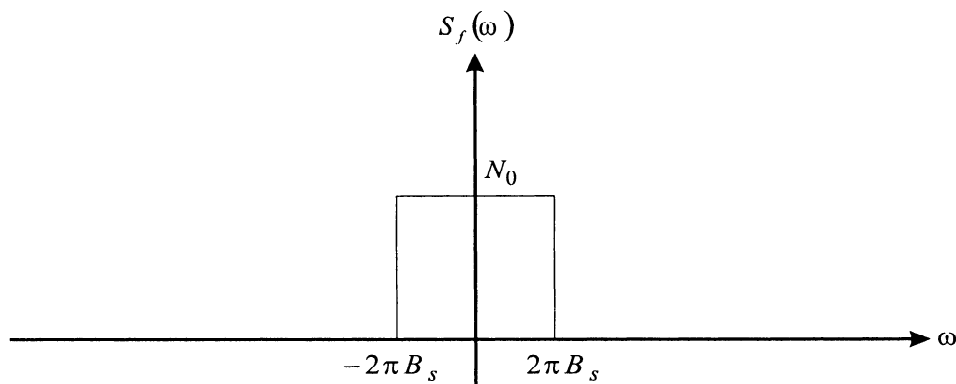
$$f = f_c + f_\Delta \quad (6.667)$$

and represent the frequency dependence in  $f_\Delta$ -space.

In Figure 6.112, we consider the case of a single plane-wave signal whose frequency spectrum is flat over  $\pm B_s/2$ . The interference consists of white noise. From Section 5.5.3, we know that, as  $B_f = B_s/f_c$  increases, the signal will have multiple eigenvalues and we will need a frequency-dependent beamformer to achieve optimum performance. For this simple model, we need to approximate pure delays over the frequency band of interest.



(a)



(b)

In Figure 6.113, we consider the same signal model as in Figure 6.112. The interference consists of a set of plane-wave interferers whose frequency spectra are identical to the signal spectrum. In this case, our processing gain will come from the spatial filtering and a frequency-dependent MVDR or MPDR beamformer will be appropriate.

From (6.14), the MVDR beamformer is

$$\mathbf{W}_{mvdr}^H(\omega) = \frac{\mathbf{v}_{\omega,u}^H(\omega, u_s) \mathbf{S}_n^{-1}(\omega)}{\mathbf{v}_{\omega,u}^H(\omega, u_s) \mathbf{S}_n^{-1}(\omega) \mathbf{v}_{\omega,u}(\omega, u_s)}.$$

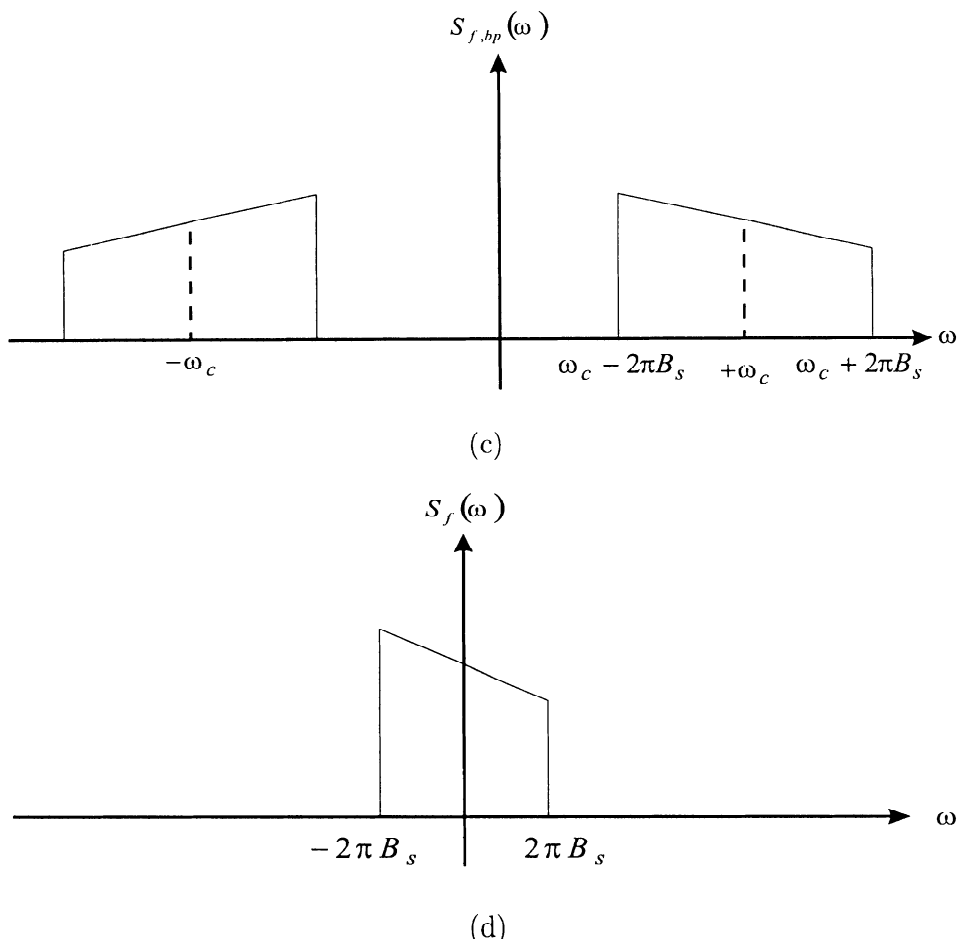


Figure 6.110 Signal spectra: (a) bandpass; (b) complex baseband; (c) bandpass; (d) complex baseband.

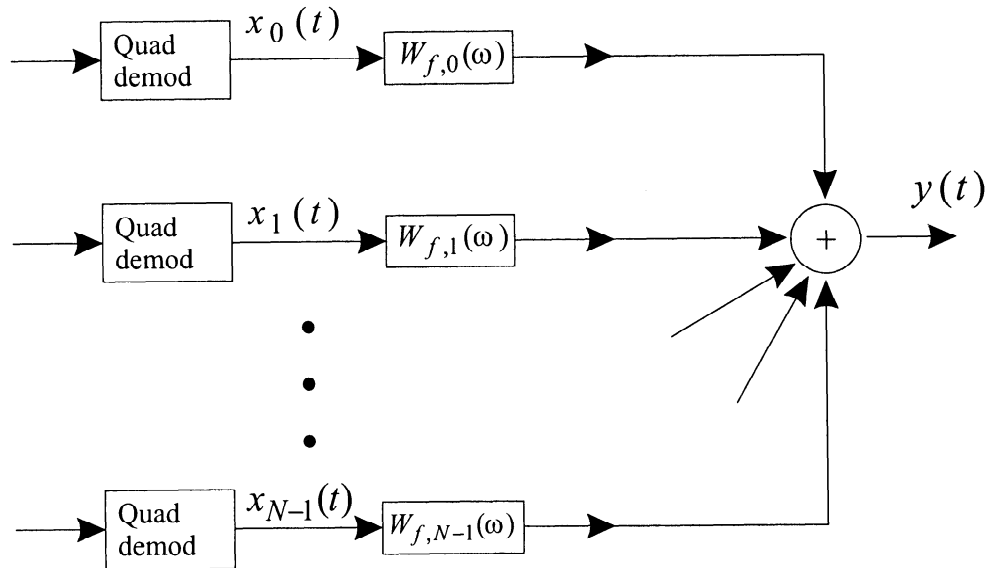
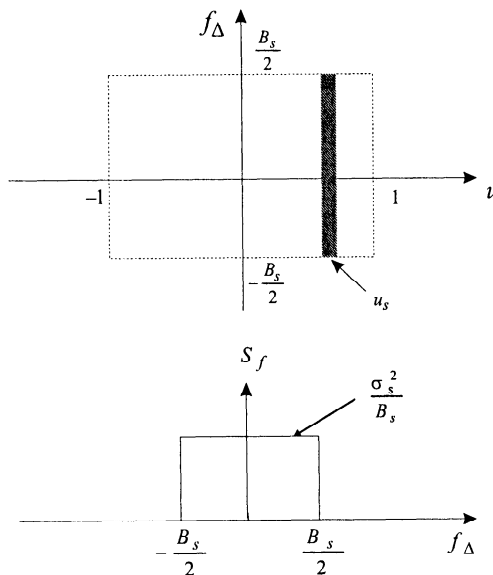


Figure 6.111 Broadband beamformer.

Figure 6.112 Plane-wave signal with flat spectrum located at  $u_s$ .

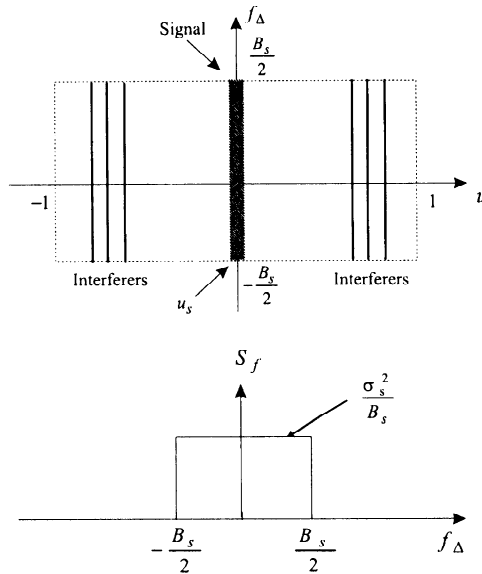


Figure 6.113 Broadband signal and interferers in  $u$ - $f_\Delta$  space.

From (6.71), the MPDR beamformer is

$$\mathbf{W}_{mpdr}^H(\omega) = \frac{\mathbf{v}_{\omega,u}^H(\omega, u_s) \mathbf{S}_x^{-1}(\omega)}{\mathbf{v}_{\omega,u}^H(\omega, u_s) \mathbf{S}_x^{-1}(\omega) \mathbf{v}_{\omega,u}(\omega, u_s)} \triangleq \Lambda_x(\omega) \mathbf{v}_{\omega,u}^H(\omega, u_s) \mathbf{S}_x^{-1}(\omega). \quad (6.668)$$

The array manifold vector is

$$\mathbf{v}_{\omega,k}(\omega, \mathbf{k}) = [ e^{-j\omega\tau_0} \quad e^{-j\omega\tau_1} \quad \dots \quad e^{-j\omega\tau_{N-1}} ]^T, \quad (6.669)$$

where  $\tau_n$  is given by (2.21). We assume the highest frequency of interest is  $\omega_u (= 2\pi f_u)$  and refer to this as the **design frequency** of the array,<sup>18</sup>

$$f_u = f_c + B_s/2. \quad (6.670)$$

The corresponding **design wavelength** is  $\lambda_u$ . For a standard linear array with design frequency  $\omega_u$ ,

$$\tau_n = \frac{-d_n u}{c}, \quad (6.671)$$

---

<sup>18</sup>Note that the subscript “ $u$ ” denotes upper and should not be confused with the directional cosine,  $u = \cos \theta$ .

and

$$d_n = \left(n - \frac{N-1}{2}\right) \frac{\lambda_u}{2}. \quad (6.672)$$

(see (2.53)). Then,

$$\begin{aligned} [\mathbf{v}_{\omega,u}(2\pi f, u)]_n &= \exp \left\{ j2\pi(f_c + f_{\Delta})(n - \frac{N-1}{2}) \frac{u}{2f_u} \right\}, \\ n &= 0, \dots, N-1. \end{aligned} \quad (6.673)$$

Defining

$$b_f = \frac{f_{\Delta}}{f_c}, \quad (6.674)$$

we can write (6.673) as

$$\begin{aligned} [\mathbf{v}_{b_f,u}(b_f, u)]_n &= \exp \left\{ j\pi u(1 + b_f)(n - \frac{N-1}{2}) \frac{f_c}{f_u} \right\}, \\ n &= 0, \dots, N-1. \end{aligned} \quad (6.675)$$

Defining

$$B_f = \frac{B_s}{f_c}, \quad (6.676)$$

(6.675) reduces to

$$\begin{aligned} [\mathbf{v}_{b_f,u}(b_f, u)]_n &= \exp \left\{ j\pi u \left( \frac{1 + b_f}{1 + \frac{B_f}{2}} \right) \left( n - \frac{N-1}{2} \right) \right\}, \\ n &= 0, \dots, N-1. \end{aligned} \quad (6.677)$$

The spectral matrix can also be written in terms of  $b_f$ .

In the cases in Figures 6.112 and 6.113, the broadside beamformer achieves gain through spatial discrimination.

In Figure 6.114, we show a case in which the signal and interferers have different frequency spectra. The desired signal is a plane wave arriving from  $u_s = 0$ . The temporal waveform of the complex envelope is modeled as a complex AR(1) process centered at  $\omega = 0$ . The interfering signal is a plane wave arriving from  $u_s = 0.2$ . The temporal waveform of the complex envelope is modeled as a complex AR(1) process centered at 0.2. In this case, we want to exploit both spatial and frequency filtering, so we use the MMSE beamformer developed in Section 6.2.2.1. From (6.42),

$$\mathbf{W}_{mmse}^H(\omega) = \mathbf{S}_{dx}^H(\omega) \mathbf{S}_x^{-1}(\omega). \quad (6.678)$$

For the plane-wave signal case in which the desired signal and the interference are uncorrelated, (6.43) applies and (6.678) reduces to

$$\mathbf{W}_{mmse}^H(\omega) = S_f(\omega) \mathbf{v}_{\omega, \mathbf{k}}^H(\omega, \mathbf{k}_s) \mathbf{S}_{\mathbf{x}}^{-1}(\omega). \quad (6.679)$$

Using (6.668), we can partition  $\mathbf{W}_{mmse}^H(\omega)$ , as shown in Figure 6.115, although this may not be the best implementation in practice.

The purpose of the rest of Section 6.13 is to develop efficient techniques for implementing the various beamformers:  $\mathbf{W}_{mpdr}^H(\omega)$ ,  $\mathbf{W}_{lcmp}^H(\omega)$ ,  $\mathbf{W}_{mmse}^H(\omega)$ , and  $\mathbf{W}_{lcmp,dl}^H(\omega)$ .

We must develop structures that can be implemented adaptively based on the data inputs. In this chapter, we consider the solution assuming the necessary statistics are known.

In the problems for Section 6.6, we discussed how frequency mismatch (Problem 6.6.11), broadband signals (Problem 6.6.12), and broadband interference (Problem 6.6.13) degrade the performance of a narrowband beamformer. The reader may want to review those problems at this point. In this section, we are concerned with scenarios in which the degradation requires us to implement some form of broadband beamformer.

In Section 6.13.2 we consider a DFT beamformer that obtains the frequency-dependent weighting by taking an FFT and weighting each frequency component separately. This FFT beamformer is the discrete realization of our frequency-domain snapshot model.

In Section 6.13.3, we consider a broadband beamformer that utilizes a tapped delay line or finite impulse response (FIR) filter at the output of each sensor to achieve a frequency-dependent weighting.

In Section 6.13.4, we summarize our results.

### 6.13.2 DFT Beamformers

In this section, we develop the DFT implementation of a frequency-domain beamformer. Because we have used a frequency-domain snapshot model in our earlier discussion, the structure of the frequency-domain beamformer follows easily from Figure 6.111. We take the finite-time Fourier transform of  $\mathbf{x}(t)$  over the time interval  $(k-1)\Delta T \leq t < k\Delta T$  at a set of frequencies  $\omega_m$  that are separated by  $\omega_\Delta = 2\pi/\Delta T$ . We assume that  $\Delta T$  is large enough that the snapshots are statistically independent. We then implement the narrowband beamformers at each of the  $M$  frequencies.

In practice, we implement the frequency-domain beamformer by sampling  $\mathbf{x}(t)$  every  $1/B_s$  seconds and obtain  $M$  samples. We then perform a

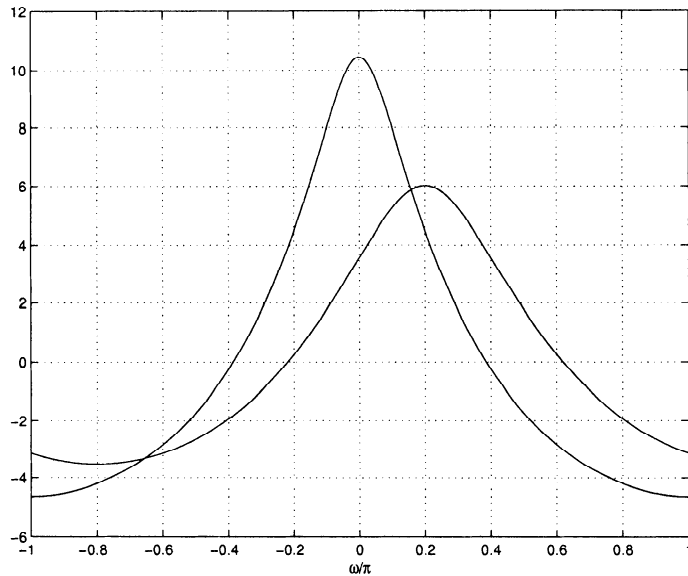


Figure 6.114 Broadband signal and interferers in  $u - f_D$  space; different frequency spectra.

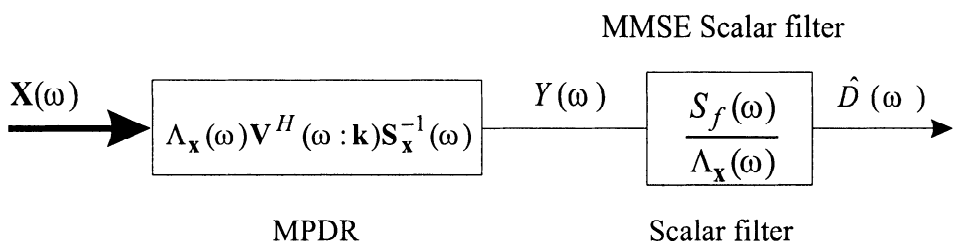


Figure 6.115 Partitioned MMSE beamformer.

DFT to obtain  $M$  frequency samples. We accomplish the DFT operation with a FFT. The concept is straightforward, but there is a fair amount of detail that must be developed to do the implementation. The bulk of this section is devoted to developing some of the necessary detail.

Frequency-domain beamformers have been discussed in a number of references. Most of these references focus on the adaptive behavior.

We assume that the signals of interest are bandlimited, as shown in Figure 6.110. The signal is a bandpass signal and the first step in the processing is to perform the quadrature demodulation to obtain a complex low-pass signal that is bandlimited to  $|f| \leq B_s/2$ . We divide our discussion into several steps.

**Step 1: Generation of frequency-domain vectors:** An array with DFT processing is shown in Figure 6.116. The output of each sensor is passed through a quadrature demodulator and is sampled every  $T_s$  seconds where

$$T_s = \frac{1}{B_s}. \quad (6.680)$$

We buffer  $M$  samples and take the DFT of the  $M$  samples. For the present discussion, we assume  $M$  is chosen to be a power of 2. The total observation interval on each snapshot is

$$\Delta T = M T_s. \quad (6.681)$$

We discuss the case in which we have to add zeros to the actual samples to obtain a power of 2 later. There are other reasons for zero padding.

The output of the DFT is a set of  $M$  frequency values (or bins) that are separated in frequency by  $1/M T_s$ . Thus, the frequency resolution is

$$\Delta f = 1/M T_s = B_s/M. \quad (6.682)$$

Many algorithms require high-frequency resolution, so  $M$  may be a large number.

In the  $m$ th frequency bin there is an  $N \times 1$  complex vector,  $\mathbf{X}\{m\}$ ,  $m = 0, \dots, M-1$ .

$$\begin{aligned} \mathbf{X}\{m\} &\triangleq [ X_0\{m\} \quad X_1\{m\} \quad \dots \quad X_{N-1}\{m\} ]^T, \\ m &= 0, \dots, M-1. \end{aligned} \quad (6.683)$$

The argument  $m$  represents the number of the bin. We will relate it to the corresponding frequency shortly. Recall that the continuous Fourier transform at frequency  $\omega_m$  is denoted  $\mathbf{X}_{\Delta T}(\omega_m)$  for a finite-time interval.

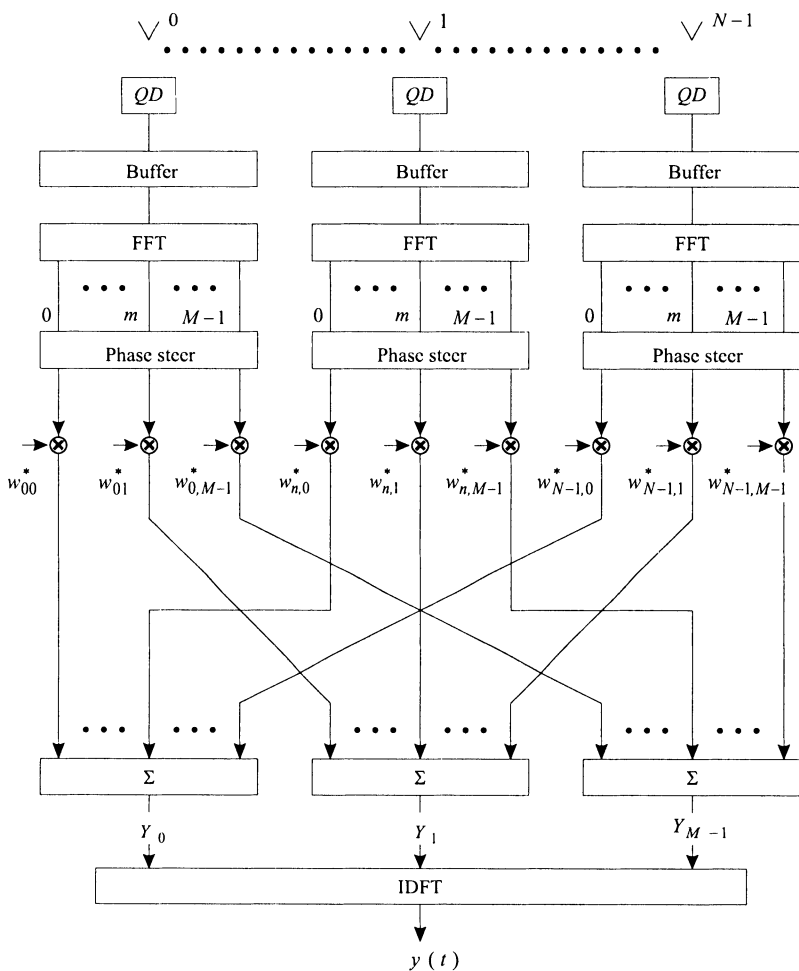


Figure 6.116 FFT processing.

We use  $\mathbf{X}\{m\}$  to denote the DFT in the  $m$ th bin. Using a different shape of the brackets is an abuse of notation but should not cause confusion due to the context.

Normally, we process each frequency bin independently using one of the narrowband algorithms we have developed in this chapter.<sup>19</sup> The result is a set of complex scalars,

$$Y\{m\} = \mathbf{w}^H\{m\} \mathbf{X}\{m\}, \quad m = 0, \dots, M-1. \quad (6.684)$$

The final step is to take an IDFT to obtain  $M$  output samples in the time domain. We refer to this procedure as **block processing**.

We next develop the equations for the DFT beamformer with block processing. There is direct correspondence with the discussion of DFT in Section 3.3.3.

We denote the time of the most recent sample as  $t_0$ . The current sample from the  $n$ th sensor is  $x_n(t_0)$ . The previous sample is  $x_n(t_0 - T_s)$ . We introduce the notation

$$x_n(t_0) = x_n(0), \quad (6.685)$$

$$x_n(t_0 - T_s) = x_n(1), \quad (6.686)$$

$$x_n(t_0 - (M-1)T_s) = x_n(M-1). \quad (6.687)$$

The subscript “ $n$ ” denotes the sensor whose output is being sampled. The argument specifies the sample.

We define a complex vector,  $\tilde{\mathbf{x}}_n$ , consisting of the time samples. To be consistent with conventional DFT notation, we reorder the time samples so that the most recent sample is at the bottom of the vector,

$$\tilde{\mathbf{x}}_n \triangleq \begin{bmatrix} x_n(t_0 - (M-1)T_s) \\ \vdots \\ x_n(t_0) \end{bmatrix} = \begin{bmatrix} x_n(M-1) \\ x_n(M-2) \\ \vdots \\ x_n(0) \end{bmatrix}, \quad n = 0, \dots, N-1. \quad (6.688)$$

This is a vector of the time samples. We use a superscript “ $\sim$ ” to distinguish it from the vector down the array.

The DFT of  $\tilde{\mathbf{x}}_n$  is

$$X_n\{m\} = \sum_{k=0}^{M-1} x_n(M-1-k) (e^{-j \frac{2\pi}{M}})^{km}$$

---

<sup>19</sup>We discuss whether this technique is optimum later in this section.

$$= \sum_{k=0}^{M-1} x_n(M-1-k) (F_M)^{km}, \quad m = 0, 1, \dots, M-1, \quad (6.689)$$

where

$$F_M \triangleq e^{-j\frac{2\pi}{M}}. \quad (6.690)$$

In matrix notation,

$$\tilde{\mathbf{X}}_n = \mathbf{F}_M \tilde{\mathbf{x}}_n, \quad (6.691)$$

where

$$[\mathbf{F}_M]_{kl} = (F_M)^{kl} = \left(e^{-j\frac{2\pi}{M}}\right)^{kl}. \quad (6.692)$$

The vector  $\tilde{\mathbf{X}}_n$  corresponds to the  $M$  frequency components at the output of sensor  $n$ ,

$$\tilde{\mathbf{X}}_n \triangleq [ X_n\{0\} \quad \dots \quad X_n\{m\} \quad \dots \quad X_n\{M-1\} ]^T. \quad (6.693)$$

Recall that the frequency samples are arranged in the following order,<sup>20</sup>

$m$	$f$
0	0
1	$\Delta f$
$\vdots$	
$\frac{M}{2}-1$	$(\frac{M}{2}-1)\Delta f$
$\frac{M}{2}$	$\frac{M}{2}\Delta f = -\frac{M}{2}\Delta f$
$\frac{M}{2}+1$	$(\frac{M}{2}+1)\Delta f = (-\frac{M}{2}+1)\Delta f$
$\vdots$	
$M-1$	$(M-1)\Delta f = -\Delta f$

The weight vector is constructed in a similar manner. We define

$$\tilde{\mathbf{w}}_n \triangleq \begin{bmatrix} w_{n,M-1} \\ w_{n,M-2} \\ \vdots \\ w_{n,0} \end{bmatrix}. \quad (6.694)$$

Then, proceeding as in (6.690)–(6.693),

$$\tilde{\mathbf{W}}_n = \mathbf{F}_M \tilde{\mathbf{w}}_n, \quad (6.695)$$

---

<sup>20</sup>For example, [OS89].

where

$$\widetilde{\mathbf{W}}_n = \begin{bmatrix} W_n\{0\} & W_n\{1\} & \cdots & W_n\{M-1\} \end{bmatrix}^T. \quad (6.696)$$

In each frequency bin we construct a vector down the array

$$\mathbf{X}\{m\} \triangleq \begin{bmatrix} X_0\{m\} & X_1\{m\} & \cdots & X_{N-1}\{m\} \end{bmatrix}^T, \quad m = 0, \dots, M-1. \quad (6.697)$$

This vector consists of the frequency components of the array in frequency bin  $m$ . We process each of these vectors with a **narrowband beamforming** algorithm to obtain a set of  $M$  scalar outputs

$$Y\{m\} = \mathbf{w}^H\{m\} \mathbf{X}\{m\}, \quad m = 0, \dots, M-1. \quad (6.698)$$

We define the vector across frequencies as

$$\widetilde{\mathbf{Y}} = \begin{bmatrix} Y\{0\} & Y\{1\} & \cdots & Y\{M-1\} \end{bmatrix}^T. \quad (6.699)$$

We take inverse DFT (IDFT) to obtain  $M$  output time samples,

$$y(M-1-k) = \frac{1}{M} \sum_{m=0}^{M-1} Y\{m\} \left(e^{j\frac{2\pi}{M}}\right)^{km}, \quad k = 0, \dots, M-1. \quad (6.700)$$

In matrix form,

$$\tilde{\mathbf{y}} = \mathbf{F}_M^{-1} \widetilde{\mathbf{Y}} = \frac{1}{M} \mathbf{F}_M^H \widetilde{\mathbf{Y}}, \quad (6.701)$$

where

$$\begin{aligned} \tilde{\mathbf{y}} &\triangleq \begin{bmatrix} y(M-1) & y(M-2) & \cdots & y(0) \end{bmatrix}^T \\ &= \begin{bmatrix} y(t_0 - (M-1)T_s) & \cdots & y(t_0) \end{bmatrix}^T. \end{aligned} \quad (6.702)$$

By using the weighting techniques in (6.698) we are treating each frequency component independently. Most DFT beamformers used in practice are implemented in this manner.

We can also use a **sliding window technique**, in which the DFT is computed each time a new sample enters the buffer. In this case, we write (6.701) as

$$y(M-1-k) = \frac{1}{M} \sum_{m=0}^{M-1} Y\{m\} \left(e^{j\frac{2\pi}{M}}\right)^{km}, \quad k = 0, \dots, M-1, \quad (6.703)$$

and observe that the first sample is

$$y(t_0 - (M-1)T_s) = \frac{1}{M} \sum_{m=0}^{M-1} Y\{m\}, \quad (6.704)$$

so that the output is obtained by summing the frequency samples. The result in (6.704) corresponds to the IDFT at  $t = t_0 - (M-1)T_s$ . We avoid doing the entire IDFT because we only want a single time sample.

If we want to consider more general processing, we would define a composite  $NM \times 1$  data vector

$$\tilde{\mathbf{X}} \triangleq \begin{bmatrix} \tilde{\mathbf{X}}\{0\} \\ \tilde{\mathbf{X}}\{1\} \\ \vdots \\ \tilde{\mathbf{X}}\{M-1\} \end{bmatrix}, \quad (6.705)$$

and a composite weight vector,

$$\tilde{\mathbf{W}} \triangleq \begin{bmatrix} \tilde{\mathbf{W}}\{0\} \\ \tilde{\mathbf{W}}\{1\} \\ \vdots \\ \tilde{\mathbf{W}}\{M-1\} \end{bmatrix}. \quad (6.706)$$

Then

$$Y = \tilde{\mathbf{W}}^H \tilde{\mathbf{X}}. \quad (6.707)$$

The model in (6.705)–(6.707) allows us to use a wider class of constraints on the frequency domain beamformers.<sup>21</sup> For the present, we utilize independent narrowband beamformers in each frequency bin and sum the output using (6.704) to obtain the output.

**Step 2: Array manifold vectors:** In order to construct the weighting for the  $m$ th frequency bin, we need the steering vector and the spatial spectral matrix.

The array manifold vector as a function of frequency is

$$\mathbf{v}_\omega = [ e^{-j2\pi f \tau_0} \ e^{-j2\pi f \tau_1} \ \dots \ e^{-j2\pi f \tau_{N-1}} ]^T,$$

---

<sup>21</sup>The more general processing in (6.705)–(6.707) is not used in any actual systems that we are aware of.

where  $\tau_n$  is the delay to the  $n$ th sensor relative to the origin of coordinates. The subscript “ $\omega$ ” denotes that we retain the frequency dependence explicitly.

The frequency at the  $m$ th frequency bin is

$$f_m = \begin{cases} f_c + m\Delta f & m = 0, \dots, \frac{M}{2} - 1, \\ f_c + (m - M)\Delta f & m = \frac{M}{2}, \dots, M - 1, \end{cases} \quad (6.708)$$

where

$$\Delta f = \frac{1}{MT_s} = \frac{B_s}{M}. \quad (6.709)$$

For simplicity, we consider a standard linear array. Then

$$\tau_n = -\frac{d_n u}{c}, \quad (6.710)$$

and

$$d_n = (n - \frac{N-1}{2})d = (n - \frac{N-1}{2})\frac{\lambda_u}{2}, \quad n = 0, \dots, N-1, \quad (6.711)$$

where  $\lambda_u$  is the wavelength corresponding to the highest (upper) frequency.

Using (6.708), (6.710), and (6.711) in (6.705) gives an expression for  $n$ th element of the array manifold vector for the  $m$ th frequency bin,

$$[\mathbf{v}_m(u)]_n = \begin{cases} \exp \left\{ j2\pi(f_c + m\Delta f)(n - \frac{N-1}{2})\frac{\lambda_u u}{2c} \right\}, \\ \quad m = 0, \dots, \frac{M}{2} - 1, \quad n = 0, \dots, N-1, \\ \exp \left\{ j2\pi(f_c + (m - M)\Delta f)(n - \frac{N-1}{2})\frac{\lambda_u u}{2c} \right\}, \\ \quad m = \frac{M}{2}, \dots, M-1, \quad n = 0, \dots, N-1. \end{cases} \quad (6.712)$$

Using

$$f_c = \frac{c}{\lambda_c}, \quad (6.713)$$

and

$$B_f = \frac{B_s}{f_c}, \quad (6.714)$$

we have

$$[\mathbf{v}_m(u)]_n = \begin{cases} \exp \left\{ j\pi u \frac{1}{1+\frac{B_f}{2}} \left[ (n - \frac{N-1}{2}) + (\frac{m}{M})(n - \frac{N-1}{2})B_f \right] \right\}, \\ \quad m = 0, \dots, \frac{M}{2} - 1, \quad n = 0, \dots, N-1. \\ \exp \left\{ j\pi u \frac{1}{1+\frac{B_f}{2}} \left[ (n - \frac{N-1}{2}) + (\frac{m}{M} - 1)(n - \frac{N-1}{2})B_f \right] \right\}, \\ \quad m = \frac{M}{2}, \dots, M-1, \quad n = 0, \dots, N-1. \end{cases}$$

(6.715)

as the desired result. The first term in the exponent is the familiar narrow-band result and the second term models the broadband effect.

**Step 3: Spatial spectral matrix:** The next step is to compute the spatial spectral matrix in frequency bin  $m$ . We use a derivation similar to that given in Godard [God95]. The spectral spatial matrix in the  $m$ th bin is

$$\mathbf{S}_X\{m\} \triangleq E \left[ \mathbf{X}\{m\} \mathbf{X}^H\{m\} \right]. \quad (6.716)$$

We use the brace to distinguish this matrix from the usual (continuous in  $\omega$ ) spectral matrix  $\mathbf{S}_X(\omega)$ .

The  $np$ -element of this matrix is

$$[\mathbf{S}_X\{m\}]_{np} = E \left[ X_n\{m\} X_p^*\{m\} \right]. \quad (6.717)$$

From the DFT relationship,

$$X_n\{m\} = \sum_{k=0}^{M-1} x_n(M-1-k) \left( e^{-j\frac{2\pi}{M}} \right)^{km}, \quad (6.718)$$

where  $x_n(k)$  is the time sample from the  $k$ th tap of the  $n$ th sensor. Using (6.718) in (6.717) gives

$$[\mathbf{S}_X\{m\}]_{np} = E \left\{ \sum_{k=0}^{M-1} x_n(M-1-k) \left( e^{-j\frac{2\pi}{M}} \right)^{km} \sum_{q=0}^{M-1} x_p^*(M-1-q) \left( e^{j\frac{2\pi}{M}} \right)^{qm} \right\}. \quad (6.719)$$

Now recall from (6.688) that

$$\tilde{\mathbf{x}}_n = \begin{bmatrix} x_n(M-1) & \cdots & x_n(1) & x_n(0) \end{bmatrix}^T. \quad (6.720)$$

We also define a vector corresponding to the  $k$ th row of the DFT matrix,

$$\mathbf{e}(m) = \begin{bmatrix} 1 \\ e^{(j\frac{2\pi}{M})m} \\ \vdots \\ e^{(j\frac{2\pi}{M})km} \\ \vdots \\ e^{(j\frac{2\pi}{M})(M-1)m} \end{bmatrix}, \quad m = 0, \dots, M-1. \quad (6.721)$$

Then, (6.719) can be written as

$$\begin{aligned} [\mathbf{S}_x\{m\}]_{np} &= \mathbf{e}^H(m) E\left[\tilde{\mathbf{x}}_n \tilde{\mathbf{x}}_p^H\right] \mathbf{e}(m) \\ &= \mathbf{e}^H(m) \left\{ [\mathbf{R}_x]_{np} \right\} \mathbf{e}(m), \end{aligned} \quad (6.722)$$

where  $[\mathbf{R}_x]_{np}$  is the temporal correlation between the tap vector at sensor  $n$  and the tap vector at sensor  $p$ .

The next step is to derive an expression for  $[\mathbf{R}_x]_{np}$ . The correlation function matrix of the complex baseband vector  $\mathbf{x}(t)$  can be written as

$$\mathbf{R}_{\mathbf{x}(t)}(\tau) = \int_{-\infty}^{\infty} \mathbf{S}_x(2\pi f_\Delta) e^{j2\pi f_\Delta \tau} df_\Delta, \quad (6.723)$$

where  $\mathbf{S}_x(2\pi f)$  is the spectral matrix of the complex baseband vector waveform

$$\mathbf{S}_x(2\pi f_\Delta) = 2 [\mathbf{S}_{x,bp}(2\pi f_\Delta + 2\pi f_c)]_{LP}. \quad (6.724)$$

Then

$$\mathbf{x}_k(t) = \mathbf{x}(t - (M - 1 - k)T_s) \quad (6.725)$$

and

$$\mathbf{x}_q^*(t) = \mathbf{x}^*(t - (M - 1 - q)T_s). \quad (6.726)$$

The correlation matrix is,

$$[\mathbf{R}_x]_{kq} = \mathbf{R}_{\mathbf{x}(t)}((k - q)T_s). \quad (6.727)$$

Using (6.723),

$$[\mathbf{R}_x]_{kq} = \int_{-\infty}^{\infty} \mathbf{S}_x(2\pi f_\Delta) e^{j2\pi f_\Delta [(k-q)T_s]} df_\Delta. \quad (6.728)$$

Now define

$$\mathbf{e}(f_\Delta) = \left[ 1 \quad e^{j2\pi f_\Delta T_s} \quad \dots \quad e^{j2\pi f_\Delta T_s q} \quad \dots \quad e^{j2\pi f_\Delta T_s(M-1)} \right]^T. \quad (6.729)$$

Using (6.729), we can write (6.728) in matrix form as

$$[\mathbf{R}_x] = \int_{-\infty}^{\infty} \mathbf{S}_x(2\pi f_\Delta) \mathbf{e}(f_\Delta) \mathbf{e}^H(f_\Delta) df_\Delta. \quad (6.730)$$

Using (6.730) in (6.722) gives

$$[\mathbf{S}_x\{m\}]_{np} = \int_{-\infty}^{\infty} \mathbf{S}_x(2\pi f_\Delta) \mathbf{e}^H\{m\} \mathbf{e}(f_\Delta) \mathbf{e}^H(f_\Delta) \mathbf{e}\{m\} df_\Delta. \quad (6.731)$$

Now define

$$a(f_\Delta, m) \triangleq \left| \mathbf{e}^H(f_\Delta) \mathbf{e}\{m\} \right|^2. \quad (6.732)$$

Using (6.732) in (6.731) gives

$$\mathbf{S}_X\{m\} = \int_{-\infty}^{\infty} \mathbf{S}_X(2\pi f_\Delta) a(f_\Delta, m) df_\Delta. \quad (6.733)$$

Then,

$$\begin{aligned} \mathbf{e}^H(f_\Delta) \mathbf{e}\{m\} &= \sum_{q=0}^{M-1} e^{-j2\pi(f_\Delta T_s - \frac{m}{M})q} \\ &= e^{-j\pi(M-1)(f_\Delta T_s - \frac{m}{M})} \frac{\sin \pi(f_\Delta T_s M - m)}{\sin \frac{\pi}{M}(f_\Delta T_s M - m)}, \end{aligned} \quad (6.734)$$

or

$$\begin{aligned} a(f_\Delta, m) &= \frac{\sin^2(\pi(f_\Delta T_s M - m))}{\sin^2(\frac{\pi}{M}(f_\Delta T_s M - m))} = \frac{\sin^2(\pi(\frac{f_\Delta}{B_s} M - m))}{\sin^2(\frac{\pi}{M}(\frac{f_\Delta}{B_s} M - m))} \\ &= \frac{\sin^2(\frac{\pi M}{B_s}(f_\Delta - m\Delta f))}{\sin^2(\frac{\pi}{B_s}(f_\Delta - m\Delta f))}, \end{aligned} \quad (6.735)$$

where

$$B_s = T_s^{-1} \quad (6.736)$$

is the sampling frequency. The function  $a(f_\Delta, m)$  provides a window on  $\mathbf{S}_X(2\pi f_\Delta)$  and reflects how power at frequencies unequal to  $f_m$  (the frequency of the  $m$ th bin) affects  $\mathbf{S}_X\{m\}$ . A normalized plot of  $a(f_\Delta, m)$  with  $m = 0$  for  $M = 16$  and  $M = 64$  is shown in Figure 6.117. The normalization constant is  $M^2$ .

For  $m = 0$ , the first zeros are at

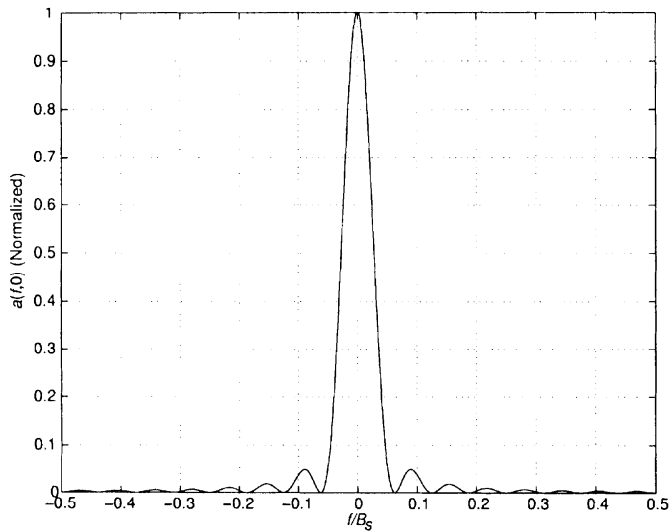
$$\frac{f_\Delta}{B_s} = \pm \frac{1}{M}. \quad (6.737)$$

The bin spacing is

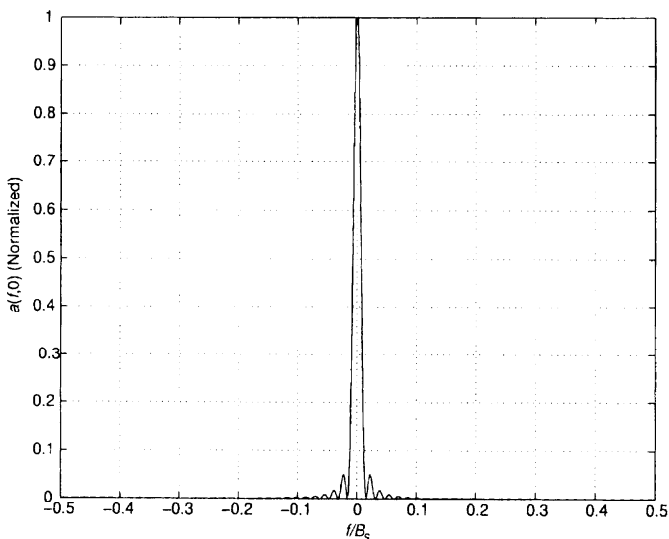
$$\frac{\Delta f}{B_s} = \frac{1}{M}. \quad (6.738)$$

If  $\mathbf{S}_x(2\pi f)$  is essentially constant over the interval,

$$-\frac{1}{2M} \leq \frac{f_\Delta}{B_s} \leq \frac{1}{2M}, \quad (6.739)$$



(a)



(b)

Figure 6.117 Normalized  $a(f, k)$  versus  $f/B_s$ : (a) $K = 16$ ; (b) $K = 64$ .

then

$$\mathbf{S}_X\{m\} \simeq M^2 \mathbf{S}_x(2\pi f_\Delta), \quad (6.740)$$

where the  $\Delta f$ -to- $m$  correspondence is given in the table following (6.693) or through the relation in (6.708).

For the special case in which the signal or interference component of  $\mathbf{x}(t)$  consists of plane waves, the corresponding spectral matrix is

$$[\mathbf{S}_X(2\pi f_\Delta)]_{np} = \mathbf{S}_f(2\pi f_\Delta) e^{j2\pi f_\Delta(\tau_p - \tau_n)}, \quad (6.741)$$

or

$$\mathbf{S}_X(2\pi f_\Delta) = \mathbf{S}_f(2\pi f_\Delta) \mathbf{v}_m(u_s) \mathbf{v}_m^H(u_s), \quad (6.742)$$

where  $\mathbf{S}_f(2\pi f_\Delta)$  is the spectrum of the complex baseband signal,  $u_s$  is the signal direction in  $u$ -space, and  $\mathbf{v}_m(u)$  is defined in (6.715) (with  $m$  and  $\Delta f$  correctly matched).

For the case of a single signal and multiple plane-wave interferers with independent white noise, the spatial spectral matrix in the  $m$ th bin is,

$$\begin{aligned} \mathbf{S}_X\{m\} &= \int_{-\infty}^{\infty} a(f_\Delta, m) [S_f(2\pi f_\Delta) \mathbf{v}_m(u_s) \mathbf{v}_m^H(u_s) \\ &\quad + \sum_{i=1}^J S_{f_i}(2\pi f_\Delta) \mathbf{v}_m(u_i) \mathbf{v}_m^H(u_i) + S_w(2\pi f_\Delta) \mathbf{I}] df_\Delta, \end{aligned} \quad (6.743)$$

where  $S_w(2\pi f_\Delta)$  has a flat spectrum over  $(-B_s/2, B_s/2)$ ,

**Step 4: Narrowband processing:** We now process each of the  $m$  frequency bins under the assumption that  $\mathbf{X}\{m_i\}$  is independent of  $\mathbf{X}\{m_j\}$ ,  $m_i \neq m_j$  (recall the discussion in Section 5.2.1).

To find  $\mathbf{W}_0\{m\}$ , we use (6.715) and (6.733) in one of the  $\mathbf{w}_0$  equations defined earlier. For example, the MPDR beamformer for the  $m$ th frequency bin is

$$\mathbf{W}_{mpdr}^H\{m\} = \frac{\mathbf{v}_m^H(u_s) \mathbf{S}_X^{-1}\{m\}}{\mathbf{v}_m^H(u_s) \mathbf{S}_X^{-1}\{m\} \mathbf{v}_m(u_s)}, \quad m = 0, \dots, M-1. \quad (6.744)$$

If the desired signal arrives from broadside or if the array has been presteered to point at the signal, then

$$\mathbf{W}_{mpdr}^H\{m\} = \frac{\mathbf{1}^T \mathbf{S}_X^{-1}\{m\}}{\mathbf{1}^T \mathbf{S}_X^{-1}\{m\} \mathbf{1}}, \quad m = 0, \dots, M-1. \quad (6.745)$$

The LCMP beamformer follows from (6.358) as

$$\mathbf{W}_{lcm}^H\{m\} = \mathbf{g}_m^H \left[ \mathbf{C}_m^H \mathbf{S}_{\mathbf{X}}^{-1}\{m\} \mathbf{C}_m \right]^{-1} \mathbf{C}_m^H \mathbf{S}_{\mathbf{X}}^{-1}\{m\}, \quad (6.746)$$

corresponding to the constraint equation,

$$\mathbf{W}^H\{m\} \mathbf{C}_m = \mathbf{g}_m^H.$$

To evaluate the output  $SNR_0$  or the array gain, we have

$$P_o = E [|y(t_0)|^2] = E [|y(0)|^2]. \quad (6.747)$$

Substituting (6.704) into (6.719) gives

$$P_o = \frac{1}{M^2} E \left[ \sum_{m=0}^{M-1} Y\{m\} \sum_{l=0}^{M-1} Y^*\{l\} \right]. \quad (6.748)$$

If we assume the  $Y\{m\}$  are uncorrelated, this reduces to

$$P_o = \frac{1}{M^2} E \left[ \sum_{m=0}^{M-1} |Y\{m\}|^2 \right]. \quad (6.749)$$

The signal component output of the  $m$ th bin is,

$$Y\{m\} = \mathbf{W}_0^H\{m\} \mathbf{F}\{m\}, \quad (6.750)$$

where  $\mathbf{F}\{m\}$  is the DFT of the signal in the  $m$ th bin. Using (6.750) in (6.749) gives

$$P_{so} = \frac{1}{M^2} \sum_{m=0}^{M-1} \mathbf{W}_0^H\{m\} \mathbf{S}_f\{m\} \mathbf{W}_0\{m\}, \quad (6.751)$$

where  $\mathbf{S}_f\{m\}$  is given by the first term on the right side of (6.743).

If each weight vector contains a distortionless constraint, then

$$P_{so} = \sigma_s^2. \quad (6.752)$$

Similarly, the output due to interference and noise is

$$P_{in,o} = \frac{1}{M^2} \sum_{m=0}^{M-1} \mathbf{W}_0^H\{m\} \mathbf{S}_n\{m\} \mathbf{W}_0\{m\}, \quad (6.753)$$

where  $\mathbf{S}_n\{m\}$  is given by the second and third term on the right side of (6.743).

Thus, the  $SNR_0$  is

$$SNR_0 = \frac{P_o}{P_{in,o}} \quad (6.754)$$

and the array gain is

$$A_0 = \frac{\sigma_n^2 P_o}{\sigma_s^2 P_{in,o}}. \quad (6.755)$$

This completes our derivation. We now consider several examples.

#### Example 6.13.1

Consider a 10-element uniform linear array with element spacing equal to  $\lambda_u/2$ . The desired signal is a plane-wave signal arriving from  $u_s$  with fractional bandwidth  $B_f$ . The signal spectrum is flat, as shown in Figure 6.112, with total power  $\sigma_s^2$ . The interference is white noise. We use a conventional beamformer in each frequency bin. For white noise, the conventional beamformer is also the MPDR beamformer. The array gain would be 10 if the signal were narrowband or if the signal arrived from broadside.

In Figure 6.118, we plot the array gain versus  $u_s/BW_{NN}$  for  $M = 1, 2, 4, 8$ , and 16. In part (a), we consider  $B_f = 0.2$ . In part (b), we consider  $B_f = 0.4$ . In part (c), we consider  $B_f = 0.6$ . In part (d), we consider  $B_f = 0.8$ .

We see that, by increasing the number of frequency bins, we can approach the same performance as in the narrowband case.

#### Example 6.13.2

Consider a 10-element uniform linear array with element spacing equal to  $\lambda_u/2$ . The desired signal arrives from broadside. It has a flat spectrum with bandwidth  $B_s$  and fractional bandwidth  $B_f$ . A single interfering plane-wave signal with the same spectrum arrives from  $u_I$ . The  $SNR$  is 0 dB and the  $INR$  is 30 dB. We use an MPDR beamformer in each frequency bin.

In Figure 6.119, we plot the array gain versus  $u_I/BW_{NN}$  for  $M = 1, 2, 4, 8$ , and 16. In part (a), we consider  $B_f = 0.4$ . In part (b), we consider  $B_f = 0.8$ .

We see that there is marginal improvement with increasing  $M$ . However, this example is misleading because the array processor is not stressed by the single interferer and uses its temporal degrees of freedom to suppress the interferer. In the next example we consider a more complicated environment.

#### Example 6.13.3

Consider the same model as in Example 6.13.1, except we assume that there are  $N - 1$  uncorrelated plane-wave interferers.  $N - 2$  narrowband interferers are fixed in orthogonal locations in  $u$ -space,

$$u_i = \pm 0.3, \pm 0.5, \pm 0.7, \pm 0.9 \quad i = 1, \dots, 4. \quad (6.756)$$

The broadband interferer arrives from  $u_I$  and we vary  $u_I$  from  $-1 \leq u_I \leq 1$ . Each interferer has a 30 dB  $INR$ .

In Figure 6.120, we plot the array gain versus  $u_I/BW_{NN}$  for  $M = 1, 2, 4, 8$ , and 16. In part (a), we consider  $B_f = 0.4$ . In part (b), we consider  $B_f = 0.8$ .

If we compare Figure 6.119(a) with Figure 6.120(a), we see that the array gain is larger with multiple interferers. The reason is that the total input of the interferers is larger by 9 dB and the beamformer can place significant nulls of the eight narrowband interferers

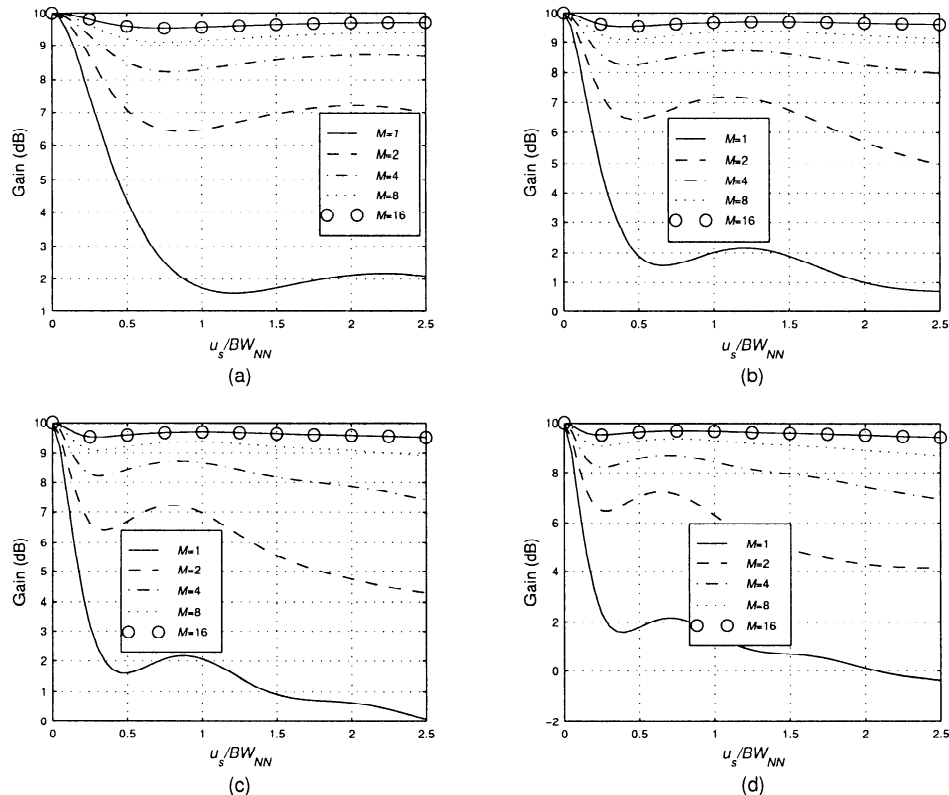


Figure 6.118 MPDR beamformer; array gain versus  $u_s/BW_{NN}$ , broadband signal in white noise,  $M = 1, 2, 4, 8$ , and 16; (a)  $B_f = 0.2$ , (b)  $B_f = 0.4$ , (c)  $B_f = 0.6$ , (d)  $B_f = 0.8$ .

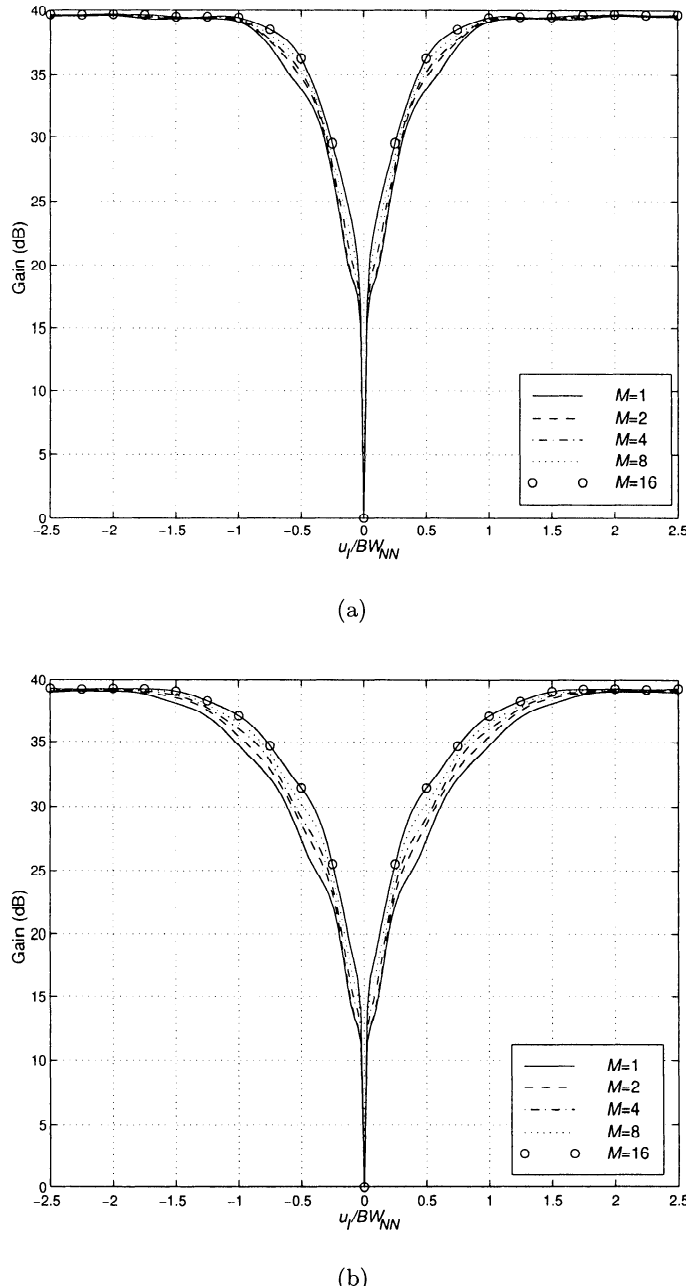
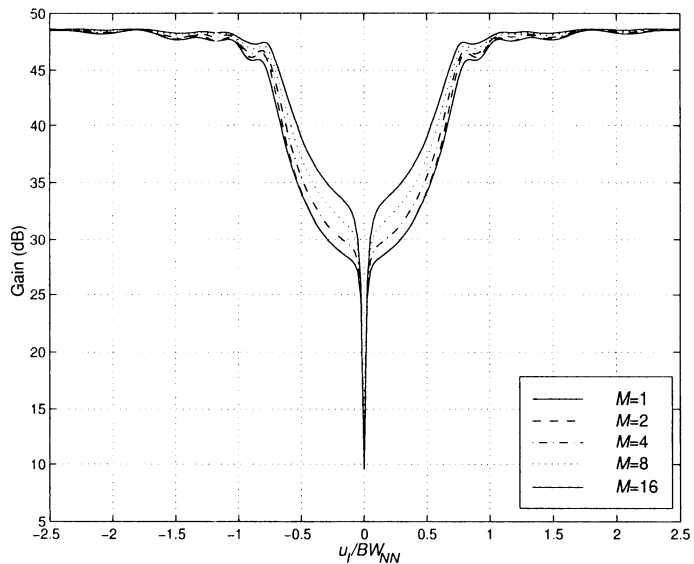
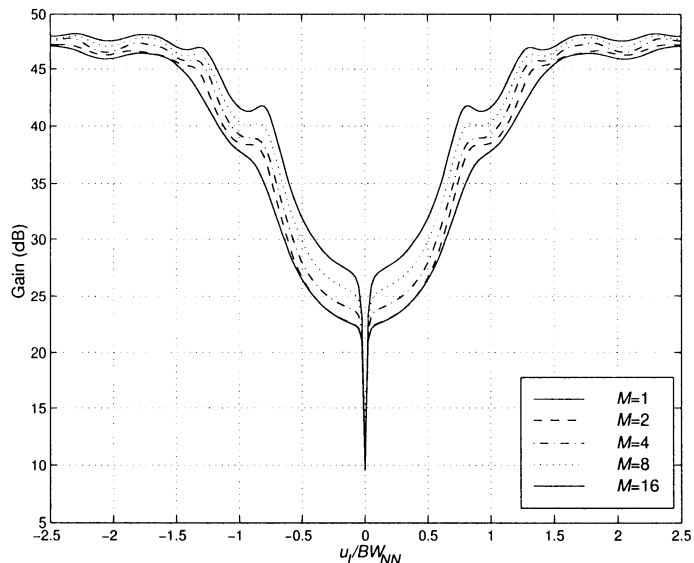


Figure 6.119 Array gain versus  $u_I/BW_{NN}$ : broadband signal in white noise;  $N = 10$ ,  $SNR = 0$  dB,  $INR = 30$  dB,  $M = 1, 2, 4, 8$ , and  $16$ : (a) $B_f = 0.4$ ; (b) $B_f = 0.8$ .



(a)



(b)

Figure 6.120 Array gain versus  $u_I/BW_{NN}$ ; broadband signal in white noise:  
 (a)  $B_f = 0.4$ ; (b)  $B_f = 0.8$ .

that are in the sidelobe region. However, this leaves only one degree of freedom to null the broadband interferer. We see that increasing  $M$  causes a larger performance improvement than in Example 6.13.2.

In Examples 6.3.2 and 6.3.3, the desired signal and the interfering signal have identical (flat) spectra. Therefore, the array gain is due to spatial filtering. In the more general case, we have an environment in which the signal and interference have different spectral characteristics as well as different spatial characteristics. In the next example, we consider environments where the interference has different spectral characteristics than the signal.

#### Example 6.13.4

Consider a 10-element uniform linear array with element spacing equal to  $\lambda_u/2$ . We implement an FFT beamformer with  $M$  frequency bins.

$$B_f = B_s/f_c = 0.8.$$

The input is sampled at  $1/B_s$ , so the normalized frequency span is  $-\pi \leq \omega \leq \pi$  in radians. The signal of interest arrives from broadside and has a flat frequency spectrum over  $0.5\pi \leq \omega \leq 1.0\pi$  (a 25% bandwidth signal).

There are four interfering signals with the following characteristics (all spectra are zero outside the indicated band):

$$(i) \quad S_{I1} = \begin{cases} 1 + \cos(10\omega - 0.8\pi) & 0.6\pi \leq \omega \leq 1.0\pi \\ 0 & \text{elsewhere} \end{cases}$$

$$INR_1 = 40 \text{ dB}, u_1 = 0.4$$

$$(ii) \quad S_{I2} = \sigma_2^2 \quad 0.6\pi \leq \omega \leq 0.9\pi$$

$$INR_2 = 30 \text{ dB}, u_2 = -0.2$$

$$(iii) \quad S_{I3} = \sigma_3^2 \quad 0.5\pi \leq \omega \leq 0.51\pi$$

$$INR_3 = 60 \text{ dB}, u_3 = -0.15$$

$$(iv) \quad S_{I4} = \sigma_4^2 \quad 0.99\pi \leq \omega \leq \pi$$

$$INR_4 = 60 \text{ dB}, u_4 = 0.7$$

Note that the signal is only present in a subset of the frequency bins

$$m_s = 0.25M, \dots, M/2 - 1, \quad M = 4, 8, 16, \dots \quad (6.757)$$

We use an MPDR beamformer in those frequency bins and set the output of the other frequency bins equal to zero. In Figure 6.121, we plot the  $SNR_o$  versus  $ASNR$  for various  $M$ . In Figure 6.122, we plot the beam pattern for representative frequency bins.

We see that the  $SNR_o$  improvement in going from  $M = 16$  to  $M = 128$  is small. However, the narrowband nulls at  $u = -0.15$  and  $u = 0.7$  become deeper.

These examples illustrate some of the properties of FFT beamformers. We are implementing a set of narrowband beamformers so all of the techniques that we developed in Sections 6.2–6.12 carry over in a straightforward manner.

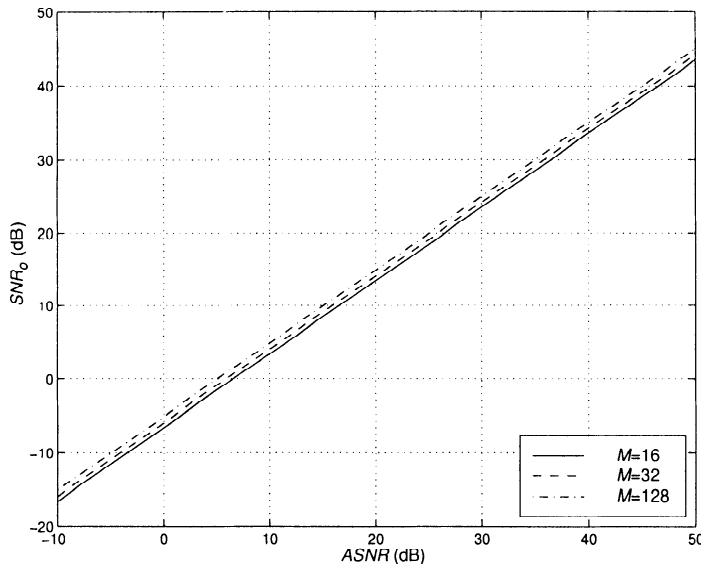


Figure 6.121 MPDR FFT beamformers:  $SNR_o$  versus  $ASNR$ , four interferers.

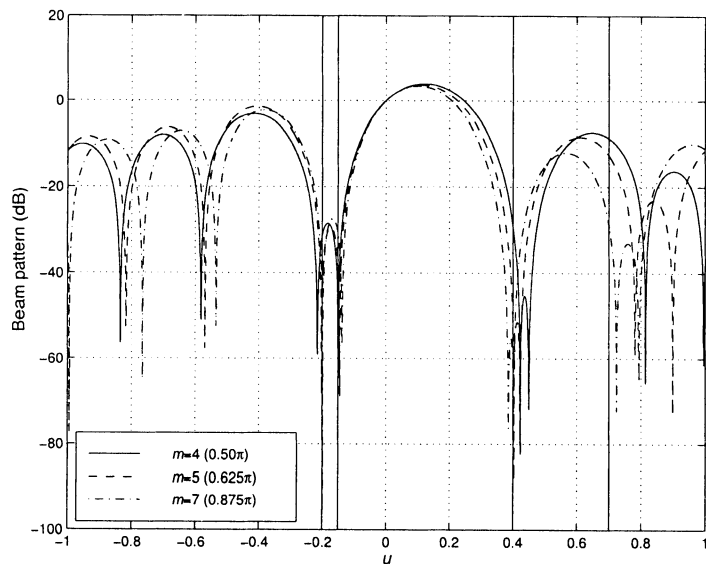
In this section we have analyzed the performance of DFT/FFT beamformer under the assumption that the relevant statistics about the signal and noise processes are known.

In the next section, we develop beamformers in which the filter behind each sensor is implemented in the time domain.

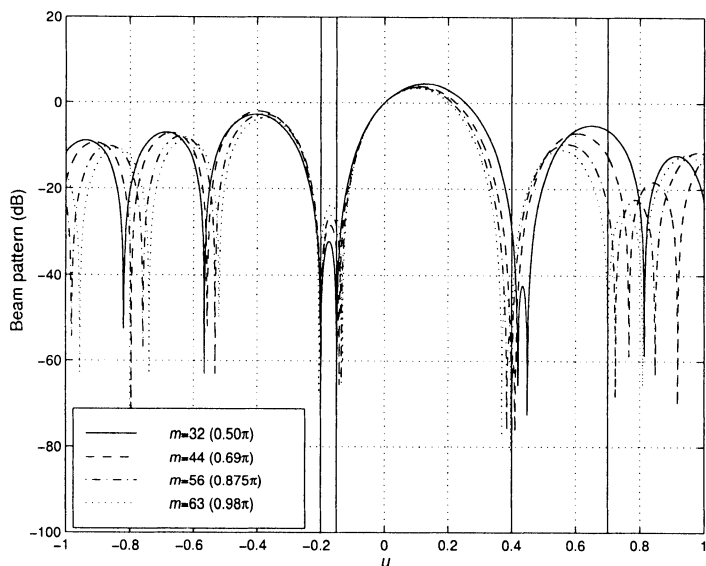
### 6.13.3 Finite impulse response (FIR) Beamformers

In this section, we study broadband beamformers that are implemented by placing a tapped delay line or finite impulse response(FIR) filter at the output of each sensor. We choose the impulse response (or tap weights) to achieve the desired frequency-wavenumber response. In practice, these weights are determined adaptively from the data. In this section, we assume that the statistics are known so the resulting beamformers correspond to the steady-state behavior. In Chapter 7, we develop the adaptive version of the FIR beamformer. An important advantage of the time domain implementation is that we can update the beamformer when each new snapshot arrives, in contrast to the FFT beamformer, which requires a block of snapshots to perform the FFT.

In Section 6.13.3.1, we develop the FIR model for a broadband beamformer. In Section 6.13.3.2, we analyze the performance.



(a)



(b)

Figure 6.122 Beam patterns at selected frequencies: (a)  $M = 16$ ; (b)  $M = 128$ .

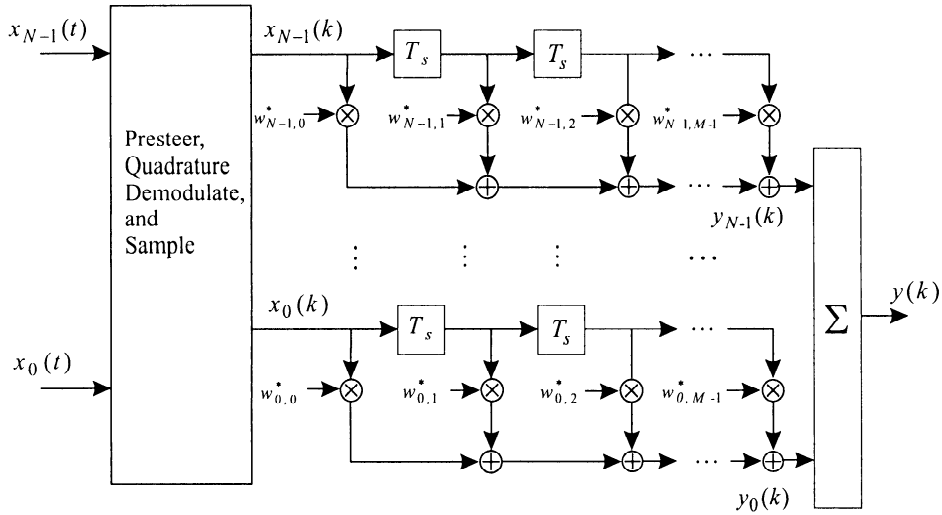


Figure 6.123 FIR beamformer.

### 6.13.3.1 FIR model

The FIR model of interest is shown in Figure 6.123. We assume that the output of each sensor has been quadrature demodulated so that the input to each of the FIR filter is a complex waveform. We are implementing the FIR at baseband.<sup>22</sup>

In order to simplify our initial discussion, we assume that the array has been pre-steered so the desired signal is aligned at the various sensors in the array.

We assume that the maximum frequency in the baseband signal is  $B_s/2$ . The tap spacing corresponds to the Nyquist sampling rate,

$$T_s = \frac{1}{B_s}. \quad (6.758)$$

The input to the first set of weights at time  $t_0$  is

$$\mathbf{x}_0(t_0) = \begin{bmatrix} x_0(t_0) \\ x_1(t_0) \\ x_2(t_0) \\ \vdots \\ x_{N-1}(t_0) \end{bmatrix} \triangleq \begin{bmatrix} x_{00} \\ x_{10} \\ x_{20} \\ \vdots \\ x_{N-1,0} \end{bmatrix} \triangleq \mathbf{x}_0. \quad (6.759)$$

<sup>22</sup>A number of discussions in the literature (e.g., [Com88a]) utilize a bandpass implementation and a tapped delay line.

The first subscript denotes the sensor. The second subscript denotes the delay from  $t = t_0$  measured in number of delays. Thus, the sensor output vector is indexed with 0. Similarly,

$$\mathbf{x}_m(t_0) = \begin{bmatrix} x_0(t_0 - mT_s) \\ x_1(t_0 - mT_s) \\ \vdots \\ x_{N-1}(t_0 - mT_s) \end{bmatrix}, \quad m = 0, \dots, M-1, \quad (6.760)$$

or

$$\mathbf{x}_m(t_0) \triangleq \begin{bmatrix} x_{0m} \\ x_{1m} \\ \vdots \\ x_{N-1,m} \end{bmatrix} \triangleq \mathbf{x}_m. \quad (6.761)$$

We can stack the vectors  $\mathbf{x}_0, \dots, \mathbf{x}_{M-1}$  to form an  $NM \times 1$  composite vector,

$$\mathbf{x} \triangleq \begin{bmatrix} \mathbf{x}_0 \\ \mathbf{x}_1 \\ \vdots \\ \mathbf{x}_{M-1} \end{bmatrix}. \quad (6.762)$$

We refer to this vector as a **tap-stacked** vector because the component vectors are indexed across the taps.

We can also specify the vector  $\mathbf{x}$  with the double index,  $[\mathbf{x}]_{nm}$ ,  $n = 0, \dots, N-1$ ,  $m = 0, \dots, M-1$ , where the ordering is given by (6.761) and (6.762).

We can define an  $NM \times 1$  array manifold vector corresponding to the tap-stacked vector  $\mathbf{x}$ . We define the spatial origin to be at the center of the array and the temporal origin to be at the sensor output. Then, the delay to a specific tap (for a linear array) is

$$\tau_{nm} = -\frac{d_n u}{c} + mT_s. \quad (6.763)$$

We first consider the case in which the quadrature demodulators are omitted. The  $NM \times 1$  array manifold vector is given by

$$[\mathbf{v}_{f,u}]_{nm} = e^{-j2\pi f \tau_{nm}}. \quad (6.764)$$

The array manifold vector down the  $m$ th tap is just the  $m$ th component vector,

$$[\mathbf{v}_{f,u}]_m = \left[ e^{-j2\pi f(\tau_0+mT_s)} \mid e^{-j2\pi f(\tau_1+mT_s)} \mid \dots \mid e^{-j2\pi f(\tau_{N-1}+mT_s)} \right]^T. \quad (6.765)$$

If the linear array is uniformly spaced at

$$d = \frac{\lambda_u}{2}, \quad (6.766)$$

where  $\lambda_u$  is the wavelength corresponding to the highest frequency, then

$$[\mathbf{v}_{f,u}]_{nm} = \exp \left\{ j2\pi f \left[ (n - \frac{N-1}{2}) \frac{u}{2f_u} - mT_s \right] \right\}. \quad (6.767)$$

If we include the quadrature demodulators, then the appropriate frequency for the taps is  $f_\Delta$ . The array manifold vector is

$$[\mathbf{v}_{f_\Delta,u}(f_\Delta, u)]_{nm} = \exp \left\{ j2\pi \left[ f(n - \frac{N-1}{2}) \frac{u}{2f_u} - f_\Delta(mT_s) \right] \right\}, \quad (6.768)$$

where

$$f_u = f_c + \frac{B_s}{2}. \quad (6.769)$$

The result in (6.768) can be rewritten as

$$[\mathbf{v}_{f_\Delta,u}(f_\Delta, u)]_{nm} = \exp \left\{ j\pi \left[ \frac{\left(1 + \frac{f_\Delta}{f_c}\right)}{\left(1 + \frac{B_f}{2}\right)} (n - \frac{N-1}{2})u - 2\frac{f_\Delta}{B_s}m \right] \right\}, \quad (6.770)$$

where

$$B_f \triangleq \frac{B_s}{f_c}. \quad (6.771)$$

The conjugate of the complex weights at the  $m$ th tap are denoted by the  $N \times 1$  vector

$$\mathbf{w}_m = \begin{bmatrix} w_{0m} \\ w_{1m} \\ \vdots \\ w_{N-1,m} \end{bmatrix}. \quad (6.772)$$

The composite tap-stacked weight vector is denoted by the  $NM \times 1$  vector,

$$\mathbf{w} = \begin{bmatrix} \mathbf{w}_0 \\ \mathbf{w}_1 \\ \mathbf{w}_2 \\ \vdots \\ \mathbf{w}_{M-1} \end{bmatrix}. \quad (6.773)$$

The array output at  $t_0$  can be written as

$$y(t_0) = \sum_{m=0}^{M-1} \mathbf{w}_m^H \mathbf{x}_m, \quad (6.774)$$

or, equivalently,

$$y(t_0) = \mathbf{w}^H \mathbf{x}. \quad (6.775)$$

The beam pattern of the TDL beamformer is obtained by replacing  $\mathbf{x}$  in (6.775) by the array manifold vector in (6.770),

$$B(f_\Delta, u) = \mathbf{w}^H \mathbf{v}_{f_\Delta, u}(f_\Delta, u). \quad (6.776)$$

For a plane-wave signal coming from the look direction, the values down the sensor at each tap are identical,

$$\begin{aligned} \mathbf{f}_0(t_0) &= f(t_0) \mathbf{1}, \\ &\vdots \\ \mathbf{f}_m(t_0) &= f(t_0 - mT_s) \mathbf{1}, \quad m = 0, \dots, M-1. \end{aligned} \quad (6.777)$$

Thus, for “look-direction” signals, we can use the equivalent tapped delay shown in Figure 6.124. The equivalent weights are

$$h_m^* = \sum_{n=0}^{N-1} w_{nm}^*, \quad m = 0, \dots, M-1, \quad (6.778)$$

and the output is

$$y(t_0) = \sum_{n=0}^{M-1} h_m^* f(t_0 - mT_s). \quad (6.779)$$

In order to implement the beamformer, we need the covariance matrix of  $\mathbf{x}$  in (6.762). In Section 6.13.2, we derived the covariance matrix of  $\tilde{\mathbf{x}}$ , which contained the same elements arranged in a different order.

Using the array manifold vector in (6.768), the  $NM \times NM$  correlation matrix is given by

$$\mathbf{R}_x = \int \mathbf{S}_x(2\pi f_\Delta) df_\Delta = \int \int S_x(f_\Delta, u) \mathbf{v}_{f_\Delta, u}(f_\Delta, u) \mathbf{v}_{f_\Delta, u}^H(f_\Delta, u) df du, \quad (6.780)$$

where  $S_x(f_\Delta, u)$  is the source spectrum in  $(f_\Delta, u)$  space. For a single plane-wave signal arriving from  $u_s$ , (6.780) reduces to

$$\mathbf{R}_x = \int_{-B_s/2}^{B_s/2} S_f(2\pi f_\Delta) \mathbf{v}_{f_\Delta, u}(f_\Delta, u) \mathbf{v}_{f_\Delta, u}^H(f_\Delta, u) df_\Delta. \quad (6.781)$$

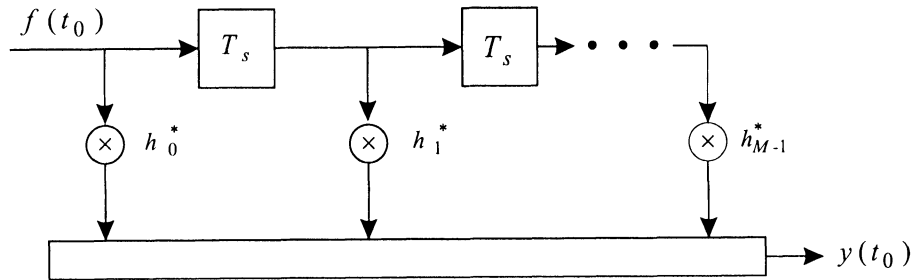
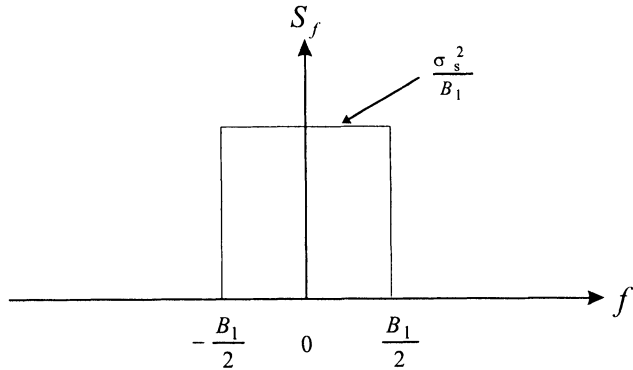


Figure 6.124 Equivalent ‘look-direction’ FIR filter.

Figure 6.125 Flat signal spectrum ( $-B_1/2, +B_1/2$ ).

Using (6.768), the  $nm, pq$  element is

$$[\mathbf{R}_x]_{nm,pq} = \int_{-B_s/2}^{B_s/2} S_f(2\pi f_\Delta) e^{j2\pi f(\tau_p - \tau_n)} e^{j2\pi f_\Delta(q-m)T_s} df_\Delta. \quad (6.782)$$

In many cases, the signals or interferers will not occupy the entire bandwidth  $[-B_s/2, B_s/2]$ . We consider a signal with the flat spectrum shown in Figure 6.125, where

$$B_1 \leq B_s. \quad (6.783)$$

Then,

$$[\mathbf{R}_x]_{nm,pq} = \int_{-B_1/2}^{B_1/2} \frac{\sigma_s^2}{B_1} e^{j2\pi f(\tau_p - \tau_n)} e^{j2\pi f_\Delta(q-m)T_s} df_\Delta. \quad (6.784)$$

Writing

$$f = f_c + f_\Delta, \quad (6.785)$$

(6.784) reduces to

$$[\mathbf{R}_x]_{nm,pq} = e^{j2\pi f_c(\tau_p - \tau_n)} \int_{-B_1/2}^{B_1/2} \frac{\sigma_s^2}{B_1} e^{j2\pi f_\Delta[(\tau_p - \tau_n) + (q - m)T_s]} df_\Delta, \quad (6.786)$$

or

$$[\mathbf{R}_x]_{nm,pq} = \frac{\sigma_s^2}{B_1} \text{sinc} [\pi B_1 ((\tau_p - \tau_n) + (q - m)T_s)] e^{j2\pi f_c(\tau_p - \tau_n)}. \quad (6.787)$$

The result in (6.787) is valid for an arbitrary array configuration.

If we restrict our attention to a standard linear array along the  $z$ -axis, then

$$\tau_n = \frac{-u_z(n - \frac{N-1}{2})}{2f_u}, \quad n = 0, \dots, N-1. \quad (6.788)$$

Then,

$$\tau_p - \tau_n = \frac{-u_z(p - n)}{2f_u} = \frac{u_z(n - p)}{2f_u}, \quad (6.789)$$

where

$$f_u = f_c + \frac{B_s}{2}. \quad (6.790)$$

If we let

$$T_s = \frac{1}{B_s}, \quad (6.791)$$

and define two fractional bandwidths,

$$B_{fs} = \frac{B_s}{f_c}, \quad (6.792)$$

and

$$B_{f1} = \frac{B_1}{f_c}, \quad (6.793)$$

we can write (6.787) as

$$[\mathbf{R}_x]_{nm,pq} = \frac{\sigma_s^2}{B_1} \text{sinc} \left[ \pi B_{f1} \frac{u_z(n-p)}{2(1+\frac{1}{2}B_{fs})} + \pi \frac{B_1}{B_s} (q-m) \right] e^{j\pi \frac{u_z(n-p)}{1+\frac{1}{2}B_{fs}}}. \quad (6.794)$$

The first term in the sinc function is due to the delay line and the second term is due to sensor location.

We now have all of the quantities necessary to specify the optimum beamformer. All of our narrowband results can be extended by suitably defining the constraint matrices.

### 6.13.3.2 Linearly constrained beamformers

In this section, we consider several types of broadband beamformers with linear constraints. In Section 6.13.3.2.1, we develop MVDR and MPDR beamformers. In Section 6.13.3.2.2, we develop LCMV and LCMP beamformers. In Section 6.13.3.2.3, we develop the generalized sidelobe canceller implementation. In Section 6.13.3.2.4, we summarize our results.

#### 6.13.3.2.1 MVDR and MPDR beamformers

We first consider MVDR and MPDR beamformers. In order to introduce a constraint on the look-direction response, we define the  $NM \times 1$  vector  $\mathbf{c}_m, m = 0, \dots, M - 1$  as

$$\mathbf{c}_m = \begin{bmatrix} \mathbf{0}_N \\ \mathbf{0}_N \\ \vdots \\ \mathbf{1}_N \\ \vdots \\ \mathbf{0}_N \end{bmatrix}, \quad (6.795)$$

where the  $\mathbf{1}_N$  vector is in the  $m$ th position. We next define an  $NM \times M$  matrix,  $\mathbf{C}$ ,

$$\mathbf{C} \triangleq \left[ \mathbf{c}_0 \ \mathbf{c}_1 \ \cdots \ \mathbf{c}_{M-1} \right]. \quad (6.796)$$

Thus,  $\mathbf{C}$  is a sparse matrix,

$$\mathbf{C} = \begin{bmatrix} 1 & 0 & \cdots & 0 \\ 0 & 1 & & \vdots \\ \vdots & 0 & \ddots & 0 \\ 0 & 0 & \cdots & 1 \end{bmatrix} = \mathbf{I}_M \otimes \mathbf{1}_N. \quad (6.797)$$

The constraint equation is

$$\mathbf{w}^H \mathbf{C} = \mathbf{g}^H, \quad (6.798)$$

where

$$\mathbf{g} \triangleq \left[ g_0 \ g_1 \ \cdots \ g_{M-1} \right]^T, \quad (6.799)$$

is an  $M \times 1$  vector.

If we impose the constraint in (6.797) on the weights, then the weight vector  $\mathbf{h}$  in Figure 6.124 is

$$\mathbf{h} = \mathbf{g}. \quad (6.800)$$

The values of  $\mathbf{g}$  will determine the temporal frequency response in the look direction. Consider a uniform linear array. If we denote the frequency response for the signal arriving from  $u$  as  $H(\omega, u)$ , then the look-direction frequency response is

$$H(\omega, 0) = \sum_{m=0}^{M-1} \int_{-\infty}^{\infty} e^{-j\omega t} g_m \delta(t - mT_s) dt. \quad (6.801)$$

Performing the integration gives

$$H(\omega, 0) = \sum_{m=0}^{M-1} g_m e^{-jm\omega T_s}. \quad (6.802)$$

The MVDR and MPDR beamformers require that the look-direction response be distortionless. In this case,

$$\mathbf{g}^H = \begin{bmatrix} 1 & 0 & \cdots & 0 \end{bmatrix}, \quad (6.803)$$

and

$$H(\omega, 0) = 1. \quad (6.804)$$

We minimize

$$P_o = \mathbf{w}^H \mathbf{R}_x \mathbf{w}, \quad (6.805)$$

subject to the constraint in (6.797). The result is

$$\boxed{\mathbf{w}_{mpdr}^H = \mathbf{g}^H \left[ \mathbf{C}^H \mathbf{R}_x^{-1} \mathbf{C} \right]^{-1} \mathbf{C}^H \mathbf{R}_x^{-1}} \quad (6.806)$$

Similarly, if  $\mathbf{R}_n$  is available, then

$$\boxed{\mathbf{w}_{mvdr}^H = \mathbf{g}^H \left[ \mathbf{C}^H \mathbf{R}_n^{-1} \mathbf{C} \right]^{-1} \mathbf{C}^H \mathbf{R}_n^{-1}} \quad (6.807)$$

Note that  $\mathbf{w}_{lcmv}^H$  and  $\mathbf{w}_{lcnp}^H$  are  $NM \times 1$  complex vectors. We use  $M$  constraints in both (6.806) and (6.807) so that there are  $(NM - M)$  degrees of freedom remaining.

The results in (6.806) and (6.807) are due to Frost [Fro72], and the resulting beamformer is sometimes referred to in the literature as the Frost beamformer. In Chapter 7, we discuss adaptive implementations of this beamformer. Frost only considered the distortionless constraint in [Fro72], but he indicated that the addition of other linear constraints was straightforward. We next consider broadband LCMV and LCMP beamformers.

### 6.13.3.2.2 LCMV and LCMP beamformers

The extension to LCMV and LCMP beamformers follows easily. The various constraint sets that we discussed for narrowband processors can be extended to the broadband TDL case. For  $N_d$  derivative constraints, we define an  $NM \times N_d$  matrix,

$$\mathbf{c}_m = \begin{bmatrix} \mathbf{0}_N \\ \mathbf{0}_N \\ \vdots \\ \mathbf{c}_{N_d} \\ \vdots \\ \mathbf{0}_N \end{bmatrix}, \quad (6.808)$$

where  $\mathbf{c}_{N_d}$  is the basic  $N \times N_d$  constraint matrix, which is in the  $m$ th position.

For three spatial derivative constraints,

$$\mathbf{c}_{N_d} = \begin{bmatrix} \mathbf{1} & \dot{\mathbf{v}}(0) & \ddot{\mathbf{v}}(0) \end{bmatrix}. \quad (6.809)$$

Then  $\mathbf{C}$  is an  $NM \times N_d M$  constraint matrix,

$$\mathbf{C} = \begin{bmatrix} \mathbf{c}_{N_d} & \mathbf{0}_{NN_d} & \cdots & \mathbf{0}_{NN_d} \\ \mathbf{0}_{NN_d} & \mathbf{c}_{N_d} & & \vdots \\ \vdots & \mathbf{0}_{NN_d} & \mathbf{c}_{N_d} & \\ \vdots & \vdots & & \ddots & \mathbf{0}_{NN_d} \\ \mathbf{0}_{NN_d} & \mathbf{0}_{NN_d} & \cdots & \mathbf{c}_{N_d} \end{bmatrix} = \mathbf{I}_M \otimes \mathbf{c}_{N_d}. \quad (6.810)$$

The  $\mathbf{g}$  matrix is an  $N_d M \times 1$  matrix,

$$\mathbf{g}^H = \begin{bmatrix} \mathbf{g}_1^H & \mathbf{0}_{N_d}^T & \cdots & \mathbf{0}_{N_d}^T \end{bmatrix}, \quad (6.811)$$

where

$$\mathbf{g}_1^H = \begin{bmatrix} 1 & g_2 & g_3 \end{bmatrix}. \quad (6.812)$$

The result for derivative constraints is due to Er and Cantoni [EC85].

Just as in the narrowband case, it is necessary to check that the columns in the constraint matrix are linearly independent.

The resulting weight vectors are

$$\mathbf{w}_{lcmp}^H = \mathbf{g}^H \left[ \mathbf{C}^H \mathbf{R}_x^{-1} \mathbf{C} \right]^{-1} \mathbf{C}^H \mathbf{R}_x^{-1}, \quad (6.813)$$

and

$$\mathbf{w}_{lcmv}^H = \mathbf{g}^H \left[ \mathbf{C}^H \mathbf{R}_n^{-1} \mathbf{C} \right]^{-1} \mathbf{C}^H \mathbf{R}_n^{-1}. \quad (6.814)$$

These are identical in form to (6.806) and (6.807). However, the  $\mathbf{g}^H$  and  $\mathbf{C}$  matrices are different.

The block structure in (6.797) and (6.810) will lead to important simplifications when we implement the beamformer adaptively.

All of the linear constraints that we studied in the narrowband case can be extended to the broadband case. However, for constraints such as multiple-direction constraints, eigenvector constraints, or quiescent pattern constraints, the constraint matrix no longer has the block structure in (6.797) or (6.810). In the adaptive implementation, the computational complexity is increased. We do not discuss these constraints in the text. A discussion of eigenvector constraints is available in Van Veen (Chapter 4 in [HS92]).

In order to improve robustness, we can also incorporate diagonal loading. We impose a quadratic constraint on the composite weight vector  $\mathbf{w}$  in (6.798),

$$\| \mathbf{w} \|^2 \leq T_0 \quad (6.815)$$

and minimize the output power. Proceeding as in the narrowband case, we obtain

$$\mathbf{w}_{lcmp,dl}^H = \mathbf{g}^H \left[ \mathbf{C}^H [\mathbf{R}_x + \lambda \mathbf{I}]^{-1} \mathbf{C} \right]^{-1} \mathbf{C}^H [\mathbf{R}_x + \lambda \mathbf{I}]^{-1}, \quad (6.816)$$

where  $\lambda$  is chosen to satisfy (6.815). Alternatively, we can choose a fixed loading level based on the expected scenario.

### 6.13.3.2.3 Generalized sidelobe canceller

In this subsection, we develop the generalized sidelobe canceller form of a broadband MPDR beamformer using tapped delay lines. The GSC form was derived independently by Griffiths and Jim [GJ82] and Byun and Gangi [BG81].

We only consider the case in which the constraint matrix  $\mathbf{C}$  has the sparse structure in (6.797) and (6.810). The broadband version of the generalized sidelobe canceller is shown in Figure 6.126. There is a preprocessing operation that steers the array in the desired direction, performs a quadrature demodulation, and samples the demodulated waveform at  $T_s = 1/B_s$  intervals. The output is a sequence of complex vectors  $\mathbf{x}(k)$ .

The upper path consists of an FIR filter of length  $M$  with fixed weights that generates the desired quiescent response. The composite  $NM \times 1$  input

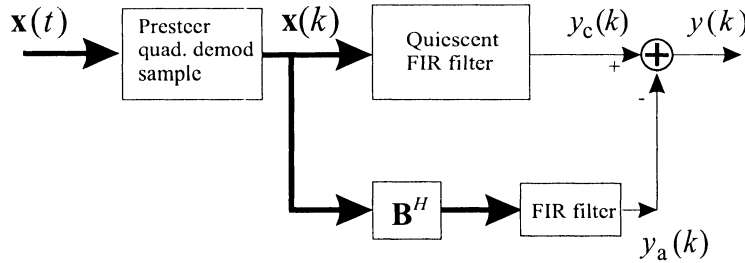


Figure 6.126 Time domain implementation of generalized sidelobe canceller.

vector in the upper filter is  $\mathbf{x}$ , as in (6.762). The  $NM \times 1$  weight vector in the upper path is designed to provide the quiescent response. From (6.813), letting  $\mathbf{R}_x = \mathbf{I}$ , we have

$$\mathbf{w}_q^H = \mathbf{g}^H [\mathbf{C}^H \mathbf{C}]^{-1} \mathbf{C}^H, \quad (6.817)$$

where  $\mathbf{g}^H$  and  $\mathbf{C}$  are given by (6.810) and (6.811), respectively. The output of the upper path is denoted by  $y_c(k)$ .

The blocking matrix  $\mathbf{B}^H$  in the lower path is an  $(N - N_d) \times N$  matrix that satisfies

$$\mathbf{C}_{N_d}^H \mathbf{B} = \mathbf{0}, \quad (6.818)$$

where  $\mathbf{C}_{N_d}$  is the basic  $N \times N_d$  constraint matrix in (6.808) and  $\mathbf{0}$  is a  $N_d \times (N - N_d)$  matrix of zeros. Note that because the constraints are spatial constraints, the blocking matrix does not require an FIR filter. As in the narrowband case, we require

$$\mathbf{B}^H \mathbf{B} = \mathbf{I}. \quad (6.819)$$

We note the output of the blocking matrix by  $\mathbf{x}_b(k)$ . At time  $t_0$ , the vector input to the  $m$ th taps in the adaptive FIR filter is

$$\mathbf{x}_{b:m} \triangleq \mathbf{x}_b(t_0 - mT_s), \quad (6.820)$$

and we can define a composite  $(N - N_d) \times M$  vector

$$\mathbf{x}_b = \begin{bmatrix} \mathbf{x}_{b:0} \\ \mathbf{x}_{b:1} \\ \vdots \\ \mathbf{x}_{b:M-1} \end{bmatrix}. \quad (6.821)$$

In order to relate  $\mathbf{x}_b$  to the original input vector  $\mathbf{x}$  in (6.819), we define a  $(N - N_d)M \times NM$  composite matrix whose blocks are  $\mathbf{B}^H$ ,

$$\mathbf{B}_{comp}^H \triangleq \begin{bmatrix} \mathbf{B}^H & \mathbf{0} & \cdots & \mathbf{0} \\ \mathbf{0} & \mathbf{B}^H & & \vdots \\ \vdots & & \ddots & \\ \mathbf{0} & \mathbf{0} & \cdots & \mathbf{B}^H \end{bmatrix} = \mathbf{I}_M \otimes \mathbf{B}^H. \quad (6.822)$$

Then,

$$\mathbf{x}_b = \mathbf{B}_{comp}^H \mathbf{x} \quad (6.823)$$

The FIR filter in the lower path is chosen to minimize the output power. Following the same approach as in (6.373)–(6.375), we obtain the  $1 \times (N - N_d)M$  weight vector

$$\hat{\mathbf{w}}_a^H = \mathbf{w}_q^H \mathbf{R}_x \mathbf{B}_{comp} \left[ \mathbf{B}_{comp}^H \mathbf{R}_x \mathbf{B}_{comp} \right]^{-1}. \quad (6.824)$$

The advantage of the generalized sidelobe canceller structure will become more apparent when we implement the adaptive version in Section 7.13. We have replaced the constrained minimization problem with an unconstrained minimization problem. In this derivation, we have implemented the FIR filter in a direct form. In Section 7.13, we mention other implementations such as lattice filters that may exhibit better adaptive behavior.

In the next subsection, we consider several examples.

#### 6.13.3.2.4 Beamformer performance

We consider several examples to illustrate the behavior of finite impulse response beamformers.

The first example uses the same signal and interference model as in the FFT beamformer discussion so we can compare performance.

**Example 6.13.5: MPDR TDL beamformer; no mismatch** (continuation; Example 6.13.2)

Consider the same signal and interference model as in Example 6.13.2. The desired signal arrives from broadside and has a flat spectrum with bandwidth  $B_s$  and fractional bandwidth  $B_f$ . A single interfering plane-wave signal with the same spectrum arrives from  $u_I$ . The  $SNR = 0$  dB and the  $INR = 30$  dB. We sample the input at  $T_s = B_s^{-1}$ . We implement an MPDR beamformer using an  $M$ -tap FIR filter.

In Figure 6.127, we show the array gain versus  $u_I/BW_{NN}$  for  $B_f = 0.4$  and  $M = 2, 4$ , and 8. As we would expect from the FFT beamformer results,  $M = 2$  provides all of the available performance improvement.

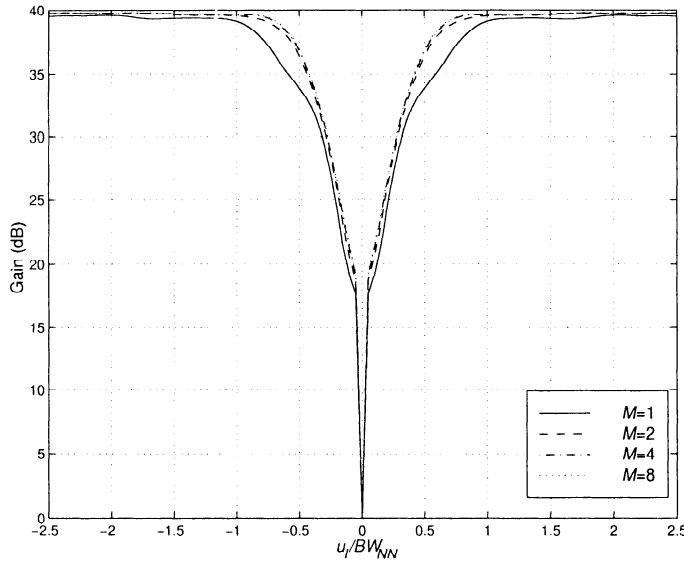


Figure 6.127 Time-domain MPDR beamformer:  $u_s = 0$ ,  $INR = 30$  dB,  $B_f = 0.4$ , array gain versus  $u_I/BW_{NN}$ .

**Example 6.13.6: LCMP beamformer with derivative constraints; signal mismatch**

Consider a uniformly spaced 10-element array. The interelement spacing is  $\lambda_u/2$ , where  $\lambda_u$  is the wavelength of the highest frequency in the input signal. There is an  $M$ -tap FIR filter at the output of each sensor.

The array is steered to broadside. We use the derivative constraint matrix in (6.809)–(6.812) with  $g_2 = 0$  and  $g_3 = \dot{B}_c(0)$ . Note that we are using  $3M$  degrees of freedom.

The signal actually arrives from  $u_a = 0.05$  and has a flat spectrum over the frequency band  $0 \leq |f_\Delta| \leq 0.5B_s$ .  $B_f = 0.4$ . The  $SNR$  varies from  $-10$  dB to  $30$  dB.

A single plane-wave interferer arrives from  $u_I = 0.45$  with the same frequency spectrum. The  $INR = 30$  dB.

In Figure 6.128(b), we plot the average  $SNR_o$  versus  $ASNR$  for  $M = 2, 4$ , and  $8$ . In Figure 6.128(a), we plot the array gain versus  $ASNR$  for  $M = 2, 4$ , and  $8$ .

In Figure 6.129, we plot the beam pattern at  $f_\Delta = 0, 0.2B_s, 0.4B_s$  for  $M = 8$  and  $SNR = 10$  dB.

For  $ASNR < 25$  dB, the derivative constraints prevent signal nulling, and the array puts a null in the interferer direction across the frequency band.

**Example 6.13.7 (continuation; Example 6.13.4)**

Consider a uniformly spaced 10-element array. The interelement spacing is  $\lambda_u/2$ , where  $\lambda_u$  is the wavelength of the highest frequency in the input signal. There is an  $M$ -tap FIR filter at the output of each sensor.

$$B_f = B_s/f_c = 0.8. \quad (6.825)$$

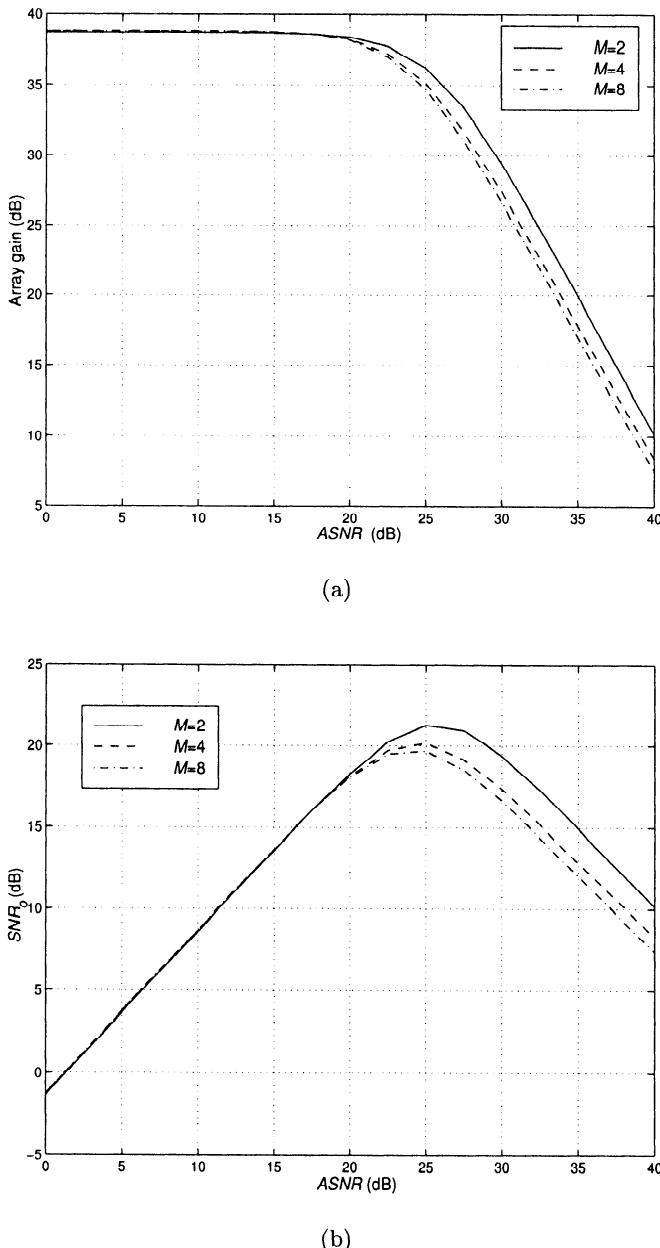


Figure 6.128 LCMP-TD beamformer with derivative constraints;  $u_s = 0$ ,  $u_a = 0.05$ ,  $u_I = 0.45$ ,  $INR = 30$  dB,  $B_{fs} = 0.4$ ,  $B_1/B_s = 0.4$ : (a)  $SNR_o$  versus  $ASNR$ ; (b) array gain versus  $ASNR$ .

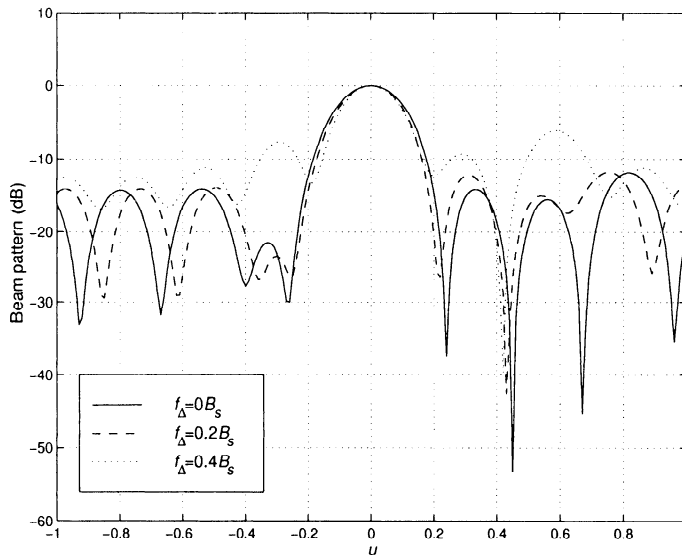


Figure 6.129 Beam pattern at various frequencies;  $M = 8$ ,  $f_\Delta = 0, 0.2B_s, 0.4B_s$ .

The input is sampled at  $1/B_s$ , so the normalized frequency span is  $-\pi \leq \omega \leq \pi$  in radians. The signal of interest arrives from broadside and has a flat frequency spectrum over  $0.5\pi \leq \omega \leq 1.0\pi$  (a 25% bandwidth signal).

There are four interfering signals with the following characteristics (all spectra are zero outside the indicated band):

$$(i) \quad S_{I1} = \begin{cases} 1 + \cos(10\omega - 0.8\pi), & 0.6\pi \leq \omega \leq 1.0\pi, \\ 0, & \text{elsewhere}, \end{cases} \quad INR_1 = 40 \text{ dB}, u_1 = 0.4; \quad (6.826)$$

$$(ii) \quad S_{I2} = \sigma_2^2 \quad 0.6\pi \leq \omega \leq 0.9\pi, \quad INR_2 = 30 \text{ dB}, u_2 = -0.2; \quad (6.827)$$

$$(iii) \quad S_{I3} = \sigma_3^2 \quad 0.5\pi \leq \omega \leq 0.51\pi, \quad INR_3 = 60 \text{ dB}, u_3 = -0.15; \quad (6.828)$$

$$(iv) \quad S_{I4} = \sigma_4^2 \quad 0.99\pi \leq \omega \leq \pi, \quad INR_4 = 60 \text{ dB}, u_4 = 0.7. \quad (6.829)$$

We implement a time-domain MPDR (MPDR-TD) beamformer using  $M$ -taps. In Figure 6.130 we plot the  $SNR_o$  versus  $ASNR$  for various  $M$ . In Figure 6.131, we plot the beam pattern at selected frequencies.

Comparing the results in Figures 6.121 and 6.130, we see that the time-domain implementation is about 4 dB better than the FFT implementation.

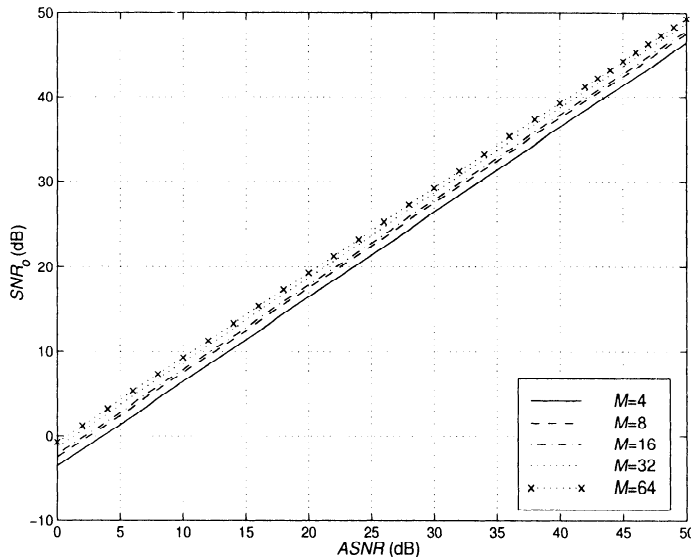


Figure 6.130 Average  $SNR_o$  versus  $ASNR$ , MPDR-TD beamformer with  $M$  taps;  $B_f = 0.8$ ;  $M = 4, \dots, 64$ .

#### 6.13.3.2.5 Summary: Time-domain beamforming

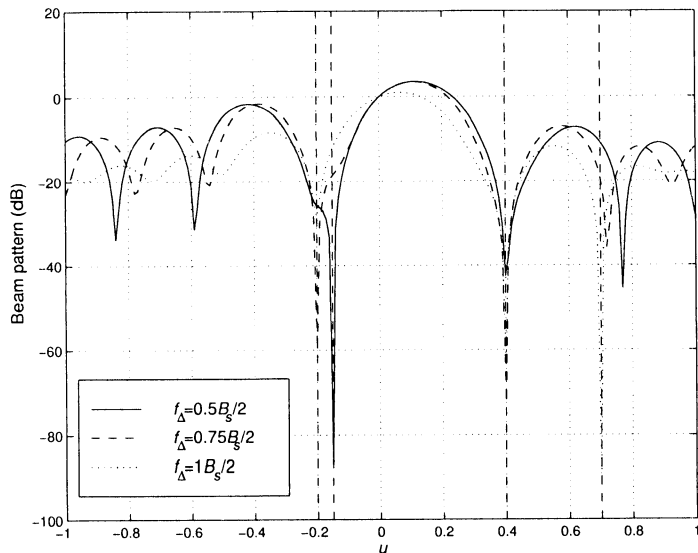
In this section, we have discussed time-domain beamforming. In Section 7.11, we develop adaptive implementations of the time-domain beamformers that we have developed in this section.

#### 6.13.4 Summary: Broadband Processing

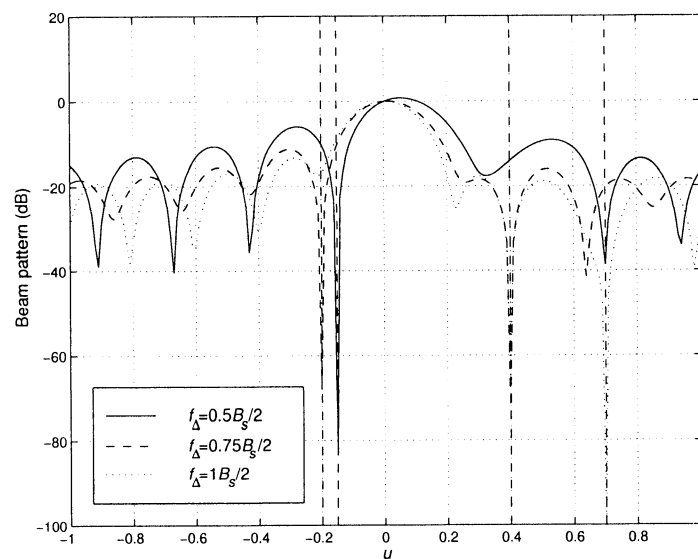
In this section we have discussed two methods of implementing broadband beamformers. In Section 6.13.1, we developed the necessary background by reintroducing the frequency dependence in the array manifold vector. The result in (6.675) was for a uniform linear array, but the extension to an arbitrary array geometry is straightforward. If we replaced the complex weights in a narrowband beamformer with a complex linear filter, then the formulas for the MPDR, LCMP, and MMSE beamformers followed easily.

In practice, we must estimate the appropriate statistics and implement these complex linear filters adaptively. The challenge is to find efficient implementations that have the capability to adapt.

In Section 6.13.2, we developed frequency-domain implementations. We sampled the output of the quadrature demodulators at the sensors to ob-



(a)



(b)

Figure 6.131 Broadband MPDR-TD beamformer:  $SNR = 0$  dB,  $B_f = 0.8$ ; beam patterns at  $f_\Delta = 0.5B_s/2, 0.75B_s/2, B_s/2$ : (a) $M = 4$ ; (b) $M = 64$ .

tain a set of complex time-domain samples. We then performed an FFT to obtain a set of complex frequency-domain samples. We chose the transform duration so that the frequency-domain samples at different frequency could be modeled as statistically independent Gaussian random vectors. We processed each frequency-domain sample using a narrowband beamformer. We then performed an IDFT to obtain an output time-domain sequence. All of the results from our narrowband beamformer discussions can be applied directly.

In Section 6.13.3, we developed time-domain implementations. We implemented the complex linear system using a complex FIR filter at the output of each quadrature demodulator. We restricted the constraint matrices to have a sparse block structure in order to restrict the computational complexity. The frequency resolution of the beamformer is a function of the length of the FIR filter.

The relative performance of the two implementations depends on the signal and interference environments. If we allow the beamformers in the various frequency bins in the FFT beamformer to be coupled, do not require that the matrix in the time-domain beamformer have a sparse block structure, and set the number of frequency bins equal to the number of taps, then we can achieve identical performances in the two implementations (e.g., Compton [Com88b] or Godara [God95]). Godara (e.g., [God95] and [GJ99]) has also developed frequency-domain techniques for computing the weights in the time-domain FIR beamformer. These techniques offer significant computational savings in certain cases.

There are other approaches to broadband beamforming that rely on a technique called focusing. The technique can be implemented in either the time domain or the frequency domain. References that discuss focusing include Wang and Kaveh [WK85], Yang and Kaveh [YK90], Sivanand and Kaveh [SK90], Simanapalli and Kaveh [SK94], and Krolik and Swingler [KS90].

We revisit broadband beamformers in Section 7.13 and discuss their adaptive behavior.

## 6.14 Summary

In this chapter, we have developed a family of optimum beamformers. Our development and analysis assumed that the statistics of the environment, either  $\mathbf{S}_x$  or  $\mathbf{S}_n$ , were known.

The discussion in Section 6.2 considered the MVDR and MPDR beam-

formers and demonstrated their optimality under a number of criteria.

Sections 6.3 and 6.4 analyzed their performance for discrete interference and spatially spread interference, respectively. We found that, when the interference was in the sidelobe region, the beam pattern was well-behaved and the beamformer was effective in reducing the output due to the interference. When the interferer was inside the main-lobe region, the beam pattern degraded and the output  $SNR_o$  decreased significantly. The resulting beamformer was also sensitive to the model assumptions. These problems of signal mismatch and main-lobe interference motivated modifications to the MPDR and MVDR beamformers in order to provide main-lobe protection.

Section 6.5 extended the results to multiple plane-wave input signals. We found that the MVDR and MPDR beamformers imposed a distortionless constraint on the signal of interest and imposed perfect nulls on the remaining signals. The MMSE beamformers treated the other signals as interferers and adjusted the gain in their direction as a function of their  $SNR$ .

Section 6.6 introduced the problems of mismatch between the model and the actual environment that are present in most applications. We studied the effects of DOA mismatch and array perturbations. We found that the MPDR beamformer was sensitive to mismatch and tried to null the signal of interest. We introduced the technique of diagonal loading to combat the problem. We found that, when the  $SNR$  was less than the individual  $INRs$ , diagonal loading provided significant improvement. Subsequent discussions in Chapter 7 lead us to the conclusion that some form of diagonal loading is an important component of most beamforming algorithms. The disadvantage of relying completely on diagonal loading to solve the mismatch or main-lobe interferer problem was that the beamformer lost its ability to form nulls on interferers with  $INRs$  less than the  $LNR$ .

Section 6.7 introduced linear constraints to improve the performance in the presence of mismatch. Directional and derivative constraints tried to control the behavior of the beam pattern at specific points (or small regions) in frequency-wavenumber space. Eigenvector and quiescent pattern constraints tried to control the behavior over larger regions. The resulting LCMV and LCMP beamformers, coupled with diagonal loading, provided significant performance improvement. We also introduced the generalized sidelobe canceller that separated the constraints and the adaptive component of the beamformer in an effective manner.

Section 6.8 exploited the result that the plane-wave signal and  $D$  plane-wave interferers define a  $(D + 1)$ -dimensional subspace that provides a sufficient statistic for the waveform estimation (or detection) problem. By

projecting the incoming waveform into this subspace, we can implement eigenspace beamformers, which have improved performance and reduced computational complexity. In Chapter 7, we find that they have good adaptive performance.

Section 6.9 developed beamspace processing. In this technique, we transform the input from element space into a reduced-dimension beamspace using a set of fixed beams (either conventional beams or one of the tapered beams developed in Chapters 3 and 4). We process the beam outputs using one of the optimum processors developed in the earlier section of the chapter. Beamspace processing provides reduced computational complexity without significant loss in performance for interferers in the beamspace sector. In Chapter 7, we find that beamspace processors provide faster adaptation to the optimum processor than the corresponding element-space processors. For conjugate symmetric array manifolds and conjugate symmetric beamspace matrix, we find that there is the additional advantage that we can use real computation to find the beamformer. The disadvantage is the loss of adaptive degrees of freedom.

Section 6.10 revisited quadratically constrained beamformers that were introduced in Section 6.6.4. The norm of the weight vector was constrained and the resulting level of diagonal loading was computed. The QC formulation in this section also leads naturally to a data-dependent variable loading in Chapter 7.

Section 6.11 revisited the problem of approximating a desired beam pattern over some region of frequency-wavenumber space that we first encountered in our discussion of eigenvector constraints in Section 6.7.1.5. We developed an algorithm that is a generalization of diagonal loading. The resulting algorithms are referred to as soft constraint algorithms and provide performance improvements in several application areas.

Section 6.12 considered the problem in which the signal and interference are temporally correlated. This model occurs in a multipath environment and other scenarios. We introduced a technique called spatial smoothing to reduce the correlation prior to beamforming.

Section 6.13 considered broadband beamformers and developed frequency domain and time domain implementations.

In this chapter we have assumed that the necessary statistics are known. In Chapter 7, we develop adaptive beamformers that rely on the observed data to develop the beamformer. If the environment is stationary, we would anticipate that the adaptive beamformers would approach one of the optimum beamformers developed in this chapter. We will develop various adaptive techniques and explore their adaptive behavior, computational complex-

ity, and numerical stability.

## 6.15 Problems

### P6.2 Optimum Beamformers

#### Problem 6.2.1

Assume that we have a sequence of statistically independent frequency-domain snapshots

$$\mathbf{X}(w) = \mathbf{F}(w) + \mathbf{N}(w), \quad (6.830)$$

where  $\mathbf{F}(w)$  and  $\mathbf{N}(w)$  are statistically independent with spectral matrices  $\mathbf{S}_f(\omega)$  and  $\mathbf{S}_n(\omega)$ .

Find the linear filter that maximizes the *SNR*.

#### Problem 6.2.2

Show that, if  $\mathbf{v}_m(\psi) = \mathbf{v}_s(\psi)$ , the MPDR beamformer in (6.71) is identical to the MVDR beamformer in (6.14).

#### Problem 6.2.3

Consider the case where

$$\mathbf{X}(\omega) = F_1(\omega)\mathbf{v}(\mathbf{k}_1) + F_2(\omega)\mathbf{v}(\mathbf{k}_2) + \mathbf{W}(\omega), \quad (6.831)$$

where

$$S_{F_1}(\omega), \quad S_{F_2}(\omega), \quad S_{F_1 F_2}(\omega), \quad \text{and} \quad S_{\mathbf{W}}(\omega) = \sigma_w^2 \mathbf{I}, \quad (6.832)$$

are known, and

$$D(\omega) = F_1(\omega). \quad (6.833)$$

- (a) Find the optimum MMSE matrix processor to estimate  $D(\omega)$ .
- (b) Assume the signals are narrowband around  $\omega_c$ . Plot  $\varepsilon_u$  as a function of  $S_{F_1 F_2}(\omega_c)$  and  $\rho_{12}(\omega_c)$ , the spatial correlation.

#### Problem 6.2.4

Consider a standard 10-element linear array. The signal is a plane wave arriving from broadside. The interference consists of a plane wave arriving from  $u_I$  with an  $INR = \sigma_I^2 / \sigma_w^2$  and white noise with spectral height  $\sigma_w^2$ .

- (a) Plot the array gain versus  $u_I / BW_{NN}$  for an MVDR beamformer. Consider  $INRs = 0, 10, 20$ , and  $30$  dB.
- (b) Plot  $\| \mathbf{w}_{mvdr} \|^2$  versus  $u_I / BW_{NN}$  for the same  $INRs$ .

#### Problem 6.2.5 (continuation)

Consider a standard  $N$ -element linear array. The rest of the model is the same as in Problem 6.2.4.

Define the normalized array gain as

$$AG_n \triangleq AG/N, \quad (6.834)$$

the array  $INR$  as

$$AINR = N \cdot INR, \quad (6.835)$$

and

$$u_{In} = u_I / BW_{NN}. \quad (6.836)$$

- (a) Plot the normalized array gain versus  $u_I / BW_{NN}$  for  $AINRs = 10, 20, 30$ , and  $40$  dB, for  $N = 4, 8, 10, 32$ , and  $64$ .
- (b) Discuss your results. Are the normalized plots essentially the same after some value of  $N$ ?

### Problem 6.2.6

Consider a standard 10-element linear array. Assume  $\mathbf{v}_{\psi_m}$  corresponds to broadside. Assume  $\mathbf{S}_n = \mathbf{I}$  and  $\sigma_s^2$  is the signal strength. The signal actually arrives from  $u_a$ , where  $|u_a| \leq 0.1$ . Plot  $A_{mpqr}$  vs  $u_a$  for the interval  $[0, -0.1]$ . Indicate the points where

$$A_{mpqr}(u_a) = 0.5A_{mpqr}(0). \quad (6.837)$$

### Problem 6.2.7 (continuation)

Repeat Problem 6.2.7 for the interference model in Problem 6.2.4.

### Problem 6.2.8: MVQR Beamformers

In many applications, we want to have a quiescent pattern with low sidelobes. We define the weight vector of the desired quiescent pattern as  $\mathbf{w}_{dq}^H$ . We define a normalized version of  $\mathbf{w}_{dq}^H$  as,

$$\overline{\mathbf{w}}_{dq}^H = \frac{\mathbf{w}_{dq}^H}{\|\mathbf{w}_{dq}\|^2}. \quad (6.838)$$

We impose the constraint

$$\overline{\mathbf{w}}_{dq}^H \mathbf{w} = 1, \quad (6.839)$$

on the weight vector and minimize

$$\mathbf{w}^H \mathbf{S}_n \mathbf{w} \quad (6.840)$$

subject to the constraint.

- (a) Show that

$$\mathbf{w}_{mvqr}^H = \Lambda_q \overline{\mathbf{w}}_{dq}^H \mathbf{S}_n^{-1}, \quad (6.841)$$

where

$$\Lambda_q = [\overline{\mathbf{w}}_{dq}^H \mathbf{S}_n^{-1} \overline{\mathbf{w}}_{dq}]^{-1}. \quad (6.842)$$

The resulting beamformer is called the **minimum variance quiescent response (MVQR)** beamformer.

- (b) Derive an expression for the array gain.

- (c) What is the array gain when

$$\mathbf{S}_n = \sigma_w^2 \mathbf{I}? \quad (6.843)$$

### Problem 6.2.9: MPQR Beamformers (continuation)

Define

$$\overline{\mathbf{w}}_{dq}^H = \frac{\mathbf{w}_{dq}^H}{\|\mathbf{w}_{dq}\|^2} \quad (6.844)$$

and impose the constraint on the weight vector

$$\bar{\mathbf{w}}_{dq}^H \mathbf{w} = 1. \quad (6.845)$$

Minimize

$$\mathbf{w}^H \mathbf{S}_x \mathbf{w} \quad (6.846)$$

subject to the constraint. The resulting beamformer is called the **minimum power quiescent response (MPQR)** beamformer.

- (a) Show that

$$\mathbf{w}_{mpqr}^H = \Lambda_{qp} \bar{\mathbf{w}}_{dq}^H \mathbf{S}_x^{-1}, \quad (6.847)$$

where

$$\Lambda_{qp} = [\bar{\mathbf{w}}_{dq}^H \mathbf{S}_x^{-1} \bar{\mathbf{w}}_{dq}]^{-1}. \quad (6.848)$$

- (b) Derive an expression for the array gain.

### P6.3 Discrete Interference

#### Problem 6.3.1

Consider a standard 10-element linear array. Compare the performance of a least squares Dolph-Chebychev beamformer ( $-40$ -dB sidelobe) with a zero-order null at  $u_I$  (see Section 3.7) with the MVDR processor with a single plane-wave interferer at  $u_I$  plus white noise ( $\sigma_w^2$ ).

- (a) Compute the array gain of the two beamformers and plot their beam patterns for  $u_I = 0.3$  and  $0.50$  and  $\sigma_I^2 = 10$  dB and  $50$  dB.
- (b) Compute the array gain of the two beamformers and plot their beam patterns for  $u_I = 0.09$  and  $0.18$  and  $\sigma_I^2 = 10$  dB and  $50$  dB.
- (c) Compute the array gain of the two beamformers and plot their beam patterns for  $u_I = 0.02$  and  $0.0433$  and  $\sigma_I^2 = 10$  dB and  $50$  dB.

#### Problem 6.3.2

Repeat Problem 6.3.1 using the Villenueve  $\bar{n}$  beamformer of Section 3.4.4 as the original weighting.

#### Problem 6.3.3

Repeat Problem 6.3.1 using the Kaiser beamformer ( $\beta = 6$ ) as the original weighting.

#### Problem 6.3.4

Repeat Problem 6.3.1 using the Hann beamformer as the original weighting.

#### Problem 6.3.5

Consider a standard 10-element linear array that uses the MVDR beamformer with a single plane-wave interferer plus white noise. Assume the MVDR beamformer is designed assuming the plane wave is at  $u_I$ .

The actual location of the plane wave in  $u$ -space is a Gaussian random variable,  $N(u_I, \sigma_u^2)$ .

- (a) Assume  $u_I$  is in the sidelobe region and  $\sigma_u$  is small. Find  $E[A_o(u_I)]$ . Plot your result for  $u_I = 0.30, \sigma_u = 0.05, \sigma_I^2 = 10$  dB and  $20$  dB.
- (b) Repeat part (a) for  $u_I = 0.18$ .

**Problem 6.3.6**

- (a) Repeat Problem 6.3.5 for the Villenueve  $\bar{n}$  beamformer in Problem 6.3.2.
- (b) Compare your result to the result in Problem 6.3.5.

**Problem 6.3.7**

Consider a standard 10-element linear array with  $d = \lambda_c/2$  where  $\lambda_c$  is the wavelength corresponding to  $f_c$ . The frequency spectrum of the single plane-wave interferer is uniform from  $f_c - B_s/2 \leq f \leq f_c + B_s/2$ . Denote the fractional bandwidth as  $B_f = B_s/f_c$ .

- (a) We design an MVDR beamformer assuming that the interferer is at  $f_c$ . Assume that

$$INR \triangleq \sigma_I^2/\sigma_w^2 = 30 \text{ dB}. \quad (6.849)$$

Plot the array gain versus  $u_I/BW_{NN}$  over the range

$$0.5 \leq u_I/BW_{NN} \leq 2.5, \quad (6.850)$$

for  $B_f = 0, 0.1, 0.2$ , and  $0.4$ . Plot the beam patterns for several values of  $u_I$ .

- (b) Repeat part (a) for the case in which the MVDR beamformer is designed using the correct frequency spectrum of the interferer. Plot the beam patterns for several values of  $u_I$ .
- (c) We want to show that a frequency-spread interferer has the same effect as a cluster of narrowband interferers. Derive a formula that allows us to replace a single frequency spread interferer with  $M$  interferers clustered around  $u_I$ . Show how the number of interferers and their spacing is related to  $u_I$  and  $B_f$ .
- (d) Discuss the results in part (c) in terms of degrees of freedom available to the beamformer.

**Problem 6.3.8**

Consider a standard 10-element linear array. We implement the MPDR beamformer in (6.71), assuming the desired signal arrives from broadside. The interference consists of two plane-wave interferers at  $u_I = 0.30$  and  $0.50$  with an  $INR = 20$  dB (each). The additive white noise has spectral height  $\sigma_w^2$ . The signal actually arrives from  $u_a$ .

- (a) Plot the array gain versus  $u_a/BW_{NN}$  over the range  $0 \leq u_a/BW_{NN} \leq 0.25$  for  $SNR = -10$  dB,  $0$  dB,  $10$  dB, and  $20$  dB.
- (b) Plot the beam patterns for  $u_a = 0.02, 0.05$ , and  $0.1$ .
- (c) Discuss your results.

**Problem 6.3.9** (continuation; Problem 6.2.8)

Consider a standard 10-element linear array. We implement the MVQR beamformer derived in Problem 6.2.8.

The desired quiescent beam pattern is a Dolph-Chebychev beam pattern with  $-40$ -dB SLL. The signal arrives from broadside. The interference consists of a single plane-wave interferer with an  $INR = 10$  dB or  $20$  dB.

Plot the array gain versus  $u_I/BW_{NN}$  for the two  $INR$  levels.

Plot the beam patterns for  $u_I = 0.50, 0.30, 0.18, 0.09, 0.0433$ , and  $0.02$ . Compare your results to the results in Figures 6.13–6.16.

**Problem 6.3.10** (continuation; Problems 6.2.9 and 6.3.8)

Consider the same signal and interference model as in Problem 6.3.8. We use the MPQR beamformer in Problem 6.2.9 with a Dolph-Chebychev quiescent beam pattern with  $-40$ -dB SLL. Repeat Problem 6.3.9.

**Problem 6.3.11** (continuation; Problem 6.2.10)

Consider the MPQR beamformer in Problem 6.3.10. We add a second constraint,

$$\mathbf{C}_2^H \mathbf{v}_s \triangleq \mathbf{P}_{\overline{\mathbf{w}}_{dq}}^\perp \mathbf{v}_s = 1, \quad (6.851)$$

where  $\mathbf{P}_{\overline{\mathbf{w}}_{dq}}$  is the projection matrix onto  $\overline{\mathbf{w}}_{dq}$ .

- (a) Derive the optimum beamformer. Verify that the quiescent pattern is unchanged.
- (b) Repeat Problem 6.3.10 and compare your results.

**Problem 6.3.12**

As a modification to the MVDR beamformer, we can require both a distortionless output at  $\mathbf{k} = \mathbf{k}_s$  and a zero-order null at  $\mathbf{k} = \mathbf{k}_I$ . Assume that the noise spectral matrix is  $\mathbf{S}_n$ .

- (a) Find the minimum variance beamformer subject to the two constraints. Find the expression for the array gain  $A_{co}$ .
- (b) Specialize your result to a 10-element standard linear array. The desired signal arrives from broadside. Assume that the interference consists of a single plane wave at  $u_I$  with an *INR* that is a parameter. The additive white noise has a spectral height  $\sigma_w^2$ . Plot  $A_{co}$  versus  $u_I/BW_{NN}$  for *INRs* = 0 dB, 10 dB, 20 dB, and 30 dB. Compare your result to (6.28). Plot  $A_{co}/A_o$  versus  $u_I/BW_{NN}$  for the above *INRs*. Discuss your results.

**Problem 6.3.13**

Consider a standard 19-element hexagonal array in the  $xy$ -plane. The desired signal arrives at  $\theta_s = 0^\circ$ . Two plane-wave interferers arrive at

$$\begin{aligned} u_r &= 0.5, \phi = 0, \\ u_r &= 0.5, \phi = 30^\circ. \end{aligned} \quad (6.852)$$

Each interferer has an *INR* = 20 dB. Design an MPDR beamformer. Compute the array gain. Plot a contour plot of the beam pattern and pattern cuts through  $\phi = 0^\circ, 10^\circ, 20^\circ$ , and  $30^\circ$ .

**Problem 6.3.14**

Repeat Problem 6.3.13 for a standard 37-element hexagonal array.

**Problem 6.3.15**

Repeat Problem 6.3.14 for a standard 61-element hexagonal array.

**Problem 6.3.16**

Consider a standard 10-element linear array. The noise consists of three plane-wave interferers located in  $u$ -space at  $u_I$ ,  $u_I + \Delta u$ ,  $u_I - \Delta u$  plus additive sensor noise of height  $\sigma_w^2$ .

- (a) The three plane waves are uncorrelated and have equal power,  $\sigma_I^2/3$ . Assume that the three plane waves are in the sidelobe region. Find the MVDR beamformer (signal is at  $u_s = 0$ ) and compute the array gain as a function of  $u_I$  and  $\Delta u$ .
- (b) Plot the beam pattern for  $u_I = 0.3$  and  $\Delta u = 0.03$  and  $\Delta u = 0.003$ .
- (c) Discuss the behavior as  $\Delta u \rightarrow 0$  in terms of the condition number of  $[\mathbf{v}_I^H \mathbf{v}_I]$ .
- (d) Compare the result in parts (b) and (c) to a constrained MVDR beamformer with zero-order, first-order, and second-order null at  $u_I$ .
- (e) Repeat parts (a) and (b) for  $u_I = 0.2$  and  $\Delta = 0.04$ .

**Problem 6.3.17**

Consider a standard 37-element hexagonal array in the  $xy$ -plane. The interference consists of 10 plane-wave interferers distributed uniformly on a circle in  $u$ -space with radius  $u_{RI} = \sqrt{u_{xI}^2 + u_{yI}^2}$ . The interferers are uncorrelated equal power signals ( $\sigma_i^2 = \sigma_I^2/10$ ) and the additive noise has variance  $\sigma_w^2$ .

- (a) Derive the MVDR beamformer and compute the array gain.
- (b) Plot pattern cuts for  $u_{RI}$  in the sidelobe region and  $\sigma_I^2/\sigma_w^2 = 20$  dB.
- (c) Repeat part (b) for the outer main-lobe region.
- (d) Assume we have  $M$  uncorrelated equal power interferers with spectrum  $\sigma_I^2/M$ . Analyze the MVDR beamformer as  $M \rightarrow \infty$ .

## P6.4 Spatially Spread Interference

**Problem 6.4.1**

Consider a vertical standard 10-element linear array. Assume the noise consists of the surface noise model in Problem 5.3.1 with  $\alpha = 0.25$  plus additive white noise with spectrum height  $\sigma_w^2$ .

Calculate the array gain as a function of  $\theta_T$ , the target signal's angle of arrival measured from the vertical for  $INR$  values of 10 dB and 20 dB.

**Problem 6.4.2**

Repeat Problem 6.4.1 for the case of high surface noise:  $\alpha = 1$ .

**Problem 6.4.3**

Repeat Problem 6.4.1 for the layer noise model in Problem 5.3.2. Assume low layer noise:  $\alpha = 0.25$ .

**Problem 6.4.4**

Repeat Problem 6.4.3 for the case of high layer noise:  $\alpha = 1$ .

**Problem 6.4.5**

Consider the sector noise model in Figure 5.8. Denote the angle of the cone boundary with the  $xy$ -plane as  $\bar{\theta}_c$ ,  $S_o(\omega) = S_o$ . Assume that we have standard 10-element linear array along the  $x$ -axis and the signal is a plane wave arriving from  $[\theta_s, \psi_s = 0]$ . In addition, there is additive white noise ( $\sigma_w^2$ ).

- (a) Find the MVDR beamformer. Plot the resulting beam pattern for (i)  $\theta_s = 30^\circ, \bar{\theta}_c = 75^\circ, INR = 20$  dB; (ii)  $\theta_s = 30^\circ, \bar{\theta}_c = 60^\circ, INR = 20$  dB; (iii)  $\theta_s = 45^\circ, \bar{\theta}_c = 75^\circ, INR = 30$  dB.

- (b) Compute the array gain for the above cases.

**Problem 6.4.6**

Repeat Problem 6.4.5 for a standard  $10 \times 10$  rectangular array in the  $xy$ -plane.

**Problem 6.4.7**

Consider a standard 21-element linear array. Assume the noise spectrum corresponds to a complex AR(2) process plus additive white noise with spectral height  $\sigma_w^2$ .

- (a) Find the MVDR receiver for a signal located at  $u_s = 0.4$ .
- (b) Find the array gain for AR spectrum in Figure 6.19, assuming  $\sigma_w^2 = 0$ . Plot the beam pattern.
- (c) Repeat part (b) for AR spectrum in Figure 6.20, assuming  $\sigma_w^2 = 0$ .
- (d) Repeat part (b) for  $\sigma_{AR}^2/\sigma_w^2 = 20$  dB.
- (e) Compare your result in part (d) to the case of two plane-wave interferers located at  $u_{I1} = 0, u_{I2} = 0.8$ .

**Problem 6.4.8**

Consider the same linear array and noise model as in Problem 6.4.7. Assume  $u_s = 0$  and  $z_1 = |z_1| \exp(-0.15\pi)$  and  $z_2 = |z_2| \exp(+0.15\pi)$ . Assume the INR is 20 dB.

- (a) Plot the beam pattern of the MVDR receiver for  $|z_1| = |z_2| = 0.5, 0.9$  and 0.99.
- (b) Find the array gain for the above cases.

**Problem 6.4.9**

Consider a standard 10-element linear array. The signal is at  $u = 0$ . The interference has a flat spatial spectrum in one dimension:

$$S_I(u) = \frac{S_I}{2u_\Delta} \quad u_I - u_\Delta \leq u \leq u_I + u_\Delta. \quad (6.853)$$

The additive white noise has spectral height  $\sigma_w^2$ . Find the optimum beam pattern and compute the array gain for

$$(a) \quad u_I = 0.3, \quad u_\Delta = 0.1, \quad S_I/\sigma_w^2 = 20 \text{ dB}. \quad (6.854)$$

$$(b) \quad u_I = 0.2, \quad u_\Delta = 0.1, \quad S_I/\sigma_w^2 = 20 \text{ dB}. \quad (6.855)$$

$$(c) \quad u_I = 0.5, \quad u_\Delta = 0.2, \quad S_I/\sigma_w^2 = 40 \text{ dB}. \quad (6.856)$$

**Problem 6.4.10**

Consider a 32-element uniformly spaced linear array with  $d = \frac{\lambda_c}{8}$ . Assume that

$$\mathbf{S}_n(\omega_c) = \sigma_I^2(\omega_c) \operatorname{sinc}\left(\frac{\omega_c}{c}|d|\right) + \sigma_w^2 \mathbf{I}, \quad (6.857)$$

which is a mixture of isotropic and white noise. The signal and noise are narrowband.

- (a) Find the array gain as a function of  $u_s$ .

- (b) Plot the magnitude of the beam pattern for  $u_s = 0, 0.5$  and  $1.0$  and various  $INR$ .  
 (c) Plot the sensitivity function for the same values as in part (b).

## P6.5 Multiple Plane-wave Signals

### Problem 6.5.1

Consider the case of  $D$  plane-wave signals impinging on the array from  $\mathbf{k}_1, \mathbf{k}_2, \dots, \mathbf{k}_D$ . The noise consists of a single plane wave at  $\mathbf{k}_J$  plus white noise with spectral height  $\sigma_w^2$ . Thus,

$$\mathbf{S}_n = \mathbf{v}^H(\mathbf{k}_J) S_J \mathbf{v}(\mathbf{k}_J) + \sigma_w^2 \mathbf{I}. \quad (6.858)$$

- (a) Find the  $D \times N$  MVDR processor. Interpret your result.  
 (b) Is the result in part (a) the same as the  $(D+1) \times N$  MVDR processor for  $D+1$  plane-wave signals impinging on the array from  $\mathbf{k}_1, \mathbf{k}_2, \dots, \mathbf{k}_D, \mathbf{k}_J$ ? Justify your answer.

### Problem 6.5.2

Assume there are two signals impinging on an array in the presence of noise that is uncorrelated with the signals and has a spectral matrix  $\mathbf{S}_n(\omega)$ :

$$\mathbf{X}(\omega) = \mathbf{V}\mathbf{F}(\omega) + \mathbf{N}(\omega). \quad (6.859)$$

Create a 2-D signal subspace

$$\mathbf{X}_s(\omega) = \mathbf{V}^H \mathbf{X}(\omega). \quad (6.860)$$

- (a) Find the MMSE processor to estimate  $\mathbf{F}(\omega)$  using  $\mathbf{X}_s(\omega)$  as the input.  
 (b) Compare your result with (6.181).

### Problem 6.5.3

Consider a standard 10-element linear array. The frequency-domain snapshots are

$$\mathbf{X}(\omega) = \mathbf{V}\mathbf{F}(\omega) + \mathbf{W}(\omega), \quad (6.861)$$

where  $\mathbf{F}(\omega)$  is  $2 \times 1$  source-signal vector,

$$\mathbf{F}(\omega) = \begin{bmatrix} F_s(\omega) \\ F_I(\omega) \end{bmatrix}, \quad (6.862)$$

with spectral matrix

$$\mathbf{S}_f(\omega) = \begin{bmatrix} \sigma_s^2 & \sigma_s \sigma_I \rho \\ \sigma_s \sigma_I \rho^* & \sigma_I^2 \end{bmatrix}. \quad (6.863)$$

The array manifold matrix  $\mathbf{V}$  is known. The source signal  $\mathbf{F}(\omega)$  and additive-noise vector  $\mathbf{W}(\omega)$  ( $\mathbf{S}_w(\omega) = \sigma_w^2 \mathbf{I}$ ) are uncorrelated.

- (a) Find the MMSE processor to estimate  $F_s(\omega)$ .  
 (b) Assume the signal arrives from broadside with an  $SNR = 10$  dB. Plot the output  $SNR_o$  and the normalized MSE versus  $\psi_I$  for  $INRs = 10, 20$ , and  $30$  dB. Discuss your result.

**Problem 6.5.4**

Derive a “pure” eigenbeam receiver. In this case the  $D + 1$  sufficient statistics are the  $D + 1$  eigenbeams.

**Problem 6.5.5**

Consider the problem of finding the MMSE estimate for multiple plane-wave signals ( $D$  signals)

$$\mathbf{S}_x = \mathbf{V} \mathbf{S}_f \mathbf{V}^H + \mathbf{S}_n, \quad (6.864)$$

$$\mathbf{V} = [ \mathbf{v}_1 \mid \mathbf{v}_2 \mid \cdots \mid \mathbf{v}_D ]. \quad (6.865)$$

The resulting MMSE filter is

$$\mathbf{H}_o = (\mathbf{I} + \mathbf{S}_f \mathbf{V}^H \mathbf{S}_n^{-1} \mathbf{V})^{-1} \mathbf{S}_f \mathbf{V}^H \mathbf{S}_n^{-1}, \quad (6.866)$$

which reduces to

$$\mathbf{H}_o = \left( \mathbf{I} + \frac{\mathbf{S}_f}{\sigma_w^2} \mathbf{V}^H \mathbf{V} \right)^{-1} \frac{\mathbf{S}_f}{\sigma_w^2} \mathbf{V}^H, \quad (6.867)$$

for white noise.

Now consider the problem of finding the MMSE estimate of the first signal in the presence of  $D - 1$  interfering signals plus white noise. This will result in a  $1 \times N$  filter that is denoted as  $\mathbf{H}_1$ .

- (a) Find  $\mathbf{H}_1$ .
- (b) Prove  $\hat{f}_1(t) = y_1(t)$ .

**Problem 6.5.6**

The received waveform is an  $N \times 1$  vector,

$$\mathbf{X}(\omega) = \sum_{i=1}^{K_1} \mathbf{v}(\omega : \mathbf{k}_i^S) F_i(\omega) + \sum_{j=1}^{K_2} \mathbf{v}(\omega : \mathbf{k}_j^N) N_j(\omega) + \mathbf{W}(\omega), \quad (6.868)$$

where

$$\mathbf{F}(\omega) = \begin{bmatrix} F_1(\omega) \\ \vdots \\ F_{K_1}(\omega) \end{bmatrix}, \quad (6.869)$$

and  $\mathbf{S}_f(\omega)$  is the corresponding signal spectral matrix

$$\mathbf{N}(\omega) = \begin{bmatrix} N_1(\omega) \\ \vdots \\ N_{K_2}(\omega) \end{bmatrix}, \quad (6.870)$$

and  $\mathbf{S}_n(\omega)$  is the corresponding noise spectral matrix and  $\mathbf{W}(\omega)$  corresponds to a white random process with spectral matrix  $\sigma_w^2 \mathbf{I}$ .

Assume  $K_1 + K_2 < N$ . Define

$$\mathbf{V}_F = [ \mathbf{v}(\omega : \mathbf{k}_1^S) \mid \cdots \mid \mathbf{v}(\omega : \mathbf{k}_{K_1}^S) ] \quad (6.871)$$

and

$$\mathbf{V}_N = [ \mathbf{v}(\omega : \mathbf{k}_1^N) \mid \cdots \mid \mathbf{v}(\omega : \mathbf{k}_{K_2}^N) ]. \quad (6.872)$$

- (a) Find  $\mathbf{H}_W(\omega)$ , the whitening filter.  $\mathbf{H}_W(\omega)$  whitens the total noise input.
- (b) Define  $\mathbf{S}_W(\omega)$  as the total output of the whitening filter when the input is signal plus noise. Find the spectrum of  $\mathbf{S}_W(\omega)$ .
- (c) What is rank of signal-component spectral matrix?
- (d) Does the result in part (c) generalize to an arbitrary  $\mathbf{S}_n(\omega)$ ?

**Problem 6.5.7**

Consider the case of a scalar Gaussian process propagating along  $\mathbf{v}(\omega : \mathbf{k}_s)$ . Then

$$\mathbf{S}_f(\omega) = \mathbf{v}(\omega : \mathbf{k}_s) S_f(\omega) \mathbf{v}^H(\omega : \mathbf{k}_s). \quad (6.873)$$

- (a) Show that  $H_1(\omega)$ , the MMSE processor is

$$\mathbf{H}_1(\omega) = \mathbf{v}_s S_f(\omega) \mathbf{v}_s^H \left[ \sigma_w^2 \mathbf{I} + \mathbf{v}_s S_f(\omega) \mathbf{v}_s^H \right]^{-1}. \quad (6.874)$$

- (b) Show that  $H_1(\omega)$  reduces to

$$\mathbf{H}_1(\omega) = \mathbf{v}_s \left\{ \frac{1}{N} \frac{S_f(\omega)}{\frac{\sigma_w^2}{N} + S_f(\omega)} \right\} \mathbf{v}_s^H. \quad (6.875)$$

Sketch the optimum processor. Note that the optimal processor is an MVDR beamformer followed by the optimum scalar processor.

**Problem 6.5.8**

The frequency-domain snapshots at a standard 10-element linear array are

$$\mathbf{X}(\omega) = F(\omega) \mathbf{v}_\psi(\psi_1) + \alpha_2 F(\omega) \mathbf{v}_\psi(\psi_2) + \alpha_3 F(\omega) \mathbf{v}_\psi(\psi_3) + \mathbf{W}(\omega), \quad (6.876)$$

where  $F(\omega)$  is the Fourier transform of the signal whose spectrum is  $S_f(\omega)$ ,  $\alpha_2$  and  $\alpha_3$  are known complex parameters, and  $\mathbf{W}(\omega)$  is spatially white noise with spectral height  $\sigma_w^2$ . The signal is narrowband so  $\omega$  can be suppressed.

- (a) Find the linear processor that provides a MMSE estimate of  $F(\omega)$ .
- (b) The array  $SNR$  is defined as

$$ASN R = \frac{N S_f(\omega)}{\sigma_w^2}. \quad (6.877)$$

Assume  $\psi_1 = 0$ ,  $\psi_3 = -\psi_2$ , and  $\alpha_2 = 0.5\alpha_3$ . Plot the the output  $SNR_o$  and the MMSE error versus  $ASN R$  for several  $\alpha_2$  and  $\psi_2$ .

## P6.6 Mismatched MVDR and MPDR Beamformers

**Problem 6.6.1**

Consider a standard 10-element linear array with white noise interference. Assume that the optimum MPDR beamformer is steered to broadside ( $\mathbf{v}_m = \mathbf{1}$  and  $u_m = 0$ ).

- (a) Assume that the desired signal actually arrives from  $u_a$ . The input  $SNR$  is  $\sigma_s^2/\sigma_w^2$ . Plot  $A_{mpdr}$  versus  $u_a$  for various  $SNR$  (-10 dB to 30 dB).
- (b) Plot  $A_{mpdr}$  versus  $SNR$  for  $u_a = 0.25BW_{NN}$  and  $u_a = 0.0433BW_{NN}$ .

- (c) Assume that  $u_a$  is a random variable whose probability density is uniform  $[-u_1 \leq u_a \leq u_1]$ . Plot  $E[A_{mpdr}]$  versus  $SNR$  for  $u_1 = 0.0433BW_{NN}$ , and  $0.25BW_{NN}$ .
- (d) Assume  $u_a$  is a zero-mean Gaussian random variable whose standard deviation is given by (6.237). Repeat part (c).

**Problem 6.6.2** (continuation; Problem 6.6.1)

Consider a standard 10-element linear array. The interference consists of two plane-wave interferers at  $u = 0.29$  and  $0.45$ , each with an  $INR = 20$  dB. We design an optimum MPDR beamformer steered to broadside.

- (a) Repeat part (a) of Problem 6.6.1.
- (b) Repeat part (b) of Problem 6.6.1.
- (c) Add a third interferer at  $u_I = 0.25BW_{NN}$  ( $u_I = 0.1$ ). Repeat part (a) for  $u_a \leq 0.05$ .
- (d) Add diagonal loading with various  $LNR$ . Repeat part (c) for representative  $LNR$ .

**Problem 6.6.3**

Consider a standard 10-element linear array. Consider the multiple plane-wave MPDR beamformer. (It corresponds to the MVDR beamformer in (6.158), with  $\mathbf{S}_n$  replaced by  $\mathbf{S}_x$ .)

There are four plane-wave signals impinging on the array plus white noise. The beamformer is designed assuming the signals arrive from

$$u_{s1} = 0, \quad u_{s2} = 0.3, \quad u_{s3} = 0.5, \quad u_{s4} = -0.7. \quad (6.878)$$

Each signal has the same  $SNR$ . The actual signals arrive from

$$u_{a1} = u_a, \quad u_{a2} = 0.3 + u_a, \quad u_{a3} = 0.5 - u_a, \quad u_{a4} = -0.7 + u_a, \quad (6.879)$$

where  $|u_a| \leq 0.05$ .

- (a) Plot the output  $SNR_o$  versus  $u_a$  for signal 1 for  $SNR = -10$  dB,  $\dots$ ,  $30$  dB in  $10$ -dB steps.
- (b) Add diagonal loading. Repeat part (a) for representative  $LNR$ .

**Problem 6.6.4** (continuation; Problem 6.3.13)

Consider the same model and environment as Problem 6.3.13. The signal actually arrives from  $(\theta_a, \phi_a)$ .

- (a) Plot the array gain versus  $u_{ra} = \sin \theta_a$  for  $\phi_a = 0^\circ, 10^\circ, 20^\circ$ , and  $30^\circ$  and  $SNR = 0, 10$ , and  $20$  dB. Assume  $|u_{ra}| \leq 0.5$
- (b) Add diagonal loading. Repeat part (a) for various  $LNR$ .

**Problem 6.6.5** (continuation; Problem 6.3.13)

Consider the same model and environment as Problem 6.3.13. The plane of the array rotates slightly around the  $y$ -axis so that the angle between the plane of the array and the  $x$ -axis is  $\gamma_x$  degrees.

Plot the array gain versus  $\gamma_x$  for  $0 < \gamma_x < 5^\circ$ . Consider  $SNR = 0, 10$ , and  $20$  dB.

**Example 6.6.6** (continuation; Example 6.6.4)

Consider the same model as in Example 6.6.4.

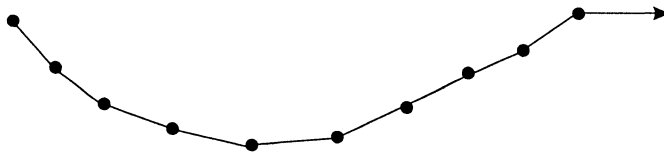


Figure 6.132 Towed array.

- (a) Assume the position perturbations are only in the  $z$ -direction. Repeat Example 6.6.4.
- (b) Assume the position perturbations occur only in the  $y$ -direction. Repeat Example 6.6.4.

In both parts, compare your results to the results in Example 6.6.4.

#### Problem 6.6.7

Consider a standard 10-element linear array. The signal arrives from broadside and two equal-power uncorrelated interferers arrive from  $u_I = 0.30$  and  $0.50$  with an  $INR = 20$  dB (each). Design an MPDR beamformer and calculate the array gain.

- (a) Assume the  $n$ th sensor fails. When the sensor fails, its output is set to zero. Calculate the resulting array gain for two cases:
  - (i) The remaining  $N - 1$  weights remain the same.
  - (ii) The MPDR weights are recomputed for the  $N - 1$  operational sensors.
 Consider different values of  $n$ .
- (b) Repeat part (a) for two sensor failures. Consider various sensor pairs.

#### Problem 6.6.8

Consider a standard 48-element towed linear array. The signal is a plane-wave signal arriving from broadside. There are two plane-wave interferers arriving from  $u_I = 3/48$  and  $5/48$  with a 30-dB  $INR$  (each).

When the vehicle towing the array turns, the array shape can be approximated as a segment of a circle in the  $xy$ -plane, as shown in Figure 6.132. The diameter of the circle measured in wavelengths is  $d_p$ .

Plot the array gain versus  $d_p$  (measured in wavelengths under two assumptions):

- (a) The MPDR weights do not change from their values calculated assuming a linear array.
- (b) The positions of sensors are known and the MPDR weights are recalculated.

#### Problem 6.6.9

Consider a standard 10-element linear array along the  $x$ -axis. The signal arrives from broadside and two plane-wave interferers arrive from  $u_I = 0.30$  and  $0.50$ . We use the array perturbation model in (6.242)–(6.247).

- (a) Consider independent gain and phase perturbations with standard derivation  $\sigma_g$  and  $\sigma_\phi$ , respectively. Plot the array gain versus  $SNR$  for various  $\sigma_g$  and  $\sigma_\phi$ . For  $SNR = -10$  dB, 0 dB, 10 dB, and 20 dB, plot a contour map showing array gain versus  $\sigma_g$  and  $\sigma_\phi$ .

- (b) Compare your results to those in Example 6.6.5. Discuss the relative importance of gain versus phase variations.

**Problem 6.6.10**

Consider a standard 10-element linear array with  $d = \lambda_c/2$  and white noise interference. Assume that the optimum MPDR beamformer is steered to  $\theta_m = 30^\circ$ .

- Assume that the desired signal arrives from  $30^\circ$ , but its frequency is  $f_c + f_a$ . The input SNR is  $\sigma_s^2/\sigma_w^2$ . Plot  $A_{mpdr}$  versus  $f_a$  for various SNR (-10 dB to 30 dB).
- Plot  $A_{mpdr}$  versus SNR for  $f_a = 0.2f_c$  and  $f_a = 0.4f_c$ .
- Assume that  $f_a$  is a random variable whose probability density is uniform  $[-f_1 \leq f_a \leq f_1]$ . Plot  $E[A_{mpdr}]$  versus SNR for  $f_1 = 0.04f_c, 0.10f_c, 0.20f_c$ .

**Problem 6.6.11: Frequency mismatch**

Consider a standard 10-element linear array designed for frequency  $f_c$ . A narrowband plane-wave signal at frequency  $f$  arrives from direction  $u_s$ . The interference is white noise. We define

$$f = f_c + f_\Delta, \quad (6.880)$$

and

$$b_f = \frac{f_\Delta}{f_c}. \quad (6.881)$$

- (a) Show that the array manifold vector  $\mathbf{v}_f$  can be written as

$$[\mathbf{v}_f]_n = \exp\left(j\pi\left(n - \frac{N-1}{2}\right)\right) u_f, \quad (6.882)$$

with

$$u_f \triangleq (1 + b_f)u. \quad (6.883)$$

- Design a MVDR beamformer for frequency  $f_c$ . Plot the array gain (normalized by the array gain when  $f_\Delta = 0$ ) versus  $u_s$  for  $b_f = 0.2, 0.4, 0.6$ , and  $0.8$ .
- Repeat part (b) for a MPDR beamformer.

**Problem 6.6.12: Broadband signal (continuation)**

Consider a standard 10-element linear array designed for frequency  $f_c$ . A plane-wave signal arrives from direction  $u_s$ . The signal has a flat frequency spectrum over the band  $f_c - B_s/2 \leq f \leq f_c + B_s/2$ . The interference is white noise. Define

$$B_f \triangleq \frac{B_s}{f_c}. \quad (6.884)$$

- Design a MVDR beamformer for frequency  $f_c$ . Plot the array gain versus  $u_s$  for  $B_f = 0.1, 0.2$ , and  $0.4$ .
- Repeat part (a) for a MPDR beamformer.

**Problem 6.6.13: Broadband interference**

Consider a standard 10-element linear array designed for frequency  $f_c$ . A narrowband plane-wave signal arrives from direction  $u_s$ .

There are two plane-wave interferers arriving from  $u_I = 0.30$  and  $0.50$  with an  $INR = 20$  dB (each). Each interferer has a flat frequency spectrum over the band

$$f_c - B_I/2 \leq f \leq f_c + B_I/2. \quad (6.885)$$

Define

$$B_{fI} \triangleq \frac{B_I}{f_c}. \quad (6.886)$$

- (a) Design a MVDR beamformer using the assumption that the interferers are narrowband. Evaluate the array gain for  $B_{fI} = 0, 0.1, 0.2$ , and  $0.4$ . Plot the beam patterns.
- (b) Let the DOA and the  $INR$  of the second interferer be a variable. Plot the array gain versus  $u_{I2}$  for various  $INR$ .
- (c) Design a MVDR beamformer using the actual spectral matrix  $\mathbf{S}_n(w)$  corresponding to the actual interferer spectra. The beamformer can only use complex weights (not complex filters). Evaluate the array gain for  $B_{fI}=0, 0.1, 0.2$ , and  $0.4$ . Plot the resulting beam patterns. Explain your results.

#### Problem 6.6.14

Consider a standard 10-element linear array whose input is given by (6.589). The various output powers  $P_{do}$ ,  $P_{io}$ , and  $P_{no}$  are given by (6.593), (6.597), and (6.598), respectively. The input  $SNR$  is  $\sigma_s^2/\sigma_w^2$ . The input  $INR$  is  $\sigma_I^2/\sigma_w^2$ .

- (a) Assume  $u_I = 0.3$ . Plot  $P_{do}$ ,  $P_{io}$ ,  $P_{no}$ , and  $SNR_o$  versus  $|\rho|$  for various  $SNR$  and  $INR$ . Does the phase of  $\rho$  affect any of the results?
- (b) Now assume that diagonal loading is used with  $\sigma_L^2$  added to  $\sigma_w^2$  for purposes of computing  $\mathbf{S}_x^{(L)}$ . Use  $\mathbf{S}_x^{(L)}$  to determine the  $\mathbf{w}_{mpdr,dl}$ . Repeat part (a) for various  $\sigma_L^2/\sigma_w^2$ . Note that  $\mathbf{S}_x$  is still given by (6.587).

#### Problem 6.6.15 (continuation)

Repeat Problem 6.6.14 for  $u_I = 0.18$ .

## P6.7 LCMV and LCMP Beamformers

#### Problem 6.7.1

Consider a standard 10-element linear array with white noise interference. Compare the performance using directional, derivative, and eigenvector constraints in a LCMP beamformer. In each case, utilize three constraints and add diagonal loading. The  $LNR$  is a design parameter. Show the MPDR-DL results for comparison.

- (a) Consider two sets of directional constraints. The first set is at  $u_1 = 0$ ,  $u_2 = 0.0433$ , and  $u_3 = -0.0433$ . The second set is  $u_1 = 0$ ,  $u_2 = 0.1$ , and  $u_3 = -0.1$ . For each set we use the  $\mathbf{g}$  given by (6.292) and (6.294). Plot  $SNR_o$  versus  $u_a/BW_{NN}$  for various  $SNR$  (0 dB, 10 dB, 20 dB). Plot the corresponding beam patterns.
- (b) Repeat part (a) for the derivative constraints in (6.312). Utilize the  $\mathbf{g}$  given by (6.313) and (6.314).
- (c) Repeat part (a) for three eigenvector constraints where we try to match a conventional beam pattern between  $\pm 0.10$ .
- (d) Compare your results and develop some design guidelines.

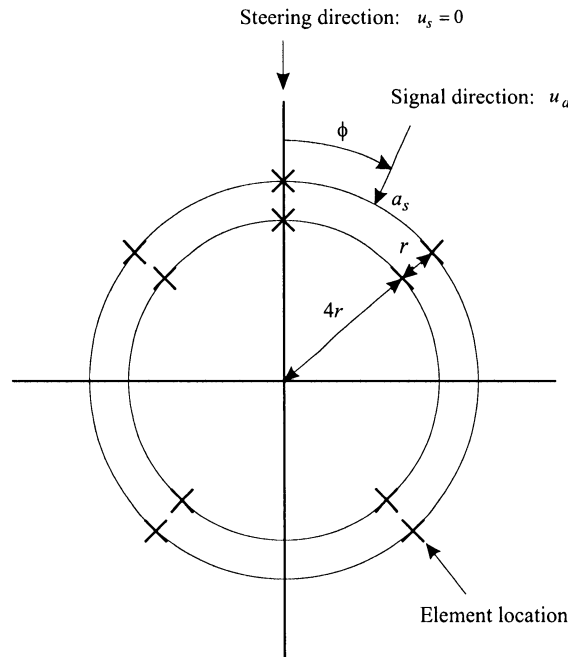


Figure 6.133 Planar dual array.

**Problem 6.7.2** (continuation)

Repeat Problem 6.7.1 for the case of a single plane-wave interferer ( $INR = 0, 10, 20$  dB) in the sidelobe region ( $u_I = 0.3$ ).

**Problem 6.7.3** (continuation)

Repeat Problem 6.7.2 for the case in which the DOA of the interferer is a variable. Study the behavior as  $u_I$  moves from the sidelobe region into the main-lobe region.

**Problem 6.7.4** (continuation; Problem 6.7.1)

Repeat Problem 6.7.1 for the case of two uncorrelated plane-wave interferers at  $u_{I1} = 0.30$  and  $u_{I2} = -0.50$ . The interferers are equal power ( $INR = 0, 10, 20$  dB each).

**Problem 6.7.5** (continuation)

Repeat Problem 6.7.4 for the case of correlated interferers. Consider  $|\rho| = 0, 0.5, 0.9, 0.95$ , and  $1.0$ .

**Problem 6.7.6** [Ste83]

Consider the 10-element planar dual ring array shown in Figure 6.133. Compare the performance using directional and derivative constraints. The array is steered to  $\phi = 0$ . The signal arrives at  $\phi_s$ . The interference consists of isotropic noise.

- (a) Use three directional constraints at  $\phi = -5^\circ, 0$ , and  $+5^\circ$ . Use a  $\mathbf{g}$  vector corresponding to a flat response and a conventional response. Plot the  $SNR_o$  (in dB) versus  $\phi$  for input  $SNR = -12$  dB,  $-6$  dB,  $0$  dB,  $6$  dB, and  $r/\lambda = 0.2$ . Discuss your

results.

- (b) Use three derivative constraints,

$$\mathbf{C} = \begin{bmatrix} \mathbf{v}(0) & \mathbf{d}_\phi(0) & \mathbf{d}_{\phi\phi}(0) \end{bmatrix}, \quad (6.887)$$

where  $\mathbf{d}_\phi$  denotes the derivative with respect to  $\phi$  and  $\mathbf{d}_{\phi\phi}$  denotes the second derivative.

In the first case,

$$\mathbf{g}^H = \begin{bmatrix} 1 & 0 & 0 \end{bmatrix}, \quad (6.888)$$

so the first two derivatives are constrained to equal zero at  $\phi_s = 0$ , the steering direction.

In the second case, match the derivatives of a conventional beamformer.

$$\mathbf{g}^H = \begin{bmatrix} 1 & \frac{\mathbf{d}_\phi^H(0)\mathbf{v}(0)}{N} & \frac{\mathbf{d}_{\phi\phi}^H(0)\mathbf{v}(0)}{N} \end{bmatrix}, \quad (6.889)$$

Repeat the plot in part (a). Compare the results with part (a).

- (c) The implementation of directional and derivative constraints requires the calculation of  $[\mathbf{C}^H \mathbf{S}_x \mathbf{C}]^{-1}$ . The condition number of a matrix is

$$\text{Condition number} = \frac{\lambda_{\max}}{\lambda_{\min}}. \quad (6.890)$$

Plot the condition number versus  $r/\lambda$  ( $0 \leq r/\lambda \leq 0.30$ ) for three directional constraints at  $1^\circ$ ,  $3^\circ$ , and  $5^\circ$  and derivative constraints. Discuss the implication of your results.

### Problem 6.7.7 [Jab86a],[Jab86b]

For directional and derivative constraints, an easy technique for constructing  $\mathbf{B}$  is to treat each column of  $\mathbf{C}$  successively. Consider a standard  $N$ -element linear array and assume that  $\mathbf{C}$  is given by (6.291). First pass  $\mathbf{X}(\omega)$  through the bidiagonal  $(N-1) \times N$  matrix  $\mathbf{B}_1^H$ ,

$$\mathbf{B}_1^H = \begin{bmatrix} 1 & -1 & & & \\ & 1 & -1 & & \mathbf{0} \\ & & 1 & -1 & \\ & 0 & & \ddots & \ddots \\ & & & & 1 & -1 \end{bmatrix}. \quad (6.891)$$

Then,

$$\mathbf{X}_1(\omega) = \mathbf{B}_1^H \mathbf{X}(\omega) \quad (6.892)$$

will not contain any components along  $\mathbf{v}(\psi_m)$ .

Then pass  $\mathbf{X}_1(\omega)$  through the bidiagonal  $(N-2) \times (N-1)$  matrix  $\mathbf{B}_2^H$ ,

$$\mathbf{B}_2^H = \begin{bmatrix} 1 & -e^{-j\psi_1} & & & & \\ & 1 & -e^{-j\psi_1} & & \mathbf{0} & \\ & & 1 & -e^{-j\psi_1} & & \\ & 0 & & \ddots & \ddots & \\ & & & & 1 & -e^{-j\psi_1} \end{bmatrix}, \quad (6.893)$$

where  $\psi_1 = \psi_m + \Delta\psi$ .

Then,

$$\mathbf{X}_2(\omega) = \mathbf{B}_2^H \mathbf{X}_1(\omega) \quad (6.894)$$

will not contain any components along  $\mathbf{v}(\psi_1)$ .

Finally, pass  $\mathbf{X}_2(\omega)$  through the bidiagonal  $(N - 3) \times (N - 2)$  matrix  $\mathbf{B}_3^H$ ,

$$\mathbf{B}_3^H = \begin{bmatrix} 1 & -e^{-j\psi_2} & & & & \\ & 1 & -e^{-j\psi_2} & & & \mathbf{0} \\ & & 1 & -e^{-j\psi_2} & & \\ & & & \ddots & \ddots & \\ \mathbf{0} & & & & & 1 & -e^{-j\psi_2} \end{bmatrix}, \quad (6.895)$$

where  $\psi_2 = \psi_m - \Delta\psi$ .

Then,

$$\mathbf{Z}(\omega) = \mathbf{B}_3^H \mathbf{X}_2(\omega) = \mathbf{B}_3^H \mathbf{B}_2^H \mathbf{B}_1^H \mathbf{X}(\omega) \quad (6.896)$$

will be orthogonal to the constraint subspace.

The advantage of this approach is that the matrices are sparse, which saves computation. A possible disadvantage is that

$$\mathbf{B}^H \mathbf{B} \neq \mathbf{I}. \quad (6.897)$$

- (a) Consider a standard 10-element linear array. Implement a LCMP beamformer using three directional constraints with  $\Delta\psi = 0.25BW_{NN}$ . Assume there is a single plane-wave interferer at  $u_I = 0.3$  ( $INR = 0, 10, 20$  dB). The signal arrives from  $u_a$ . ( $SNR = 0, 10, 20$  dB). Plot the array gain versus  $u_a/BW_{NN}$  for  $0 \leq u_a/BW_{NN} \leq 0.25$ .
- (b) Discuss the implications of (6.897).

#### Problem 6.7.8 (continuation)

The same technique can be used for derivative constraints. Pass  $\mathbf{X}_1(\omega)$  through the tridiagonal  $(N - 2) \times N$  matrix  $\mathbf{B}_2^H$ ,

$$\mathbf{B}_2^H = \begin{bmatrix} -1 & 2 & -1 & & & & \mathbf{0} \\ & -1 & 2 & -1 & & & \\ & & -1 & 2 & -1 & & \\ & & & \ddots & \ddots & \ddots & \\ \mathbf{0} & & & & & -1 & 2 & -1 \end{bmatrix}. \quad (6.898)$$

Then

$$\mathbf{X}_2(\omega) = \mathbf{B}_2^H \mathbf{B}_1^H \mathbf{X}(\omega), \quad (6.899)$$

where  $\mathbf{B}_1^H$  is defined in (6.891), contains no components in the constraint space.

To include the second derivative constraint in (6.310) with  $\psi = 0$ , use the  $(N - 3) \times N$  matrix  $\mathbf{B}_3^H$ ,

$$\mathbf{B}_3^H = \begin{bmatrix} -1 & 3 & -3 & 1 & & & & \mathbf{0} \\ & -1 & 3 & -3 & 1 & & & \\ & & -1 & 3 & -3 & 1 & & \\ & & & \ddots & \ddots & \ddots & \ddots & \\ \mathbf{0} & & & & & -1 & 3 & -3 & 1 \end{bmatrix}. \quad (6.900)$$

Then,

$$\mathbf{Z}(\omega) = \mathbf{B}_3^H \mathbf{B}_2^H \mathbf{B}_1^H \mathbf{X}(\omega), \quad (6.901)$$

contains no components in the constraint space.

- (a) Consider a standard 10-element linear array. Repeat part (b) of Problem 6.7.2.
- (b) Discuss the implications of (6.897).

### Problem 6.7.9

Analyze the behavior of a LCMP-GSC beamformer in which fixed nulls are placed in the direction of strong interferers whose direction has been previously determined. Implement the beamformer as a GSC.

Consider a standard 20-element linear array. The nominal signal direction is broadside. There are four uncorrelated plane-wave interferers at  $u_{I1} = 0.30$  ( $INR = 40$  dB),  $u_{I2} = 0.50$  ( $INR = 30$  dB),  $u_{I3} = 0.70$  ( $INR = 50$  dB),  $u_{I4} = -0.50$  ( $INR = 10$  dB).

There is an additional interferer at  $u_I = -0.3$  (variable  $INR$ ).

- (a) Design a LCMP-GSC beamformer in which the second through fifth columns of  $\mathbf{C}$  force perfect nulls on the four interferers. Calculate the array for various  $INR$  of the additional interferer. Compare your results to a single distortionless constraint MPDR beamformer.
- (b) Assume that the location of the interferers has been estimated and that the error in the estimate is a zero-mean Gaussian random variable with standard deviation  $\sigma_e$  (in  $u$ -space). The estimate associated with each interferer is independent. Use a Monte Carlo procedure to evaluate the loss in array gain for several  $\sigma_e$ . How can you make the beamformer more robust to estimation errors?

### Problem 6.7.10

Consider a standard 21-element linear array. The desired quiescent pattern is a Dolph-Chebychev pattern with  $-40$ -dB SLL.

The nominal signal DOA is broadside. The actual signal arrives from  $u_a$  where  $u_a$  is a uniform random variable,  $|u_a| \leq 0.1$ . Implement a LCMP-DL beamformer using a quiescent pattern constraint and diagonal loading.

There are two uncorrelated interferers arriving from  $u_{I1}$  and  $u_{I2}$ . Consider  $INRs$  of 10, 20, and 30 dB.

- (a) Assume  $u_{I1} = 3/21$  and  $u_{I2} = -3/21$ . Plot the array gain versus  $SNR$  for the three  $INR$ . Use appropriate loading. Plot the beam patterns. Explain the behavior of the beamformer.
- (b) Repeat part (a) for  $u_{I1} = 3/21$  and  $u_{I2} = -5/21$ .

### Problem 6.7.11 (continuation; Problem 6.7.10)

Consider a standard 21-element linear array. The desired quiescent pattern is a Dolph-Chebychev pattern with  $-40$ -dB SLL. Use the same signal and interference model as in Problem 6.7.10.

Consider the following constraints:

- (i)  $\mathbf{w}_{dq}/\|\mathbf{w}_{dq}\|^2$  is the only constraint.
- (ii)  $\mathbf{w}_{dq}/\|\mathbf{w}_{dq}\|^2$  plus first- and second-order derivative constraints. Use an appropriate diagonal loading level.

- (a) Repeat part (a) of Problem 6.7.10.
- (b) Repeat part (b) of Problem 6.7.10.
- (c) Compare your results to those in Problem 6.7.10.

**Problem 6.7.12**

Consider a standard 21-element linear array. The nominal signal arrival angle is  $u_s = 0$ . The actual signal arrival angle is  $u_a$ , where  $u_a$  is a random variable with uniform probability density,  $0 \leq |u_a| \leq 0.1$ . The desired quiescent beam pattern is a Dolph-Chebychev beam pattern with -40-dB SLL.

Use the constraints in (6.416) and diagonal loading.

- (a) Assume there are four plane-wave interferers:

$$\begin{aligned} u_I1 &= 0.3, & INR &= 50 \text{ dB}, \\ u_I2 &= -0.4, & INR &= 40 \text{ dB}, \\ u_I3 &= 0.5, & INR &= 30 \text{ dB}, \\ u_I4 &= -0.6, & INR &= 20 \text{ dB}. \end{aligned} \quad (6.902)$$

Use a total of three constraints,  $\bar{\mathbf{w}}_{dq}$ , and two eigenvectors. Choose an appropriate  $LNR$ . Plot the expected value of the array gain versus  $SNR$ .

- (b) Let the number of eigenvectors constraints be a design parameter. Repeat part (a). Explain your results. How would they change if the number of interferers or their strength changed.

**Problem 6.7.13** (continuation; Problem 6.7.12)

Consider a standard 21-element linear array. Use the quiescent pattern technique and investigate how the choice of the quiescent pattern affects the performance. Consider the following quiescent patterns:

- (i) Hann
- (ii) Hamming
- (iii) Blackman-Harris
- (iv) Dolph-Chebychev (-20-dB SLL)
- (v) Dolph-Chebychev (-30-dB SLL)
- (vi) Taylor (-30-dB SLL,  $\bar{n} = 6$ )

Repeat Problem 6.7.12.

## P6.8 Eigenvector Beamformers

**Problem 6.8.1**

Consider a standard 10-element array. The nominal signal direction is broadside. The actual signal arrives from  $u_a$ , where  $|u_a| \leq 0.1$  with an  $SNR = -10, 0, 10$ , or  $20$  dB. There are two equal-power uncorrelated interferers at  $u_I = 0.29$  and  $0.45$ . Consider  $INRs$  of  $0, 10, 20$ , and  $30$  dB.

Use an eigenspace beamformer and plot the array gain versus  $u_a/BW_{NN}$  for three scenarios.

- (a) The dimension of the  $S + I$  subspace is correctly estimated at 3. Plot the array gain versus  $u_a/BW_{NN}$ . Note that the eigenspace space is based on the actual  $u_a$ . Consider the  $SNR$  and  $INR$  values specified above.

- (b) The dimension of the  $S + I$  subspace is underestimated at 2. The eigenspace consists of the eigenvectors with the two largest eigenvalues. Repeat part (a).
- (c) The dimension of the  $S + I$  subspace is overestimated at 4. One eigenvector due to the white noise is added to the eigenspace in part (a). Repeat part (a).
- (d) Compare your results in parts (a)–(c).

**Problem 6.8.2** (continuation; Problem 6.8.1)

Consider the same model as in Problem 6.8.1 except there are four interferers:

$$\begin{aligned} u_{I1} &= 0.29, & INR &= 30 \text{ dB}, \\ u_{I2} &= 0.45, & INR &= 20 \text{ dB}, \\ u_{I3} &= 0.55, & INR &= 10 \text{ dB}, \\ u_{I4} &= -0.50, & INR &= 10 \text{ dB}, \end{aligned} \quad (6.903)$$

The  $SNR$  varies from  $-10$  dB to  $30$  dB in  $10$ -dB steps. Consider eigenspace dimensions of 4, 5, and 6. Repeat Problem 6.8.1. Discuss your results.

**Problem 6.8.3** (continuation; Problem 6.8.2)

Consider the model as in Problem 6.8.2. Impose second-order derivative constraints in (6.464). Repeat Problem 6.8.2 for the case in which the eigenspace dimension is 5.

**Problem 6.8.4**

Consider a 10-element uniform linear array with  $d = \lambda/4$ . The nominal signal direction is broadside. The interference consists of isotropic noise and white noise. Define

$$INR_{ISO} = \sigma_{ISO}^2 / \sigma_w^2.$$

- (a) Assume the signal arrives from broadside. Consider  $INR_{ISO} = 0, 10, 20$ , and  $30$  dB. Plot the array gain versus the dimension of the eigenspace for the indicated  $INR_{ISO}$ .
- (b) Now assume the signal arrives from  $u_a$  where  $|u_a| \leq 0.1$ . Plot the array gain versus  $u_a/BW_{NN}$  for the indicated  $INR_{ISO}$ . Choose the dimension based on the results in part (a).
- (c) Repeat parts (a) and (b) for the cross-spectral beamformer in Section 6.8.2.

**Problem 6.8.5** (continuation)

Consider the same model and isotropic noise environment as in Problem 6.8.4. There are also two equal-power uncorrelated plane-wave interferers at  $u_I = -0.25$  and  $0.3$  with  $INRs$  that vary from  $0$  dB to  $30$  dB in  $10$ -dB steps.

Repeat Problem 6.8.4.

**Problem 6.8.6**

Consider a standard 10-element array. The steering direction is broadside ( $u_s = 0$ ). The interference consists of three plane waves,

$$\begin{aligned} u_{I1} &= 0.30, & INR &= 20 \text{ dB}, \\ u_{I2} &= -0.50, & INR &= 25 \text{ dB}, \\ u_{I3} &\text{ is variable,} & INR &= 30 \text{ dB}. \end{aligned} \quad (6.904)$$

The  $SNR$  is  $10$  dB. We use  $D_m = 4$  and  $15$  dB of diagonal loading. Read [CP97] or [CPL98]. Implement the robust DMR algorithm.

Plot the output  $SNR_o$  versus  $u_{I3}$ .

**Problem 6.8.7**

Consider a standard 32-element linear array.

The signal is a plane wave arriving from  $u_a = 0.01$ . There are four interferers at:

$$\begin{aligned} u_{I1} &= 5/32, \quad INR = 20 \text{ dB}, \\ u_{I2} &= 8/32, \quad INR = 30 \text{ dB}, \\ u_{I3} &= 13/32, \quad INR = 20 \text{ dB}, \\ u_{I4} &= -17/32, \quad INR = 30 \text{ dB}. \end{aligned} \quad (6.905)$$

- (a) Design an eigenspace beamformer and plot the array gain versus  $SNR$ . Plot the beam pattern for  $SNR = 10$  dB.
- (b) Assume there are eight interferers. The location in  $u$ -space of the  $i$ th interferer is a uniform random variable  $(-1 \leq u_i \leq 1)$ ,  $i = 1, \dots, 8$ . The location random variables are statistically independent. The  $INR$  of each interferer is one of five values, 0, 10, 20, 30, 40 dB with equal probability. The  $INR$  is independent of the location.

Design an eigenspace beamformer. Specify the assumptions you use in the design.

Find the array gain and plot the beam pattern for a single trial.

- (c) Run 50 trials of part (b) and compute the average array gain.

## P6.9 Beamspace (BS) Beamformers

**Problem 6.9.1** (continuation; Example 6.9.1)

Consider a standard 32-element linear array and a  $7 \times 32$  beamspace matrix using conventional beams. The signal is a plane-wave signal arriving from  $u_s$  where  $|u_s| \leq 0.25BW_{NN}$ . The signal arrival direction  $u_s$  is known to the beamformer. The interferers consist of two equal-power uncorrelated plane-wave interferers at  $u_I = 3/32$  and  $5/32$ .

- (a) Find the optimum beamspace MPDR beamformer. Compute the array gain and compare it to the result in Example 6.9.1. Discuss your results.
- (b) Discuss various ways to improve performance and evaluate one of them.

**Problem 6.9.2** (continuation; Example 6.9.2)

Consider the same model and environment as in Example 6.9.2. Design a LCMP beamformer using second-order derivative constraints and diagonal loading.

- (a) Plot the array gain versus  $u_a$  and compare the results to those in Figure 6.84.
- (b) Add three out-of-sector interferers at  $u_I = -11/32, 9/32$ , and  $15/32$ , each with an  $INR$  of 20 dB. Plot the array gain versus  $u_a$  and compare the results to part (a).

**Problem 6.9.3** (continuation; Example 6.9.2)

Consider the model in Example 6.9.2 except we use Dolph-Chebychev beams with  $-40$ -dB SLL to form  $\mathbf{B}_{no}^H$  and orthonormalize them to form  $\mathbf{B}_{bs}^H$ .

- (a) Repeat Example 6.9.2 and compare your results to Figure 6.84.
- (b) Repeat Problem 6.9.2 and compare your results.

**Problem 6.9.4** (continuation; Example 6.9.6)

Consider a standard 32-element linear array and a  $7 \times 32$  beampspace matrix. Assume there are 10 uncorrelated interferers at  $3/32, 7/32, 11/32, 15/32, 19/32$  and  $-5/32, -9/32, -13/32, -17/32, -21/32$ . Each interferer has a 20-dB *INR*.

Consider various beampspace matrices such as:

- (i) Conventional beams.
- (ii) Dolph-Chebychev (-30-dB SLL, -40-dB SLL) beams.
- (iii) Taylor beams.

Design an MPDR beamformer for a signal arriving from  $u_s = 0$ . Evaluate the array gain for the various beampspace matrices. Compare the result to the array gain for element-space MPDR.

**Problem 6.9.5** (continuation; Example 6.9.2)

Consider a standard 32-element linear array and the  $7 \times 32$  beampspace matrix given in Example 6.9.1. The interference environment is the same as in Example 6.9.2. Use an LCMP beampspace beamformer with a quiescent pattern constraint and fixed diagonal loading. The desired quiescent beam corresponds to  $\cos^6(\pi\tilde{n}/N)$  weighting.

- (a) Plot the array gain versus  $u_a/BW_{NN}$  for an *SNR* = 0 and 10 dB and several levels of diagonal loading.
- (b) Compare your results to those in Figure 6.84. Suggest some design guidelines.

**Problem 6.9.6**

Consider a standard 32-element linear array and a  $6 \times 32$  beampspace matrix. The beam sector is centered at broadside. The rows of the beampspace matrix are conventional beams with steering directions,

$$u_s = \pm 1/32, \pm 3/32, \pm 5/32. \quad (6.906)$$

The interference consists of two equal-power uncorrelated plane-wave interferers at  $4/32$  and  $6/32$ . Consider *INRs* of 10, 20, and 30 dB. Consider *SNRs* of 0, 10 dB, and 20 dB.

- (a) Evaluate the performance of an MPDR beamformer. Assuming no signal mismatch. Plot the beam pattern and evaluate the array gain. Compare your result to the results in Example 6.9.1.
- (b) Consider the case of signal mismatch where  $|u_a| \leq 1/32$ . Use an appropriate level of fixed diagonal loading. Plot the array gain versus  $u_a/BW_{NN}$ . Compare your result to the results in Example 6.9.2.
- (c) Assume the signal arrives from  $u_a$  where  $|u_a| \leq 1/32$ . We estimate  $u_a$ . We assume that the estimate  $\hat{u}_a$  is unbiased and its standard deviation is given by (6.237)

$$(E [|\hat{u}_a - u_a|^2])^{1/2} = \frac{4}{N} \left( \frac{3}{8K} \left[ \frac{1}{ASNR} + \frac{1}{ASNR^2} \right] \frac{1}{1 - 1/N^2} \right)^{1/2}. \quad (6.907)$$

We construct a MPDR beamformer steered at  $\hat{u}_a$ . Evaluate the performance. Plot the array gain versus  $u_a$  for representative *SNR*. Plot the array gain versus *SNR* for representative  $u_a$ . Use  $K/N = 2$  and  $K/N = 10$ .

**Problem 6.9.7** (continuation; Problem 6.9.6)

Consider the same model as in Problem 6.9.5. Define a quiescent beam corresponding to a  $\cos^5(\pi n/N)$  weighting. We construct a beamformer that satisfies the constraint

$$\bar{\mathbf{w}}_{dq}^H \mathbf{w} = 1. \quad (6.908)$$

- (a) Repeat part (a) of Problem 6.9.6.
- (b) Repeat part (b) of Problem 6.9.6.
- (c) Design a beamspace LCMP beamformer using the quiescent pattern constraint and appropriate fixed loading. Plot the array gain versus  $u_a/BW_{NN}$ . Compare your result to the results in Example 6.9.2 and Problem 6.9.6.

**Problem 6.9.8**

Consider a standard 32-element linear array and a  $5 \times 32$  beamspace matrix centered at broadside. The rows of the beamspace matrix are conventional beams with steering directions,

$$u_s = 0, \pm 2/32, \pm 4/32. \quad (6.909)$$

The interference consists of two equal-power uncorrelated plane-wave interferers at  $3/32$  and  $5/32$ . Consider  $INRs$  of 10, 20, 30 dB. Consider  $SNRs$  of 0, 10, and 20 dB.

- (a) Evaluate the performance of a MPDR beamformer assuming no signal mismatch. Plot the beam pattern and evaluate the array gain. Compare your result to the result in Example 6.9.1.
- (b) Repeat part (a) for signal mismatch.

**Problem 6.9.9** (continuation; Problem 6.9.8)

Consider the same model as in Problem 6.9.8. Consider two quiescent beam patterns:

- (i) Blackman-Harris
- (ii)  $\cos^4(\pi n/N)$

- (a) Construct a beamformer that satisfies the constraint,

$$\bar{\mathbf{w}}_{dq}^H \mathbf{w} = 1 \quad (6.910)$$

and uses fixed diagonal loading with appropriate  $LNR$ . Consider the signal mismatch problem where  $|u_a| \leq 1/32$ . Plot the array gain versus  $u_a/BW_{NN}$ . Compare your results to the results in Example 6.9.2.

- (b) Design a beamspace LCMP beamformer using the a quiescent pattern constraint. Repeat part (a).
- (c) Discuss your results and suggest design guidelines.

**Problem 6.9.10**

Consider a standard 32-element linear array and a  $4 \times 32$  beamspace matrix centered at broadside. The rows of the beamspace matrix are conventional beams with steering directions,

$$u_s = \pm 1/32, \pm 3/32. \quad (6.911)$$

The interference consists of two equal power uncorrelated plane-wave interferers at  $2/32$  and  $4/32$ . We consider  $INRs$  of 10, 20, 30 dB. We consider  $SNRs$  of 0, 10, and 20 dB.

Evaluate the performance of a MPDR beamformer assuming no signal mismatch. Plot the beam pattern and evaluate the array gain. Compare your result to the results in Example 6.9.1.

**Problem 6.9.11**

Consider the same model as in Problem 6.9.10. Consider a quiescent beam pattern of  $\cos^3(\pi n/N)$ .

- (a) Construct a beamformer that satisfies the constraint,

$$\bar{\mathbf{w}}_{dq}^H \mathbf{w} = 1 \quad (6.912)$$

and uses fixed diagonal loading with appropriate  $LNR$ . Consider the signal mismatch problem where  $|u_a| \leq 1/32$ . Plot the array gain versus  $u_a/BW_{NN}$ . Compare your results to the results in Example 6.9.2.

- (b) Discuss your results. What are the limitations of this low-dimensional beamspace?

**Problem 6.9.12**

As an alternative to eigenspace processing, consider the following beamspace algorithm.

In order to construct the beamspace matrix, scan a conventional beam over  $u$ -space with a scan step size of  $2/N$ . Detect the presence or absence of the a signal (or interferer) at each scan location and estimate its power. If the  $SNR$  exceeds 10 dB, form a conventional beam steered at it and use that beam as a row in the beamspace matrix. For the beamspace sector centered at  $u_s = 0$ , always include a beam centered at  $u_s = 0$ . Then form a MPDR beamformer in beamspace.

Consider a standard 32-element linear array and a  $N_{bs} \times N$  beamspace matrix. The signal is a plane wave with an  $SNR = 10$  dB arriving from  $u_a = 0.01$ .

- (a) Assume that the scan detects four interferers at:

$$\begin{aligned} u_{I1} &= 5/32, & INR &= 20 \text{ dB}, \\ u_{I2} &= 8/32, & INR &= 30 \text{ dB}, \\ u_{I3} &= 13/32, & INR &= 20 \text{ dB}, \\ u_{I4} &= -17/32, & INR &= 30 \text{ dB}. \end{aligned} \quad (6.913)$$

Form a  $5 \times 32$  beamspace matrix and then use an MPDR beamformer in beamspace. Find the array gain and plot the beam pattern. Compare your result to the result in Problem 6.8.7 and to an element-space beamformer.

- (b) Assume there are eight interferers. The location in  $u$ -space of the  $i$ th interferer is a uniform random variable  $(-1 \leq u_i \leq 1)$ ,  $i = 1, \dots, 8$ . The location random variables are statistically independent. The  $INR$  of each interferer is one of five values; 0, 10, 20, 30, 40 dB with equal probability. The  $INR$  is independent of the location. (Note that a 0-dB interferer will not be detected.) Find the array gain and plot the beam pattern for a single trial. Compare your result to the result in Problem 6.8.7 and to an element-space beamformer. Use the same data set.
- (c) Run 50 trials of part (b) and compute the average array gain.

**Problem 6.9.13** (continuation; Example 6.9.1)

Consider a standard 32-element linear array and a  $7 \times 32$  beamspace matrix. The rows of the beamspace matrix are determined adaptively.

Each row of the beamspace processor is an MPDR beamformer with a distortionless constraint in its steering direction. Assume that the beamspace beams can be formed during a period in which there are no signals or interferers arriving in the beamspace sector.

There are eight interferers at:

$$\begin{aligned} u &= 11/32, -13/32, 19/32 : INR = 40 \text{ dB}, \\ u &= 15/32, 23/32, -17/32 : INR = 30 \text{ dB}, \\ u &= -21/32, 27/32 : INR = 20 \text{ dB}, \end{aligned} \quad (6.914)$$

present during the beamspace matrix construction. After the beamspace matrix is established, two interferers, each with an  $INR=20$  dB, arrive from  $3/32$  and  $5/32$ . The eight interferers remain.

- (a) Design a beamspace MPDR processor for a signal arrival direction  $u_s = 0$ . Evaluate its array gain and plot its beam pattern.
- (b) Compare the performance in part (a) to an element-space MPDR beamformer.

#### Problem 6.9.14 (continuation; Problem 6.9.13)

Consider the same model as in Problem 6.9.13. In order to construct the beamspace matrix, scan a conventional beam over  $u$ -space with a scan step size of  $2/N$ . Detect the presence or absence of a signal (or interferer) at each scan location and estimate its power. If the  $SNR$  exceeds 10 dB and it is outside the beamspace sector, place a null on it in each of the beamspace rows.

After the beamspace matrix is established, the two interferers appear at  $5/32$  and  $7/32$  ( $INR = 20$  dB each).

- (a) Repeat Problem 6.9.13. Compare your result to the results in Problem 6.9.13.
- (b) How does the scan step size affect performance?

#### Problem 6.9.15

Consider a standard 32-element linear array and a  $5 \times 32$  beamspace matrix using conventional beams centered at  $u = 0, \pm 2/32$ , and  $\pm 4/32$ . The desired quiescent beam is the Blackman-Harris beam.

The nominal signal arrival direction is  $u_s = 0$ . The actual signal arrival angle is  $u_a$ , where  $|u_a| \leq 1/32$ . There are four uncorrelated plane-wave interferers:

$$\begin{aligned} u_1 &= 5/32, INR = 20 \text{ dB}, \\ u_2 &= 13/32, INR = 50 \text{ dB}, \\ u_3 &= 19/32, INR = 50 \text{ dB}, \\ u_4 \text{ variable: } &3/32 \leq u_4 \leq 21/32, INR = 20 \text{ dB}. \end{aligned} \quad (6.915)$$

Design a beamspace LCMP-DL beamformer using a quiescent pattern constraint. Evaluate the performance for various  $u_a$ ,  $u_4$ , and  $SNR$ . Discuss the trade-offs between low out-of-sector sidelobes and the ability to null in-sector interferers.

## P6.10 Quadratically Constrained Beamformers

#### Problem 6.10.1 (continuation; Example 6.10.1)

Consider a standard 10-element linear array. The array is steered to broadside. The

interference consists of two uncorrelated equal-power interferers at  $u = 0.29$  and  $0.45$ . The signal arrives at  $u_a$ . The  $SNR$ ,  $INR$ , and  $T_o$  are parameters that we want to investigate.

- (a) The  $SNR$  is 0 dB. Consider  $INRs$  of 0, 10, 20, and 30 dB. Plot the output  $SNR_o$  versus  $u_a/BW_{NN}$  for various  $T_o$ , where  $1/N \leq T_o \leq 2/N$ . Explain your results. Use the optimum  $\beta$ . Plot  $\beta$  versus  $u_a/BW_{NN}$ .
- (b) Repeat part (a) for an  $SNR = 10$  dB.
- (c) Repeat part (a) for an  $SNR = 20$  dB.
- (d) Based on the results of parts (a)–(c), suggest guidelines for choosing  $T_o$ .

**Problem 6.10.2** (continuation)

Consider the same model as in Problem 6.10.1 with  $u_a = 0$ . Add a third interferer with an  $INR_3 = 20$  dB whose location  $u_{I3}$  is a parameter.

- (a) Consider  $INRs$  of 0, 10, 20, and 30 dB for the original two interferers. Plot the output  $SNR_o$  versus  $u_{I3}/BW_{NN}$  for various  $T_o$ , where  $1/N \leq T_o \leq 2/N$ . Use the optimum  $\beta$  and the approximate  $\beta$ .
- (b) Suggest guidelines for choosing  $T_o$ .

**Problem 6.10.3** (continuation)

Consider the same model as in Problems 6.10.1 and 6.10.2. Investigate the sensitivity to the choice of  $\beta$ . Use these sensitivity results to develop criteria for how accurate the value of  $\beta$  should be in order to preserve almost optimum performance.

**Problem 6.10.4** (continuation; Example 6.10.1)

Consider the same model as in Example 6.10.1. Implement an LCMP-QC beamformer with second order derivative constraints,

$$\mathbf{C} = [ \begin{array}{ccc} 1 & \mathbf{d}(0) & \dot{\mathbf{d}}(0) \end{array} ], \quad (6.916)$$

$$\mathbf{g}^H = [ \begin{array}{ccc} 1 & \mathbf{0} & \ddot{\mathbf{B}}_c(0) \end{array} ], \quad (6.917)$$

and

$$\mathbf{w}^H \mathbf{w} \leq T_o \quad (6.918)$$

- (a) The  $SNR$  is 0 dB. Consider  $INRs$  of 0, 10, 20, and 30 dB. Plot the output  $SNR_o$  versus  $u_a/BW_{NN}$  for various  $T_o$ . Explain your results. Use the optimum  $\beta$ . Plot  $\beta$  versus  $u_a/BW_{NN}$ .
- (b) Repeat part (a) for an  $SNR = 10$  dB.
- (c) Repeat part (a) for an  $SNR = 20$  dB.
- (d) Based on the results of parts (a)–(c), suggest guidelines for choosing  $T_o$ .
- (e) In Example 6.10.1 and Problems 6.10.1–6.10.3 the beamformer relied on QC to provide main-lobe protection. In Example 6.10.2 and Problems 6.10.4–6.10.5, the beamformer relied on both linear constraints and QC to provide main-lobe protection. Discuss the advantages and disadvantages of the two approaches in the context of the environment.

**Problem 6.10.5** (continuation; Problem 6.10.4)

Consider the same model as in Problem 6.10.4 with  $u_a = 0$ . Add a third interferer with an  $INR_3 = 20$  dB whose location  $u_{I3}$  is a parameter.

- (a) Consider INRs of 0, 10, 20, and 30 dB for the original two interferers. Plot the output  $SNR_o$  versus  $u_{I3}/BW_{NN}$  for various  $T_o$ . Use the optimum  $\beta$ .
- (b) Suggest guidelines for choosing  $T_o$ .

**Problem 6.10.6** (continuation; Problem 6.10.1)

Consider a standard 10-element linear array and the signal and interference environment described in Problem 6.10.1. Use the quiescent pattern constraint technique in Section 6.7.5 to determine the linear constraints. Consider two quiescent patterns: Hamming, and Dolph-Chebychev with -40-dB SLL. Impose a quadratic constraint.

Repeat the analyses in Problem 6.10.1.

**Problem 6.10.7** (continuation; Problem 6.7.5)

Consider a standard 21-element linear array. Use the quiescent pattern constraint technique in Section 6.7.5 to determine the linear constraint. In addition, impose a quadratic constraint. Consider the six quiescent patterns in Problem 6.7.13. The nominal signal direction is broadside and  $u_a$  is a uniform random variable ( $-1/21 \leq u_a \leq 1/21$ ). There are six interferers in the sidelobe region  $(3/21, 5/21, 11/21, -7/21, -9/21, -15/21)$ .

- (a) The  $SNR$  is 0 dB. Consider INRs of 0, 10, 20, and 30 dB. Plot the output  $SNR_o$  versus  $u_a/BW_{NN}$  for various  $T_o$ . Consider up to five constraints. Do not simply generate a large set of plots. Determine the important factors and illustrate them. Use the optimum  $\beta$ . Plot  $\beta$  versus  $u_a/BW_{NN}$ . Explain your results.
- (b) Repeat part(a) for an  $SNR = 10$  dB.
- (c) Repeat part(a) for an  $SNR = 20$  dB.
- (d) Based on the results of parts (a)–(c), suggest guidelines for choosing the quiescent pattern, the number of constraints, and  $T_o$ .

**Problem 6.10.8: Beamspace-QC algorithms**

Consider a standard 32-element linear array and a  $7 \times 32$  beamspace matrix using conventional beams. Use the signal mismatch and interference model in Example 6.9.2. Consider two quadratically constrained beamformers.

- (i) MPDR (see Example 6.9.2).
- (ii) LCMP using a quiescent pattern constraint, with  $\cos^6(\pi\tilde{n}/N)$  the quiescent pattern.
- (a) Plot the array gain versus  $u_a/BW_{NN}$  for the two beamformers (consider various values of  $T_o$ ). Plot the resulting beam patterns. Compare your results to those in Example 6.9.2 and Problem 6.9.5.
- (b) Discuss your results and suggest design guidelines.

**Problem 6.10.9** (continuation; Problem 6.9.6)

Consider a standard 32-element linear array and the  $6 \times 32$  beamspace matrix described in Problem 6.9.6. Consider two quadratically constrained beamformers:

- (i) MPDR (see Example 6.9.6).
- (ii) LCMP-QP-QC with  $\cos^5(\pi\tilde{n}/N)$  quiescent pattern (see Problem 6.9.7).

The signal and interference environment is the same as Problem 6.9.6.

- (a) Plot the array gain versus  $u_a/BW_{NN}$  for the two beamformers (consider various values of  $T_o$ ). Plot the resulting beam patterns. Compare your results to those in Problem 6.9.6 and 6.9.7.
- (b) Discuss your results and suggest design guidelines. What are the advantages and disadvantages of this beamspace processor compared to the  $7 \times 32$  processor in Problem 6.10.8.

### P6.11 Soft Constraint Beamformers

#### Problem 6.11.1 (continuation; Example 6.11.1)

Consider the same signal and interference model as in Example 6.11.1. Study the effect of the choice of  $\mathbf{w}_d$  in (6.567). Consider Dolph-Chebychev beam patterns with SLLs of  $-20$ ,  $-30$ , and  $-40$  dB. Use  $\psi_0 = 0.1\pi$  and  $\alpha = 0.03$ .

- (a) Plot the normalized  $SNR_o$  versus  $u_a/BW_{NN}$  for the MPSC beamformer. Consider  $SNR = 0$  dB and 10 dB. Compare your results to the results in Figures 6.94 and 6.95.
- (b) Vary  $\alpha$  and study the effect on  $SNR_o$ .

#### Problem 6.11.2

Three of the algorithms developed in this chapter use the  $\mathbf{Q}$  matrix in (6.571) as a starting point:

- (i) Eigenvector constraints in Section 6.7.4.3.
- (ii) Quiescent pattern constraints in Section 6.7.5.
- (iii) Soft constraints in Section 6.11.

Consider several signal-and-interference scenarios and compare the performance of the three algorithms. Based on these analyses, discuss the trade-offs involved and suggest design guidelines.

#### Problem 6.11.3

A general formulation of the  $\mathbf{Q}$  matrix is given in (6.412). For a linear array,  $\mathbf{Q}$  can be written as

$$\mathbf{Q} = \int_F \int_\psi \mathbf{v}(\psi, f) \mathbf{v}^H(\psi, f) d\psi df. \quad (6.919)$$

Consider a 10-element uniform linear array with spacing  $d = \lambda_c/2$  where  $\lambda_c$  is the wavelength corresponding to the design frequency  $f_c$ . Assume the interval is

$$f_c - 0.2f_c \leq f \leq f_c + 0.2f_c. \quad (6.920)$$

Use the signal and interference model in Example 6.11.1. Consider different frequencies for the signal. Denote the frequency of the signal as  $f_s$ .

- (a) Assume  $u_a = 0.5$ . Plot the normalized  $SNR_o$  versus  $\Delta f/f_c$ , for the MPSC beamformer where

$$\Delta f = f_s - f_c.$$

Consider various  $\alpha$ .

- (b) Assume  $\Delta f = 0$ . Plot the normalized  $SNR_o$  versus  $u_a/BW_{NN}$ . Compare your results to those in Figures 6.94 and 6.95 and in part (a). Does the addition of a soft-frequency constraint impact the performance?

- (c) Plot a contour plot of the normalized  $SNR_o$  versus  $(\Delta f/f_c, u_a/BW_{NN})$ . Discuss your results.

**Problem 6.11.4**

In some applications, it is easier to specify  $\mathbf{Q}$  as a sum of points in the  $(f, \theta, \phi)$  space rather than an integral. Then,

$$\mathbf{Q} = \sum_{m=1}^M c_m \mathbf{v}(f_m, \theta_m, \phi_m) \mathbf{v}^H(f_m, \theta_m, \phi_m) \quad (6.921)$$

where  $c_m$  is a weighting function to allow emphasis on certain points.

As a special case, consider a standard 10-element linear array and the signal-and-interference model in Example 6.11.1. There is no frequency mismatch. Thus

$$\mathbf{Q} = \sum_{m=1}^{M_c} c_m \mathbf{v}(\psi_m) \mathbf{v}^H(\psi_m). \quad (6.922)$$

- (a) Choose  $M_c$  in order to achieve equivalent performance to Example 6.11.1.
- (b) Now assume that  $M_c = 3$  and that  $\psi_m = 0, \pm 0.1$ . Plot the normalized  $SNR_o$  versus  $u_a/BW_{NN}$ . Compare your results to an LCMP beamformer using three directional constraints and diagonal loading.

**Problem 6.11.5**

Consider an algorithm in which both a soft constraint and a quadratic constraint are imposed.

- (a) Show that the resulting optimum weight vector is

$$\hat{\mathbf{w}}_p = [[\mathbf{S}_x + \lambda_2 \mathbf{I}] + \lambda_1 \mathbf{Q}]^{-1} [\mathbf{S}_x + \lambda_2 \mathbf{I}] \mathbf{w}_d, \quad (6.923)$$

where  $\lambda_1$  and  $\lambda_2$  are chosen to satisfy the two constraints,

$$\hat{\mathbf{w}}_p^H \mathbf{Q} \hat{\mathbf{w}}_p \leq e_0^2, \quad (6.924)$$

and

$$(\mathbf{w}_d - \mathbf{w}_p)^H (\mathbf{w}_d - \mathbf{w}_p) \leq T_o. \quad (6.925)$$

- (b) Consider various signal-and-interference scenarios and see if there are cases in which the added complexity leads to a significant performance improvement.

**Problem 6.11.6** (continuation; Example 6.11.1)

Consider the same model as in Example 6.11.1. As an alternative to the approach in Problem 6.11.5, define

$$\mathbf{Q}_{au} = \gamma \mathbf{Q} + (1 - \gamma) \mathbf{I}, \quad 0 \leq \gamma \leq 1, \quad (6.926)$$

where  $\mathbf{Q}$  is defined in (6.571). Plot  $SNR_o$  versus  $u_a/BW_{NN}$  for various values of  $\gamma$  and  $\alpha$ . Compare your results to the results in Example 6.11.1

**Problem 6.11.7** (continuation; Example 6.7.10)

Extend the technique of soft constraints to derivative constraints. Derive the optimum  $\mathbf{w}_p$ .

Consider the signal-and-interference model in Example 6.7.10. Plot the array gain versus  $u_a/BW_{NN}$  and compare your results to the results in Figure 6.59.

**Problem 6.11.8: Beamspace soft constraints** (continuation; Example 6.9.2 and Problem 6.10.15)

Consider a standard 32-element linear array and the  $7 \times 32$  standard beamspace matrix given in Example 6.9.1. Use the same signal-and-interference model as in Example 6.9.2. Consider two desired beam patterns (conventional and  $\cos^6(\pi\tilde{n}/N)$ ). Utilize soft constraints over the interval  $-1/32 \leq u \leq 1/32$ .

- (a) Plot the array gain versus  $u_a/BW_{NN}$  and compare your results to those in Example 6.9.2.
- (b) Discuss your comparison. How dependent is it on the specific signal-and-interference model?

## P6.12 Beamforming for Correlated Signal and Interferences

**Problem 6.12.1**

Consider the spatial smoothing approach in which the subarray spectral matrices are averaged with different weights. Then, from (6.622),

$$\mathbf{S}_{SSFB} = \frac{1}{2} \sum_{i=1}^L w_i (\mathbf{S}_M^{(i)} + \mathbf{S}_{MB}^{(i)}), \quad (6.927)$$

where the weights are real and

$$\sum_{i=1}^L w_i = 1. \quad (6.928)$$

- (a) Derive the equation corresponding to (6.637).
- (b) Assume the  $w_i$  are chosen to correspond to an  $L$ -element Hamming weighting. Plot the results analogous to those in Figure 6.104 for this weighting
- (c) Discuss your results. Is the  $u_I = 0.30$  case representative?

**Problem 6.12.2** (continuation)

Consider a standard 32-element linear array. Repeat Problem 6.12.1 for the following sub-array weightings:

- (i) Uniform
- (ii) Hamming
- (iii) Dolph-Chebychev

Test various  $u_I$  in the sidelobe region.

**Problem 6.12.3**

Consider a standard rectangular array with  $N = M$ . Extend the technique of spatial smoothing to the rectangular array.

- (a) Derive the necessary equations
- (b) Develop plots similar to Figure 6.104 for several interference scenarios.

## P6.13 Broadband Beamformers

### Problem 6.13.1

Consider a uniformly spaced 10-element array. The interelement spacing is  $\lambda_u/2$ , where  $\lambda_u$  is the wavelength of the highest frequency in the input signal. Implement an FFT beamformer with  $M$  frequency bins.

$$B_f = B_s/f_c = 0.6. \quad (6.929)$$

The input is sampled at  $1/B_s$  so the normalized frequency span is  $-\pi \leq \omega \leq \pi$  in radians. The signal of interest arrives from  $u_s = 0.3$  and has a flat frequency spectrum over  $-0.25\pi \leq \omega \leq 0.25\pi$  (a 50% bandwidth signal).

There are three interfering signals with the following characteristics (all spectra are zero outside the indicated band):

$$S_{I1} = \sigma_1^2, \quad -0.25\pi < \omega < 0, \quad u_I = 0, \quad INR_1 = 40 \text{ dB}. \quad (6.930)$$

$$S_{I2} = \sigma_2^2, \quad -0.01 \leq \omega \leq 0.01, \quad u_I = 0.5, \quad INR_2 = 60 \text{ dB}. \quad (6.931)$$

$$S_{I3} = \sigma_3^2, \quad 0 < \omega \leq 0.25\pi, \quad u_I = -0.2, \quad INR_2 = 30 \text{ dB}. \quad (6.932)$$

Consider  $M = 4, 8, 16, 32$ , and  $64$ . Use an MPDR beamformer in the appropriate bins and set the output of the other frequency bins equal to 0.

Plot the  $SNR_o$  versus  $ASNR$  for the various  $M$ . Discuss your results.

### Problem 6.13.2 (continuation)

Consider the same model as in Problem 6.13.1, except the signal spectrum is

$$S_s = \begin{cases} 1 + \cos 10\omega & -0.25\pi \leq \omega \leq 0.25\pi, \\ 0 & \text{elsewhere.} \end{cases} \quad (6.933)$$

Repeat Problem 6.13.1.

### Problem 6.13.3 (continuation)

Consider the same model as in Problem 6.13.1, except there is a single narrowband interferer,

$$\begin{aligned} S_{I1} &= \sigma_1^2, \quad \omega_1 - 0.01 \leq \omega \leq \omega_1 + 0.01, \\ INR_1 &= 50 \text{ dB}. \end{aligned} \quad (6.934)$$

Investigate the behavior as a function of  $u_I$ ,  $\omega_1$ , and  $M$ . Plot the  $SNR_o$  versus  $ASNR$  for various combinations. Discuss your results.

## Bibliography

- [AC76] S. P. Applebaum and D. J. Chapman. Adaptive arrays with main beam constraints. *IEEE Trans. Antennas Propag.*, vol.AP-24, pp. 650–662, September 1976.
- [AO90] D.A. Abraham and N.L. Owsley. Beamforming with dominant mode rejection. *Proc. IEEE Oceans 90*, pp. 470–475, 1990.
- [BAB90] J. F. Bull, M. A. Arnao, and L. R. Burgess. Hypersensitivity effects in adaptive antenna arrays. *Proc. IEEE Antennas Propag. Soc. Symp.*, pp. 396–399, May 1990.

- [Bag76] A. B. Baggeroer. Space-time processes and optimal array processing. Technical Report 506, Navy Undersea Center, San Diego, California, December 1976.
- [BC65] C. J. Becker and B. F. Cron. Optimum array gain for directional noise. Technical Report 656, Underwater Systems Lab, October 1965.
- [BG81] B. S. Byun and A. F. Gangi. A constraint-elimination technique for linearly constrained arrays. *IEEE Trans. Geosci. Remote Sensing*, vol.GE-19, pp. 8–15, January 1981.
- [BG86] K. M. Buckley and L. J. Griffiths. An adaptive generalized sidelobe canceller with derivative constraints. *IEEE Trans. Antennas Propag.*, vol.AP-34, pp. 311–319, March 1986.
- [BH86] E. Brookner and J.M. Howell. Adaptive-adaptive array processing. *Proc. IEEE*, vol.74, pp. 602–604, April 1986.
- [BKS88] A. B. Baggeroer, W. A. Kuperman, and H. Schmidt. Matched field processing: Source localization in correlated noise as an optimum parameter estimation problem. *J. Acoust. Soc. Am.*, vol.83, pp. 571–587, February 1988.
- [BN62] R. G. Brown and J. W. Nilsson. *Introduction to Linear Systems Analysis*. Wiley, New York, 1962.
- [BR89] K. A. Byerly and R. A. Roberts. Output power based partially adaptive array design. *Proc. 23rd Asilomar Conf. on Signals, Systems and Computers*, Pacific Grove, California, pp. 576–580, November 1989.
- [BRK88] Y. Bresler, V. U. Reddy, and T. Kailath. Optimum beamforming for coherent signal and interferences. *IEEE Trans. Acoust., Speech, Signal Process.*, vol.ASSP-36, pp. 833–842, June 1988.
- [Bry62] F. Bryn. Optimum signal processing of three-dimensional array operating on Gaussian signals and noise. *J. Acoust. Soc. Am.*, vol.34, pp. 289–297, March 1962.
- [Buc87] K. M. Buckley. Spatial/spectral filtering with linearly constrained minimum variance beamformers. *IEEE Trans. Acoust., Speech, Signal Process.*, vol.ASSP-35, pp. 249–266, March 1987.
- [Bur64] J. P. Burg. Three-dimensional filtering with an array of seismometers. *Geophysics*, vol.XXIX, no.5, pp. 693–713, October 1964.
- [Cap69] J. Capon. High-resolution frequency-wavenumber spectrum analysis. *Proc. IEEE*, vol.57, pp. 1408–1418, August 1969.
- [CG80] A. Cantoni and L.C. Godara. Resolving the direction of sources in a correlated field incident on an array. *J. Acoust. Soc. Am.*, vol.67, pp. 1247–1255, April 1980.
- [CGK67] J. Capon, R. J. Greenfield, and R. J. Kolker. Multidimensional maximum-likelihood processing of a large aperture seismic array. *Proc. IEEE*, vol.56, pp. 192–211, February 1967.
- [Cha76] D. J. Chapman. Partial adaptivity for the large array. *IEEE Trans. Antennas Propag.*, vol.AP-24, pp. 685–696, September 1976.
- [CK84] T. K. Citron and T. Kailath. An improved eigenvector beamformer. *Proc. ICASSP*, San Diego, California, 1984.

- [Com88a] R. T. Compton, Jr. *Adaptive Antennas (Concepts and Performance)*. Prentice-Hall, Englewood Cliffs, New Jersey, 1988.
- [Com88b] R. T. Compton, Jr. The relationship between tapped delay-line and FFT processing in adaptive arrays. *IEEE Trans. Antennas Propag.*, vol.AP36, pp. 15–26, January 1988.
- [Cox73] H. Cox. Resolving power and sensitivity to mismatch of optimum array processors. *J. Acoust. Soc. Am.*, vol.ASSP-54, pp. 771–785, September 1973.
- [Cox00] H. Cox. Multi-Rate Adaptive Beamforming (MRABF). *Proc. IEEE Sensor Array and Multichannel Signal Processing Workshop*, Cambridge, Massachusetts, pp. 306–309, March 2000.
- [CP97] H. Cox. and R. Pitre. Robust DMR and multi-rate adaptive beamforming. *Proc. 31st Asilomar Conf. on Signals, Systems and Computers*, Pacific Grove, California, November 1997.
- [CPL98] H. Cox, R. Pitre, and H. Lai. Robust adaptive matched field processing. *Proc. 32nd Asilomar Conf. on Signals, Systems and Computers*, Pacific Grove, California, November 1998.
- [CR65] D. Childers and I. Reed. On the theory of continuous array processing. *IEEE Trans. Aerosp. Navig. Electron.*, vol.AES-12, pp. 103–109, June 1965.
- [CY92] L. Chang and C. Yeh. Performance of DMI and eigenspace-based beamformers. *IEEE Trans. Antennas Propag.*, vol.AP-40, pp. 1336–1347, November 1992.
- [CZO87] H. Cox, R. M. Zeskind, and M. M. Owen. Robust adaptive beamforming. *IEEE Trans. Acoust., Speech, Signal Process.*, vol.-ASSP-35, pp. 1365–1376, October 1987.
- [Dar58] S. Darlington. Linear least-squares smoothing and prediction, with applications. *Bell Syst. Tech. J.*, vol.37, pp. 1221–1294, September 1958.
- [EC81] M. H. Er and A. Cantoni. An alternative formulation for an optimum beamformer with robustness capability. *Proc. IEE*, vol. 132, pt. F, pp. 447–460, October 1985.
- [EC83] M. H. Er and A. Cantoni. Derivative constraints for broad-band element space antenna array processors. *IEEE Trans. Acoust., Speech, Signal Process.*, vol.ASSP-31, pp. 1378–1393, December 1983.
- [EC85] M. H. Er and A. Cantoni. An alternative formulation for an optimum beamformer with robustness capability. *Proc. IEE*, vol.132 pt. F, pp. 447–460, October 1985.
- [EC90] M. H. Er and A. Cantoni. A unified approach to the design of robust narrow-band antenna array processors. *IEEE Trans. Antennas Propag.*, vol.AP-38, pp. 17–23, January 1990.
- [EFK67] D.J. Edelblute, J.M. Fisk, and G.L. Kinnison. Criteria for optimum-signal-detection theory for arrays. *J. Acoust. Soc. Am.*, vol.41, pp. 199–205, January 1967.
- [EJS82] J.E. Evans, J.R. Johnson, and D.F. Sun. Application of advanced signal processing techniques to angle of arrival estimation in ATC navigation and surveillance systems. Technical Report, M.I.T. Lincoln Laboratory, Lexington, Massachusetts, June 1982.

- [Far83] D.R. Farrier. Gain of an array of sensors subjected to processor perturbation. *Proc. IEE*, vol.72, pt. H, pp. 251–254, June 1983.
- [FG91] D. D. Feldman and L. J. Griffiths. A constraint projection approach for robust adaptive beamforming. *Proc. ICASSP*, Toronto, Canada, vol.2, pp. 1381–1384, May 1991.
- [FG94] D. D. Feldman and L. J. Griffiths. A projection approach for robust adaptive beamforming. *IEEE Trans. Signal Process.*, vol.SP-42, pp. 867–876, April 1994.
- [FH53] J. J. Faran and R. Hills. Wide-band directivity of receiving arrays. Technical Report 31, Acoustic Research Laboratory, Harvard University, Cambridge, Massachusetts, May 1953.
- [FT98] B.E. Freburger and D.W. Tufts. Case study of principal component inverse and cross spectral metric for low rank interference adaptation. *Proc. ICASSP*, Seattle, Washington, vol.4, pp. 1977–1980, May 1998.
- [Fri88] B. Friedlander. A signal subspace method for adaptive interference cancellation. *IEEE Trans. Acoust., Speech, Signal Process.*, vol.ASSP-36, pp. 1835–1845, December 1988.
- [Fro72] O. L. Frost III. An algorithm for linearly constrained adaptive array processing. *Proc. IEEE*, vol.60, pp. 926–935, August 1972.
- [Gaa66] N.T. Gaarder. The design of point detector arrays: II. *IEEE Trans. Inf. Theory*, vol.IT-12, pp. 112–120, April 1966.
- [Gaa67] N.T. Gaarder. The design of point detector arrays: I. *IEEE Trans. Inf. Theory*, vol.IT-13, pp. 42–50, January 1967.
- [Gab76a] W. F. Gabriel. Adaptive arrays – An introduction. *Proc. IEEE*, vol.64, pp. 239–271, February 1976.
- [Gab76b] W. F. Gabriel. Preface-Special issue on adaptive antennas. *IEEE Trans. Antennas Propag.*, vol.AP-24, pp. 573–574, September 1976.
- [Gab86] W. F. Gabriel. Using spectral estimation technique in adaptive processing antenna system. *IEEE Trans. Antennas Propag.*, vol.AP-34, pp. 291–300, March 1986.
- [Gab87] W. F. Gabriel. *Adaptive Processing Antenna Systems*. IEEE Antennas and Propagation Short Course. Naval Research Laboratory, Virginia Polytechnic Institute and State University, Blacksburg, Virginia , June 1987.
- [GB87] L. J. Griffiths and K. M. Buckley. Quiescent pattern control in linearly constrained adaptive arrays. *IEEE Trans. Acoust., Speech, Signal Process.*, vol.ASSP-35, pp. 917–926, July 1987.
- [GE91] A. B. Gershman and V. T. Ermolaev. Synthesis of the weight distribution of an adaptive array with wide dips in the directional pattern. *Radiophys. Quantum Electron.*, vol.34, pp. 720–724, August 1991.
- [GJ82] L. J. Griffiths and C. W. Jim. An alternative approach to linearly constrained adaptive beamforming. *IEEE Trans. Antennas Propag.*, vol.AP-30, pp. 27–34, January 1982.
- [GJ99] L. C. Godara and M. R. S. Jahromi. Limitations and capabilities of frequency domain broadband constrained beamforming schemes. *IEEE Trans. Signal Process.*, vol.SP-47, pp. 2386–2395, September 1999.

- [GM55] E.N. Gilbert and S.P. Morgan. Optimum design of directive antenna arrays subject to random variations. *Bell Syst. Tech. J.*, vol.34, pp. 637–663, May 1955.
- [God85] L.C. Godara. The effect of phase-shifter error and the performance of an antenna array beamformer. *IEEE J. Oceanogr. Eng.*, vol.OE-10, pp. 278–284, July 1985.
- [God86] L. C. Godara. Error analysis of the optimal antenna array processors. *IEEE Trans. Aerosp. Electron. Syst.*, vol.AES-22, pp. 395–409, July 1986.
- [God90] L. C. Godara. Beamforming in the presence of correlated arrivals using structured correlation matrix. *IEEE Trans. Acoust., Speech, Signal Process.*, vol.ASSP-38, pp. 1–15, January 1990.
- [God95] L. C. Godara. Application of the fast Fourier transform to broadband beamforming. *J. Acoust. Soc. Am.*, vol.98, pp. 230–239, July 1995.
- [GR97a] J. Goldstein and I. Reed. Reduced rank adaptive filtering. *IEEE Trans. Acoust., Speech, Signal Process.*, vol.ASSP-45, p. 492, February 1997.
- [GR97b] J. Goldstein and I. Reed. Subspace selection for partially adaptive sensor array processing. *IEEE Trans. Acoust., Speech, Signal Process.*, vol.ASSP-33, pp. 539-544, April, 1997.
- [GR97c] J. Goldstein and I. Reed. Theory of partially adaptive radar. *IEEE Trans. Acoust., Speech, Signal Process.*, vol.ASSP-33, pp. 1309-1325, October 1997.
- [Gra82] D. A. Gray. Formulation of the maximum signal-to-noise array processor in beam space. *J. Acoust. Soc. Am.*, vol.72, pp. 1195-1201, October 1982.
- [Gri77] L.J. Griffiths. An adaptive beamformer which implements constraints using an auxiliary array processor. In G. Tacconi Ed., *Aspects of Signal Processing, PROC. NATO ASI*, Reidel, Dordrecht, The Netherlands, pp. 517–522, 1977.
- [GSB96] A. B.Gershman, G. V. Serebryakov, and J. F. Bohme. Constrained Hung-Turner adaptive beamforming algorithm with additional robustness to wideband and moving jammers. *IEEE Trans. Antennas Propag.*, vol.AP-44, pp. 361-367, 1996.
- [Gue99] J.R. Guerci. Theory and application of covariance matrix tapers for robust adaptive beamforming. *IEEE Trans. Signal Process.*, vol.SP-47, pp. 997-985, April 1999.
- [GVL89] G. H. Golub and C. F. Van Loan. *Matrix Computations*. The Johns Hopkins University Press, Baltimore, Maryland, 1989.
- [HBN88] A. M. Haimovich and Y. Bar-Ness. Adaptive antenna arrays using eigenvector methods. *IEEE Int. Conf. Antennas Propagat.*, 1988.
- [HBN91] A. M. Haimovich and Y. Bar-Ness. An eigenanalysis interference canceller. *IEEE Trans. Acoust., Speech, Signal Process.*, vol.ASSP-39, pp. 76–84, January 1991.
- [HS92] S. Haykin and A. Steinhardt, Editors. *Adaptive Radar Detection and Estimation*. Wiley, New York, 1992.
- [HT83] E. K. L. Hung and R. M. Turner. A fast beamforming algorithm for large arrays. *IEEE Trans. Aerosp. Electron. Syst.*, vol.AES-19, pp. 598–607, July 1983.

- [Jab86a] N. K. Jablon. Adaptive beamforming with the generalized sidelobe canceller in the presence of array imperfections. *IEEE Trans. Antennas Propag.*, vol.AP-34, pp. 996–1012, August 1986.
- [Jab86b] N. K. Jablon. Steady state analysis of the generalized sidelobe canceller by adaptive noise cancelling techniques. *IEEE Trans. Antennas Propag.*, vol.AP-34, pp. 330–337, March 1986.
- [KBK85] S. B. Kesler, S. Boodaghians, and J. Kesler. Resolving uncorrelated and correlated sources by linear prediction. *IEEE Trans. Antennas Propag.*, vol.AP-33, pp. 1221–1227, November 1985.
- [Kel65] E. J. Kelly. A comparison of seismic array processing schemes. Technical Report 1965-21, M.I.T. Lincoln Laboratory, Lexington, Massachusetts, June 1965.
- [KL64] E. J. Kelly, Jr. and M.J. Levin. Signal parameter estimation for seismometer arrays. MIT DDC 435-489 Technical Report 339, M.I.T. Lincoln Laboratory, Lexington, Massachusetts, January 1964.
- [Kle80] L. I. Kleinberg. Array gain for signals and noise having amplitude and phase fluctuations. *J. Acoust. Soc. Am.*, vol.67, pp. 572–576, February 1980.
- [KS90] J. Krolik and D. Swigler. Focused wideband array processing by spatial resampling. *IEEE Trans. Acoust., Speech, Signal Process.*, vol.ASSP-38, pp. 356–360, February 1990.
- [KT85] I. P. Kirsteins and D. W. Tufts. On the probability density of signal-to-noise ratio in an improved adaptive detector. *Proc. ICASSP*, Tampa, Florida, vol.1, pp. 572–575, 1985.
- [Lev64] M.J. Levin. Maximum-likelihood array processing. Technical Report DDC 455743, M.I.T. Lincoln Laboratory, Lexington, Massachusetts, December 1964.
- [Lut86] A. K. Luthra. A solution to the adaptive nulling problem with a look-direction constraint in the presence of coherent jammers. *IEEE Trans. Antennas Propag.*, vol.AP-34, pp. 702–710, May 1986.
- [Mai95] R.J. Mailloux. Covariance matrix augmentation to produce adaptive array pattern troughs. *Electron. Lett.*, vol.31, pp. 771–772, July 1995.
- [Mer64] H.F. Mermoz. Filtrage adapté et utilisation optimale d'une antenne. In *NATO Adavanced Study Institute Signal Processing Emphasis Underwater Acoustics*, Grenoble, France, 1964.
- [MG64] D. Middleton and H. Groginsky. Detection of random acoustic signals with distributed elements: Optimum receiver structures for normal signal and noise fields. *Proc. Acoustic Society Symposium of 1964*, 1964.
- [MG88] T.T. Ma and L.J. Griffiths. A solution space approach to achieving partially adaptive arrays. *Proc. ICASSP*, NewYork, New York, vol.V, pp. 2869–2872, April 1988.
- [Mid60] D. Middleton. *An Introduction to Statistical Communication Theory*. McGraw-Hill, New York, 1960.
- [Mor78] D.R. Morgan. Partially adaptive array techniques. *IEEE Trans. Antennas Propag.*, vol.AP-26, pp. 823–833, November 1978.

- [MP81] R.A. Mucci and R.G. Pridham. Impact of beam steering errors on shifted sideband and phase shift beamforming techniques. *J. Acoust. Soc. Am.*, vol.69, pp. 1360–1368, May 1981.
- [MSC81] J. T. Mayhan, A. J. Simmons, and W. C. Cummings. Wide-band adaptive antenna nulling using tapped delay lines. *IEEE Trans. Antennas Propag.*, vol.AP-29, pp. 923–936, November 1981.
- [Nit76] R. Nitzberg. Effect of errors in adaptive weights. *IEEE Trans. Aerosp. Electron. Syst.*, vol.AES-12, pp. 369–373, May 1976.
- [OS89] A. V. Oppenheim and R. W. Schafer. *Discrete-Time Signal Processing*. Prentice-Hall, Englewood Cliffs, New Jersey, 1989.
- [Ows71] N. L. Owsley. Source location with an adaptive antenna array. Technical Report, Naval Underwater Systems Center, National Technical Information Service, Springfield, Virginia, January 1971.
- [Ows73] N. L. Owsley. A recent trend in adaptive spatial processing for sensor arrays: Constrained adaptation. In *Proc. NATO Advanced Study Institute on Signal Processing*, London and New York, pp. 591–604, 1973.
- [Ows74] N. L. Owsley. Noise cancellation in the presence of correlated signal and noise. Technical Report 4639, Naval Underwater Systems Center, New London, Connecticut, January 1974.
- [Ows80] N. L. Owsley. An overview of optimum-adaptive control in sonar array processing. In K. S. Narendra and R. V. Monopoli, editors, *Applications of Adaptive Control*, pp. 131–164. Academic Press, New York, 1980.
- [Ows85] N. L. Owsley. Sonar array processing. In S. Haykin, editor, *Array Signal Processing*. Prentice-Hall, Englewood Cliffs, New Jersey, 1985.
- [PK85] A. Paulraj and T. Kailath. On beamforming in the presence of multipath. *Proc. ICASSP*, vol.1, pp. 564–567, Tampa, Florida, March 1985.
- [PK89] S. U. Pillai and B. H. Kwon. Forward/backward spatial smoothing techniques for coherent signal identification. *IEEE Trans. Acoust., Speech, Signal Process.*, vol.ASSP-37, pp. 8–15, January 1989.
- [Pri51] R. L. Pritchard. Directivity of acoustic linear point arrays. Technical Report 21, Acoustic Research Laboratory, Harvard University, Cambridge, Massachusetts, January 1951.
- [Pri53] R. Price. Statistical theory applied to communication through multipath disturbances. Technical Report, M.I.T. Research Laboratory of Electronics, Lexington, Massachusetts, September 1953.
- [Pri54] R. Price. The detection of signals perturbed by scatter and noise. *IRE Trans.*, vol.PGIT-4, pp. 163–170, September 1954.
- [Pri56] R. Price. Optimum detection of random signals in noise with application to scatter-multipath communication. *IRE Trans.*, vol.PGIT, pp. 125–135, December 1956.
- [Pri63] R. Pritchard. Optimum directivity patterns for linear point arrays. *J. Acoust. Soc. Am.*, vol.25, pp. 879–891, September 1953.
- [PRK87] A. Paulraj, V. U. Reddy, and T. Kailath. Analysis of signal cancellation due to multipath in optimum beamformers for moving arrays. *IEEE J. Oceanogr. Eng.*, vol.OE-12, pp. 163–172, January 1987.

- [Qua82] A. H. Quazi. Array beam response in the presence of amplitude and phase fluctuations. *J. Acoust. Soc. Am.*, vol.72, pp. 171–180, July 1982.
- [RC79] W.E. Rodgers and R. T. Compton, Jr. Adaptive array bandwidth with tapped delay-line processing. *IEEE Trans. Aerosp. Electron. Syst.*, vol.AES-15, pp. 21–28, January 1979.
- [RPK87a] V. U. Reddy, A. Paulraj, and T. Kailath. Performance analysis of the optimum beamformer in the presence of correlated sources and its behavior under spatial smoothing. *IEEE Trans. Acoust., Speech, Signal Process.*, vol.ASSP-35, pp. 927–936, July 1987.
- [RPK87b] R. Roy, A. Paulraj, and T. Kailath. Comparative performance of ESPRIT and MUSIC for direction-of-arrival estimation. *Proc. ICASSP*, vol.IV, pp. 2344–2347, Dallas, Texas, April 1987.
- [RR92a] K. J. Raghunath and V. U. Reddy. Finite data analysis of MVDR beamformer: With and without spatial smoothing. *IEEE Trans. Antennas Propag.*, vol.ASSP-11, pp. 1226–1236, November 1992.
- [RR92b] K. J. Raghunath and V. U. Reddy. A note on spatially weighted subarray covariance averaging schemes. *IEEE Trans. Antennas Propag.*, vol.ASSP-40, pp. 720–723, June 1992.
- [Sch68] F. Schweppe. Sensor array data processing for multiple signal sources. *IEEE Trans. Inf. Theory*, vol.IT-4, pp. 294–305, March 1968.
- [Sid58] M. M. Siddiqui. On the inversion of the sample covariance matrix in a stationary autoregressive process. *Ann. Math. Statist.*, vol.58, pp. 585–588, 1958.
- [SK85a] V. Shahmirian and S. Kesler. Bias and resolution of the vector space methods in the presence of coherent planewaves. In *Proc. ICASSP*, Tampa, Florida, vol.IV, pp. 2320–2323, 1985.
- [SK85b] T.-J. Shan and T. Kailath. Adaptive beamforming for coherent signals and interference. *IEEE Trans. Acoustics, Speech, Signal Process.*, vol.ASSP-33, pp. 527–534, June 1985.
- [SK90] S. Sivanand and M. Kaveh. New results in broadband adaptive beamforming. *Proc. Asilomar Conference on Communications, Signal Processing and Computers*, Pacific Grove, California, November 1990.
- [SK94] S. Simanapalli and M. Kaveh. Broadband focusing for partially adaptive beamforming. *IEEE Trans. Aerosp. Electron. Syst.*, vol.AES-30, pp. 68–79, January 1994.
- [SSW86] Y.-L. Su, T.-J. Shan, and B. Widrow. Parallel spatial processing: A cure for signal cancellation in adaptive arrays. *IEEE Trans. Antennas Propag.*, vol.AP-34, pp. 347–355, March 1986.
- [Ste83] A.K. Steele. Comparison of directional and derivative constraints for beamformers subject to multiple linear constraints. *Proc. IEE*, vol.130, pts. F and H, pp. 41–45, 1983.
- [TBV98] Z. Tian, K. L. Bell, and H. L. Van Trees. A recursive least squares implementation for adaptive beamforming under quadratic constraint. *Proc. ICASSP*, Seattle, Washington, vol.IV, pp. 2053–2056, May 1998.

- [TCL95] I. Thng, A. Cantoni, and Y. H. Leung. Constraints for maximally flat optimum broadband antenna arrays. *IEEE Trans. Signal Process.*, vol.SP-43, pp. 1334–1347, June 1995.
- [TG92a] C-Y. Tseng and L. J. Griffiths. A simple algorithm to achieve desired pattern for arbitrary arrays. *IEEE Trans. Signal Process.*, vol.SP-40, pp. 2737–2746, November 1992.
- [TG92b] C-Y. Tseng and L. J. Griffiths. A unified approach to the design of linear constraints in minimum variance adaptive beamformers. *IEEE Trans. Antennas Propag.*, vol.AP-40, pp. 1533–1542, December 1992.
- [TK87] K. Takao and N. Kikuma. Adaptive array utilizing an adaptive spatial averaging technique for multipath environments. *IEEE Trans. Antennas Propag.*, vol.AP-35, pp. 1389–1396, December 1987.
- [TKY86] K. Takao, N. Kikuma, and T. Yano. Toeplitzization of correlation matrix in multipath environment. *Proc. ICASSP*, vol.III, pp. 1873–1876, Tokyo, Japan, April 1986.
- [Tse92] C.-Y. Tseng. Minimum variance beamforming with phase-independent derivative constraints. *IEEE Trans. Antennas Propag.*, vol.AP-40, pp. 285–294, March 1992.
- [TYS95] C.-J. Tsai, J.-F. Yang, and T.-H. Shiu. Performance analysis of beamformers using effective SINR on array parameters. *IEEE Trans. Signal Process.*, vol.SP-43, pp. 300–303, January 1995.
- [US56] M. Uzsoky and L. Solymár. Theory of superdirective linear arrays. *Acta Phys. Acad. Sci. Hung.*, vol.6, pp. 185–205, June 1956.
- [Van63] V. Vanderkulk. Optimum processing for acoustic arrays. *J. Br. IRE*, vol.26, pp. 286–292, October 1963.
- [VT64] H. L. Van Trees. *Optimum Signal Design and Processing for Reverberation-Limited Environments*, Report No. 1501064, pp. 1–115. Arthur D. Little, Cambridge, Massachusetts, October 1964.
- [VT65] H. L. Van Trees. Optimum signal design and processing for reverberation-limited environments. *IEEE Trans. Mil. Electron.*, vol.MIL-9, pp. 212–229, July–October 1965.
- [VT66a] H. L. Van Trees. Optimum processing for passive sonar arrays. In *Proc. IEEE Ocean Electronics Symp.*, pp. 41–65, Honolulu, Hawaii, 1966.
- [VT66b] H. L. Van Trees. A unified theory for optimum array processing. Technical Report 4160866, Dept. of the Navy, Naval Ship Systems Command, Arthur D. Little, Cambridge, Massachusetts, August 1966.
- [VT68] H. L. Van Trees. *Detection, Estimation, and Modulation Theory, Part I*. Wiley, New York, 1968.
- [VT01a] H. L. Van Trees. *Detection, Estimation, and Modulation Theory, Part I*. Wiley Interscience, New York, 2001.
- [VT69] H. L. Van Trees. *Multi-Dimensional and Multi-Variable Processes*. unpublished class notes, 1969.
- [VT71] H. L. Van Trees. *Detection, Estimation, and Modulation Theory, Part III*. Wiley, New York, 1971.

- [VT01b] H. L. Van Trees. *Detection, Estimation, and Modulation Theory, Part III*. Wiley Interscience, New York, 2001.
- [Vur77] A.M. Vural. A comparative performance study of adaptive array processors. *Proc. ICASSP*, Hartford, Connecticut, vol.I, pp. 695–700, May 1977.
- [Vur79] A.M. Vural. Effects of perturbations on the performance of optimum/adaptive arrays. *IEEE Trans. Aerosp. Electron. Syst.*, vol.AES-15, pp. 76–87, January 1979.
- [VV88] B. D. Van Veen. Eigenstructure based partially adaptive array design. *IEEE Trans. Antennas Propag.*, vol.AP-36, pp. 357–362, March 1988.
- [VV89] B. D. Van Veen. An analysis of several partially adaptive beamformer designs. *IEEE Trans. Acoust., Speech, Signal Process.*, vol.ASSP-37, pp. 192–203, February 1989.
- [VV91] B. D. Van Veen. Minimum variance beamforming with soft response constraints. *IEEE Trans. Signal Process.*, vol.SP-39, pp. 1964–1972, September 1991.
- [VVR87] B.D. Van Veen and R.A. Roberts. Partially adaptive beamformer design via output power minimization. *IEEE Trans. Acoust., Speech, Signal Process.*, vol.ASSP-35, pp. 1524–1532, November 1987.
- [WAN84] H. Watanabe, R. Azuma, and A. Noguchi. Interference rejection characteristics of spatially averaged learning adaptive antenna. Tech. Group on Antennas Propagat., IECE Japan, No.AP84-94, 1984
- [WDGN82] B. Widrow, K. M. Duvall, R. P. Gooch, and W. C. Newman. Signal cancellation phenomena in adaptive antennas: Causes and cures. *IEEE Trans. Antennas Propag.*, vol.AP-30, pp. 469–478, 1982.
- [Whi76] W.D. White. Cascade preprocessors for adaptive antennas. *IEEE Trans. Antennas Propag.*, vol.AP-24, pp. 670–684, September 1976.
- [WK85] H. Wang and M. Kaveh. Coherent signal subspace processing for the detection and estimation of angles of arrival of multiple wideband sources. *IEEE Trans. Acoust., Speech, Signal Process.*, pp. 823–831, August 1985.
- [Wol59] J. K. Wolf. *On the Detection and Estimation Problem for Multiple Non-Stationary Random Processes*. PhD thesis, Department of Electrical Engineering, Princeton University, Princeton, New Jersey, 1959.
- [WPMS88] R. T. Williams, S. Prasad, A. K. Mahalanabis, and L. H. Sibul. An improved spatial smoothing technique for bearing estimation in a multipath environment. *IEEE Trans. Acoust., Speech, Signal Process.*, vol.ASSP-36, pp. 425–431, April 1988.
- [WS74] L. P. Winkler and M. Schwartz. Constrained array optimization by penalty function techniques. *J. Acoust. Soc. Am.*, vol.55, pp. 1042–1048, May 1974.
- [YK90] J. F. Yang and M. Kaveh. Coherent signal-subspace transformation beamformer. *IEE Proc.*, vol. 137, Pt. F, No. 4, pp. 267–275, August 1990.
- [YU94] W. S. Youn and C. K. Un. Robust adaptive beamforming based on the eigenstructure method. *IEEE Trans. Signal Process.*, vol.SP-42, pp. 1543–1547, June 1994.

- [YY95] J.-L. Yu and C.-C. Yeh. Generalized eigenspace-based beamformers. *IEEE Trans. Signal Process.*, vol.SP-43, pp. 2453–2461, November 1995.
- [Zat95] M. Zatman. Production of adaptive array troughs by dispersion synthesis. *Electron. Lett.*, vol.31, pp. 2141-2142, 1995.
- [Zat99] M. Zatman. The relationship between covariance matrix tapers and multiple constraints. M.I.T. Lincoln Laboratory, Internal Memo. 1-6, Cambridge, Massachusetts, February 1999.
- [Zat00] M. Zatman. Comments on “Theory and application of covariance matrix tapers for robust adaptive beamforming.” *IEEE Trans. Signal Process.*, vol.SP-48, pp. 1796-1800, June 2000.
- [ZG91] G. T. Zunich and L. J. Griffiths. A robust method in adaptive array processing for random phase errors. *Proc. ICASSP*, Toronto, Canada, vol.II, pp. 1357-1360, May 1991.
- [ZL91a] M. D. Zoltowski and T. Lee. Maximum likelihood based sensor array signal processing in the beampspace domain for low-angle radar tracking. *IEEE Trans. Acoust., Speech, Signal Process.*, vol.ASSP-39, pp. 656-671, 1991.
- [ZL91b] M. D. Zoltowski and T. Lee. Beamspace. ML bearing estimation incorporating low-angle geometry. *IEEE Trans. Acoust., Speech, Signal Process.*, vol.ASSP-27, pp. 441-458, 1991.
- [ZL91c] M. D. Zoltowski and T. Lee. Interference cancellation matrix beamforming for 3-D beampspace ML/MUSIC bearing estimation. *IEEE Trans. Acoust., Speech, Signal Process.*, vol.ASSP-39, pp. 1858-1876, 1991.
- [Zol88] M. D. Zoltowski. On the performance analysis of the MVDR beamformer in the presence of correlated interference. *IEEE Trans. Acoust., Speech, Signal Process.*, vol.ASSP-36, pp. 945-947, June 1988.

Copyright of Optimum Array Processing is the property of John Wiley & Sons, Inc. 2002 and its content may not be copied or emailed to multiple sites or posted to a listserv without the copyright holder's express written permission. However, users may print, download, or email articles for individual use.